LBL-13605

Lawrence Berkeley Laboratory
UNIVERSITY OF CALIFORNIA

Materials & Molecular
Research Division

STUDY OF CORRELATIONS IN MOLECULAR MOTION BY MULTIPLE QUANTUM NMR

Jau-Huei Tang
(Ph.D. thesis)

November 1981

Prepared for the U.S. Department of Energy under Contract W-7405-ENG-48

LBL 13605

Study of Correlations in Molecular Motion by Multiple Quantum NMR

by

Jau-Huei Tang

Ph.D. Thesis

Materials and Molecular Research Division
Lawrence Berkeley Laboratory
University of California
Berkeley, CA 94720

November 1981

This work was supported by the Director, Office of Energy Research, Office of Basic Energy Sciences, Materials Sciences Division of the U. S. Department of Energy under Contract Number W-7405-ENG-48.

STUDY OF CORRELATIONS IN MOLECULAR MOTION

BY

MULTIPLE QUANTUM NMR

Jau-Huei Tang

Materials and Molecular Research Division
Lawrence Berkeley Laboratory
University of California
Berkeley, CA 94720

Abstract

Nuclear magnetic resonance is a very useful tool for characterizing molecular configurations through the measurement of transition frequencies and dipolar couplings. The measurement of spectral lineshapes, spin-lattice relaxation times, and transverse relaxation times also provide us with valuable information about correlations in molecular motion. The new technique of multiple qauntum nuclear magnetic resonance has numerous advantages over the conventional single quantum NMR techniques in obtaining information about static and dynamic interactions of coupled spin systems.

In the first two chapters, we discuss the theoretical background of spin Hamiltonians and the density matrix formalism of multiple quantum NMR. The creation and detection of multiple quantum coherence by multiple pulse sequence are discussed in chapter III. Prototype multiple quantum spectra of oriented benzene are presented. Redfield relaxation theory and the

application of multiple quantum NMR to the study of correlations in fluctuations are presented in chapter IV. A specific example of an oriented methyl group relaxed by paramagnetic impurities is studied in detail. In chapter V we present the study of possible correlated motion between two coupled methyl groups by multiple quantum NMR. For a six spin system it is shown that the four-quantum spectrum is sensitive to two-body correlations, and serves a ready test of correlated motion. In chapter VII we present the study of the spin-lattice relaxation dynamics of orienting or tunneling methyl groups (CH_3 and CD_3) at low temperatures. The anisotropic spin-lattice relaxation of deuterated hexamethylbenzene, caused by the sixfold reorientation of the molecules, is investigated in chapter VIII. The NMR spectrometers and other experimental details are discussed in chapter IX.

ACKNOWLEDGEMENT

I would like to express my gratitude to Professor Alexander Pines for his continuous support of me. By sharing his intuitions and novel ideas, he greatly inspired my exploration of the Multiple Quantum NMR Spectroscopy and other related topics discussed in this document.

I am grateful also to Dr. Soemi Emid. He initiated my interest in understanding the physics of methyl groups. Without him, and Dr. Shan Hsi's help in building a low temperature probe, the work of studying relaxation of methyl groups (in chapter VII) would have been impossible. I enjoyed the experience of collaborating with Larry Sterna in the experiments described in chapter VIII, and with Yu-Sze Yen, Dr. Jin-Feng Wong in the study of the correlation of two methyl groups described in chapter V. For many stimulating discussions and help with experiments, I am grateful to Gary Drobny, Steve Sinton, Dick Eckman, Dave Wemmer, Jim Murdoch, Dan Weitekamp, Warren Warren, George Wolf, Joel Garbow, John Millar, David Zax, Rob Tycko, Jean Baum, and visiting scientists: Dr. Chaohui Ye and Dr. Luciano Mueller.

Sidney Wolfe and Herbert Zimmerman have been very helpful in the synthesis of compounds and the growing of single crystals. Dione Carmichael's and Carol Hacker's excellent typing of the drafts of this thesis, Dr. Ye's help in proofreading the final draft, and Marshall Tuttle's work on the figures are greatly appreciated.

Finally, I would like to thank my wife Nen-Hua for her encouragement. My grandmother and parents also deserve a wealth of gratitude for supporting me during all my years of study.

This research was supported in part by the Director, Office of Energy Research, Office of Basic Energy Sciences, Materials Sciences Division of the U.S. Department of Energy under Contract Number W-7405-ENG-48.

Berkeley

September 1981 Jau-Huei Tang

Contents

Page

Page

I

THE SPIN HAMILTONIAN

1.1 Introduction

Nuclei, as well as fundamental particles, have individual attributes. Some examples are mass, charge, and spin. The spin angular momentum of any particle only takes the value of a non-negative integer or a positive half-integer in the unit of $\hbar$. For example, the spin of electron, proton, neutron, nuclei of ^{13}C and ^{19}F is one half. Nuclei of ^{2}H and ^{14}N have a spin 1, whereas the nuclei of ^{12}C and ^{16}O have no spin. A particle with spin I has a magnetic dipole moment $\vec{\mu}$ associated with it, and

$$\vec{\mu} = \hbar\gamma\vec{I} \quad , \tag{I.1}$$

where γ is a magnetogyric ratio of the particle. Table I.1 shows the value of γ for several common particles.[1]

We are primarily interested in the nuclear magnetic resonance (NMR) of organic molecules; hence we shall focus mainly on the nuclei of hydrogen and deuterium atoms--namely, the proton and the deuteron.

The nuclear spins in a molecule can interact with neighbor spins by direct dipole-dipole interaction, and also by indirect spin-spin interaction via orbiting electrons. Also, they can interact with an external static field or an oscillating magnetic field of an electromagnetic wave. For nuclei with spins greater than one half, the spins can interact with their local electric field gradients, also known as nuclear quadrupole interaction.

1.2 The Zeeman interaction

In the presence of an external magnetic field, quantum theory demands that spin cannot have an arbitrary orientation. Only a few states are allowed and they are characterized by the spin magnetic quantum number m. The z-component of the spin angular momentum $\hbar I_z$ is quantized, and I_z can take on one of a set of discrete values -I, -I+1, ..., I. The interaction between spin and an external magnetic field B_o along the z-axis is described by the Zeeman Hamiltonian H_z,

$$\begin{aligned} H_z &= -\gamma\hbar\vec{I}\cdot\vec{B}_o \\ &= -\gamma\hbar I_z B_o \quad , \end{aligned} \tag{I.2}$$

or

$$\begin{aligned} E_m &= -\gamma\hbar B_o m \\ &= -m\hbar\omega_o \quad , \end{aligned} \tag{I.3}$$

where ω_o is the Larmor frequency. The Larmor frequency of several common particles is listed in Table I.1.[2] In a typical field of 50 kG, the proton has a resonant frequency at about 210 MHz. The energy levels of spin I in a magnetic field consist of 2I+1 multiplets with an energy separation of $\hbar\omega_o$.

Because of the shielding effect of the surrounding electrons, the nuclear spins do not experience a common magnetic field $\vec{B}_o$. They experience slightly different local fields $\vec{B}_i$'s, and[3]

Table I.1

The Resonance Frequency and Magnetogyric Ratio

	I	γ(radians/sec 10 KGauss)	Frequency (MHz/10 KGauss)
e	1/2	1.759×10^3	2.800×10^4
^1H	1/2	2.675	42.577
n	1/2	1.833	29.175
^{13}C	1/2	0.673	10.705
^{19}F	1/2	2.518	40.055
^2H	1	0.411	6.542
^{14}N	1	0.193	3.072

$$H_z = -\hbar\gamma \sum_i \vec{I}_i \cdot (\underset{\sim}{1}-\underset{\sim i}{\sigma_i}) \cdot \vec{B}_o$$

$$= -\hbar\gamma \sum_i I_{i,z}(1-\sigma_{i,zz})B_o$$

$$= -\hbar\omega_o \sum_i I_{i,z}(1-\sigma_{i,zz}) \quad , \qquad (I.4)$$

where $\underset{\sim}{1}$ is a unit tensor, and $\underset{\sim i}{\sigma_i}$ is the local shielding tensor of the second rank. The shielding is determined by the local electronic structure, and has a magnitude order of 10^{-6}. It is small but plays a very important role in identifying molecular structure.

1.3 The dipole-dipole interaction

The nuclear spin can interact with the magnetic field produced by neighboring spins. The dipole-dipole interaction is described by the dipolar Hamiltonian H_D as[1,3]

$$H_D = \sum_{i<j} \vec{I}_i \cdot \underset{\sim ij}{D} \cdot \vec{I}_j$$

$$= \sum_{i<j} \gamma_i \gamma_j \hbar^2 \left[\frac{\vec{I}_i \cdot \vec{I}_j}{r_{ij}^3} - \frac{3(\vec{I}_i \cdot \vec{r})(\vec{I}_j \cdot \vec{r})}{r_{ij}^5}\right] \quad , \qquad (I.5)$$

where r_{ij} is the internuclear distance. $\underset{\sim ij}{D}$ is a traceless, symmetric tensor of the second rank. Since the dipolar coupling strength is much weaker than the Larmor frequency, we may ignore the non-secular part of the dipolar Hamiltonian that does not commute with the Zeeman Hamiltonian. The secular part (truncated Hamiltonian) can be expressed by[3]

$$H_D = \sum_{i<j} D_{ij} \, (3I_{i,z}I_{j,z} - \vec{I}_i \cdot \vec{I}_j) \quad , \tag{I.6}$$

and

$$D_{ij} = - \frac{\hbar^2 \gamma_i \gamma_j}{r_{ij}^3} \cdot \frac{1}{2} \, (3 \cos^2\theta_{ij} - 1) \quad , \tag{I.7}$$

where θ_{ij} is the angle between the z-axis and the internuclear vector.

For heteronuclear dipole-dipole interaction, the flip-flop term $I_{i+}I_{j-} + I_{i-}I_{j+}$ in $\vec{I}_i \cdot \vec{I}_j$ may also be neglected, since it does not commute with the Zeeman Hamiltonian if nuclei i and j are different species.

Assume we have two unlike species I and S; the secular part of the dipolar coupling between them is given by

$$H_D = \sum_{i<j} 2D_{ij} \, I_{i,z} \, S_{j,z} \quad . \tag{I.8}$$

1.4 The indirect spin-spin coupling

The nuclear spins can interact with each other through the second order effect of hyperfine coupling via electrons. The indirect spin-spin interaction can be written as

$$H_J = \sum_{i<j} \vec{I}_i \cdot \underset{\sim}{J}_{ij} \cdot \vec{I}_j \quad , \tag{I.9}$$

where $\underset{\sim}{J}_{ij}$ is a second-rank tensor.

If we neglect the non-secular part, the remaining secular term is given by[3]

$$H_J = \sum_{i<j} J_{ij}\, \vec{I}_i \cdot \vec{I}_j + \sum_{i<j} J_{ij}^{aniso}(3\, I_{i,z} I_{j,z} - \vec{I}_i \cdot \vec{I}_j) \quad , \quad (I.10)$$

where J_{ij} is the isotropic average of the tensor $\underset{\sim}{J}_{ij}$. J_{ij}^{aniso} is the anisotropic component that vanishes if the molecule undergoes isotropic tumbling as happens in liquid phase.

1.5 The quadrupole interaction

Nuclei with spin I greater than one half possess an electric quadrupole moment because of the non-spherical distribution of charge on the nuclei. In the molecule, the nuclear quadrupole moment will interact with the local electric field gradient that is produced by surrounding valence electrons. The nuclear quadrupole interaction is described by[4]

$$H_Q = \sum_i \frac{eQ_i}{2I_i(2I_i-1)}\, \vec{I}_i \cdot \underset{\sim}{V}_i \cdot \vec{I}_i \quad , \quad (I.11)$$

where Q_i is the quadrupole moment of nucleus i and $V_{i,\alpha\beta}$ (α,β = x,y, or z) is the second-rank tensor component of the electric field gradient at site i. Laplace's equation demands that the tensor $\underset{\sim}{V}$ be traceless and symmetric.

In the presence of a large magnetic field, the Hamiltonian becomes[4]

$$H_Q = \sum_i \frac{eQ_i V_{i,zz}}{4I_i(2I_i-1)} [3I_{i,z}^2 - I_i(I_i+1) + \frac{1}{2}\eta_i(I_{i,+}^2 + I_{i,-}^2)] \quad , \quad (I.12)$$

where η_i is the asymmetric parameter defined by

$$\eta_i = (V_{i,xx} - V_{i,yy})/V_{i,zz} \qquad 0 \le \eta \le 1 \quad . \quad (I.13)$$

$|V_{zz}| \geq |V_{xx}| \geq |V_{yy}|$ are the principle values of the electric field gradient tensor. For axially symmetric nuclear surroundings η vanishes, and

$$H_Q = \sum_i \frac{\hbar\omega_{Q,i}}{3} [3I_{i,z}^2 - I_i(I_i+1)] \quad , \tag{I.14}$$

where the quadrupole strength $\omega_{Q,i}$ is defined by

$$\omega_{Q,i} = \frac{3eQ_i V_{i,zz}}{4\hbar I_i(2I_i-1)} \quad . \tag{I.15}$$

1.6 Discussion

In general, the Hamiltonian of a spin system consists of four parts:

$$H = H_z + H_D + H_J + H_Q \quad . \tag{I.16}$$

In an isotropic liquid phase, all molecules undergo rapid diffusion and rotation. Consequently, the anisotropic parts of the interactions, such as dipolar and quadrupole interactions vanish in the time scale of NMR; and only the isotropic parts remain, namely,

$$H = -\hbar\omega_o \sum_i (1-\sigma_{i,zz})I_{i,zz} + \sum_{i<j} J_{ij} \vec{I}_i \cdot \vec{I}_j \quad . \tag{I.17}$$

Molecules dissolved in an anisotropic solvent such as liquid crystal are forced to align themselves in a preferential direction. Although the molecules are free in translational motion, their freedom of isotropic tumbling is impaired. As a result, the

anisotropic interactions do not vanish though their strength is generally reduced.

The dipolar interaction between solute molecules and liquid crystal, or among solute molecules, vanishes due to fast diffusion. Only intramolecular dipolar interaction remains.

For protons, the anisotropic spin-spin coupling J_{ij}^{aniso} is negligible and $H_Q = 0$. The Hamiltonian is given by[3]

$$H = -\hbar\omega_o \sum_i (1-\sigma_{i,zz})I_{i,z} + \sum_{i<j} J_{ij}\, \vec{I}_i \cdot \vec{I}_j + \sum_{i<j} D_{ij}(3I_{i,z}I_{j,z} - \vec{I}_i \cdot \vec{I}_j) \quad , \tag{I.18}$$

where

$$D_{ij} = -\frac{\hbar^2 \gamma_i \gamma_j}{\langle r_{ij}^3 \rangle} \cdot \frac{1}{2} \langle 3\cos^2\theta_{ij} - 1 \rangle \quad . \tag{I.19}$$

The coupling constant D_{ij} in the laboratory frame can be expressed in terms of the ordering parameters $S_{\alpha\beta}$'s of the liquid crystal. The coupling constants in the molecular frame can be expressed as[3,5]

$$\begin{aligned} D_{ij} = -\frac{\hbar^2 \gamma_i \gamma_j}{2\langle r_{ij}^3 \rangle} [& S_{aa} \langle 3\cos^2\theta_{ij,a} - 1 \rangle \\ & + (S_{bb} - S_{cc}) \langle \cos^2\theta_{ij,b} - \cos^2\theta_{ij,c} \rangle \\ & + 2 S_{ab} \langle \cos\theta_{ij,a} \cos\theta_{ij,b} \rangle \\ & + 2 S_{ac} \langle \cos\theta_{ij,a} \cos\theta_{ij,c} \rangle \\ & + 2 S_{bc} \langle \cos\theta_{ij,b} \cos\theta_{ij,c} \rangle] \quad , \end{aligned} \tag{I.20}$$

and

$$S_{\alpha\beta} = \frac{1}{2} \langle 3 \cos\theta_{\alpha z} \cos\theta_{\beta z} - \delta_{\alpha\beta} \rangle \quad , \quad \alpha,\beta = a,b, \text{ or } c \quad , \quad (I.21)$$

where $\theta_{\alpha z}$ is the angle made by the α-axis in the molecular frame (with respect to the field direction).

The matrix $\underset{\sim}{S}$ is traceless, symmetric, and has at most five independent components. The number of independent elements depends on the symmetry of the molecule.[3] For example, there is only one element for the benzene molecule and methyl group. There are two elements for the para disubstituted benzene.

The NMR study of partially oriented molecules in liquid crystal allows us to obtain valuable information about molecular structure by measuring the dipolar coupling constants that depend on internuclear distance and relative orientation. This information is generally not available by an NMR study of molecules in the liquid or solid phase.

1.7 References

1. A. Carrington and A. D. McLachlan, Introduction to Magnetic Resonance, Chapter 1 (Harper & Row, New York, 1967).

2. J. A. Pople, W. G. Schneider, and H. J. Bernstein, High-Resolution Nuclear Magnetic Resonance, Appendix A (McGraw-Hill, New York, 1959).

3. J. W. Emsley and J. C. Lindon, NMR Spectroscopy Using Liquid Crystal Solvents, Chapter 2 (Pergamon, Oxford, 1975).

4. A. Abragam, The Principles of Nuclear Magnetism, Chapter 6 (Oxford Univ. Press, London, 1961).

5. P. Diehl and C. L. Dhetrapal, NMR Basic Principles and Progress, Vol. 1, ed. by P. Diehl, et al. (Springer-Verlag, Berlin, 1969).

II

THE DENSITY MATRIX AND FICTITIOUS SPIN OPERATORS

2.1 Density matrix

For a given quantum mechanical system, any pure state $|\psi\rangle$ is a superposition of all the eigenstates $|i\rangle$,

$$|\psi\rangle = \sum_i \langle j_i|i\rangle \quad . \tag{II.1}$$

The expectation value of a physical observable operator A at that state is given by

$$\begin{aligned}\langle A\rangle &= \langle\psi|A|\psi\rangle = \sum A_i A_j^k \langle j|A|i\rangle \\ &= \sum \rho_{ij} A_{ji} = \mathrm{Tr}(\rho A) \quad .\end{aligned} \tag{II.2}$$

where $\rho_{ij} = a_i a_j^*$. The diagonal element ρ_{ii} of the density matrix is the population at state $|i\rangle$. The off-diagonal element ρ_{ij} describes the phase relation between states $|i\rangle$ and $|j\rangle$.

In general, the Hamiltonian of a system consists of two parts, the static Hamiltonian $H_0(t)$ and the fluctuating Hamiltonian $H_1(t)$. In most cases, the time dependent Hamiltonian $H_1(t)$ is much weaker than the static Hamiltonian and can be treated as a small perturbation.

By using a high temperature approximation ($\beta||H|| << i$) which is generally true for a spin system, the density matrix at thermal equilibrium can be expressed by[1]

$$\begin{aligned}\rho_o &= e^{-\beta H}/\mathrm{Tr}(e^{-\beta H}) \\ &\propto 1-\beta H_0 \quad ,\end{aligned} \tag{II.3}$$

where $\beta = 1/kT$.

The density matrix ρ_o is diagonal in the basis set of the eigenvectors of the Hamiltonian H_0. The irreversible fluctuation $H_1(t)$ drives the non-diagonal element of the density matrix toward zero at a time constant characterized by the transverse relaxation time. The non-equilibrium distribution of the population recovers at a different rate--called the longitudinal relaxation time.

The equation of motion for the density matris is given by[2]

$$\frac{d}{dt}\rho(t) = -i[H_o,\rho(t)] \quad , \quad (\hbar = 1) \tag{II.4}$$

where the time-dependent Hamiltonian $H_1(t)$ is neglected. The solution for the above equation is very simple and can be expressed by

$$\rho(t) = \exp(-iH_o t)\ \rho(0)\ \exp(iH_o t) \quad . \tag{II.5}$$

2.2 Rotating frame

The concept of rotating frame that synchronizes with the rotation of applied radio-frequency electromagnetic wave is convenient to use.

In the laboratory frame, the rf field along the coil is composed of clockwise and counterclockwise components. Only the component that rotates in the same way as the precession of nuclear spins is effective. The other component, which is off resonance by $2\omega_o$, can be neglected. This is the basis of the rotating-wave approximation. The assumption is justified because the strength of rf field is much weaker than the Larmor frequency ω_o.

Assuming U is a unitary transformation operator that transforms the wavefunction ψ or the density matrix from laboratory frame to rotating frame:[3]

$$|\psi>^* = U|\psi> \quad , \tag{II.6}$$

or

$$\rho^* = U\rho U^+ \quad , \tag{II.7}$$

then

$$\frac{d}{dt}\rho^* = -i[H^*,\rho^*] \quad , \tag{II.8}$$

and

$$\begin{aligned} H^* &= UHU^+ + i(\frac{d}{dt}U)U^+ \\ &= UHU^+ - iU(\frac{d}{dt}U^+) \quad , \end{aligned} \tag{II.9}$$

where the asterisk mark is referred to the rotating frame.

The Hamiltonian of a spins system in the presence of an rf field at frequency ω is given by

$$\begin{aligned} H &= H_z + H_{rf} \\ &= -\omega_o I_z - 2\,\omega_1\, I_x \cos\omega t \quad , \end{aligned} \tag{II.10}$$

where ω_1 is the strength of the oscillating field.

Using an explicit form for the unitary transformation operator

$$U = \exp(-i\omega I_z t) \quad ,$$

the Hamiltonian at rotating frame becomes

$$H^* = -(\omega_o - \omega)I_z - 2\omega_1 I_x \cos^2\omega t + \omega_1 I_y \sin 2\omega t$$

$$= -\Delta\omega I_z - \omega_1 I_x \quad , \qquad \text{(II.11)}$$

where $\Delta\omega$ is the frequency offset. The term with $\sin 2\omega t$ oscillates at a very high frequency and is averaged to zero, and $\cos^2\omega t$ has an average value of one half.

Evidently, the above expression shows that the effective Hamiltonian at the rotating frame is time-independent, and that the Larmor frequency ω_o is reduced to $\Delta\omega$.

2.3 The effect of symmetry on density matrix

For a system of N coupled spin-1/2 particles, the density matrix has a dimension of $2^N \times 2^N$. To characterize a general quantum state for such a system, one needs to know $2^{2N}-1$ matrix elements. Even for a system of a small number N, such as benzene, the number of matrix elements is quite huge. Fortunately, the actual number of independent and non-zero elements is not so large if the spin system possesses some kind of symmetry.

Let us assume that operator R corresponds to a symmetry operation of the system, and that the operator leaves the Hamiltonian invariant, namely,

$$R\, H_o\, R^+ = H_o \quad , \qquad \text{(II.12)}$$

or

$$[R, H_o] = 0 \quad . \qquad \text{(II.13)}$$

We can then show that the density matrix will also commute with R.[4]

The reasons are as follows. The density matrix at an equilibrium given by

$$\rho_o = e^{-\beta H_o}/Tr(e^{-\beta H_o}) \quad ,$$

is invariant under operator R, namely,

$$R\rho_o R^+ = e^{-\beta R H_o R^+}/Tr(e^{-\beta H_o})$$

$$= \rho_o \quad . \tag{II.14}$$

Since the radio frequency Hamiltonian H_{rf} has an A-type symmetry, it also commutes with R. In the rotating frame, the density matrix at an arbitrary time $\rho(t)$ given by

$$\rho(t) = e^{-it(H_o+H_{rf})}\ \rho(0)\ e^{it(H_o+H_{rf})}$$

commutes with R, that is,

$$R\ \rho(t)\ R^+ = \rho(t) \quad , \tag{II.15}$$

or

$$R\ \rho(t) = \rho(t)\ R \quad . \tag{II.16}$$

The above equation can be expressed in a matrix form based on eigenvectors of R such as

$$R_{\alpha\alpha}\rho_{\alpha\beta}(t) = \rho_{\alpha\beta}(t)R_{\beta\beta} \quad ,$$

or

$$(R_{\alpha\alpha}-R_{\beta\beta})\ \rho_{\alpha\beta}(t) = 0 \quad . \tag{II.17}$$

Thus $\rho_{\alpha\beta}(t) = 0$ if α and β refer to different eigenvalues of R, that is, no off-diagonal elements of ρ will connect states of a different symmetry.

As a result, the density matrix can be reduced to a simple block form such as

$$\begin{pmatrix} \rho^{(1)} & 0 & 0 \\ 0 & \rho^{(2)} & 0 \\ 0 & 0 & \cdots \end{pmatrix} , \tag{II.18}$$

where $\rho^{(i)}$ refers to i-th irreducible representation.

By using symmetry-adapted wavefunctions, we can greatly reduce the task of evaluating a density matrix or diagonalizing a Hamiltonian matrix.

We shall see later that no multiple quantum coherence exists among states of different symmetry.

2.4 Two-level system and fictitious spin

The most simple and fundamental quantum system of physical

interest is a two-level system. The system with a spin-1/2 particle in a magnetic field is a typical example. Its density matrix is given by a 2 x 2 matrix, and can be expressed by a linear combination of an unit matrix and the other three Pauli's matrices as follows[2]

$$\rho = 1/2(1 + \vec{P}\cdot\vec{\sigma}) \quad . \tag{II.19}$$

The Pauli's matrices are given by

$$\sigma_x = \begin{pmatrix} 0 & 1 \\ 1 & 0 \end{pmatrix}, \quad \sigma_y = \begin{pmatrix} 0 & -i \\ i & 0 \end{pmatrix}, \quad \sigma_z = \begin{pmatrix} 1 & 0 \\ 0 & -1 \end{pmatrix} \quad . \tag{II.20}$$

We can show that the Pauli's matrices are mutually orthogonal, namely, $Tr(\sigma_i\sigma_j) = 2\delta_{ij}$, where δ_{ij} is the Kronecker delta function. The vector $\vec{P}$ describes the polarization and is given by

$$\vec{P} = Tr(\rho\vec{\sigma}) \quad . \tag{II.21}$$

Any given quantum state is completely determined, except for an overall constant phase, if the polarization vector is known. The time-evolution of the polarization is governed by an equation of motion for the density matrix or for the Pauli's matrices. Both of these approaches are equivalent.

Usually, we will use a spin operator $\vec{I}$ instead of $\vec{\sigma}$. They are related to each other by

$$\vec{I} = \frac{1}{2}\vec{\sigma} \quad . \tag{II.22}$$

We can demonstrate this important commutation relationship:

$$[I_\alpha, I_\beta] = iI_\gamma, \quad \alpha,\beta,\gamma \text{ in cyclic ordering.} \tag{II.23}$$

The motion for the operator $\vec{I}$ is given by Heisenberg's equation

$$\frac{d}{dt}\vec{I} = i[\mathcal{H},\vec{I}] \tag{II.24}$$

where we use the usual convention $\hbar = 1$.

Any physical observable can be expressed in terms of operator $\vec{I}$, and can be calculated by knowing the equation of motion for $\vec{I}$.

Since the operator I is so important, we shall discuss it in more detail. Instead of a matrix representation, we may also express $\vec{I}$ in the second quantization operators for boson. For a two level system, there are two states $|\alpha\rangle$ and $|\beta\rangle$. We can define the creation operator C_i^+ which creates a particle in state $|i\rangle$ out of vacuum. The annihilation operator C_j destroys a particle in state $|j\rangle$. If we define a projection operator C_{ij} as $C_i^+ C_j$, we can express the operator $\vec{I}$ in terms of them as[5]

$$I_x = \frac{1}{2}(C_{\alpha\beta}+C_{\beta\alpha}) = \frac{1}{2}(|\alpha\rangle\langle\beta| + |\beta\rangle\langle\alpha|)$$

$$I_y = -\frac{i}{2}(C_{\alpha\beta}-C_{\beta\alpha}) = -\frac{i}{2}(|\alpha\rangle\langle\beta| - |\beta\rangle\langle\alpha|)$$

$$I_z = \frac{1}{2}(C_{\alpha\alpha}-C_{\beta\beta}) = \frac{1}{2}(|\alpha\rangle\langle\alpha| - |\beta\rangle\langle\beta|) \quad . \tag{II.25}$$

This approach was first devised by Schwinger.

We can expand Schwinger's ideas to include any N-level system. Given a pair of states $|i\rangle$ and $|j\rangle$, we can define fictitious

spin operators in a similar way as

$$X_x^{ij} = \frac{1}{2}(C_{ij}+C_{ji}) = \frac{1}{2}(|i><j| + |j><i|)$$

$$I_y^{ij} = -\frac{i}{2}(C_{ij}-C_{ji}) = -\frac{i}{2}(|i><j| - |j><i|)$$

$$I_z^{ij} = \frac{1}{2}(C_{ii}-C_{jj}) = \frac{1}{2}(|i><i| - |j><j|) \quad . \tag{II.26}$$

We may notice that

$$I_x^{ij} = I_x^{ji} \quad , \quad I_y^{ij} = -I_y^{ji} \quad , \quad I_z^{ij} = -I_z^{ji} \quad , \tag{II.27}$$

and that they are all hermitian operators. As ordinary spin operators, the fictitious spin operators also follow a similar communication relation:

$$[I_\alpha^{ij}, I_\beta^{ij}] = i\, I_\gamma^{ij} \quad , \quad \alpha,\beta,\gamma \text{ in cyclic ordering.} \tag{II.28}$$

Since there are more than two states, the commutation relationship of the fictitious spin operators among different states is also important. They are listed below:

1) $[I_\alpha^{ij}, I_\beta^{km}] = 0$, if $i, j \neq k, m$

2) $[I_z^{ij}, I_z^{km}] = 0$, for any i, j, k, m

3) $[I_x^{ij}, K_x^{km}] = \frac{i}{2}(\delta_{jk}I_y^{im} - \delta_{im}I_y^{kj} + \delta_{jm}I_y^{ik} - \delta_{ik}I_y^{mj})$

4) $[I_y^{ij}, I_y^{km}] = -\frac{i}{2}(\delta_{jk}I_y^{im} - \delta_{im}I_y^{kj} - \delta_{jm}I_y^{ik} + \delta_{ik}I_x^{mj})$

5) $[I_x^{ij}, I_y^{km}] = \frac{i}{2}(-\delta_{jk}I_x^{im} + \delta_{im}I_x^{kj} + \delta_{jm}I_x^{ik} - \delta_{ik}I_x^{mj})$

6) $[I_x^{ij}, I_z^{km}] = \frac{i}{2}(\delta_{jk}I_y^{ij} + \delta_{im}I_y^{ij} - \delta_{ik}I_y^{ij} - \delta_{jm}I_y^{ij})$

$$7)\quad [I_y^{ij}, I_z^{km}] = -\frac{i}{2}\left({}_{jk}I_x^{ij} + {}_{im}I_x^{ij} - {}_{ik}I_x^{ij} - {}_{jm}I_x^{ij}\right)$$

$$8)\quad I_z^{ij} + I_z^{jk} + I_z^{kp} + \ldots + I_z^{sm} + I_z^{mn} = I_z^{in} \quad . \tag{II.29}$$

The above equations are very useful. In particular, they are frequently used for finding the commutation relationship among generators of SU(3). These will be discussed in the next section.

The time-evolution of the projection operator $C_{\alpha\beta}(t)$ is governed by Heisenberg's equation, and is given by

$$C_{\alpha,\beta}(t) = e^{-iHt}|\alpha><\beta|e^{iHt} = e^{-i\omega_{\alpha\beta}t}|\alpha><\beta|$$

$$= e^{-i\omega_{\alpha\beta}t} C_{\alpha\beta}(o) \tag{II.30}$$

where $\omega_{\alpha\beta} = \omega_\alpha - \omega_\beta$. ω_α and ω_β are the eigenfrequencies of the states $|\alpha>$ and $|\beta>$. Consequently, the evolution of the fictitious spin operators follows a simple relation:

$$I_x^{ij}(t) = I_x^{ij}(o)\ \cos\omega_{ij}t - I_y^{ij}(o)\ \sin\omega_{ij}t \quad ,$$

$$I_y^{ij}(t) = I_x^{ij}(o)\ \sin\omega_{ij}t + I_y^{ij}(o)\ \cos\omega_{ij}t \quad ,$$

$$I_z^{ij}(t) = I_z^{ij}(o) \quad . \tag{II.31}$$

The transverse polarizations I_x^{ij} and I_y^{ij} rotate in the fictitious spin space at a frequency ω_{ij} (Figure II.1). The dependence of the transverse polarizations of multiple quantum coherence upon the phase shift ϕ varies for a different order of coherence as follows:

$$e^{i\phi I_z} I_x^{ij} e^{-i\phi I_z} = I_x^{ij}\ \cos(m_i - m_j)\phi - I_y^{ij}\ \sin(m_i - m_j)\phi \quad ,$$

$$e^{i\phi I_z} I_y^{ij} e^{-i\phi I_z} = I_x^{ij} \sin(m_i - m_j)\phi + I_y^{ij} \cos(m_i - m_j)\phi \quad .(II.32)$$

Thus, n-quantum coherence has a phase shift by $n\phi$.

2.5 Three-Level System

As we discussed previously, for any general n-level system, the density matrix of the system has a dimension of n x n. Because of the conservation of probability, the total population among each state should remain constant. Consequently, to completely specify a general quantum state of a n-level system, we must know n^2-1 independent parameters about the system.

For two-level systems, the quantum state is completely determined if we know their three polarization components. The polarization is actually the expectation value of the Pauli's matrices. Any physical transformation of a given quantum state can be characterized by an unitary transformation U and is related to the Pauli's matrices by[6]

$$U = \exp(i \sum \sigma_i \theta_i) \quad , \qquad i = 1,2,3 \qquad (II.33)$$

Mathematically speaking, the Pauli's matrices are generators of the SU(2) group and U is a group element.

Generally in a n-level system, any physical transformation is characterized by a group element of SU(n). The SU(n) group has n^2-1 generators.[6] For each generator, it associates with a parameter θ. Therefore, it needs n^2-1 parameters to completely specify any general quantum state.

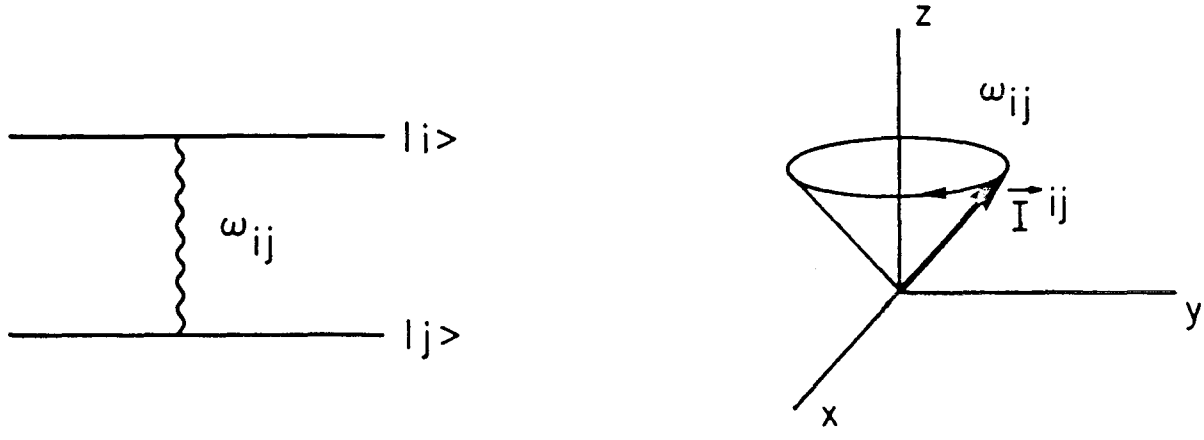

$$\langle \vec{I} \rangle = \mathrm{Tr}(\vec{I}^{ij}\rho)$$

$$\langle I_x^{ij} \rangle = 2\mathrm{Re}\rho_{ij}$$

$$\langle I_y^{ij} \rangle = -2\,\mathrm{Im}\,\rho_{ij}$$

$$\langle I_z^{ij} \rangle = \rho_{ii} - \rho_{jj}$$

XBL 816-10418

Figure II.1 Correspondence between the fictitious spin polarization and the density matrix. The polarization in the fictitions spin space precesses about the z-axis at the transition frequency. The longitudinal and transverse polarizations correspond to the population difference and phase coherence.

In the case of a spin-1 particle, such as the deuteron, it is a three-level system. Using NMR techniques on deuteron, we can explore many interesting properties of the SU(3) group.[7] There are eight generators in all. Our choice of these generators depends on the physical situation and convenience. Usually the generator set consists of three components of the spin operator $\vec{I}$ and five components of the second-rank tensor $T^{(m)}$, where m = 0, ±1, and ±2. They have following commutation relations:[8]

$$[I_\alpha, I_\beta] = iI_\gamma \quad , \quad \alpha,\beta,\gamma \text{ in cyclic ordering}$$

$$[I_z, T^{(m)}] = m\, T^{(m)}$$

$$[I_\pm, T^{(m)}] = \sqrt{j(j+1)-m(m\pm1)}\; T^{(m\pm1)} \quad , \quad j=2 \quad . \tag{II.34}$$

The generators can be represented by matrices with states $|m=1\rangle$, $|m=0\rangle$, $|m=-1\rangle$ as bases,

$$I_x = \frac{1}{\sqrt{2}} \begin{pmatrix} 0 & 1 & 0 \\ 1 & 0 & 1 \\ 0 & 1 & 0 \end{pmatrix} \quad , \quad I_y = \frac{i}{\sqrt{2}} \begin{pmatrix} 0 & -1 & 0 \\ 1 & 0 & -1 \\ 0 & 1 & 0 \end{pmatrix}$$

$$I_z = \begin{pmatrix} 1 & 0 & 0 \\ 0 & 0 & 0 \\ 0 & 0 & -1 \end{pmatrix} \quad , \quad T^{(0)} = \begin{pmatrix} 1 & 0 & 0 \\ 0 & -2 & 0 \\ 0 & 0 & 1 \end{pmatrix} \tag{II.35}$$

$$T^{(1)} = \sqrt{3} \begin{pmatrix} 0 & -1 & 0 \\ 0 & 0 & 0 \\ 0 & 0 & 0 \end{pmatrix} \quad , \quad T^{(2)} = \sqrt{6} \begin{pmatrix} 0 & 0 & 1 \\ 0 & 0 & 0 \\ 0 & 0 & 0 \end{pmatrix}$$

and $T^{(-m)} = (-1)^m T^m$. All the above generators are traceless and $Tr((-1)^m T^{(m)} T^{(-m)}) = 6$.

Another usual set of generators are fictitions spin operators given by I_α^{ij}, where $\alpha = x, y, z$ and $i,j = 1, 2, 3$. Their matrix representations are shown as follows:

$$I_x^{12} = \frac{1}{2}\begin{pmatrix} 0 & 1 & 0 \\ -1 & 0 & 0 \\ 0 & 0 & 0 \end{pmatrix} \quad I_y^{12} = \frac{i}{2}\begin{pmatrix} 0 & -1 & 0 \\ 1 & 0 & 0 \\ 0 & 0 & 0 \end{pmatrix} \quad I_z^{12} = \frac{1}{2}\begin{pmatrix} 1 & 0 & 0 \\ 0 & -1 & 0 \\ 0 & 0 & 0 \end{pmatrix}$$

$$I_x^{23} = \frac{1}{2}\begin{pmatrix} 0 & 0 & 0 \\ 0 & 0 & 1 \\ 0 & 1 & 0 \end{pmatrix} \quad I_y^{23} = \frac{i}{2}\begin{pmatrix} 0 & 0 & 0 \\ 0 & 0 & -1 \\ 0 & 1 & 0 \end{pmatrix} \quad I_z^{23} = \frac{1}{2}\begin{pmatrix} 0 & 0 & 0 \\ 0 & 1 & 0 \\ 0 & 0 & -1 \end{pmatrix}$$

$$I_x^{13} = \frac{1}{2}\begin{pmatrix} 0 & 0 & 1 \\ 0 & 0 & 0 \\ 1 & 0 & 0 \end{pmatrix} \quad I_y^{13} = \frac{i}{2}\begin{pmatrix} 0 & 0 & -1 \\ 0 & 0 & 0 \\ 1 & 0 & 0 \end{pmatrix} \quad I_z^{13} = \frac{1}{2}\begin{pmatrix} 1 & 0 & 0 \\ 0 & 0 & 0 \\ 0 & 0 & -1 \end{pmatrix}$$

(II.36)

The above nine operators are not linearly independent, since $I_z^{13} = I_z^{12} + I_z^{23}$. Nevertheless, the remaining eight operators are linearly independent and form the complete set of generators for SU(3). We can show that

$$Tr(I_\alpha^{ij})^2 = \frac{1}{2}$$

$$Tr(I_z^{12} I_z^{23}) = -Tr(I_z^{12} I_z^{13}) = -Tr(I_z^{23} I_z^{13}) = -\frac{1}{4} \quad , \qquad \text{(II.37)}$$

and that for all other combinations $I_\alpha^{ij} I_\beta^{lm}$ are traceless, namely,

$$\mathrm{Tr}(I_\alpha^{ij} I_\beta^{lm}) = 0 \quad . \tag{II.38}$$

These fictitious spin operators are convenient for solving the problem of weak, selective perturbation.[9]

Many interesting NMR phenomena of spin-1 system arise from the peculiar properties of transforming these SU(3) generators. Before exploring their peculiar transformation and commutative relationship, we shall prove two important lemmas:

Lemma 1. If operators A, B, and C satisfy the following relations

$$[A,B] = i\alpha C$$

$$[A,B] = -i\alpha B$$

$$\text{then } e^{i\theta A} B e^{-i\theta A} = B\cos\alpha\theta - C\sin\alpha\theta \quad , \tag{II.39}$$

Proof: $\dfrac{\partial^n}{\partial\theta^n}(e^{i\theta A} B e^{-i\theta A}) = \underbrace{[A[A,\ldots[A,B]\ldots]]}_{n \text{ times}}$

$$e^{i\theta A} B e^{-i\theta A} = \sum_{n=0}^{\infty} \frac{(i\theta)^n}{n!} [A[A\ldots[A,B]\ldots]]$$

$$= \sum_{\substack{n=0 \\ (\text{even})}} \frac{(i\theta)^n}{n!} \alpha^n B + \sum_{\substack{n=1 \\ (\text{odd})}} \frac{(i\theta)^n}{n!} (i\alpha)^n C$$

$$= B\cos\alpha\theta - C\sin\alpha\theta \quad .$$

Lemma 2. If operators A, B, C, and D satisfy

$$[A,B] = i\beta\alpha C$$

$$[A,C] = -i\alpha D$$

$$[A,D] = i\alpha C \quad ,$$

then

$$e^{i\theta A} B e^{-i\theta A} = B - \beta D(1-\cos\alpha\theta) - \beta C \sin\alpha\theta \quad . \tag{II.40}$$

Proof:

$$e^{i\theta A} B e^{-i\theta A} = B + \sum_{n=1}^{\infty} \frac{(i\theta)^n}{n!} [A[A...[A,B]...]]$$

$$= B + \sum_{\substack{n=1 \\ (odd)}} \beta \frac{(i\theta)^n}{n!} (i\alpha)^n C + \sum_{\substack{n=2 \\ (even)}} \beta \frac{(i\theta)^n}{n!} \alpha^n D$$

$$= B - \beta D(1-\cos\alpha\theta) - \beta C \sin\alpha\theta \quad .$$

2.6 Transformation of fictitious spin operator

The transformation of the SU(2) group has a very special property. If A, B, and C are its generators--as are Pauli's matrices σ_x, σ_y and σ_z--their commutation relationship is given by

$$[A,B] = \frac{i}{2} C \quad , \quad A, B, C, \text{ in cyclic ordering.}$$

Using Lemma 1, we can show

$$E^{i\theta A} B e^{-i\theta A} = B \cos\frac{\theta}{2} - C \sin\frac{\theta}{2} \quad . \tag{II.41}$$

The transformation of a state is only half the angle of the spatial rotation. Consequently, a 2π pulse will change the sign of the wave function and will not bring it back to its original state. Actually this is a special property of a spinor that is a half-rank tensor. We can show that the following sets of operators generate their own SU(2) groups.

These are subgroups of SU(3):

(1) $I_x^{12}, I_x^{23}, I_y^{13}$,

(2) $I_y^{12}, I_y^{13}, I_y^{23}$,

(3) $I_x^{13}, I_x^{23}, I_y^{12}$

(4) $I_x^{12}, I_x^{13}, I_y^{23}$.

The following sets of operators however, generate O(3) groups[5] (orthogonal group) that are also subgroups of SU(3)

(1) $I_x^{12}, I_y^{12}, I_z^{12}$,

(2) $I_x^{23}, I_y^{23}, I_z^{23}$,

(3) $I_x^{13}, I_y^{13}, I_z^{13}$.

They follow a different commutation relationship such as

$$[A,B] = iC \quad , \quad A, B, C, \text{ in cyclic ordering,}$$

and

$$e^{i\theta A} B e^{-i\theta A} = B\cos\theta - C\sin\theta \quad . \tag{II.42}$$

Unlike spinors, they make a full rotation and behave as ordinary vectors.

2.7 Transformation of tensor operator

The transformation of a tensor operator is very important in studying the NMR of spin-1 system. Both quadrupole and dipole-dipole interaction Hamiltonian consist of tensor operators of the

second rank. They are bilinear operators in spin operators I_α, that is, they are formed by the product of two spin operators. Their transformation is completely different from vectors and spinors. A tensor of second rank two has five components $T^{(m)}$ with indices m = 0, ±1 and ±2. The index m is the magnetic quantum number. Because of the closure property of similarity transformation, a spatial transformation will change any component into a linear combination of the five components.

Using the lemma 1 and the lemma 2, we are able to show some important transformations of the tensor operators.

$$\text{(A)}\quad e^{-i\beta I_x} T^{(0)} e^{i\beta I_x} = T^{(0)} + \frac{\sqrt{6}}{8}(T^{(2)}+T^{(-2)}+\sqrt{6}\,T^{(0)})(\cos 2\beta - 1) - i\frac{\sqrt{6}}{4}(T^{(1)}+T^{(-1)})\sin 2\beta \quad ,$$

$$= T^{(0)}\frac{1}{2}(3\cos^2\beta - 1) - i\frac{\sqrt{6}}{4}(T^{(1)}+T^{(-1)})\sin 2\beta + \frac{\sqrt{6}}{8}(T^{(2)}+T^{(-2)})(\cos 2\beta - 1) \quad . \qquad \text{(II.43)}$$

Proof: Because of follwoing commutation relations:

$$[I_x, T^{(0)}] = 2\frac{\sqrt{6}}{4}(T^{(1)}+T^{(-1)}) \quad ,$$

$$[I_x, \frac{\sqrt{6}}{4}(T^{(1)}+T^{(-1)})] = 2\frac{\sqrt{6}}{8}(T^{(2)}+T^{(-2)}+\sqrt{6}\,T^{(0)}) \quad ,$$

$$[I_x, \frac{\sqrt{6}}{8}(T^{(2)}+T^{(-2)}+\sqrt{6}\,T^{(0)}] = 2\frac{\sqrt{6}}{4}(T^{(1)}+T^{(-1)}) \quad ,$$

together with the lemma 2, it is easily proven.

We may notice that the angular dependece of $T^{(0)}$ is given by the Legrendre polynomial $P_2(\cos\theta)$. It has a zero value at the magic angle $\theta_m = \cos^{-1}\frac{1}{\sqrt{3}} \simeq 54.74°$.

$$(B)\quad e^{-i\beta I_x}\,(T^{(2)}-T^{(-2)})\,e^{i\beta I_x} = (T^{(2)}-T^{(-2)})\,\cos\beta - i(T^{(1)}-T^{(-1)})\sin\beta. \tag{II.44}$$

It can be proved by lemma 1; using the following relation,

$$[I_x, T^{(2)}-T^{(-2)}] = T^{(1)}-T^{(-1)} \quad ,$$

$$[I_x, T^{(1)}-T^{(-1)}] = T^{(2)}-T^{(-2)} \quad .$$

$$(C)\quad e^{-i\beta I_x}\,(T^{(1)}-T^{(-1)})\,e^{i\beta I_x} = (T^{(1)}-T^{(-1)})\,\cos\beta - i(T^{(2)}-T^{(-2)})\sin\beta \tag{II.45}$$

It can be easily proven by using a method similar to the one used in (B).

$$(D)\quad e^{-i\beta I_x}\,(T^{(1)}+T^{(-1)})\,e^{i\beta I_x}$$

$$= 2\left[\frac{1}{2}\,(T^{(1)}+T^{(-1)})\,\cos\alpha\beta - i\,\frac{1}{4}\,(T^{(2)}+T^{(-2)} + \sqrt{6}\,T^{(0)})\,\sin 2\beta\right] \tag{II.46}$$

$$(E)\quad e^{-i\beta I_x}\,(T^{(2)}+T^{(-2)})\,e^{i\beta I_x}$$

$$= T^{(2)} + T^{(-2)} - \frac{1}{4}\,(T^{(2)}+T^{(-2)}+\sqrt{6}\,T^{(0)}(1-\cos 2\beta)$$

$$- i\,\frac{1}{2}\,(T^{(1)}+T^{(-1)})\,\sin 2\beta \quad . \tag{II.47}$$

The above relations can be proved by using

$$[I_x, T^{(2)}+T^{(-2)}] = 2\cdot\frac{1}{2}(T^{(1)}+T^{(-1)}) \quad ,$$

$$[I_x, \frac{1}{2}(T^{(1)}+T^{(-1)}] = 2\cdot\frac{1}{4}(T^{(2)}+T^{(-2)}+\sqrt{6}\,T^{(0)}) \quad ,$$

$$[I_x, \frac{1}{4}(T^{(2)}+T^{(-2)}+\sqrt{6}\,T^{(0)})] = 2\cdot\frac{1}{2}(T^{(1)}+T^{(-1)}) \quad ,$$

and the lemmas 1 and 2.

$$(F)\quad e^{-i\phi I_z}\, T^{(m)}\, e^{i\phi I_z} = T^{(m)}\, e^{-im\phi} \tag{II.48}$$

It can be proved using

$$[I_z, T^{(m)}] = mT^{(m)} \quad .$$

The rotation about the y axis $e^{-i\theta I_y}$ is equivalent to the transformation $e^{-i\frac{\pi}{2} I_z}\, e^{-i\theta I_x}\, e^{i\frac{\pi}{2} I_z}$; for any arbitrary rotation, it can be characterized by several successive rotations about the z and x axes. Consequently, we can obtain any transformation of $T^{(m)}$ without too much difficulty. We shall use them quite often in the study of spin-lattice relaxation of CD_3 groups and deuterated hexamethylbenzene molecules in solids.

2.8 Quadrupole echo in SU(2) space--an analogy to Hahn spin-echo

In a recent paper,[7] the eight-dimensional spin space of a spin-1 particle is studied by NMR. It illustrates that the SU(3) group has three kinds of SU(2) subgroups that transform under rotation with the angles $\beta/2$, β, and 2β. The quadrupole echo that follows a $90^\circ_x - \tau - 90^\circ_y$ pulse sequence is actually the behavior of the fictitious spin in the SU(2) space of rotation with angle 2β. In a typical Hahn spin-echo experiment in high-resolution NMR, the pulse sequence $90^\circ_x - \tau - 180^\circ_y$ is used to refocus the transverse magnetization that has dephased because of field inhomogeneity.[10] In a powder sample of a spin-1 system, the dephasing mechanism is caused mainly by the distribution of quadrupole splittings over all possible orientations. Because

of the characteristic feature of a 2β-rotation in the fictitious spin space, a 90°_y pulse is used instead of a 180°_y pulse to rephase the incoherence.

To illustrate this, let us consider the behavior of a spin-1 system in the rotating frame at the Larmor frequency. Followed by a 90°_x pulse, a net magnetization is created along the y-axis as is shown in Figure II.2(a). Each spin begins to precess at a rate of ω_Q as described by

$$e^{-iH\tau} I_y e^{iH\tau} = I_y \cos\omega_Q\tau + \sqrt{2}\,(I_x^{12}-I_x^{23}) \sin\omega_Q\tau$$

$$\equiv S_y \cos\omega_Q\tau + S_x \sin\omega_Q\tau \quad . \tag{II.49}$$

Owing to the orientation dependence of ω_Q, each spin does not precess at the same rate, and they begin to fan out as shown in Figure II.2(b). The effect of the second 90°_y pulse is to reverse S_x,

$$\exp(i\,\frac{\pi}{2}\,I_y)(S_y \cos\omega_Q\tau+S_x\sin\omega_Q\tau)\exp(-i\,\frac{\pi}{2}\,I_y)$$

$$= S_y\cos\omega_Q\tau - S_x\sin\omega_Q\tau \tag{II.50}$$

and is shown in Figure II.2(c).

The spins shown in Figure II.2(d) begin to refocus as time goes on. At time τ after the second pulse, all spins align along the y-axis as shown in Figure II.2(e),

$$e^{-iH\tau}(S_y\cos\omega_Q\tau - S_x\sin\omega_Q\tau)e^{iH\tau}$$

$$= S_y = I_y \tag{II.51}$$

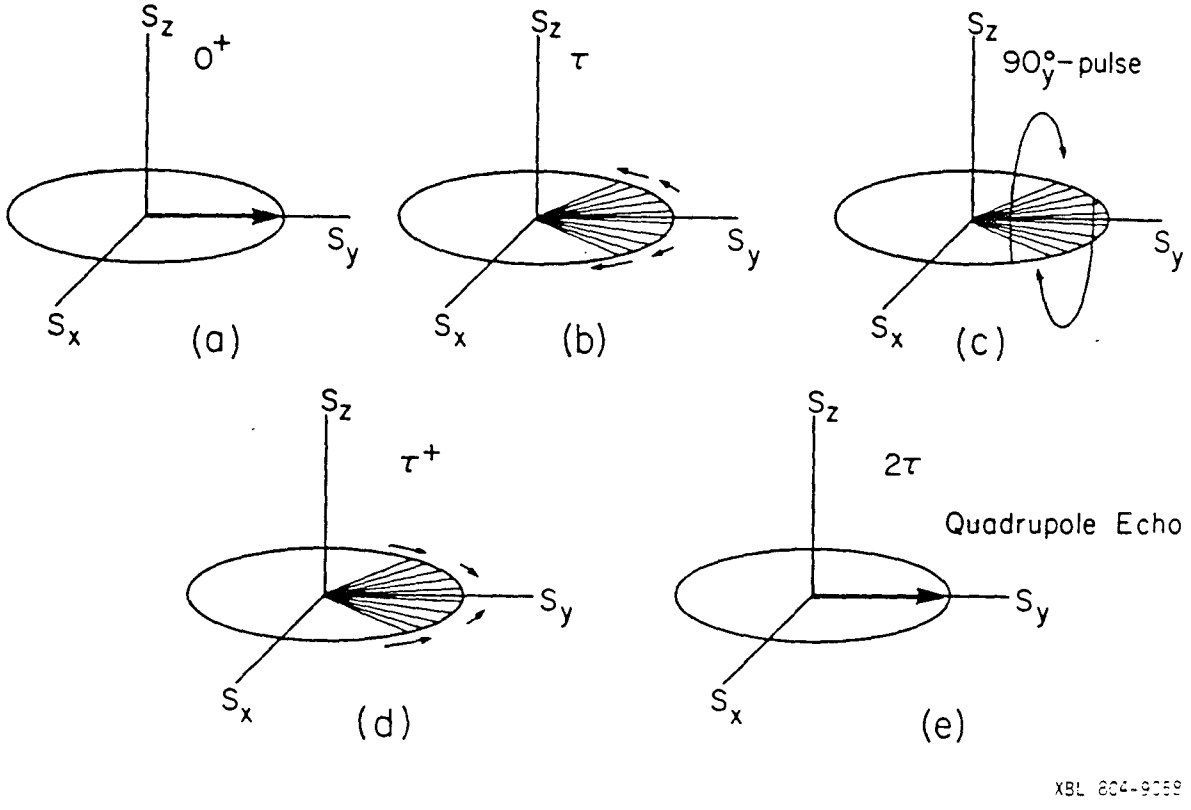

Figure II.2 Evolution of the fictitions spin in the SU(2) space of rotation with angle 2β followed by a $90°_x$-τ-$90°_y$ sequence is shown as an analogy to the Hahn spin-echo experiment.

and a quadrupole echo can be detected.

2.9 References

1. A. Abragam, The Principles of Nuclear Magnetism, Chapter 3 (Oxford Univ. Press, London, 1961).
2. E. Merzbacher, Quantum Mechanics, Chapter 13 (John Wiley & Sons, New York, 1970).
3. Reference 1, Chapter 2.
4. M. Tinkham, Group Theory and Quantum Mechanics, Chapter 1 (McGraw-Hill, New York, 1971).
5. G. Baym, Lectures on Quantum Mechanics, Chapter 17 (W. A. Benjamin, New York, 1969).
6. L. I. Schiff, Quantum Mechanics, Chapter 7 (McGraw-Hill, New York, 1968).
7. M. Mehring, E. K. Wolff, and M. E. Stoll, J. Magn. Reson. 37, 475 (1980).
8. Reference 4, Chapter 5.
9. S. Vega, T. W. Shattuck, and A. Pines, Phys. Rev. Lett. 37, 43 (1976).
10. E. L. Hahn, Phys. Rev. 80, 580 (1950).

III

MULTIPLE QUANTUM NMR SPECTROSCOPY

3.1 Introduction

The conventional NMR spectra are usually obtained by a continuous wave method[1] or Fourier transform of the FID following a single pulse excitation.[2] In both cases, the spectra consist of allowed magnetic dipole radiation, that is, the transitions that change the magnetic quantum number m by 1 or -1.[3]

For the dipole-coupled spin system, the NMR spectrum is generally very complicated, not well resolved, and sometimes difficult to analyze.[4] To illustrate this, let us consider the system of non-symmetric six dipole-coupled spin 1/2 particles. The energy levels can be classified into several manifolds of varying magnetic quantum number m as we have shown in Figure III.1. The multiplet inside the same manifold is caused by the dipole-dipole interaction. The ordinary single quantum NMR spectrum is very complicated and has about eight hundred transitions.

For a molecule with symmetric configuration, the number of allowed transitions becomes fewer because of the additional selection rule imposed by the symmetry of the molecule. For example, the benzene molecule has a hexagonal symmetry with symmetry group D_{6h}.[5] The energy levels should be classified by the magnetic quantum number m and also by the irreducible representation of the symmetry group as shown in Figure III.2.

Because of the additional selection rule, only the transitions within the same representation are allowed. Consequently, the

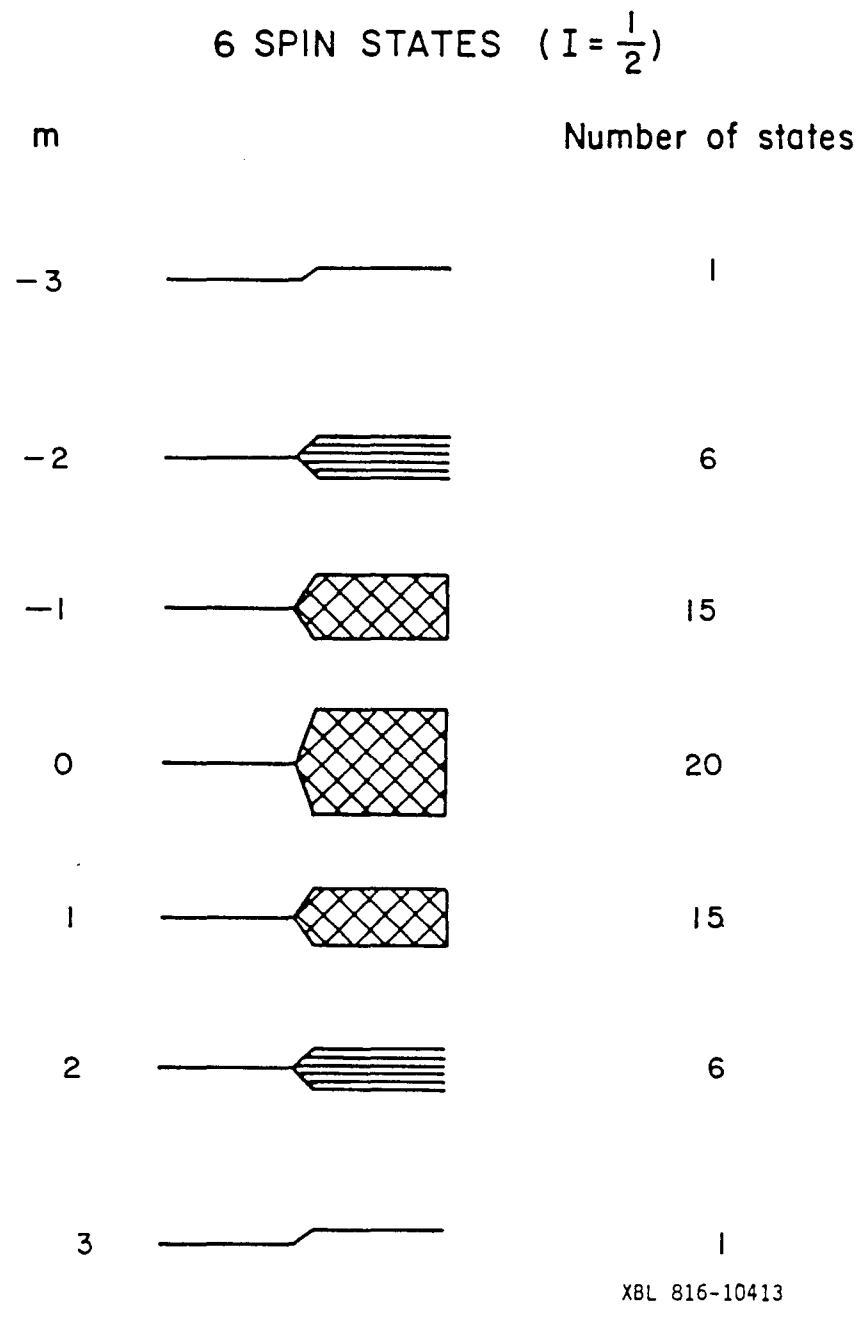

Figure III.1 Energy level diagram of a non-symmetric six spin-1/2 system in a strong magnetic field. The multiplet splitting inside the m manifolds is due to dipole-dipole interactions.

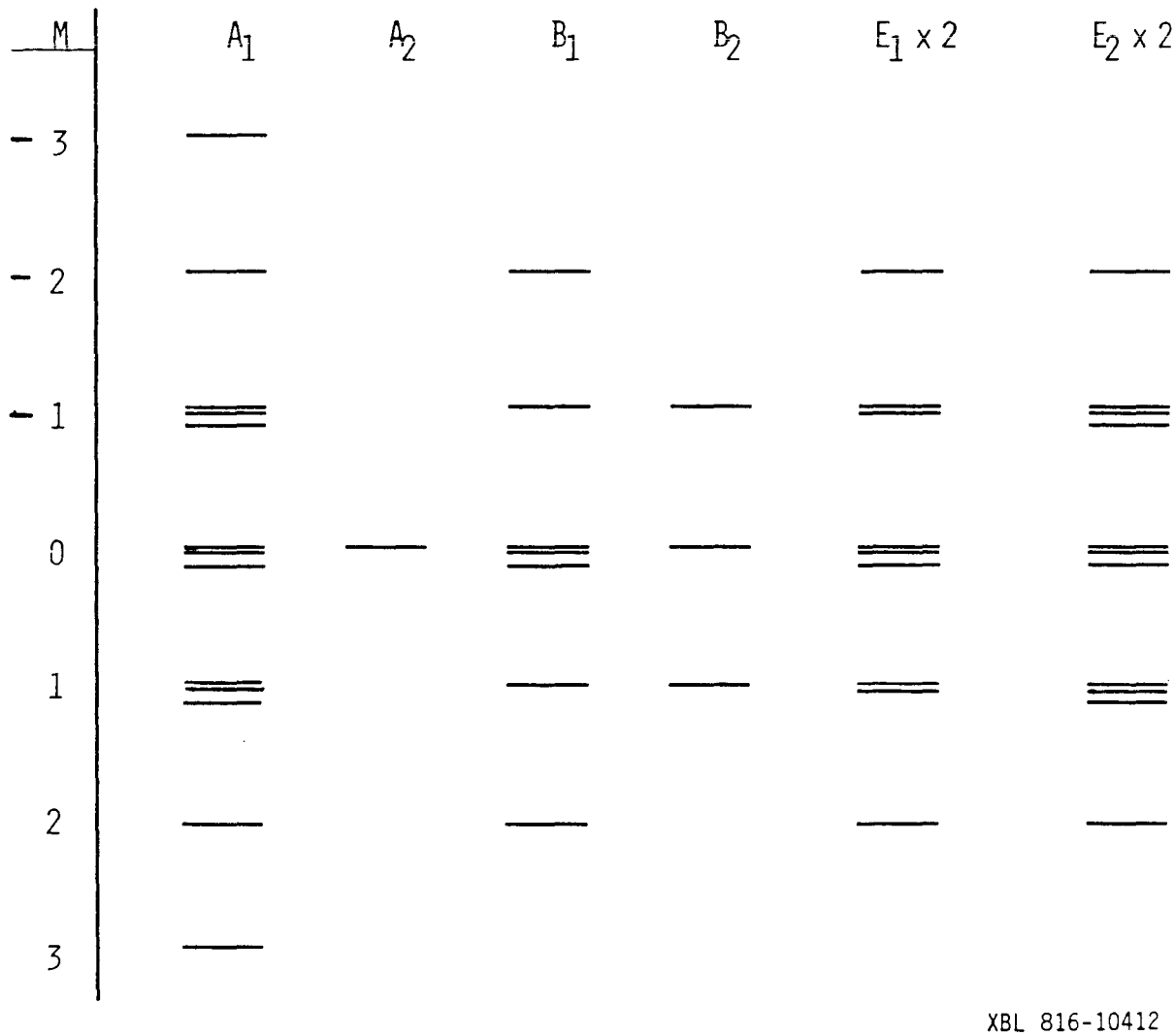

Figure III.2 Energy level diagram of proton spins in oriented benzene. The energy levels are classified into six classes: A_1, A_2, B_1, B_2, E_1, and E_2, where the E_1 and E_2 representations are doubly degenerate.

number of single quantum transitions is fewer and is approximately seventy.

By examining the energy diagram of benzene, we can find three important features of the multiple quantum NMR spectroscopy.

First of all, the number of multiple quantum transitions becomes fewer as the number of quanta Δm increases[6,7]. There is only a six-quantum transition between the state with all the spins up and the state with all the spins down. There are two five-quantum transitions and seven four-quantum transitions. Since the higher multiple quantum spectra have fewer transitions, they are much easier to analyze. We should notice that the highest multiple quantum transition contains no information about the dipole couplings because the associated states are image states and have the same dipolar shift. Generally speaking, the well-resolved multiple quantum NMR spectra provides an easier way to study molecular structure and conformation.

Secondly, since we can observe forbidden transitions (non-single quantum transitions), more information about the couplings between spins becomes available. It allows for a much more complete determination of the molecular structure. Besides, the measurement of the spin-lattice relaxation time and the transverse relaxation time of the multiple quantum transitions provides more information about the dynamics of the system.[8-10]

Thirdly, the zero-quantum transitions among the multiplet within the manifold of the same magnetic quantum number depend on the dipole couplings but not the Larmor frequency. Consequently they

are independent of the external magnetic field and are free of inhomogeneous field broadening.[11]

3.2 Creation of multiple quantum coherence

Multiple quantum coherence is a non-linear process as in the harmonic generation of a non-linear oscillator. The Zeeman coupling between spins and the external field is a linear interaction. Nevertheless, the dipole-dipole interaction and the quadrupole interaction are all bi-linear and contain products of two spin operators. They are responsible for the generation of multiple quantum coherence.

When followed by a single strong pulse the FID S(t) is actually a correlation function of the spin operator I_x or I_y in time,

$$\begin{aligned} S(t) &= \mathrm{Tr}(I_x\, e^{-iHt}\, I_x\, e^{iHt}) \\ &= \mathrm{Tr}(I_x(0)\; I_x(t)) \\ &= \sum_{\alpha,\beta} \exp(-i\omega_{\alpha\beta}t)\,|\langle\alpha|I_x|\beta\rangle|^2 \quad . \end{aligned} \tag{III.1}$$

Since I_x and I_y are linear in raising and lowering oeprators I_+ and I_- that are single quantum operators, the FID S(t) consists of only single quantum coherence.

Evidently, a single pulse can excite only single quantum transition. The simplest way to create a multiple quantum coherence is achieved by employing two strong pulses with an appropriate time interval. This allows the dipole-dipole interaction to mix the phase coherence.

Although there are many possible ways to create multiple quantum coherence, we shall direct our attention to the simplest way of suing two pulses. Following two 90° pulses of x and $\bar{x}$ phases with time interval (Figure III.3), the density matrix in the rotating frame is given by

$$\rho^{x\bar{x}}(\tau) = \exp(-i\tfrac{\pi}{2}I_x)\exp(-iH\tau)\exp(i\tfrac{\pi}{2}I_x)I_z\exp(-i\tfrac{\pi}{2}I_x)\exp(iH\tau)\exp(i\tfrac{\pi}{2}I_x)$$

$$= \exp(-iH_{yy}\tau)\exp(-i\Delta\omega\tau I_y)I_z\exp(i\Delta\omega\tau I_y)\exp(iH_{yy}\tau)$$

$$= \exp(-iH_{yy}\tau)I_z\exp(iH_{yy}\tau)\cos\Delta\omega\tau + \exp(-iH_{yy}\tau)I_x\exp(iH_{yy}\tau)\sin\Delta\omega\tau$$

$$\equiv U_z(\tau)\cos\Delta\omega\tau + U_x(\tau)\sin\Delta\omega\tau \quad , \qquad \text{(III.2)}$$

where $H = -\Delta\omega I_z + H_{zz}$, $H_{zz} = \sum_{i<j} D_{ij}(3I_{iz}I_{jz} - \vec{I}_i\cdot\vec{I}_j)$ is the secular part of the dipole-dipole coupling Hamiltonian, $\Delta\omega$ is the resonance frequency offset, and

$$H_{yy} = \exp(-i\tfrac{\pi}{2}I_x)H_{zz}\exp(i\tfrac{\pi}{2}I_x) = \sum_{i<j} D_{ij}(3I_{iy}I_{jy} - \vec{I}_i\cdot\vec{I}_j) \quad . \qquad \text{(III.3)}$$

Similarly, if the phase of the second pulse is y (Figure III.3) the density matrix becomes

$$\rho^{xy}(\tau) = \exp(-iH_{xx}\tau)I_y\exp(iH_{xx}\tau)\cos\Delta\omega\tau + \exp(-iH_{xx}\tau)I_z\exp(iH_{xx}\tau)\sin\Delta\omega\tau$$

$$\equiv V_y(\tau)\cos\Delta\omega\tau + V_z(\tau)\sin\Delta\omega\tau \qquad \text{(III.4)}$$

where

$$H_{xx} = \sum_{i<j} D_{ij}(3I_{ix}I_{jx} - \vec{I}_i\cdot\vec{I}_j) \quad . \qquad \text{(III.5)}$$

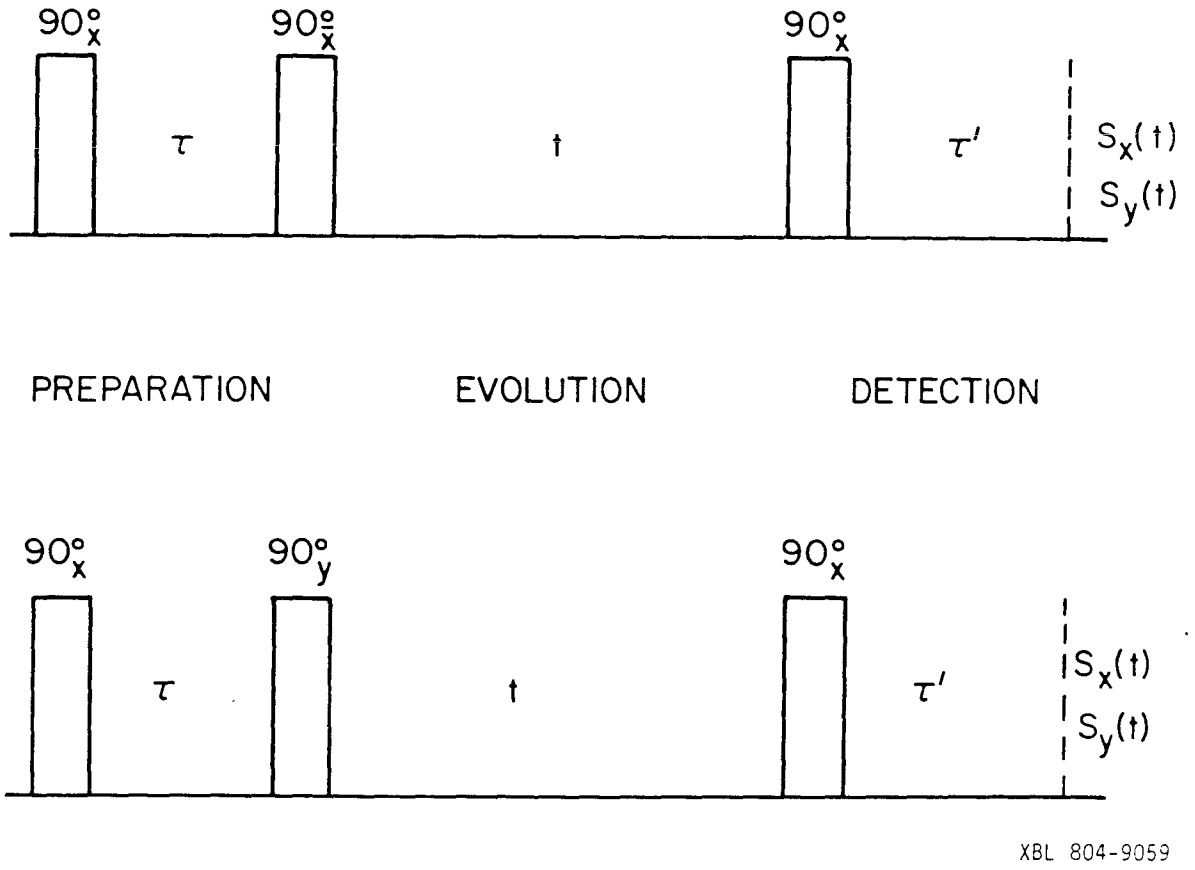

Figure III.3 Pulse sequences for creation and detection of multiple quantum coherence. The first two pulses establish a phase relationship among eigenstates whose magnetic quantum number may differ from unity. In the interval t, each multiple quantum coherence oscillates at its own characteristic frequency. A third pulse is applied at the end of the evolution period to transfer the multiple quantum coherence into detectable single quantum coherence. Signals $S_x(t)$ and $S_y(t)$ are detected by a quadrature detector.

$Exp(\pm iH_{xx}\tau)$ and $exp(\pm iH_{yy}\tau)$ are even-quantum operators that connect eigenstates with a difference in magnetic quantum number by even number of Δm. As a consequence, $U_z(\tau)$ and $V_z(\tau)$ are even-quantum operators. Conversely, $U_x(\tau)$ and $V_y(\tau)$ are odd-quantum operators. As a special case of zero frequency offset, i.e., $\Delta\omega = 0$, $\rho^{x\bar{x}}(\tau)$ and $\rho^{xy}(\tau)$ contain only even-quantum and odd-quantum coherences. Even in the presence of an inhomogeneous field, we can apply a π pulse (Hahn-echo pulse) in the middle of the preparation period to eliminate the frequency offset (Figure III.4). Consequently, by simply arranging the phase of the pulses, we may be able to selectively create even-quantum or odd-quantum coherences (Figure III.4). Imperfection in the selectivity may be caused by a deviation in the flipping angle from $\pi/2$ in the pulses.

3.3 Examples of spin-1 and spin-3/2 particles

Our approach in the previous section can also be applied to a isolated particle system with spin $I \geq 1$ because of the similarity in the transformation by rotation between the quadrupole Hamiltonian and dipole-dipole interaction Hamiltonian. Specifically, the density matrices $\rho^{x\bar{x}}(\tau)$ and $\rho^{xy}(\tau)$ are calculated in terms of the fictitious multiple quantum transition operators.

(1) $I = 1$, $H_Q = \omega_Q (3 I_z^2 - I(I+1))/3$

The energy level diagram is shown in Figure III.5a. It consists of three states $|m = -1\rangle$, $|m = 0\rangle$, and $|m = 1\rangle$. They are denoted by $|1\rangle$, $|2\rangle$, and $|3\rangle$ in sequence. Only two single quantum transitions are allowed. The splitting is caused by quadrupole

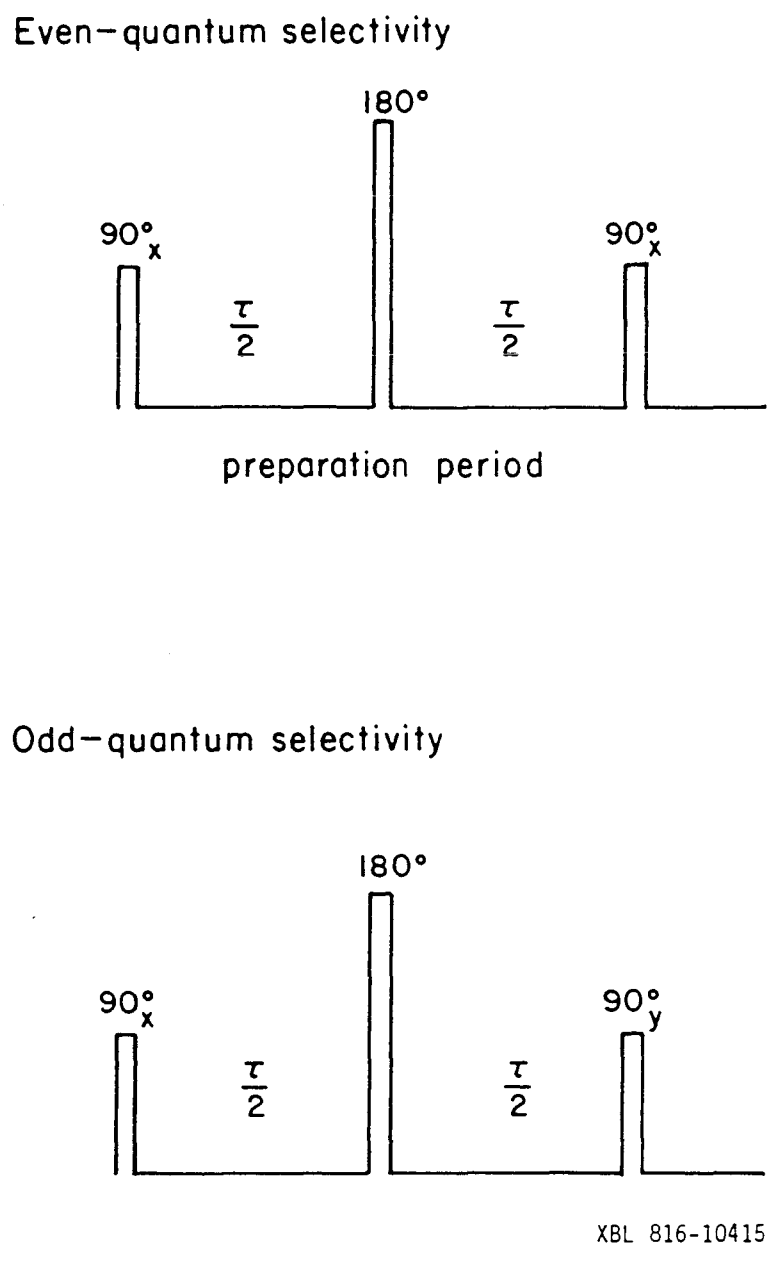

Figure III.4 Pulse sequence for selective excitation of even-quantum and odd-quantum coherence. The phase of the 180° pulse is arbitrary.

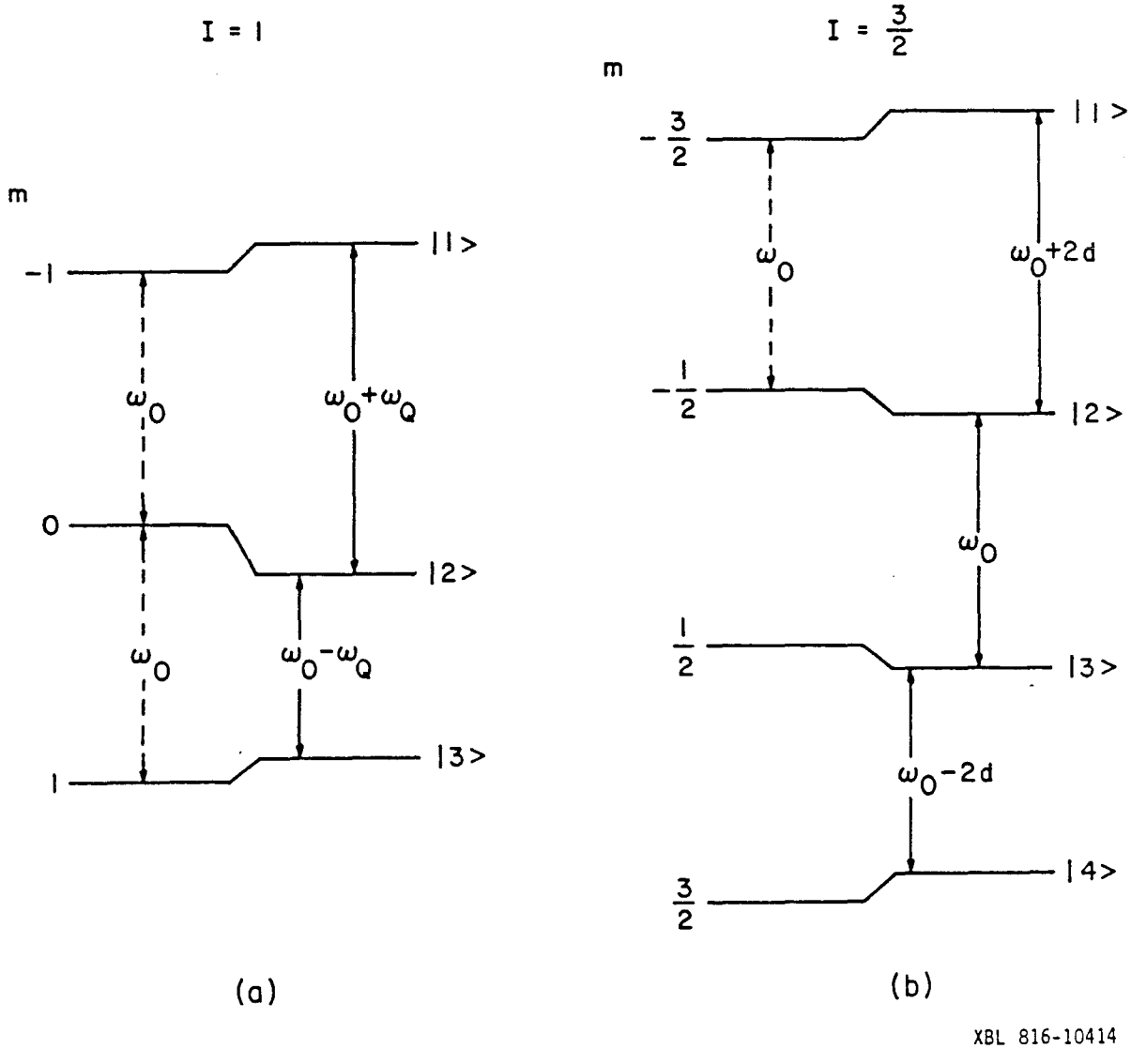

Figure III.5 Energy level diagrams of spin-1 and spin-3/2 particles. The Zeeman levels are shifted by the quadrupole interaction.

interaction. We may observe that the double quantum transition between $|1>$ and $|3>$ contains no information about the quadrupole strength. It is free of quadrupole anisotropy in the polycrystalline or glassy state. As a consequence, we may obtain a high resolution double quantum spectrum of deuterons in solids. Thus,information about chemical shift can be obtained.

After the second 90° pulse of $\bar{x}$ and y phases the density matrices are given by

$$\rho^{x\bar{x}}(\tau) = 2\cos\Delta\omega\tau\{I_z^{13}\cos\omega_Q\tau - I_y^{13}\sin\omega_Q\tau\} + \sqrt{2}\sin\Delta\omega\tau\{(I_x^{12}+I_x^{23})\cos\omega_Q\tau + (I_y^{12}-I_y^{23})\sin\omega_Q\tau\}, \quad \text{(III.6)}$$

$$\rho^{xy}(\tau) = 2\sin\Delta\omega\tau\{I_z^{13}\cos\omega_Q\tau + I_y^{13}\sin\omega_Q\tau\} + \sqrt{2}\cos\Delta\omega\tau\{(I_y^{12}+I_y^{23})\cos\omega_Q\tau - (I_x^{12}-I_x^{23})\sin\omega_Q\tau\}. \quad \text{(III.7)}$$

The multiple quantum transition operators are defined in equation (II.26). The operator I_y^{13} describes the double quantum coherence between states $|1>$ and $|3>$. Its intensity depends on the pumping period τ. If we assume the condition of perfect field homogeneity and exactly on resonance, or using a Hahn-echo pulse as described earlier, the density matrices $\rho^{x\bar{x}}(\tau)$ and $\rho^{xy}(\tau)$ have pure even-quantum and odd-quantum coherence. The above result also applies to the general dipole-coupled spin system.

(2) $I = 3/2$, $H_Q = d(3I_z^2 - I(I+1))/3$

The energy level diagram is shown in Figure III.5b. It

consists of a quartet $|m=-3/2\rangle$, $|m=-1/2\rangle$, $|m=1/2\rangle$, $|m=3/2\rangle$. They are denoted by $|1\rangle$, $|2\rangle$, $|3\rangle$, and $|4\rangle$ in sequence. There are three single quantum, two double quantum, and only one triple quantum transitions. Again, the highest order of multiple quantum transition--the triple quantum transition--has a transition frequency independent of the quadrupole strength.

The density matrices after the second 90° pulse are given by

$$\begin{aligned}\rho^{x\bar{x}}(\tau) = \cos\Delta\omega\tau\{&I_z\cos^2 d\tau - 2I_z^{23}\sin^2 d\tau + 2\sqrt{3}(I_y^{13}+I_y^{24})\sin d\tau\cos d\tau \\ &+ \sqrt{3}(I_x^{13}-I_x^{24})\sin^2 d\tau\} \\ + \sin\Delta\omega\tau\{&\sqrt{3}(I_x^{12}+I_x^{34})\cos^2 d\tau - 2\sqrt{3}(I_y^{12}-I_y^{34})\sin d\tau\cos d\tau \\ &+ I_x^{23}(3\cos^2 d\tau-1) - 3I_x^{14}\sin^2 d\tau\} \quad , \qquad \text{(III.8)}\end{aligned}$$

$$\begin{aligned}\rho^{xy}(\tau) = \sin\Delta\omega\tau\{&I_z\cos^2 d\tau - 2I_z^{23}\sin^2 d\tau - 2\sqrt{3}(I_y^{13}+I_y^{24})\sin d\tau\cos d\tau \\ &- \sqrt{3}(I_x^{13}-I_x^{24})\sin^2 d\tau\} \\ + \cos\Delta\omega\tau\{&\sqrt{3}(I_y^{12}+I_y^{34})\cos^2 d\tau + 2\sqrt{3}(I_x^{12}-I_x^{34})\sin d\tau\cos d\tau \\ &+ I_y^{23}(3\cos^2 d\tau-1) - 3\,I_y^{14}\sin^2 d\tau\} \quad . \qquad \text{(III.9)}\end{aligned}$$

The transition operators I_x^{13}, I_y^{13}, I_x^{24}, and I_y^{24} are double-quantum operators, whereas I_x^{14} and I_y^{14} are triple quantum operators. The allowed multiple quantum spectrum contains three single quantum, two double quantum, and one triple quantum transitions.

The dipole-dipole coupling Hamiltonian of some molecules that contain only I = 1/2 spins may look like a quadrupole interaction Hamiltonian. For example, the eigenstates of methyl group contain

one quartet of A symmetry and two doublets of E symmetry.[10] The subsystem of A-symmetry quartet behaves similar to a particle of I = 3/2; the other two doublets behave similar to particles of I = 1/2. A second example of this is the system of an isolated pair of spin 1/2 particles. The eigenstates consist of a triplet and a singlet. The triplet behaves similar to a particle of I = 1 and the singlet behaves similar to a scalar particle without spin. A third example is the system of tetrahedral group. It contains one quintet, three triplets, and two singlets as quasiparticles of spin I = 2, 1 and 0. The density matrices illustrated for spins I = 1 and 3/2 are applicable to those quasiparticle of triplet and quartet. The calculation of the density matrix for scalar particle and spin 1/2 particle is trivial and will not be discussed.

3.4 Detection of multiple quantum coherence

The multiple quantum coherence created in the preparation period oscillate at their own characteristic frequencies in the evolution period (Figure III.3) as shown in equation (II.31), and

$$I_x^{\alpha\beta}(t) = I_x^{\alpha\beta} \cos\omega_{\alpha\beta}t - I_y^{\alpha\beta}\sin\omega_{\alpha\beta}t \quad ,$$

$$I_y^{\alpha\beta}(t) = I_y^{\alpha\beta} \cos\omega_{\alpha\beta}t + I_x^{\alpha\beta}\sin\omega_{\alpha\beta}t \quad ,$$

$$I_z^{\alpha\beta}(t) = I_z^{\alpha\beta} \quad , \qquad \text{(III.10)}$$

where $\omega_{\alpha\beta}$ is the transition frequency between states $|\alpha>$ and $|\beta>$, i.e.,

$$\omega_{\alpha\beta} = -(m_\alpha - m_\beta)\Delta\omega + D_\alpha - D_\beta \quad .$$

D_α and D_β are eigenvalues of the Hamiltonian H_{zz} on states $|\alpha>$ and $|\beta>$. The offset term in above equation indicates that the n-quantum transition has a frequency offset of $n\Delta\omega$.[6]

Since the multiple quantum coherence cannot be detected directly, a monitoring $\pi/2$ pulse is usually applied at the end of the evolution period. This transfers the multiple quantum coherence into an observable single quantum coherence that is detected at time τ' after the monitoring pulse is shown in Figure III.3.

Using the quadrature detection, signals are detected in x and y channels such as $S_x(t)$ and $S_y(t)$. They are evaluated for both pulse sequences in Figure III.3 as follows,

1) $90^\circ_x - \tau - (90^\circ_{\bar{x}}) - t - 90^\circ_x - \tau'$

$$S_x(t) = \sum_{\alpha,\beta} \rho^{x\bar{x}}_{\alpha\beta}(\tau)\ \rho^{\bar{y}\bar{x}}_{\beta\alpha}(-\tau')\ \exp(-i\omega_{\alpha\beta}t) \quad ,$$

$$S_y(t) = \sum_{\alpha,\beta} \rho^{x\bar{x}}_{\alpha\beta}(\tau)\ \rho^{x\bar{x}}_{\beta\alpha}(-\tau')\ \exp(-i\omega_{\alpha\beta}t) \quad , \qquad \text{(III.11)}$$

2) $90^\circ_x - \tau - (90^\circ_y) - t - 90^\circ_x - \tau'$

$$S_x(t) = \sum_{\alpha,\beta} \rho^{xy}_{\alpha\beta}(\tau)\ \rho^{\bar{y}\bar{x}}_{\beta\alpha}(-\tau')\ \exp(-i\omega_{\alpha\beta}t) \quad ,$$

$$S_y(t) = \sum_{\alpha,\beta} \rho^{xy}_{\alpha\beta}(\tau)\ \rho^{x\bar{x}}_{\beta\alpha}(-\tau')\ \exp(-i\omega_{\alpha\beta}t) \quad , \qquad \text{(III.12)}$$

where $\rho^{x\bar{x}}_{\alpha\beta}$, $\rho^{xy}_{\alpha\beta}$ are elements of the density matrices in the equations (III.8) and (III.9), and

$$\rho^{\bar{y}\bar{x}}_{\alpha\beta}(-\tau') = U_x(-\tau')\cos\Delta\omega\tau' + U_z(-\tau')\sin\Delta\omega\tau' \quad . \qquad \text{(III.13)}$$

Multiple quantum spectrum can be obtained by Fourier transformation of $S_x(t)$ and $S_y(t)$ on variable t. Each order of multiple quantum

spectrum can be made in separate domains because the n-quantum transitions have a frequency that offset $n\Delta\omega$.[5] The higher order of multiple quantum transition, however, may be broadened substantially in the presence of an inhomogeneous field. A technique that uses a π pulse in the middle of the evolution period and also uses a phase increment in the first two pulses to create an artificial frequency offset, can remove the inhomogeneous broadening; meanwhile it preserves the ordering of each n-quantum transitions[7] as is shown in Figure III.6.

The phase change ϕ of the first two 90° pulses in the preparation period is equivalent to the rotation of the density matrix by angling about z axis. It is given explicitly by

$$\rho_{\phi}^{x\bar{x}}(\tau) = \exp(-i\phi I_z)\, U_z(\tau)\, \exp(i\phi I_z)\, \cos\Delta\omega\tau + \exp(-i\phi I_z)\, U_x(\tau)\, \exp(i\phi I_z)\, \sin\Delta\omega\tau \quad , \qquad \text{(III.14)}$$

where $U_z(\tau)$ and $U_x(\tau)$ are defined in equation (III.2). In deriving the above result, the following relation is used:

$$\exp(-i\,\frac{\pi}{2}(I_x\cos\phi + I_y\sin\phi)) = \exp(-i\phi I_z)\, \exp(-i\,\frac{\pi}{2}\, I_x)\, \exp(i\phi I_z) \quad .$$

The rotation of the operators $U_z(\tau)$, $U_x(\tau)$ about z axis by angle $\Delta\phi$ changes the phase of the multiple quantum operators in proportion to its order m; that is, the m-quantum operator has a phase change by $m\Delta\phi$ as shown in equation (II.32). This important property allows us to selectively monitor and pump a particular order of coherence.

Furthermore, it is used in the TPPI method to create a fictitious frequency offset $\Delta\omega = \Delta\phi/\Delta t$, where Δt is the inverse

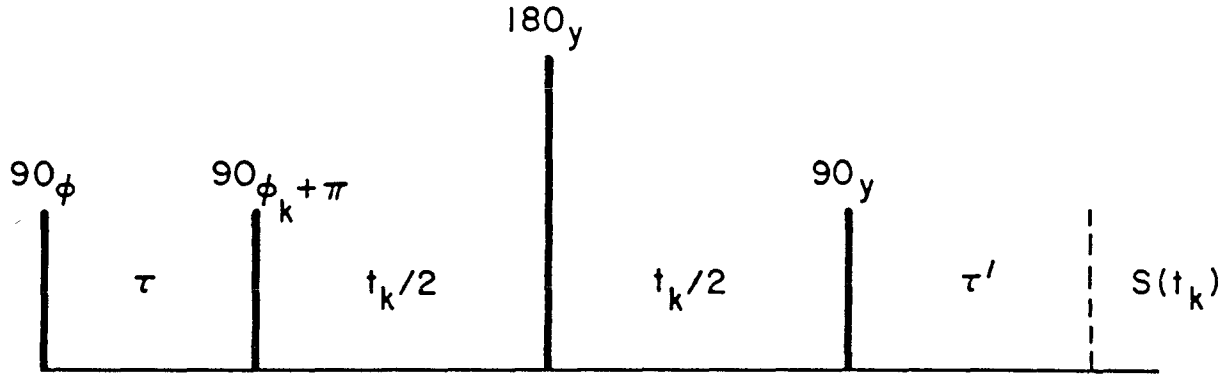

$\phi_k = k\Delta\phi$ $\quad k = 0, 1, \ldots, N-1$

$t_k = k\Delta t$ $\quad N$ = number of FID

$\Delta\omega = \Delta\phi/\Delta t$ (Fictitious frequency offset)

XBL 816-10416

Figure III.6 Time Proportional Phase Incrementation (TPPI) pulse sequence. The phases of the first two pulses are increased in proportion to the time interval in the evolution period.

of the sampling rate in the evolution period. The selective detection of a particular order n of a multiple quantum coherence can be obtained by summing up n multiple quantum FID's with a different phase shift $\phi_k = 2\ k/n$, k = 0, 1, ..., n-1 as shown in Figure III.7. Actually, besides the n-quantum spectrum, the other harmonics, such as 0, 2n, 3n, etc., are also selected out. In the above discussion, we did not take the relaxation process into account. Practically, τ and τ' should be made shorter than T_2 and be of order of the inverse of the dipolar or quadrupole strength.

Since the intensity for each multiple quantum transition is individually dependent on the preparation and detection periods, an ensemble average of the magnitude spectra is usually taken for the different values of τ and τ'.

3.5 Experimental spectra of oriented benzene

Small molecules dissolved in an anisotropic solvent such as liquid crystal at the nematic phase have characteristics of high resolution NMR. Usually, the transition has a linewidth of approximately a few hertz to a few ten hertz .

Several molecules have been studied by multiple quantum NMR techniques.[6,12-13] We, however, shall illustrate the prototype experiments on partially oriented benzene in particular.[6] We have chosen to examine the benzene molecule because of its simple structure, high degree of symmetry, and reasonable number of spins. The schematic energy level diagram is shown in Figure III.2. The energy levels are classified into several irreducible representations of the symmetry group D_{6h}. There are six different classes A_1, A_2,

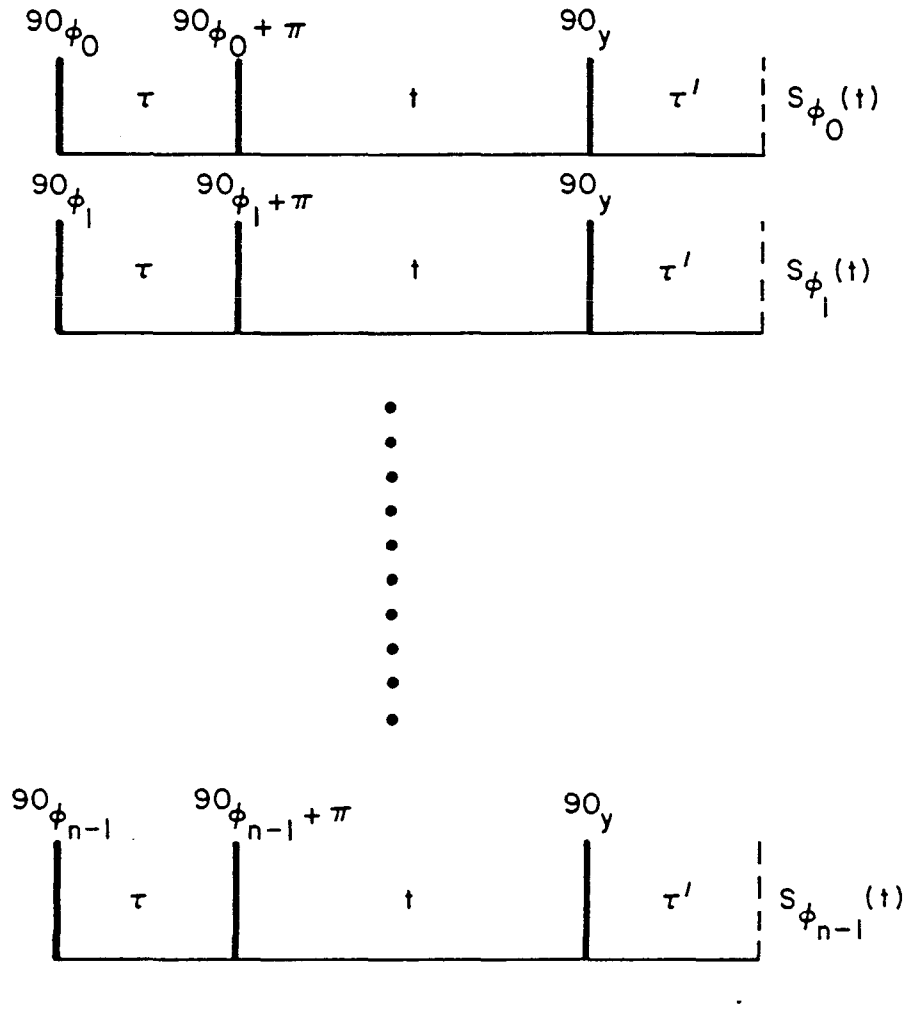

$$S_{total}(t) = \sum_{k=0}^{n-1} S_{\phi_k}(t)$$

XBL 816-10417

Figure III.7 Pulse sequences to selectively monitor a particular order of multiple quantum spectra. Many FID's with different phase shifts $\phi_k = 2\pi k/n$, k = 0, 1, ..., n-1 are added.

B_1, B_2, E_1, and E_2, where states of E_1 and E_2 representations are doubly degenerate.

The ensemble-averaged magnitude spectra of multiple quantum transitions are shown in Figure III.8. The timer intervals τ_1 and τ_2 were set equal for several values between 9.6 msec and 10.7 msec. The r.f. frequency are set at 5.97 kHz off resonance so that each order of the multiple quantum spectra is well separated by the frequency offset. The multiple quantum transitions of a higher order have a larger linewidth because of the field inhomogeneity. During experimentation, we found that the linewidth is linearly proportional to the number of quanta, that is, the six-quantum transition has a linewidth six times larger than that of single quantum transitions. Also, since they are independent of field inhomogeneity the zero-quantum transitions have a very narrow linewidth of only a few hertz. The spectral lines seen in the figure are substantially broadened because of the FID truncation.

Using the TPPI method, the field inhomogeneity in the spectrum can be removed, and meanwhile retain the separation of the order.

The multiple quantum spectra of benzene obtained by the TPPI method are shown in Figure III.9. Several magnitude spectra have been averaged for different τ (or τ').

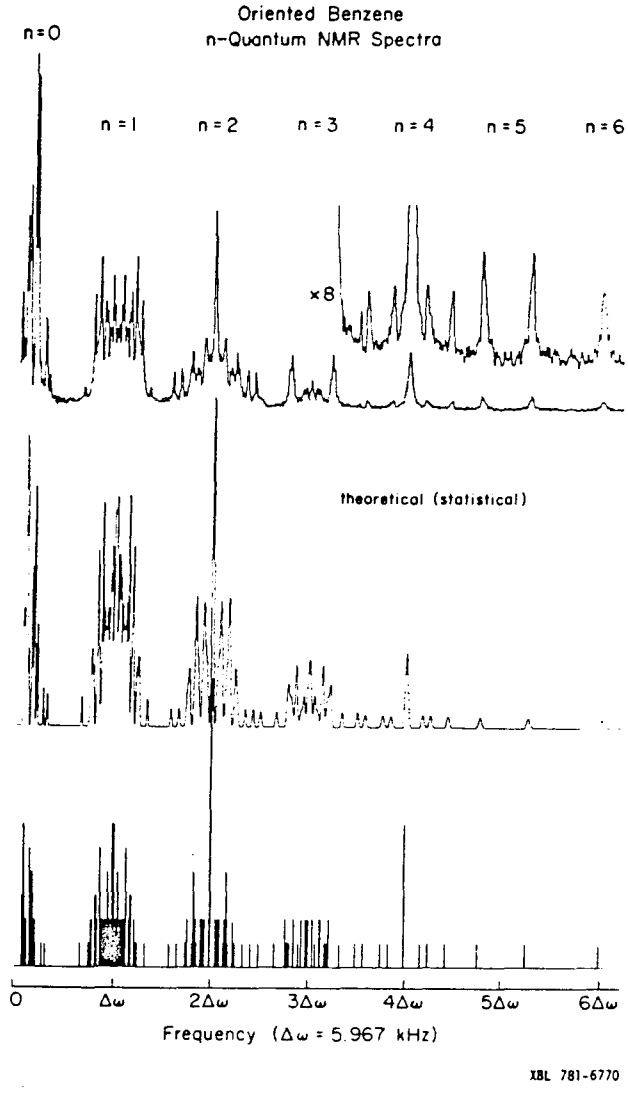

Figure III.8 Experimental and theoretical multiple quantum spectrum of benzene with a three pulse sequence. The broadening of the transitions in the top figure is caused by field inhomogeneity.

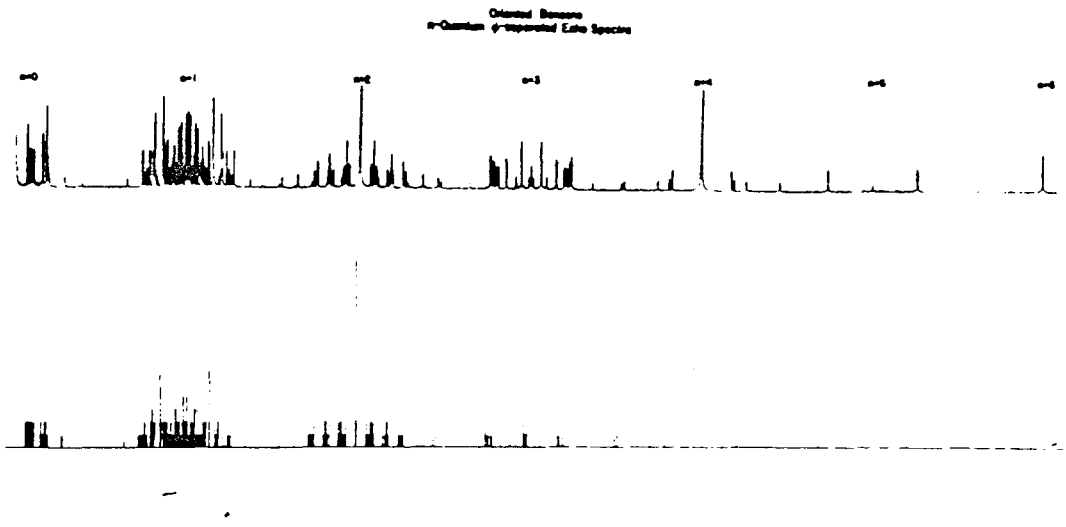

Figure III.9 Experimental and theoretical multiple quantum spectra of benzene using the TPPI pulse sequence. The inhomogeneous line-broadening was removed by a π pulse in the middle of the evolution period. The artificial frequency offset is created by phase cycling.

3.6 References

1. J. A. Pople, W. G. Schneider, and H. J. Bernstein, High-Resolution Nuclear Magnetic Resonance (McGraw-Hill, New York, 1959).
2. T. C. Farrar and E. D. Becker, Pulse and Fourier Transform NMR (Academic Press, New York, 1971).
3. Reference 1, Chapter 6.
4. J. W. Emsley and L. C. Lindon, NMR Spectroscopy Using Liquid Crystal Solvents, Chapter 3 (Pergamon, Oxford, 1975).
5. M. Tinkham, Group Theory and Quantum Mechanics, Chapter 7 (McGraw-Hill, New York, 1964).
6. A. Pines, D. Wemmer, J. Tang, and S. Sinton, Bull. Am. Phys. Soc. 23, 21 (1978).
7. G. Drobny, A. Pines, S. Sinton, D. Weitekamp, and D. Wemmer, Faraday Div. of the Chem. Soc. Symposium 13, 49 (1979).
8. A. Wokaun and R. R. Ernst, Mol. Phys. 36, 317 (1978).
9. R. Poupko, R. L. Vold, and R. R. Vold, J. Magn. Reson. 34, 67 (1979).
10. J. Tank and A. Pines, J. Chem. Phys. 72, 3290 (1980).
11. A. Wokaun and R. R. Ernst, Chem. Phys. Lett. 52, 407 (1977).
12. J. Tang and A. Pines, J. Chem. Phys. 73, 2512 (1980).
13. S. Sinton and A. Pines, Chem. Phys. Lett. 76, 263 (1980).

IV

RELAXATION OF MULTIPLE QUANTUM COHERENCE AND APPLICATIONS

4.1 Redfield's relaxation theory

The first phenomenological description of time evolution for the spin system was proposed by Bloch, and is known as the Bloch equation,[1]

$$\frac{d}{dt}\vec{M} = \gamma\vec{M} \times \vec{B} - (M_x\vec{i} + M_y\vec{j})/T_2 - (M_z - M_o)\vec{k}/T_1 \quad . \tag{IV.1}$$

This equation of motion describes the evolution of magnetization $\vec{M}$ in a strong magnetic field $\vec{B}$. The transverse magnetizations M_x and M_y decay at a rate of $1/T_2$, and the longitudinal magnetization M_z recovers back to its thermal equilibrium value M_o at a rate of $1/T_1$. The Block equation fails to describe a general coupled spin system. An accurate general approach using the density matrix formalism is contained in Redfield's studies.[2,3]

The Hamiltonian of a general system is composed of two parts, a static part H_0 and a small fluctuating part $H_1(t)$,

$$H = H_0 + H_1(t) \quad . \tag{IV.2}$$

The time-dependent term $H_1(t)$ describes the random fluctuation of the coupling between the spin system and the bath (or the lattice). The fluctuation is an irreversible process which relaxes the non-equilibrium distribution of population and the coherence among spin states back to thermal equilibrium.

The equation of motion of the density matrix ρ for the system is given by

$$\frac{d}{dt}\rho = \frac{1}{i}[H_0 + H_1(t),\rho] \quad . \tag{IV.3}$$

In the interaction representation with

$$\rho^* = \exp(iH_0t)\rho\ \exp(-iH_0t) \tag{IV.4}$$

and

$$H_1^* = \exp(iH_0t)\ H_1(t)\ \exp(-iH_0t) \tag{IV.5}$$

the equation of motion becomes

$$\frac{d}{dt}\rho^* = \frac{1}{i}[H_1^*(t),\rho^*] \quad . \tag{IV.6}$$

To the first order approximation, it can be shown

$$\rho^*(t) \simeq \rho^*(0) + \int_0^t [H_1^*(t'),\rho^*(0)]dt' \quad . \tag{IV.7}$$

By substituting the density matrix ρ^* inside the commutator of the equation (IV.6) and by using the above approximated form, we obtain

$$\frac{d}{dt}\rho^* = -i[H_1^*(t),\rho^*(0)] - \int_0^t dt'[H_1^*(t),\ [H_1^*(t'),\rho^*(0)]]; \tag{IV.8}$$

or, by introducing a new variable $\tau = t-t'$

$$\frac{d}{dt}\ ^* = -i[H_1^*(t),\rho^*(0)] - \int_0^t d\tau\ [H_1^*(t),\ [H_1^*(t-\tau),\rho^*(0)]] \ . \tag{IV.9}$$

We shall take an ensemble average of the above equation and replace $\rho^*(0)$ by $\rho^*(t)$. It can always be assumed that $\overline{H_1(t)} = 0$.

If the average is different from zero, it can be included into the unperturbed Hamiltonian. In the case of a finite lattice temperature, we must replace ρ^* by $\rho^*-\rho_0$ where ρ_0 is the density matrix at the thermal equilibrium,

$$\rho_0 = \exp(-\beta H_0)/\mathrm{Tr}\,[\exp(-\beta H_0)] \quad , \quad \beta = 1/kT \tag{IV.10}$$

The master equation of motion becomes[3,4]

$$\frac{d}{dt}\rho = \frac{1}{i}[H_0,\rho] - \int_0^\infty d\tau\, \overline{[e^{-iH_0\tau} H_1(t+\tau)\, e^{iH_0\tau}, [H_1(t),\rho-\rho_0]]} \quad , \tag{IV.11}$$

or

$$\frac{d}{dt}\rho_{\alpha,\beta} = -i\omega_{\alpha\beta}\,\rho_{\alpha\beta} - \sum_{\alpha',\beta'} \exp(i(\omega_{\alpha\beta}-\omega_{\alpha'\beta'})t) R_{\alpha\beta,\alpha'\beta'} \cdot (\rho_{\alpha'\beta'}-\delta_{\alpha'\beta'}\rho_{0,\alpha'\alpha'}) \quad . \tag{IV.12}$$

The relaxation matrix element $R_{\alpha\beta,\alpha'\beta'}$ is related to the spectral densities of fluctuation by

$$R_{\alpha\beta,\alpha'\beta'} = \frac{1}{2\hbar^2}[-J_{\alpha\alpha',\beta\beta'}(\omega_{\alpha'\beta'}) - J_{\alpha\alpha',\beta\beta'}(\omega_{\alpha\beta}) + \delta_{\alpha\alpha'}\sum_\gamma J_{\gamma\beta,\gamma\beta'}(\omega_{\beta\gamma}) + \delta_{\beta\beta'}\sum_\gamma J_{\gamma\alpha',\gamma\alpha}(\omega_{\gamma\alpha})] \quad , \tag{IV.13}$$

where the spectral densities is defined by

$$J_{\alpha\beta,\alpha'\beta'} = \int_{-\infty}^{\infty} d\tau \exp(-i\omega\tau)\, \overline{\langle\alpha|H_1(t)|\beta\rangle\langle\beta'|H_1(t+\tau)|\alpha\rangle} \quad . \tag{IV.14}$$

If no other resonance frequencies of the system overlap the transition $\omega_{\alpha\beta}$, i.e.,

$$|\omega_{\alpha\beta}-\omega_{\alpha'\beta'}| >> R_{\alpha\beta,\alpha'\beta'} \quad , \tag{IV.15}$$

the rapidly oscillating function $\exp[i(\omega_{\alpha\beta}-\omega_{\alpha'\beta'})t]$ can be neglected. The equation of motion for the off-diagonal element $\rho_{\alpha\beta}$ that describes the phase coherence between states $|\alpha>$ and $|\beta>$ is given by

$$\frac{d}{dt}\rho_{\alpha\beta} = -i\,\omega_{\alpha\beta}\,\rho_{\alpha\beta}(t) + R_{\alpha\beta,\alpha\beta}\,\rho_{\alpha\beta}(t) \quad . \tag{IV.16}$$

Here $\omega_{\alpha\beta}$ is the transition frequency between states $|\alpha>$ and $|\beta>$. The transition is characterized by a single exponential decay rate $R_{\alpha\beta,\alpha\beta}$.

If another transition frequency $\omega_{\alpha'\beta'}$ overlaps the transition $\omega_{\alpha\beta}$, namely,

$$|\omega_{\alpha\beta}-\omega_{\alpha'\beta'}| >> R_{\alpha\beta,\alpha'\beta'} \quad , \tag{IV.17}$$

the equation of motion for $\rho_{\alpha\beta}$ is coupled to $\rho_{\alpha'\beta'}$, and

$$\begin{cases} \frac{d}{dt}\rho_{\alpha\beta} = (-i\omega_{\alpha\beta}-R_{\alpha\beta,\alpha\beta})\,\rho_{\alpha\beta}-R_{\alpha\beta,\alpha'\beta'}\,\rho_{\alpha'\beta'} \\ \frac{d}{dt}\rho_{\alpha'\beta'} = (-i\omega_{\alpha'\beta'}-R_{\alpha'\beta',\alpha'\beta'})\,\rho_{\alpha'\beta'}-R_{\alpha'\beta',\alpha\beta}\,\rho_{\alpha\beta} \end{cases} \quad . \tag{IV.18}$$

By solving the secular equation, the complex eigenvalues correspond to the new transition frequencies and decay rates.

The equation of motion for the diagonal elements describes the spin-lattice relaxation and is given by

$$\frac{d}{dt}\rho_{\alpha\alpha} = -\sum_{\beta} R_{\alpha\alpha,\beta\beta}(\rho_{\beta\beta}-\rho_{0,\beta\beta}) \quad . \tag{IV.19}$$

Following a perturbation, relaxation of the populations towards their equilibrium values is governed by a set of coupled differential equations. Often, the spin-lattice relaxation is characterized by several exponents.

We shall focus in this chapter on the transverse relaxation of the multiple quantum coherence. The decay rate for a non-degenerate transition between states $|\alpha\rangle$ and $|\beta\rangle$ is given by[3,5]

$$\Gamma_{\alpha\beta} = R_{\alpha\beta,\alpha\beta} = \frac{1}{2\hbar^2}\left[-2\, J_{\alpha\alpha,\beta\beta}(0) + \sum_{\gamma} J_{\gamma\alpha,\gamma\alpha}(\omega_{\gamma\alpha}) + \sum_{\gamma} J_{\gamma\beta,\gamma\beta}(\omega_{\gamma\beta})\right]$$

$$= \Gamma^{(0)}_{\alpha\beta} + \Gamma'_{\alpha\beta} \quad , \tag{IV.20}$$

where

$$\Gamma^{(0)}_{\alpha\beta} = \frac{1}{2\hbar^2}\left[J_{\alpha\alpha,\alpha\alpha}(0) + J_{\beta\beta,\beta\beta}(0) - 2\, J_{\alpha\alpha,\beta\beta}(0)\right] \quad , \tag{IV.21}$$

and

$$\Gamma'_{\alpha\beta} = \frac{1}{2\hbar^2}\left[\sum_{\gamma\neq\alpha} J_{\gamma\alpha,\gamma\alpha}(\omega_{\gamma\alpha}) + \sum_{\gamma\neq\beta} J_{\gamma\beta,\gamma\beta}(\omega_{\gamma\beta})\right] \quad . \tag{IV.22}$$

The first term is referred to as the adiabatic term--a special characteristic of transverse relaxation. It does not contribute to the longitudinal relaxation. It can also be expressed as[5]

$$\Gamma^{(0)}_{\alpha\beta} = \frac{1}{2\hbar^2} \int_{-\infty}^{\infty} d\tau \, \overline{[\langle\alpha|H_1(t)|\alpha\rangle - \langle\beta|H_1(t)|\beta\rangle]} \cdot \overline{[\langle\alpha|H_1(t-\tau)|\alpha\rangle - \langle\beta|H_1(t-\tau)|\beta\rangle]} \quad . \tag{IV.23}$$

The adiabatic relaxation involves the process that conserves the Zeeman energy. It depends exclusively on the fluctuation of the energy difference between the two states $|\alpha\rangle$ and $|\beta\rangle$; it is also known as the elastic process (Figure IV.1).

The second term (nonadiabatic term) is related to the lifetimes t_α and t_β as states $|\alpha\rangle$ and $|\beta\rangle$ through[5,6]

$$\Gamma'_{\alpha\beta} = \frac{1}{2}\left(\frac{1}{t_\alpha} + \frac{1}{t_\beta}\right) \quad , \tag{IV.24}$$

where

$$\frac{1}{t_\alpha} = \frac{1}{\hbar^2} \int_{-\infty}^{\infty} d\tau \sum_{\gamma\neq\beta} \overline{\langle\alpha|H_1(t)|\gamma\rangle\langle\gamma|H_1(t-\tau)|\alpha\rangle} \exp\langle i\omega_{\alpha\gamma}\tau\rangle \quad ,$$

$$\frac{1}{t_\beta} = \frac{1}{\hbar^2} \int_{-\infty}^{\infty} d\tau \sum_{\gamma\neq\beta} \overline{\langle\beta|H_1(t)|\gamma\rangle\langle\gamma|H_1(t-\tau)|\beta\rangle} \exp\langle i\omega_{\beta\gamma}\tau\rangle \quad . \tag{IV.25}$$

The nonadiabatic term contributes to the linewidth of the finite lifetime of states $|\alpha\rangle$ and $|\beta\rangle$ caused by the longitudinal relaxation mechanisms. Because the nonadiabatic process involves changing Zeeman energy, they are also known as inelastic process (Figure IV.1).

The nonadiabatic relaxation is dominant when the fluctuation rate is close to the Larmor frequency or its higher harmonics. Adiabatic relaxation, however, is dominant for a low fluctuation rate. In the extremely short correlation time when $\omega_0^2\tau_c^2 >> 1$, both

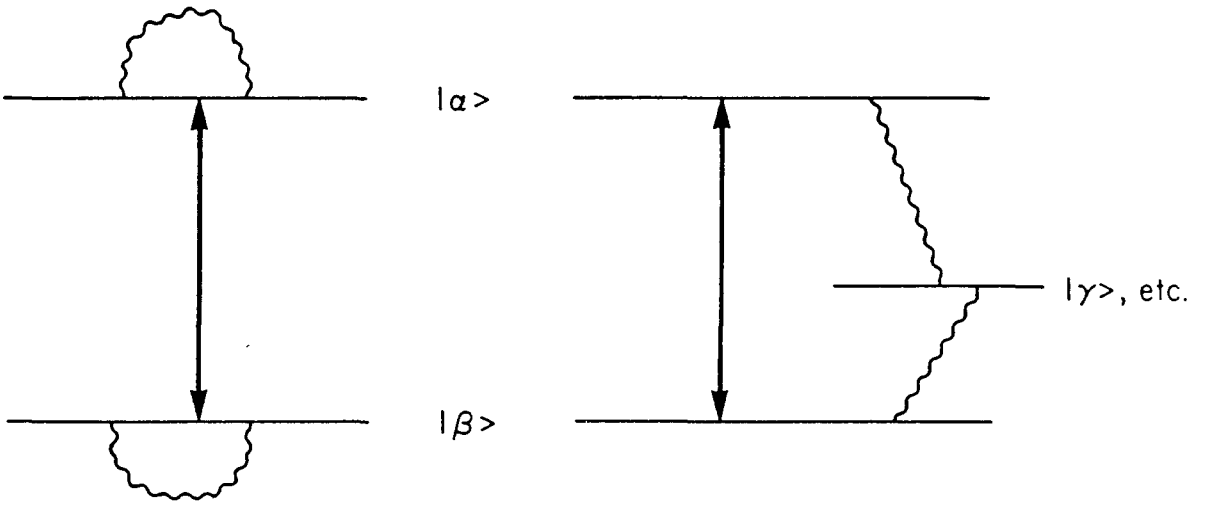

Figure IV.1 Transverse relaxation channels for the transition between states $|\alpha\rangle$ and $|\beta\rangle$. The broadening of a transition comes from two sources--the adiabatic broadening (elastic process) and lifetime broadening (inelastic process).

relaxation processes are comparable, and T_1, T_2 are of the same order of magnitude.

It can be shown that the relaxation matrix elements obey the following identities:[7]

$$R_{\alpha\beta,\alpha'\beta'} = R_{\alpha\beta,\alpha'\beta'} = R_{\alpha'\beta',\alpha\beta}$$

$$R_{\alpha\alpha,\alpha\alpha} = -\sum_{\gamma\neq\alpha} R_{\alpha\alpha\,\gamma\gamma} \quad (\text{or } \sum_{\gamma} R_{\alpha\alpha,\gamma\gamma} = 0)$$

$$R_{\alpha\beta,\alpha'\beta'} = R_{\Lambda\alpha\Lambda\beta,\Lambda\alpha'\beta'} \qquad \text{(IV.26)}$$

where Λ is the spin inversion operator. The nonadiabatic term of relaxation rate elements follows a triangular relation

$$\Gamma'_{\alpha\beta} \leq \Gamma'_{\alpha\gamma} + \Gamma'_{\gamma\beta} \quad . \qquad \text{(IV.27)}$$

Their value can be calculated from the conventionally selective T_1 measurement. There are, however, no similar properties for the adiabatic term of the relaxation rate element. The value of spectral densities for the adiabatic relaxation process can be determined from the multiple quantum relaxation; a complete determination of the relaxation matrix R becomes possible by using multiple quantum techniques.

The time-dependent Hamiltonian $H_1(t)$ can generally be classified into two categories. The part which is bilinear in the spin operators represents the intradipolar interaction or quadrupolar interaction. The part linear in the spin operators consists of an anisotropic Zeeman interaction, and a dipolar or scalar interaction with magnetic dipoles outside the considered system.

The paramagnetic molecules of external impurities has unpaired electron spin, and acts as a strong relaxation agent. The gyromagnetic ratio of electron spin is 658 times larger than the proton spin. Since the relaxation rate is proportional to the square of the electron gyromagnetic ratio, the relaxation of electron spins is very effective with even a small amount of impurities.

The dipole-dipole interaction between the electron spin and the proton spin is given by[6]

$$H_1(t) = \frac{\hbar^2 \gamma_I \gamma_S}{r^3} [\vec{I}\cdot\vec{S} - 3(\vec{I}\cdot\hat{r})(\vec{S}\cdot\hat{r})]$$

$$= K \sum_{m=-1}^{1} (-1)^m V^{(m)} f^{(-m)}(t) \qquad \text{(IV.28)}$$

where

$$V^{(0)} = I_z \ , \ V^{(1)} = -\frac{1}{\sqrt{2}} I_+ \ , \ V^{(-1)} = \frac{1}{\sqrt{2}} I_- \ , \qquad \text{(IV.29)}$$

and

$$K = \hbar^2 \gamma_I \gamma_S / r^3 \ .$$

The random fluctuation functions $f^{(m)}(t)$ are given by[6]

$$f^{(0)}(t) = F_0(t)\, S_z(t) + F_1(t)\, S_+(t) + F_{-1}(t)\, S_-(t) \ ,$$

$$f^{(1)}(t) = \sqrt{2}\, (-\frac{1}{4} F_0(t)\, S_-(t) + F_1(t)\, S_z(t) + F_2(t)\, S_+(t)) \ ,$$

$$f^{(-1)}(t) = -\,(f^{(1)}(t))^+ \ ,$$

$$f^{(m)}(t-\tau) = \exp(iH_0\tau)\, f^{(m)}(t)\, \exp(-iH_0\tau) \ . \qquad \text{(IV.30)}$$

Here the spherical harmonic functions of the second rank $F_m(t)$ are defined as

$$F_0 = 1-3\cos^2\theta \quad ,$$

$$F_1 = -\frac{3}{2}\sin\cos\theta e^{i\phi} \quad ,$$

$$F_2 = -\frac{3}{4}\sin^2\theta\, e^{2i\phi} \quad ,$$

$$F_{-m} = F_m^* \quad . \qquad \text{(IV.31)}$$

Using the definition of the correlation function in the frequency domain given by

$$G^{(m)}(m\omega_I) = \frac{1}{2}\int_{-\infty}^{\infty} d\tau\ (-1)^m\ \overline{f^{(-m)}(t)\, f^{(m)}(t-\tau)}\ \exp(-im\omega_I\tau) \quad , \qquad \text{(IV.32)}$$

we obtain[6]

$$G^{(0)}(0) = \frac{1}{5}K^2\tau_c + \frac{3}{10}K^2\tau_c\ \frac{1}{1+\omega_s^2\tau_c^2} \quad ,$$

$$G^{(1)}(\omega_I) = G^{(-1)}(\omega_I) = \frac{3}{20}\ K^2\tau_c\ \frac{1}{1+\omega_I^2\tau_c^2} + \frac{7}{20}K^2\tau_c\ \frac{1}{1+\omega_s^2\tau_c^2} \quad .$$

(IV.33)

Without losing generality, the dipole-dipole interaction between the protons of the measured system and the unpaired electron can be treated as a random local field.[6,8] It can be expressed as

$$H_1(t) = -\hbar\gamma_I \sum_i \vec{I}_i\cdot\vec{B}_i(t) = \sum_{m=0,\pm1}\ \sum_i (-1)^m\, V_i^{(m)}\, f_i^{(-m)}(t), \qquad \text{(IV.34)}$$

where $\vec{B}_i$ is the local field at the i-th proton site due to the electron spin, and

$$\vec{B}_i = \frac{\hbar\gamma_s}{\gamma_i^3}\left[3\hat{\gamma}_i(\vec{S}\cdot\hat{\gamma}_i) - \vec{S}\right] \quad , \tag{IV.35}$$

where $\hat{\gamma}_i$ is the unit vector of $\hat{\gamma}_i$.

4.2 Relaxation of Weakly Coupled System

In the case of a weakly coupled spin system, the magnetic quantum m of individual spin is a good quantum number. Any eigenstate is a direct product of states for each individual spin.

The longitudinal relaxation or the non-adiabatic relaxation is completely determined from the life-time of states,[8]

$$\frac{1}{t_\alpha} = \frac{1}{\hbar^2}\int_{-\infty}^{\infty} d\tau \sum_{\gamma\neq\alpha} \overline{\langle\alpha|H_1(t)|\gamma\rangle\langle\gamma|H_1(t-\tau)|\alpha\rangle}\ \exp(i\omega_{\alpha\gamma}\tau)$$

$$= \frac{1}{\hbar^2}\int_{-\infty}^{\infty} d\tau \sum_{\gamma\neq\alpha} \exp(i\omega_{\alpha\gamma}\tau) \sum_{p,q}\sum_{i,j} \hbar^2\gamma_I^2\ \overline{B_{p,i}(t)\ B_{q,j}(t-\tau)}$$

$$\cdot\ \langle\alpha|I_{p,i}|\gamma\rangle\langle\gamma|I_{q,j}|\alpha\rangle$$

$$= \frac{1}{\hbar^2}\int_{-\infty}^{\infty} d\tau \sum_{\gamma\neq\alpha} \exp(i\omega_{\alpha\gamma}\tau) \sum_{p,i} \hbar^2\gamma_I^2\ \overline{B_{p,i}(t)\ B_{p,i}(t-\tau)}$$

$$\cdot\ |\langle\alpha|I_{p,i}|\gamma\rangle|^2 \quad . \tag{IV.36}$$

Since only the autocorrelation function, $\overline{B_{p,i}(t)\ B_{p,i}(t-\tau)}$, of

the random field $\vec{B}_p$ at nucleus p enters the above equation, no information on cross-correlation is available from the measurements of longitudinal relaxation rates.

The adiabatic relaxation rate is given by[8]

$$\Gamma^{(0)}_{\alpha\beta} = \frac{\gamma_I^2}{2} \sum_{p,q} (m_{\alpha,p} - m_{\beta,p})(m_{\alpha,q} - m_{\beta,q}) \int_{-\infty}^{\infty} \overline{B_{p,z}(t)\, B_{q,z}(t-\tau)}\, d\tau \qquad \text{(IV.37)}$$

where $m_{\alpha,p}$ is the magnetic quantum number of nucleus p in the state $|\alpha\rangle$.

For an allowed single quantum transition, characterized by a flip of spin s, the only non-vanishing contribution to $\Gamma^{(0)}_{\alpha\beta}$ is that of p = q = s, that is,

$$\Gamma^{(0)}_{\alpha\beta} = \frac{1}{2}\gamma_I^2 \int_{-\infty}^{\infty} d\tau\ \overline{B_{s,z}(t)\, B_{s,z}(t-\tau)} \quad . \qquad \text{(VI.38)}$$

Consequently, information on cross-correlation cannot be obtained from the adiabatic linewidth of the allowed transitions.

Nevertheless, the adiabatic linewidth of multiple quantum and forbidden single quantum transitions depends on the cross-correlation of fluctuating local fields between various sites. That valuable information on cross-correlation can only be obtained from multiple quantum relaxation measurements.

4.3 Relaxation of Strongly Coupled System

For a strongly coupled system, the magnetic quantum number for

each individual spin is no longer a good quantum number. The strong couplings mix the product of spin states. Usually, observable single quantum transitions simultaneously flip polarizations of several spins. Therefore, both longitudinal and transverse relaxation of allowed single quantum transitions are influenced by internuclear correlated fluctuation. Without a doubt, the multiple quantum relaxation measurements provide more independent information on relaxation mechanism.[6,8-11]

We shall discuss in the following sections two systems of dipole-coupled spins that are released by paramagnetic electron spins. In both systems, the strong dipole-dipole interaction mixes the spin states. The linewidth measurements of the multiple quantum transitions allow a complete determination of the auto and cross-correlated fluctuations.[6]

4.4 Multiple quantum NMR and relaxation of an oriented CH_3 group

4.4.1 Introduction

We have been interested in the multiple quantum NMR of strongly dipolar coupled spin-1/2 nuclei in oriented systems (solids and liquid crystals). These illustrate the behavior of systems with high symmetry--for example a CH_3 group or benzene. Normally, radiofrequency irradiation only can induce the transitions between eigenstates that belong to the same irreducible representations of the spin Hamiltonian. Relaxation by fluctuating random fields may, however, induce symmetry-breaking transitions. The study of n-quantum spectra and their relaxation should allow a complete determination of the fluctuations, correlations, and symmetry-breaking pathways.[6] This provides a useful tool in combination

with the elegant selective excitation and normal mode relaxation techniques in 1-quantum spectroscopy that Werbelow and Grant[12] described. In the following sections we shall present an initial study of the dipolar coupled 3-proton system (CH_3 group) which is relaxed by paramagnetic impurities. The 1-, 2-, and 3-quantum linewidths were studied over a wide concentration range, and the accurate linewidth ratios allowed us to determine that the fluctuations are correlated and are a measurement of the correlation times.[6]

Section 4.4.2 describes the n-quantum spectra of a dipolar coupled CH_3 group, and Section 4.4.3 provides a concise theory of n-quantum relaxation for this symmetry group. Experimental results and discussion are presented in Section 4.4.4.

4.4.2 Multiple quantum spectra of methyl group

The NMR spectrum of an oriented solute in a liquid crystal is generally dominated by dipolar structure. It is caused by the incomplete motional averaging-out of the intramolecular dipolar interactions. The methyl protons of acetonitrile, for example, have a C_3 symmetry with the symmetry axis perpendicular to the proton plane. The eigenstates can be classified by their symmetry characteristics; they contain one quartet and two doublets.[13] The observable multiple quantum transitions connect the states of the same irreducible representation. The energy diagram and the possible multiple quantum transitions are shown in Figure IV.2. The eigenstates are given by:

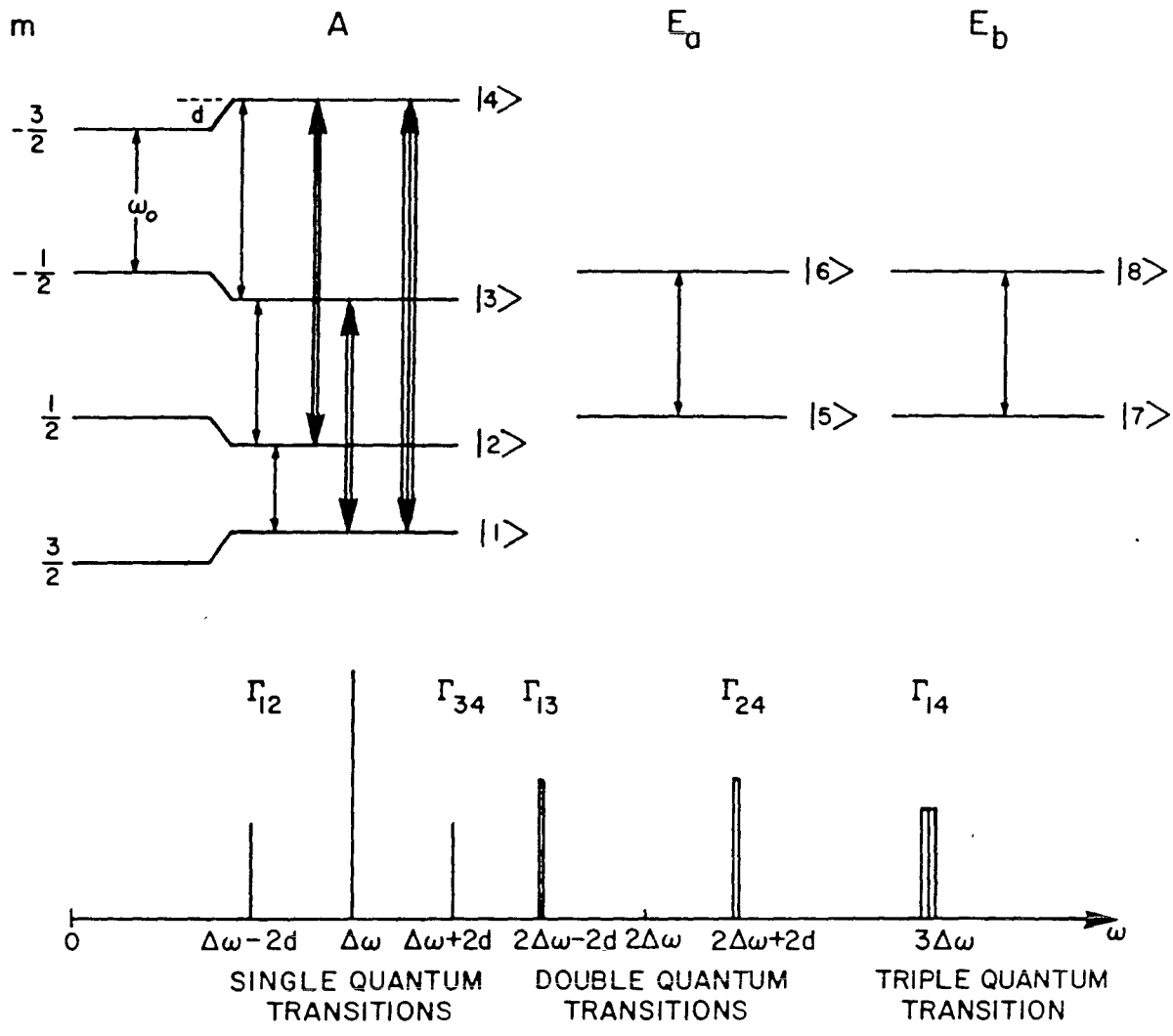

XBL 796-10115

Figure IV.2 Energy level diagram of dipolar-coupled methyl protons in a magnetic field. $\Delta\omega$ is the frequency offset in the rotating frame and d is the dipolar shift. The lower half shows a stick spectrum of the multiple quantum transitions. The associated relaxation rates Γ_{ij} are related to their linewidths.

$$|1\rangle = |A_{3/2}\rangle = |\uparrow\uparrow\uparrow\rangle$$

$$|2\rangle = |A_{1/2}\rangle = \frac{1}{\sqrt{3}}(|\downarrow\uparrow\uparrow\rangle + |\uparrow\downarrow\uparrow\rangle + |\uparrow\uparrow\downarrow\rangle)$$

$$|3\rangle = |A_{-1/2}\rangle = \frac{1}{\sqrt{3}}(|\uparrow\downarrow\downarrow\rangle + |\downarrow\uparrow\downarrow\rangle + |\downarrow\downarrow\uparrow\rangle)$$

$$|4\rangle = |A_{-3/2}\rangle = |\downarrow\downarrow\downarrow\rangle$$

$$|5\rangle = |E^{a}_{1/2}\rangle = \frac{1}{\sqrt{3}}(|\uparrow\uparrow\downarrow\rangle + \varepsilon|\uparrow\downarrow\uparrow\rangle + \varepsilon^{*}|\downarrow\uparrow\uparrow\rangle)$$

$$|6\rangle = |E^{a}_{-1/2}\rangle = \frac{1}{\sqrt{3}}(|\downarrow\downarrow\uparrow\rangle + \varepsilon|\downarrow\uparrow\downarrow\rangle + \varepsilon^{*}|\uparrow\downarrow\downarrow\rangle)$$

$$|7\rangle = |E^{b}_{1/2}\rangle = \frac{1}{\sqrt{3}}(|\uparrow\uparrow\downarrow\rangle + \varepsilon^{*}|\uparrow\downarrow\uparrow\rangle + \varepsilon|\downarrow\uparrow\uparrow\rangle)$$

$$|8\rangle = |E^{b}_{-1/2}\rangle = \frac{1}{\sqrt{3}}(|\downarrow\downarrow\uparrow\rangle + \varepsilon^{*}|\downarrow\uparrow\downarrow\rangle + \varepsilon|\uparrow\downarrow\downarrow\rangle) \qquad \text{(IV.39)}$$

where $\varepsilon = \exp(i2\pi/3)$.

The frequencies of the allowed multiple quantum transitions in the rotating frame (resonance offset $\Delta\omega$) are listed in Table 4.1.

The method used to observe the multiple quantum spectra is the TPPI method previously described in Reference 14. In this method, the frequency offset $\Delta\omega$ is created artificially by phase increments. A theoretical stick spectrum is shown in Figure IV.2. The intensity of each transition depends on the length of the preparation and mixing periods of the multiple pulse sequence, dipolar coupling strength, and real frequency offset.

The experimental spectrum shown in Figure IV.3 exhibits the expected multiple quantum transitions. They are all separated according to order. Truncation of the multiple quantum free induction decay limits the resolution. The actual linewidth is less than 5 Hz.

Table 4.1

Allowed Multiple Quantum Transitions

Transition Origin	Frequency	M
$A_{1/2}-A_{3/2}$	$\Delta\omega-2d$	$\Delta M=1$
$A_{-1/2}-A_{1/2}$	$\Delta\omega$	single quantum transition
$A_{-3/2}-A_{-1/2}$	$\Delta\omega+2d$	
$E^a_{-1/2}-E^a_{1/2}$	$\Delta\omega$	
$E^b_{-1/2}-E^b_{1/2}$	$\Delta\omega$	
$A_{-1/2}-A_{3/2}$	$2\Delta\omega-2d$	$\Delta M=2$
$A_{-3/2}-A_{1/2}$	$2\Delta\omega+2d$	double quantum transition
$A_{-3/2}-A_{3/2}$	$3\Delta\omega$	$\Delta M=3$ triple quantum transition

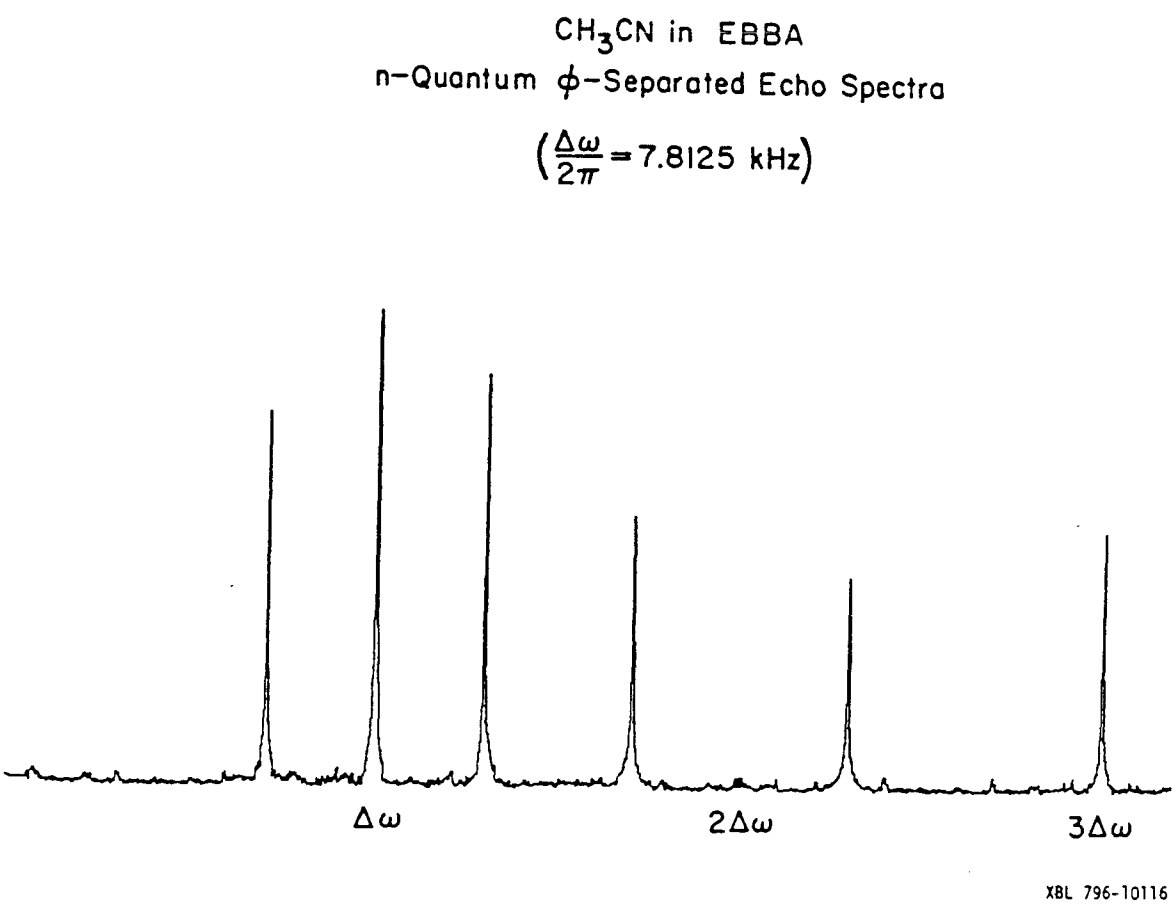

Figure IV.3 Multiple quantum spectrum of oriented methyl protons. It consists of three single quantum transitions, two double quantum transitions, and one triple quantum transition. Truncation of the multiple quantum free induction decay limits the resolution. Inhomogeneous broadening was removed by echoes in the TPPI sequence.

4.4.3 Relaxation by paramagnetic impurity

The effect of the NMR line broadening by the addition of small quantities of paramagnetic species to a sample was first observed by Bloch and others.[15] This effect was interpreted as a fluctuating electron-nuclear dipole-dipole interaction.[16] Even at small concentrations, this mechanism can be more important than intra- and inter-nuclear dipolar interactions because the magnetic moment of an unpaired electron is of the order of 10^3 times larger than the moment of a nucleus. We predict that the relaxation rate should be proportional to the concentration of the paramagnetic impurity and the square of the effective magnetic moment of the electron on the impurity.[16]

The dipole-dipole interaction between the unpaired electron and the methyl protons is given by

$$H_1(t) = \sum_{i=1,2,3} \hbar^2 \gamma_I \gamma_S \left(\frac{\vec{I}_i \cdot \vec{S}}{r_i^3} - 3 \frac{(\vec{I}_i \cdot \vec{r}_i)(\vec{S} \cdot \vec{r}_i)}{r_i^5} \right) \qquad \text{(IV.40)}$$

where γ_I and γ_S are the gyromagnetic ratios of the proton and electron. The vector $\vec{r}_i$ defines the position of the proton as shown in Figure IV.4. If the concentration is low, it is legitimate to expand the above expression in δ/r. Using symmetry-adapted operators, we obtain[17]

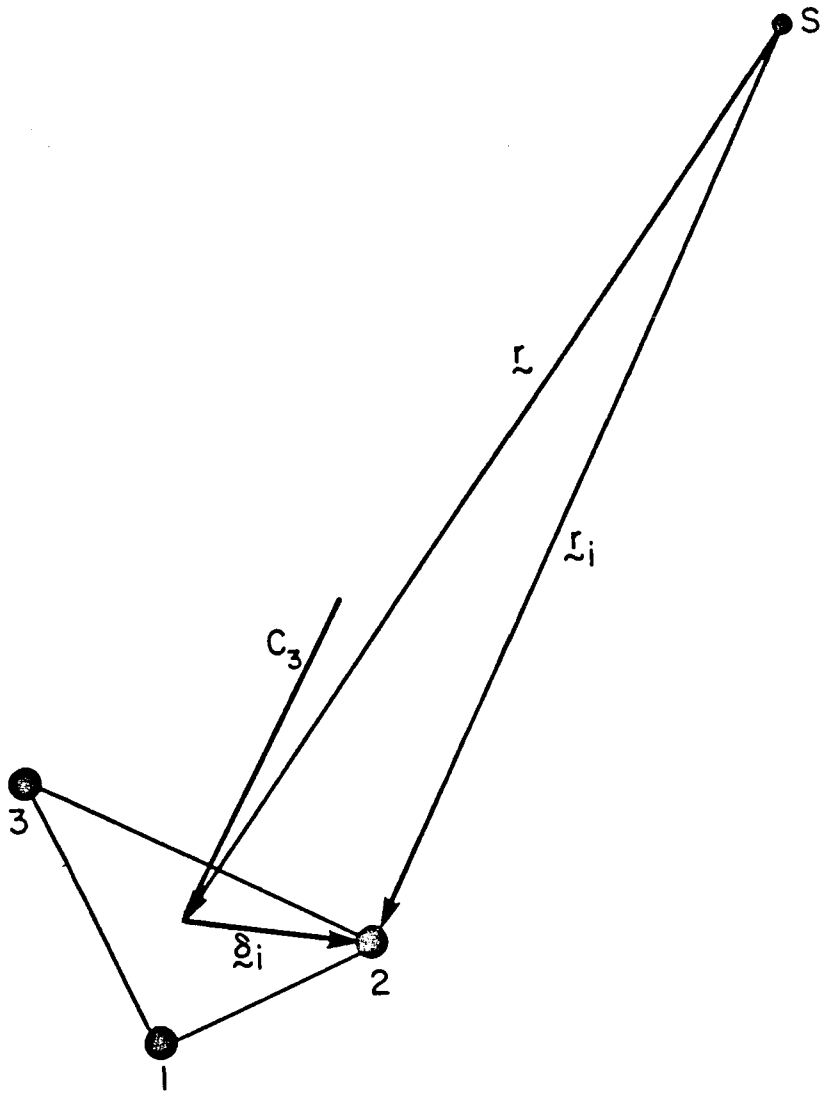

XBL 796-10117

Figure IV.4 Geometry of interacting methyl group and electron. $\vec{r}_i$ is the vector from the electron of the paramagnetic impurity to one of the methyl protons. The vector $\vec{r}$ defines the center position of the methyl protons triangle with respect to the electron. $\vec{\delta}$ is the vector from the center of the triangle to one of the protons.

$$H_1(t) = \sqrt{3}\hbar^2 \gamma_I\gamma_S \left(\frac{\vec{I}_A\cdot\vec{S}}{r^3} - \frac{3(\vec{I}_A\cdot\vec{r})(\vec{S}\cdot\vec{r})}{r^5} \right)$$

$$- \frac{3\hbar^2\gamma_I\gamma_S}{r^5} \sum_{\mu=E^a,E^b} [(\vec{I}_\mu\cdot\vec{\sigma}_{-\mu})(\vec{S}\cdot\vec{r}) + (\vec{I}_\mu\cdot\vec{r})(\vec{S}\cdot\sigma_{-\mu})$$

$$+ (\vec{I}_\mu\cdot\vec{S})(\vec{r}\cdot\vec{\sigma}_{-\mu})]$$

$$+ \frac{15\hbar^2\gamma_I\gamma_S}{r^7} \sum_{\mu=E^a,E^b} (\vec{I}_\mu\cdot\vec{r})(\vec{S}\cdot\vec{r})(\vec{r}\cdot\vec{\sigma}_{-\mu}) \qquad \text{(VI.41)}$$

where

$$\vec{I}_\mu = \frac{1}{\sqrt{3}} (\vec{I}_1 + \lambda\,\vec{I}_2 + \lambda^*\,\vec{I}_3),\ \frac{\vec{\delta}}{\mu} = \frac{1}{\sqrt{3}} (\vec{\delta}_1 + \lambda^*\,\vec{\delta}_2 + \lambda\,\vec{\delta}_3)$$

$$\mu = A,\ E^a \text{ or } E^b \text{ for } \lambda = 1,\ \varepsilon \text{ or } \varepsilon^* \quad . \qquad \text{(IV.42)}$$

The first term in the above equation contains only A symmetry operators and connects states of the same irreducible representation of the C_3 symmetry group. The second and third terms containing E^a and E^b symmetry operators, will violate the symmetry, and cause symmetry-breaking relaxation pathways.

Without loss of generality, the dipole-dipole interaction between the methyl protons and the unpaired electron can be expressed as a product of tensor operators.[18,19]

$$H_1(t) = -\hbar\gamma_I \sum_{i=1,2,3} \vec{I}_i \vec{B}_i(t) = \sum_{\substack{m=0,\pm1 \\ i=1,2,3}} (-1)^m V_i^{(m)} f_1^{(-m)}(t)$$

$$= \sum_{\substack{m=0,\pm1 \\ \mu=A,E^a,E^b}} (-1)^m V_\mu^{(m)} f_{\bar{\mu}}^{(m)}(t) \qquad \text{(IV.43)}$$

where

$$V_i^{(0)} = I_{i,z}, V_i^{(1)} = -\frac{1}{\sqrt{2}}(V_{i,x} + iV_{i,y}) \text{ and } V_i^{(-1)} = \frac{1}{\sqrt{2}}(V_{i,x} - iV_{i,y}) \quad .$$

(IV.44)

The symmetry-adapted form $V_\mu^{(m)}$ is related to $V_i^{(m)}$ by the same transformation as we used in equation (IV.11). The fluctuating local field $\vec{B}_i(t)$ experienced by the proton spin $\vec{I}_i$, is produced by the unpaired electron.

Two kinds of correlation functions are involved in our discussion. These are the auto-correlation functions $G_a(\tau)$ and the cross-correlation function $G_c(\tau)$ which are given by

$$(-1)^m \overline{f_i^{(-m)}(t)\, f_1^{(n)}(t-\tau)} = \delta_{mn} G_a^{(m)}(\tau) \quad , \qquad \text{(IV.45)}$$

$$(-1)^m \overline{f_i^{(-m)}\, f_j^{(n)}(t-\tau)} = \delta_{mn}\, G_c^{(m)}(\tau) \quad \text{for } i \neq j \ . \qquad \text{(IV.46)}$$

We can express the correlation function in terms of the molecule's symmetry by

$$(-1)^m \overline{f_\mu^{(-m)}(t)\, f_{\mu'}^{(n)}(t-\tau)} = \delta_{mn}\, \delta_{\mu\mu'}\, G_\mu^{(m)}(\tau) \quad . \qquad \text{(IV.47)}$$

It can be shown that the symmetry-adapted correlation function is closely related to both the auto-correlation function and the cross-correlation function by

$$G_\mu^{(m)}(\tau) = \begin{cases} G_a^{(m)}(\tau) + 2\, G_c^{(m)}(\tau) & \text{if } \mu = A \\ G_a^{(m)}(\tau) - G_c^{(m)}(\tau) & \text{if } \mu = E^a, E^b . \end{cases} \qquad \text{(IV.48)}$$

The transitions between states $(A_{1/2}, A_{-1/2})$, $(E^a_{1/2}, E^a_{-1/2})$, and $(E^b_{1/2}, E^b_{-1/2})$ have the same frequency. The decay of the coherence for these degenerate transitions is generally non-exponential and complicated. The decay rates for the non-degenerate multiple quantum transitions are evaluated and given as follows:

$$\left.\begin{aligned} \hbar^2\Gamma_{14} &= \tfrac{3}{2} J_A^{(0)} + \tfrac{1}{2} J_A^{(1)} + J_{E^a}^{(1)} \quad , \\ \hbar^2\Gamma_{13} = \hbar^2\Gamma_{24} &= \tfrac{2}{3} J_A^{(0)} + \tfrac{5}{6} J_A^{(1)} + \tfrac{1}{3} J_{E^a}^{(0)} + \tfrac{2}{3} J_{E^a}^{(1)} \quad , \\ \hbar^2\Gamma_{12} = \hbar^2\Gamma_{34} &= \tfrac{1}{6} J_A^{(0)} + \tfrac{5}{6} J_A^{(1)} + \tfrac{1}{3} J_{E^a}^{(0)} + \tfrac{2}{3} J_{E^a}^{(1)} \quad . \end{aligned}\right\} \qquad \text{(IV.49)}$$

The spectral densities are related to Fourier transformations of correlation functions by

$$\left.\begin{aligned} J_A^{(0)} &= 2\, G_a^{(0)}(0)\ (1+2\xi) \quad , \\ J_A^{(1)} &= 2\, G_a^{(1)}(\omega_I)\ (1+2\xi) \quad , \\ J_E{}^{a(0)} &= J_E{}^{b(0)} = 2\, G_a^{(0)}(0)(1-\xi) \quad , \\ J_E{}^{a(1)} &= J_E{}^{b(1)} = 2\, G_a^{(1)}(\omega_I)(1-\xi) \quad , \end{aligned}\right\} \qquad \text{(IV.50)}$$

where

$$\xi = G_c^{(0)}/G_a^{(0)} = G_c^{(1)}/Ga^{(1)} \quad , \qquad \text{(IV.51)}$$

and ω_I is the Lamor frequency of the proton. The asymmetry parameter (or correlation parameter) ξ is a measure of the extent of the symmetry-breaking relaxation (Figure IV.5).

(1) Completely correlated fluctuation, $\xi = 1$.

In this case each proton in the methyl group experiences the same field produced by the unpaired electron. It implies that the auto-correlation function and cross-correlation function be equal, namely, $\xi = 1$. We readily obtain

$$\left.\begin{aligned} G_A^{(m)}(\tau) &= 3\, G_a^{(m)}(\tau) \quad , \\ G_E{}^{a(m)}(\tau) &= G_E{}^{b(m)}(\tau) = 0 \quad , \end{aligned}\right\} \qquad \text{(IV.52)}$$

The allowed relaxation channels are those transitions that conserve symmetry.

(2) Completely uncorrelated fluctuation, $\xi = 0$.

In this case each proton spin is relaxed independently by the electron. The inter-symmetry-crossing relaxation is allowed and the cross-correlation function vanishes; namely,

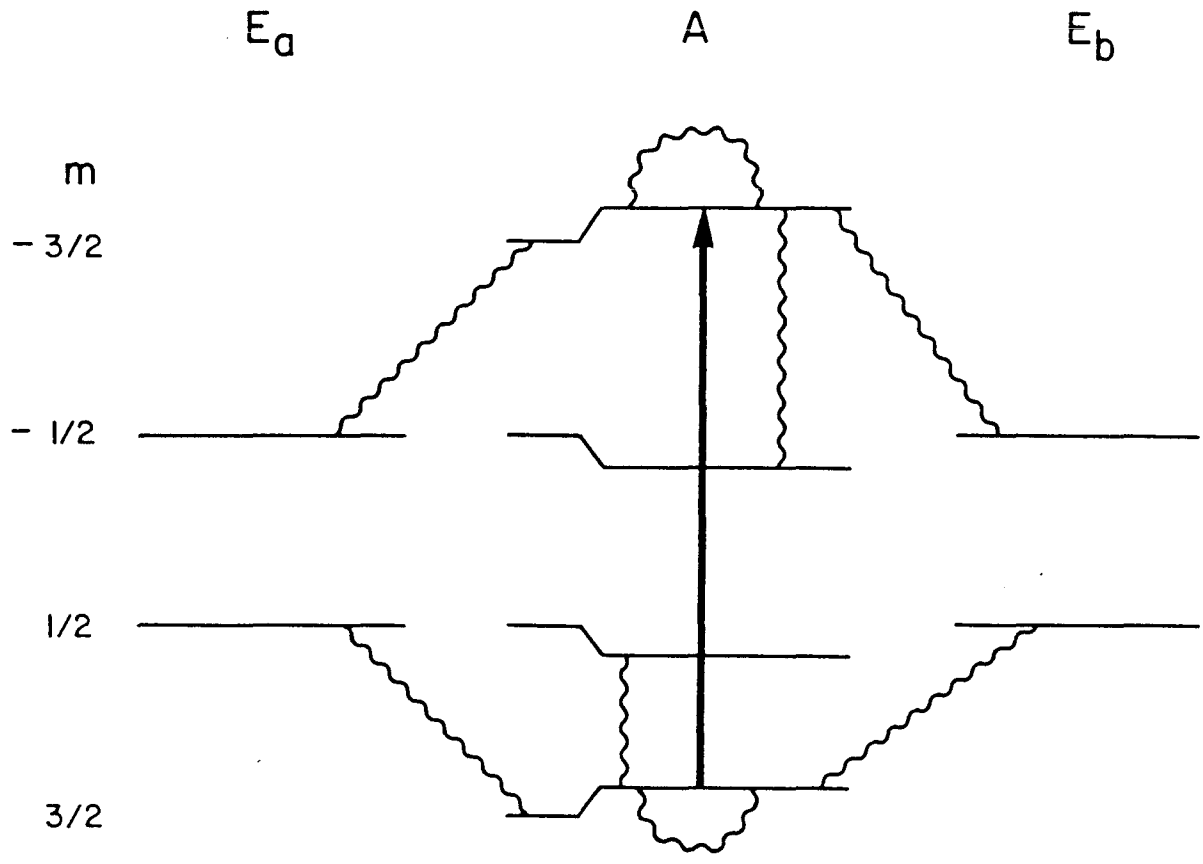

Figure IV.5 Possible relaxation pathways for the triple-quantum transition. The spectral density of A-type (symmetry-conserving) corresponds to relaxation among states of the same symmetry. Spectral densities of E^a or E^b-type (symmetry-breaking) correspond to relaxation between the states of A-symmetry and states of E^a or E^b-symmetry.

$$G_A^{(m)}(\tau) = G_E a^{(m)}(\tau) = G_E b^{(m)}(\tau) = G_a^{(m)}(\tau) \quad . \qquad \text{(IV.53)}$$

(3) General case.

The ratios of the decay rates of multiple quantum coherences depend on the asymmetry parameter ξ and the ratio of $G_a^{(0)}/Ga^{(1)}(\omega_I)$ (which depends on the correlation time τ_c of the fluctuation and the Lamor frequencies ω_I, ω_S of proton and electron). As we evaluated in an earlier section, the correlation functions are given by:

$$G_a^{(0)}(0) = \frac{1}{5} K^2 \tau_c + \frac{3}{10} K^2 \tau_c \frac{1}{1+\omega_s^2\tau_c^2} \quad , \qquad \text{(IV.54)}$$

$$G_a^{(1)}(\omega_I) = G_a^{(-1)}(\omega_I) = \frac{3}{20} K^2 \tau_c \frac{1}{1+\omega_I^2\tau_c^2} + \frac{7}{20} K^2 \tau_c \frac{1}{1+\omega_s^2\tau_c^2} \qquad \text{(IV.55)}$$

where

$$K^2 = \left\langle \left(\frac{\hbar^2 \gamma_I \gamma_S}{r^3} \right)^2 \right\rangle \quad .$$

The dependence of the decay rates on the concentration of paramagnetic impurity is through the average distance between the electron and methyl proton.

The ratios of the relaxation rates (independent of the concentration of impurity in the experimental range) provide a measurement of the correlation time and the asymmetry parameter.

To illustrate the sensitivity of the n-quantum relaxation to the fluctuation model, the ratios of the decay rates are shown for three extreme cases that are classified by the value of τ_c.

(a) Short correlation time limit, $\omega_s^2\tau_c^2 << 1$.

The ratios of decay rates is given by

$$\frac{\Gamma_{14}}{\Gamma_{12}} = \frac{3(1+\xi)}{2+\xi} \quad , \quad \frac{\Gamma_{13}}{\Gamma_{12}} = \frac{\frac{5}{2}+2\xi}{2+\xi} \quad . \tag{IV.56}$$

Their dependence on ξ is indicated by the two curves A and A' in Figure IV.6.

(b) Long correlation time limit, $\omega_I^2\tau_c^2 >> 1$.

In this case, we have

$$\frac{\Gamma_{14}}{\Gamma_{12}} = 3 + 6\xi \quad , \quad \frac{\Gamma_{13}}{\Gamma_{12}} = 2 + 2\xi \quad . \tag{IV.57}$$

The dependence of the ratios on ξ is indicated by the two curves B and B' in Figure IV.6.

(c) Intermediate case, $\omega_I^2\tau_c^2 << 1$, $\omega_s^2\tau_c^2 >> 1$.

The ratios are given by

$$\frac{\Gamma_{14}}{\Gamma_{12}} = \frac{21 + 24\xi}{13 + 6\xi} \quad , \quad \frac{\Gamma_{13}}{\Gamma_{12}} = \frac{17 + 14\xi}{13 + 6\xi} \quad . \tag{IV.58}$$

Their dependence on ξ is indicated by the two curves C and C' in Figure IV.6.

4.4.4 Experimental results and discussion

4.4.4.1 Samples and spectrometer

Experiments were done in a field of 42.5 KG provided by a Bruker superconducting solenoid. The corresponding operating frequency for protons is 185 MHz. The pulsed r.f. power of 200 Watts generated by a tuned transmitter, produced a rotating field

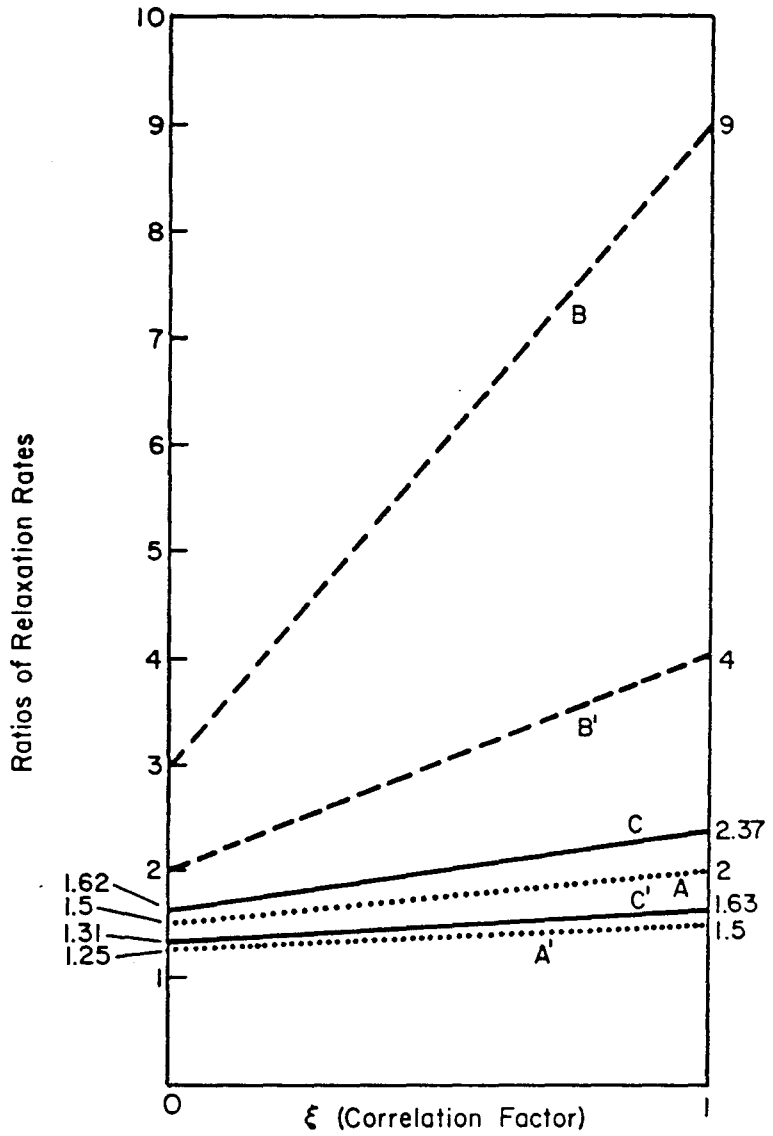

XBL 796-10119

Fig. IV.6 The ratios of relaxation rates of double and triple quantum coherences to single quantum Γ_{13}/Γ_{12} and Γ_{14}/Γ_{12} depends on the correlation factor ξ and the correlation time τ_c. Curves A and A' show the case of short correlation time limit, $\omega_s^2\tau_c^2 << 1$. Lines B and B' show the case of long correlation time limit, $\omega_I^2\ \tau_c^2 >> 1$. The intermediate case, $\omega_I^2\ \tau_c^2 << 1$, $\omega_s^2\ \tau_c^2 >> 1$, is shown by curves C and C'.

of 20 G in a solenoidal coil of 8 mm in diameter. Samples of acetonitrile ($\sim$ 12% in mole) dissolved in EBBA (p-ethoxy-benzylidine n-butylaniline), with different concentrations of di-t-butyl-nitroxide (DTBN) radical, were observed over a range of temperature 21.5° $\sim$ 23.0°C. The temperature was controlled by a feedback system within $\pm$ 0.1°. The change of the observed dipolar splitting by temperature fluctuation caused linebroadening by an amount less than a few hertz.

4.4.4.2 Pulse sequence

Multiple quantum transitions were observed by using the TPPI-Echo method.[14] The line broadening by field inhomogeneity ($\sim$ 1 ppm) was removed by the echo pulse[20] during the evolution period of multiple quantum coherences as we have shown in Figure IV.7. An artificial frequency offset was created by the phase increment of the first two 90° pulses relative to that of the third 90° pulse. When the r.f. phase is incremented by ϕ, the n-quantum transitions "see" this as $n\phi$.[15,16]

4.4.4.3 Spectra and results

The linewidths of multiple quantum transitions for a given concentration of DTBN were measured by taking the averages of the particular linewidth of spectra obtained from various τ ranging from 250 μsec to 500 μsec. Four typical spectra with different concentrations of DTBN are shown in Figure IV.8.

The full widths at half height of each transition, related to the relaxation rate by Γ/π, were found to vary linearly with respect to the concentration of the impurity as is shown in Figure

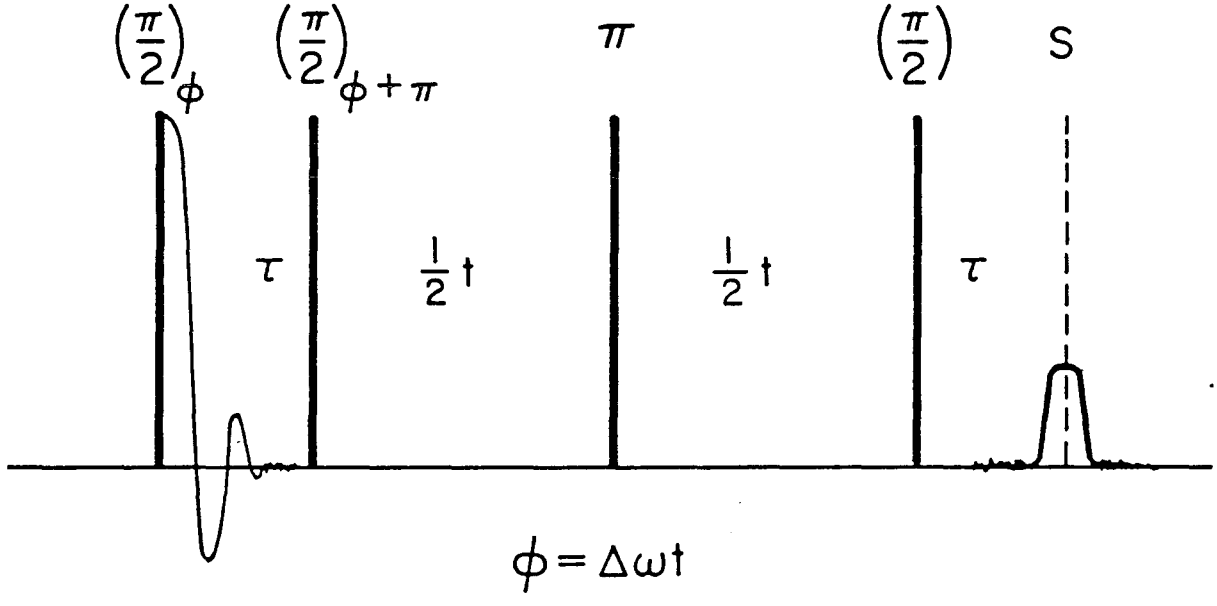

XBL 794-9146

Figure IV.7 The TPPI-Echo pulse sequence is used to remove inhomogeneous line broadening, and to restore the frequency offset by the time proportional phase increment. The artificial frequency offset is merely the rate of phase increment. The time during the period of preparation and mixing is set to be 250 μsec ∿ 500 μsec. The multiple quantum spectrum is obtained by a Fourier transformation of the signal in time domain t.

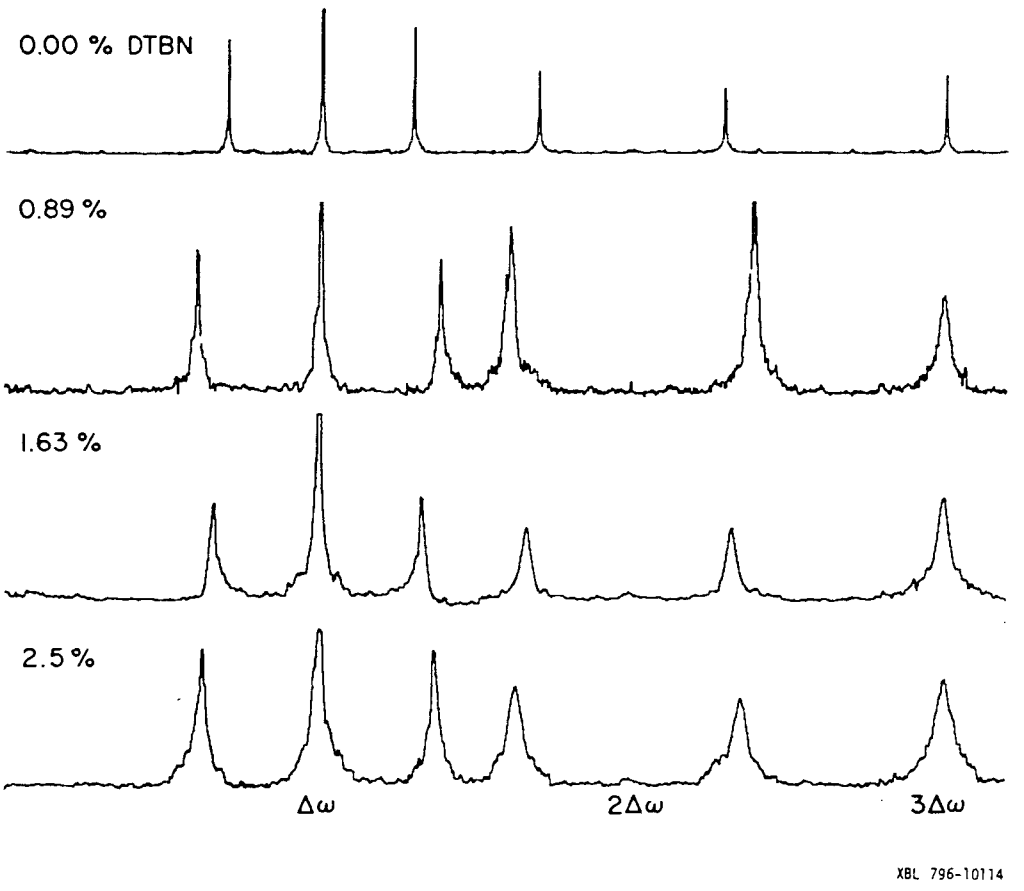

Fig. IV.8 The relaxation rates of multiple quantum coherences depend on the concentration of the paramagnetic impurity. Shown are illustrative multiple quantum spectra with different concentrations of DTBN in mole per cent. The frequency offset $\Delta\omega/2\pi$ is 7.8125 KHz.

IV.9. Their relations are given by linear fits:

$$\Gamma_{12} = \Gamma_{34} = (336 \pm 5)[C]\text{Sec}^{-1}$$

$$\Gamma_{13} = \Gamma_{24} \quad (565 \pm 10)[C]\text{Sec}^{-1}$$

$$\Gamma_{14} = (850 \pm 90)[C]\text{Sec}^{-1}$$

where [C] is the concentration of DTBN in mole per cent.

The ratios of the decay rates Γ_{14}/Γ_{12} and Γ_{13}/Γ_{12} are then:

$$\Gamma_{13}/\Gamma_{12} = 1.68 \pm 0.02$$

$$\Gamma_{14}/\Gamma_{12} = 2.53 \pm 0.15 \quad .$$

4.4.4.4 Discussion

We shall now compare the various models of correlation time τ_c and correlation parameter ξ (Figure IV.6) with these data. The model with the condition $\omega_s^2\tau_c^2 << 1$ is completely ruled out since it predicts (Curves A and A' in Figure IV.6)

$$\Gamma_{13}/\Gamma_{12} = 1.25 - 1.50$$

$$\Gamma_{14}/\Gamma_{12} = 1.50 - 2.00 \qquad \text{for } \xi = 0\text{-}1.$$

Similarly, $\tau_I^2\omega_c^2 >> 1$ is not possible since it predicts (Curves B and B' in Figure IV.6)

$$\Gamma_{13}/\Gamma_{12} = 2.0 - 4.0$$

$$\Gamma_{14}/\Gamma_{12} = 3.0 - 9.0 \qquad \text{for } \xi = 0\text{-}1,$$

By looking at Curves C and C' in Figure IV.6 we see that the

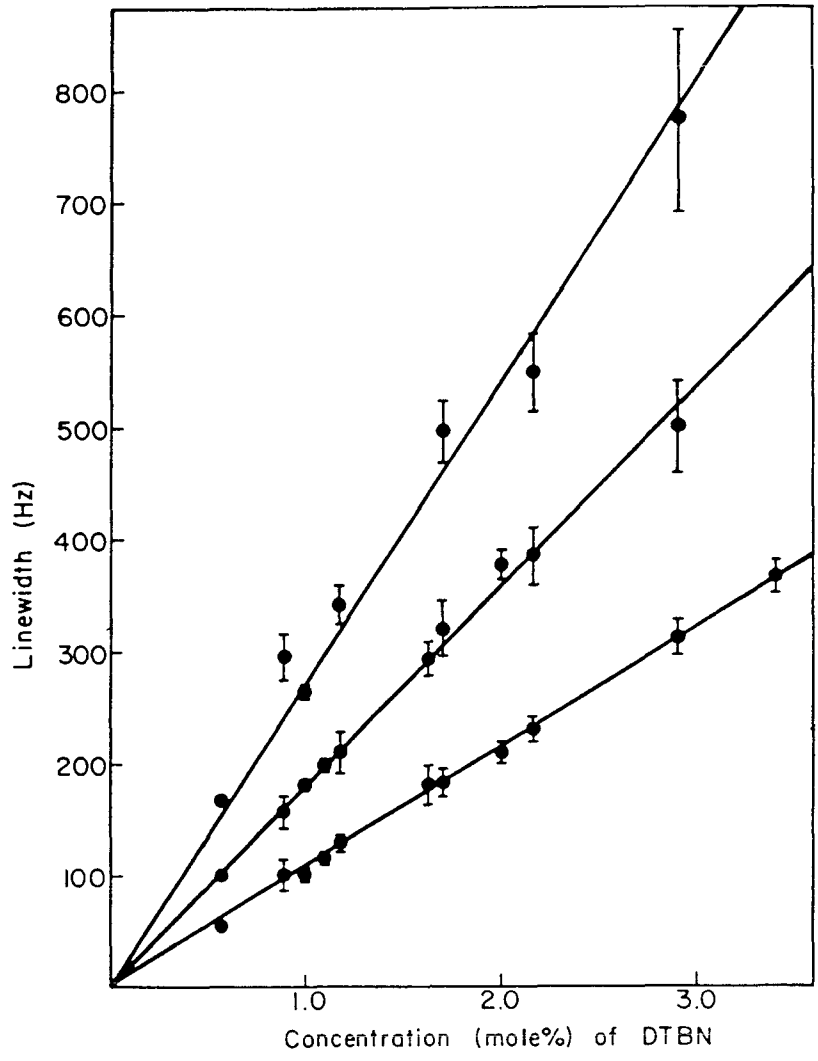

Fig. IV.9 The linewidth of multiple quantum transitions is linearly proportional to the concentration of DTBN. The ratios of the relaxation rates can be determined accurately by measuring the ratios of the slope.

data fits quite well with the assumption that $\omega_s^2\tau_c^2 >> 1$ and $\omega_I^2\tau_c^2 << 1$ with $\xi = 1$. This predicts:

$$\Gamma_{13}/\Gamma_{14} = 1.63$$

$$\xi = 1.$$

$$\Gamma_{14}/\Gamma_{13} = 2.37$$

The fit can be made very good by keeping $\xi = 1$, but $y = (1+\omega_I^2\tau_c^2)^{-1} = 0.91 \pm 0.04$. With these values we find $\tau_c = (2.7 \pm 0.6) \times 10^{-10}$ sec.

The conclusions that $\xi = 1$, namely, that a complete correlation in the fluctuation is not unreasonable, since $\tau_c \sim 10^{-10}$ sec; whereas the rotation time for the CH_3 group (permuting the proton positions) is of the order of 10^{-12} sec. In addition, the average distance between the electron spin and the methyl protons is much larger than the dimensions of the methyl group. Simple geometric calculations (using δ/γ), predict that the extent of symmetry breaking transitions should be less than 1%. Thus we see that the measurement of n-quantum relaxation indeed gives a very sensitive measure of correlation and correlation times.

4.4.4.5 Summary and comments

In a system of strongly coupled spins, we have shown that the longitudinal and transverse relaxation of normal single quantum transitions usually provides information about inter-nuclear correlation functions. They alone, however, are not adequate to determine the relaxation mechanism characterized by a number of auto- and cross-correlation functions. The

advantages of using multiple quantum spectroscopy to study relaxation effect have been illustrated by the system of oriented actionotrile in a liquid crystal matrix containing paramagnetic impurities.

We estimate that the broadening of linewidths of paramagnetic impurity becomes dominant over those by intra- and inter-proton relaxation if the molar concentration of paramagnetic impurity is larger than 0.01%. The estimated contribution of linebroadening by symmetry-breaking channels is rather small (<1%), even with molar concentrations as high as 35%.

The presence of the echo pulse during the evolution period of multiple quantum coherences reverses the magnetic quantum number m, and changes the density matrix element $\rho_{\alpha\beta}$ into $\rho_{\alpha'\beta'}$ where $|\alpha'>$, $|\beta'>$ are mirror-imaged states of $|\alpha>$ and $|\beta>$ by reversing m. The associated dipolar splitting and relaxation rates, however, remain unchanged.

We shall now point out some features of completely correlated fluctuations. The adiabatic term of the relaxation rate, originated from the elastic scattering (energy-conserving) processes, can be written as

$$\Gamma_{\alpha\beta}^{(0)} = \frac{1}{2\hbar^2} J_A^{(0)}(0) \ (m_\alpha - m_\beta)^2 \quad . \tag{IV.59}$$

It has a simple quadratic dependence of the decay rate on the number of quanta. In the case of a long correlation time limit ($\omega_I^2 \tau_c^2 >> 1$), the non-adiabatic contribution by inelastic scattering processes becomes negligible. The linewidth of n-quantum

coherence depends on N quadratically. It is a general property of the case of completely correlated fluctuations but does not refer particularly to the system of methyl protons. As the correlation time becomes shorter, the non-adiabatic contribution becomes as important as the adiabatic term. The non-adiabatic term can be found by evaluating the lifetimes of the associated states.

The expression of the adiabatic term in the case of completely uncorrelated fluctuations is generally complicated. There is, however, a simple relation if either $|\alpha\rangle$ or $|\beta\rangle$ is the highest or lowest state. In this case, the adiabatic term linearly depends on the number of quanta of the multiple quantum coherence, such as:

$$\Gamma_{\alpha\beta}^{(0)} = \frac{1}{2\hbar^2} J^{(0)}(0) \; |m_\alpha - m_\beta| \quad . \tag{IV.60}$$

For a system of N coupled spins, the non-adiabatic term has a simple form in the case of completely uncorrelated fluctuations:

$$\Gamma'_{\alpha\beta} = \frac{1}{2\hbar^2} J^{(1)}(\omega_I) N \quad . \tag{IV.61}$$

Because each spin relaxes independently, it contributes to the decay rate equally.

There is only one transition between the state with all spins up and the state with all spins down. The adiabatic term of its linewidth depends on the number of quanta quadratically in the case of completely correlated fluctuation, and linearly in

the case of completely uncorrelated fluctuations.

4.5 Multiple quantum NMR and relaxation of two coupled methyl groups

In the previous multiple quantum NMR study of an oriented methyl group relaxed by paramagnetic impurities, we found that the fluctuating magnetic fields at each site of methyl protons are correlated.[6] The dominant relaxation mechanism is caused by the A-type fluctuation that conserves the symmetry of the spin states. The relaxation caused by the fluctuation of symmetry-breaking types E^a and E^b is negligibly small.

We have studied the multiple quantum NMR of two coupled methyl groups at room temperature. The experiments showed no evidence of correlated motion between them in the time scale of a millisecond, that is, two methyl groups rotates quite independently.[21]

We shall demonstrate the application of multiple quantum NMR to the study of two dipole-coupled methyl groups in the presence of paramagnetic electron spins. The measurements of the transverse relaxation time for four, five, and six-quantum transitions allow a complete determination of the fluctuation spectral densities and relaxation pathways.

As shown in Figure IV.10, each of the two methyl groups experiences a fluctuating magnetic field that is produced by a distant electron spin. Since the methyl group rotates very rapidly at a rate of 10^{12} Hz, the protons of same group feel an equally fluctuating field. This assumption is reasonable and has been verified by our previous experiments on the multiple quantum study of an methyl group.[6] Although each methyl proton of the

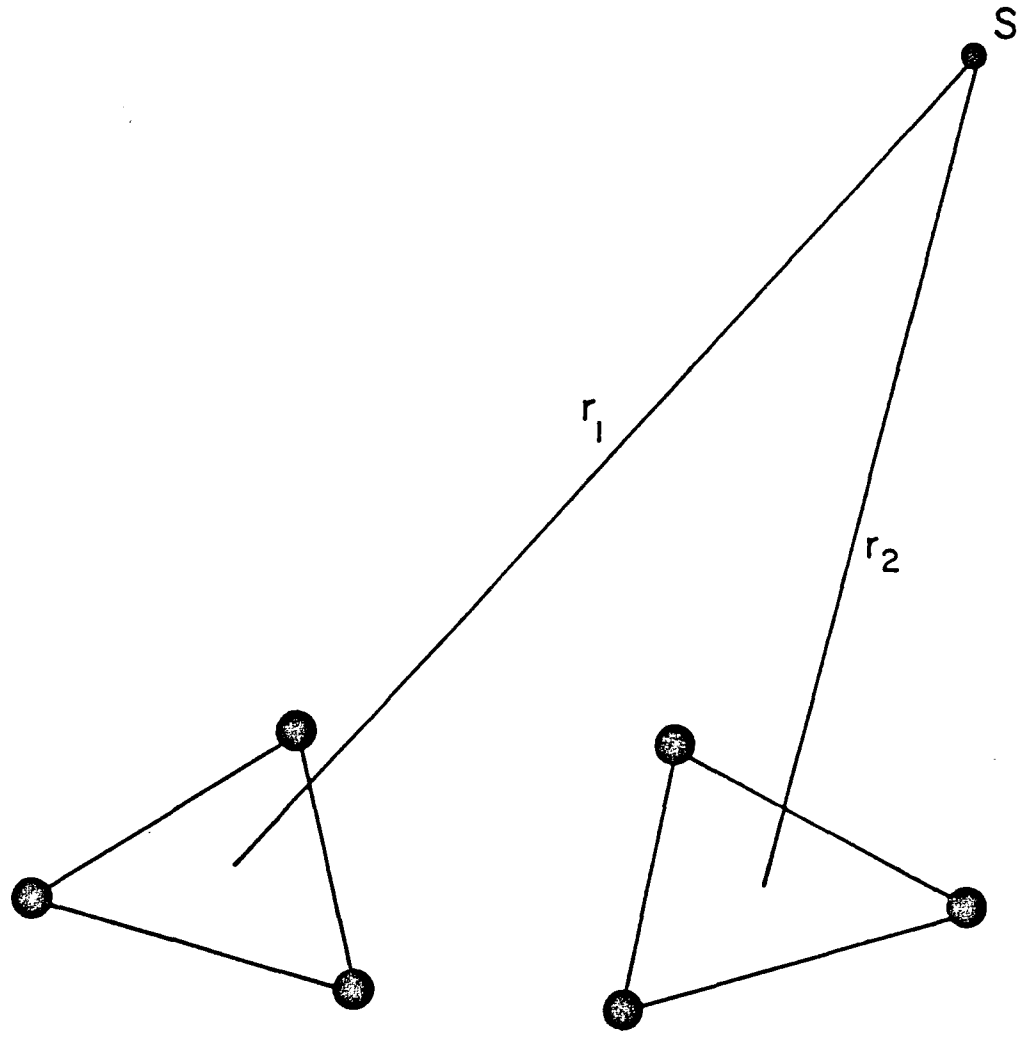

XBL 811-7663

Figure IV.10 Geometry of two methyl groups. The electron spin S produces a large random field at each site of the methyl groups.

same group experiences the same field, the fluctuating field at the site of different groups may not be equal. Different degrees of correlation between these two fluctuating magnetic fields $B_1(t)$ and $B_2(t)$ affects the linewidth of the multiple quantum spectrum differently.

The interaction between the methyl protons and the magnetic field produced by the unpaired electron is given by the time-dependent Hamiltonian $H_1(t)$ as

$$H_1(t) = - \hbar \gamma_I \sum_{i=1,2,3} \vec{I}_i \cdot \vec{B}_1(t) - \hbar \gamma_I \sum_{i=4,5,6} \vec{I}_i \cdot \vec{B}_2(t) \quad . \tag{IV.62}$$

We may rearrange the functions $\vec{I}_i$ and $\vec{B}_{1,2}(t)$ in terms of the symmetry-adapted form to read

$$\begin{aligned} H_1(t) &= - \hbar \gamma_I (\vec{I}_1 + \vec{I}_2 + \vec{I}_3 + \vec{I}_4 + \vec{I}_5 + \vec{I}_6) \cdot \frac{1}{2} (\vec{B}_1 + \vec{B}_2) \\ &\quad - \hbar \gamma_I (\vec{I}_1 + \vec{I}_2 + \vec{I}_3 - \vec{I}_4 - \vec{I}_5 - \vec{I}_6) \cdot \frac{1}{2} (\vec{B}_1 - \vec{B}_2) \\ &= - \hbar \gamma_I \vec{I}_g \cdot \vec{B}_g - \hbar \gamma_I \vec{I}_u \cdot \vec{B}_u \\ &= \sum_{\substack{m=0,\pm 1 \\ =g,u}} (-1)^m V_\mu^{(m)} f_{-\mu}^{(-m)}(t) \end{aligned} \tag{IV.63}$$

where $\vec{B}_g$ is the symmetrized function, $\vec{B}_u$ is the anti-symmetrized function

$$\vec{B}_g(t) = \frac{1}{2} (\vec{B}_1(t) + \vec{B}_2(t)) \quad ,$$

$$\vec{B}_u(t) = \frac{1}{2} (\vec{B}_1(t) - \vec{B}_2(t)) \quad , \tag{IV.64}$$

and

$$V_\mu^{(0)} = I_{\mu,z} \ , \ V_\mu^{(1)} = -\frac{1}{\sqrt{2}} I_{\mu,+} \ , \ V_\mu^{(-1)} = \frac{1}{\sqrt{2}} I_{\mu,-} \ . \quad \text{(IV.65)}$$

The fluctuating function

$$f_\mu^{(m)} = -\hbar \gamma_I B_\mu^{(m)}(t) \quad \text{(IV.66)}$$

is related in a similar way to $f_i^{(m)}$ by

$$f_i^{(m)} = -\hbar \gamma_I B_i^{(m)}(t) \quad . \quad \text{(IV.67)}$$

There are two distinctive kinds of correlation function--the autocorrelation function $G_a^{(m)}(\tau)$ and the cross-correlation function $G_c^{(m)}(\tau)$. They are defined by

$$\begin{cases} (-1)^m \ \overline{f_i^{(-m)}(t) \ f_i^{(n)}(t-\tau)} = \delta_{mn} \ G_a^{(m)}(\tau) \quad , \\ (-1)^m \ \overline{f_i^{(-m)}(t) \ f_j^{(n)}(t-\tau)} = \delta_{mn} \ G_c^{(m)}(\tau) \quad \text{for } i \neq j. \end{cases} \quad \text{(IV.68)}$$

We can introduce the symmetry-adapted correlation function $G^{(m)}(\tau)$ as

$$(-1)^m \ \overline{f_\mu^{(-m)}(t) \ f_{\mu'}^{(n)}(t-\tau)} = \delta_{mn} \ \delta_{\mu\mu'} \ G_\mu^{(m)}(\tau) \quad . \quad \text{(IV.69)}$$

The function $G_\mu^{(m)}(\tau)$ is closely related to both the autocorrelation function and cross-correlation function by

$$\begin{cases} G_g^{(m)}(\tau) = \frac{1}{2} G_a^{(m)}(\tau) + \frac{1}{2} G_c^{(m)}(\tau) \quad , \\ G_u^{(m)}(\tau) = \frac{1}{2} G_a^{(m)}(\tau) - \frac{1}{2} G_c^{(m)}(\tau) \quad . \end{cases} \quad \text{(IV.70)}$$

In the case of a completely correlated fluctuation, the fluctuating magnetic fields at both methyl groups are equal and correlated. The autocorrelation function is thus equal to the cross-correlation function, hence, the antisymmetric correlation function $G_u^{(m)}$ vanishes. If the fluctuating fields at each methyl group are completely uncorrelated, the cross-correlation term should be an identical zero. In this case, the symmetric correlation function $G_g^{(m)}$ is equal to the anti-symmetric correlation function.

Generally, there are four different fluctuation spectral density functions: $G_g^{(0)}$, $G_g^{(1)}$, $G_u^{(0)}$, and $G_u^{(1)}$. To completely determine their values and the relaxation pathways, we should at least measure the linewidth of four different multiple quantum transitions. We shall calculate the linewidth for the two satellite four-quantum transitions, one satellite five-quantum transition, and the central six-quantum transition. The four above transitions are all of A_g-type.

By using the expression for relaxation rate in the equation IV.20 and the fluctuation Hamiltonian in the equation IV.63, we can calculate the decay rates for the nondegenerate multiple quantum transitions. Their values are given as follows:

(1) six-quantum transition $A_g(-3) - A_g(3)$

$$\hbar^2\Gamma_6 = 18\, J_g^{(0)}(0) + 3\, J_g^{(1)}(\omega_I) + 3\, J_u^{(1)}(\omega_I) \quad . \qquad \text{(IV.71)}$$

(2) five-quantum transitions $A_g(-2) - A_g(3)$, $A_g(-3) - A_g(2)$

$$\hbar^2\Gamma_5 = \frac{25}{2}\, J_g^{(0)}(0) + \frac{11}{2}\, J_g^{(1)}(\omega_I) + \frac{1}{2}\, J_u^{(0)}(0) + \frac{5}{2}\, J_u^{(1)}(\omega_I) \quad . \qquad \text{(IV.72)}$$

(3) four-quantum transitions ${}^1A_g(-1) - A_g(3)$, ${}^2A_g(-1) - A_g(3)$, $A_g(-3) - {}^1A_g(1)$, $A_g(-3) - {}^2A_g(1)$

$$\hbar^2\Gamma_4 = 8\, J_g^{(0)}(0) + \frac{9}{2} J_g^{(1)}(\omega_I) + J_u^{(0)}(0) + \frac{9}{2} J_k^{(1)}(\omega_I) \quad . \text{(IV.73)}$$

Since there are two kinds of fluctuation G_g and G_u, we need to consider only two types of symmetry representations, A_g and A_u. To illustrate this, the relaxation channels for the six and five-quantum transitions are shown in Figure IV.11.

Expressing the decay rate for the two four-quantum transitions is very complicated. It depends on the strength of the dipole couplings. If we change to a different sample, the dipole coupling will also change. As a consequence, we cannot study the effects using different concentration of impurities. Nevertheless, we can show that the average value of the decay rates for the two four-quantum transitions does not depend on the strength of dipole couplings. Its value was given in the previous rate equation.

It is reasonable to assume that the ratio between $G_c^{(m)}$ and $G_a^{(m)}$ is characterized by the same correlatin parameter ξ as

$$\xi = G_c^{(0)}/G_a^{(0)} = G_c^{(1)}/G_a^{(1)} \quad . \text{(IV.74)}$$

We can rewrite the equations for the relaxation rates as

$$\begin{cases} \hbar^2\Gamma_6 = 18\, G_a^{(0)}(1+\xi) + 6\, G_a^{(1)} \\ \hbar^2\Gamma_5 = (13 + 12\xi)G_a^{(0)} + (8 + 3\xi)G_a^{(1)} \\ \hbar^2\Gamma_4 = (9 + 7\xi)G_a^{(0)} + 9\, G_a^{(1)} \end{cases} \quad . \text{(IV.75)}$$

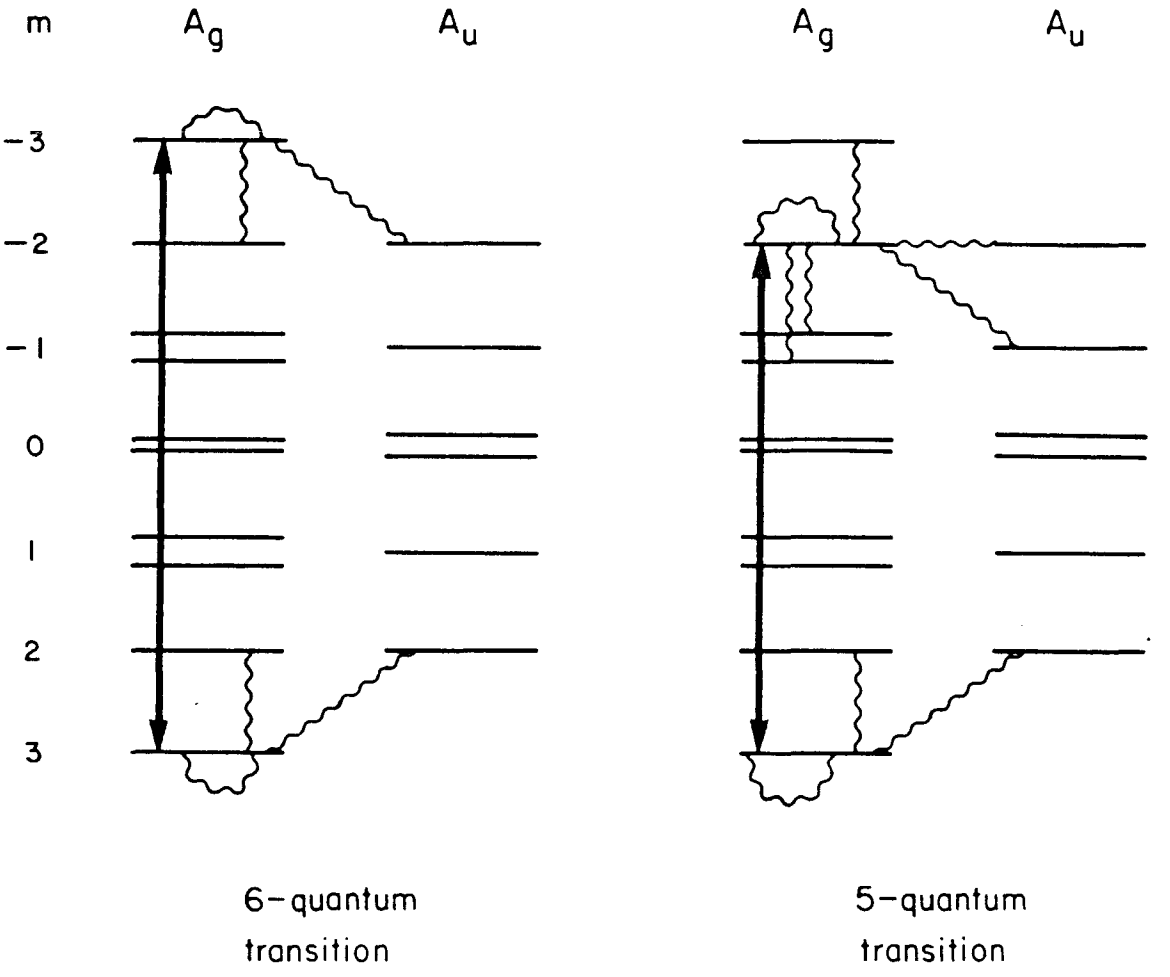

Figure IV.11 Relaxation channels for 5 and 6-quantum transitions. Pathways which connect the A_g and A_u states are caused by antisymmetric fluctuations. Symmetry-conserving relaxation channels are caused by symmetric fluctuations.

The explicit expression of $G_a^{(0)}(0)$ and $G_a^{(1)}(\omega_I)$ has already been shown in equations (IV.54) and (IV.55).

We shall illustrate the dependence of the relaxation rate on the correlation parameter ξ by using three extreme cases.

(a) Short correlation time, $\omega_s^2\tau_c^2 << 1$.

In this case, one has $G_a^{(0)} = G_a^{(1)}$ and

$$\frac{\Gamma_6}{\Gamma_4} = \frac{24 + 18\xi}{18 + 7\xi} \quad , \quad \frac{\Gamma_5}{\Gamma_4} = \frac{21 + 15\xi}{18 + 7\xi} \quad . \tag{IV.76}$$

Their dependence on ξ is indicated by the two curves A and A' in Figures IV.12 and IV.13.

(b) Long correlation time, $\omega_I^2\tau_c^2 >> 1$.

In this case, we have $G_a^{(1)} << G_a^{(0)}$ and

$$\frac{\Gamma_6}{\Gamma_4} = \frac{18 + 18\xi}{9 + 7\xi} \quad , \quad \frac{\Gamma_5}{\Gamma_4} = \frac{13 + 12\xi}{9 + 7\xi} \quad . \tag{IV.77}$$

Their dependence on ξ is shown by the two curves B and B' in Figures IV.12 and IV.13.

(c) Intermediate case, $\omega_I^2\tau_c^2 << 1$, $\omega_s^2\tau_c^2 >> 1$.

$$\frac{\Gamma_6}{\Gamma_4} = \frac{90 + 72\xi}{63 + 28\xi} \quad , \quad \frac{\Gamma_5}{\Gamma_4} = \frac{76 + 57\xi}{63 + 28\xi} \quad . \tag{IV.78}$$

Their dependence on ξ is indicated by the two curves C and C' in Figures IV.12 and IV.13.

From the linewidth measurements of four, five, and six-quantum transitions with different concentrations of paramagnetic

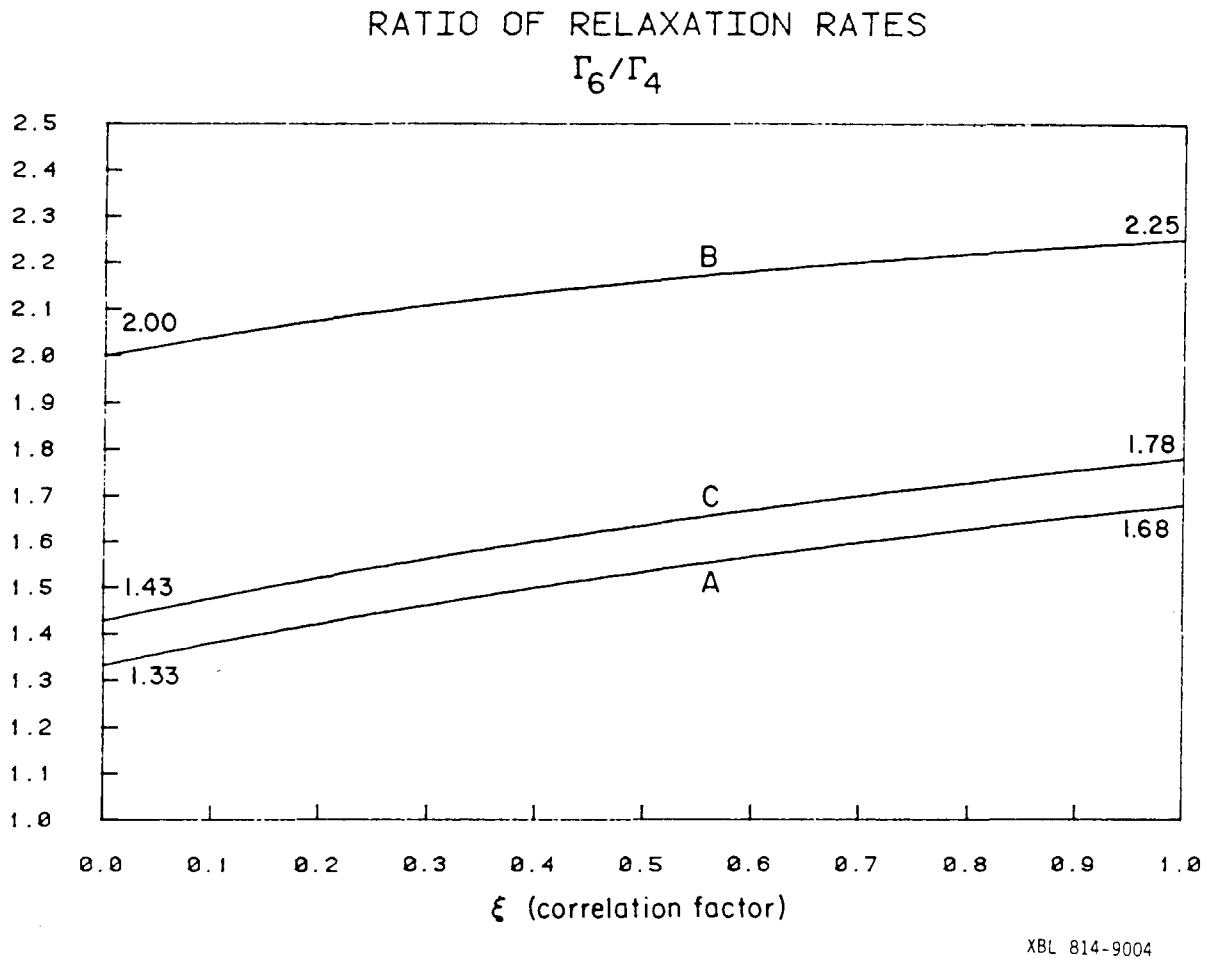

Figure IV.12 Ratios of relaxation rates of 6-quantum coherence to 4-quantum coherence. Γ_6/Γ_4 depends on the correlation factor ξ and the correlation time τ_c. Curves A shows the case of the short correlation time limit, $\omega_s^2\tau_c^2 << 1$. Curves B shows the case of the long correlation time limit, $\omega_I^2\tau_c^2 >> 1$. The intermediate case, $\omega_I^2\tau_c^2 << 1$, $\omega_s^2\tau_c^2 >> 1$, is shown by curve C.

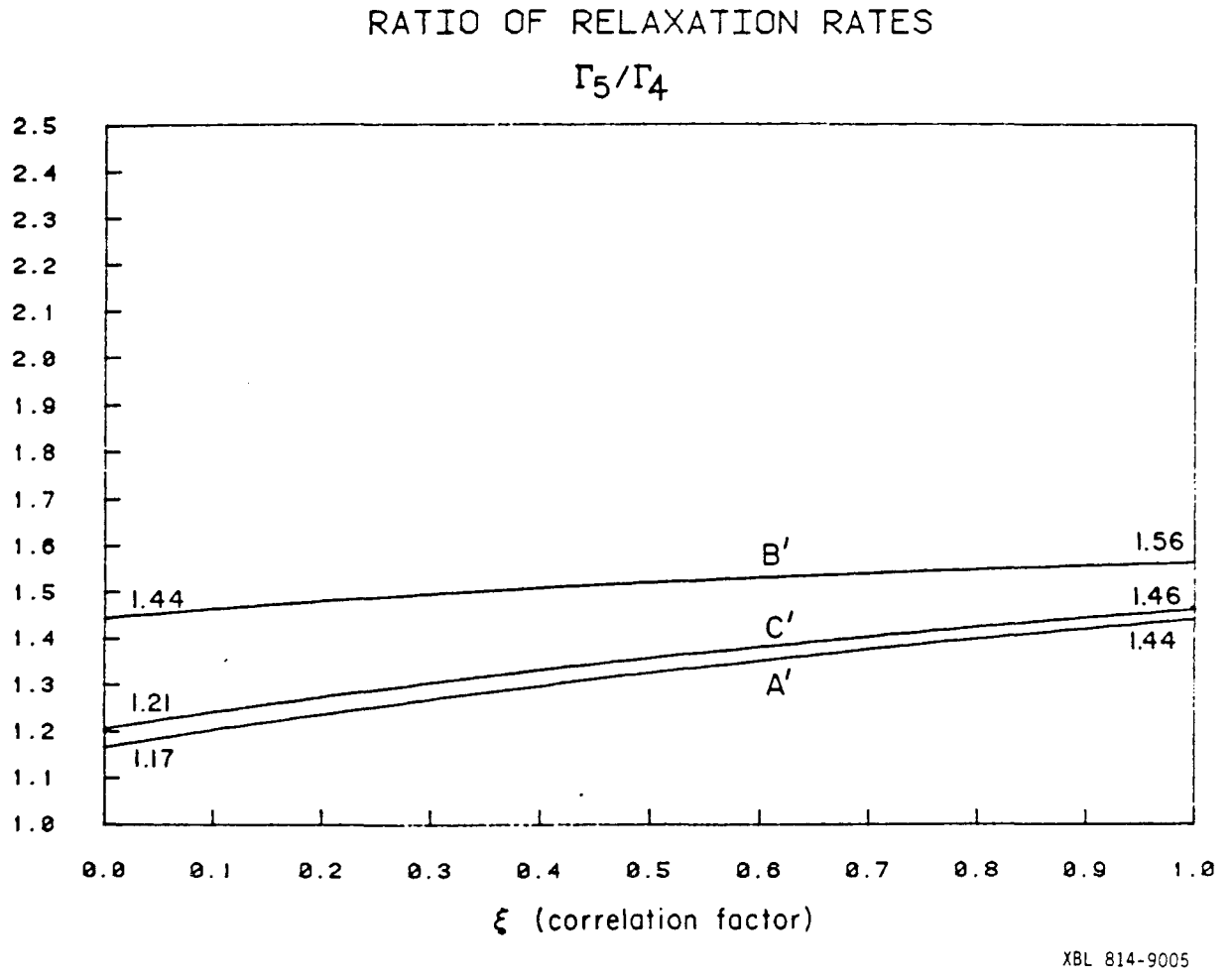

Figure IV.13 Ratios of the relaxation rates of 5-quantum coherence to 4-quantum coherence. Γ_5/Γ_4 depends also on the correlation factor ξ and the correlation time τ_c. Curves A', B', and C' show the case of the short correlation time limit, long correlation time limit, and intermediate case.

impurities, we can determine the ratios of the decay rates more accurately. The degree of the correlated fluctuation can be calculated from the experimental measurements of these ratios. By knowing the correlation factor ξ, we can completely determine the relaxation pathways.

4.6 Relaxation by an external random field

As we have pointed out in the earlier discussion of the completely correlated fluctuations, the adiabatic part of the relaxation rate is given by

$$\Gamma_{\alpha\beta}^{(0)} = \frac{1}{2\hbar^2} J_A^{(0)}(0) (m_\alpha - m_\beta)^2 \quad . \tag{IV.79}$$

For a n-quantum transition, the adiabatic relaxation time is n^2 times faster than that of a single quantum transition.[6]

This interesting phenomena can be verified by irradiating external random electromagnetic waves at audio frequency. The nuclear spins couple to the fluctuating magnetic field that is produced by a tuned coil along the z-axis; its interaction Hamiltonian is given by

$$H_1(t) = -\hbar \gamma_I \left(\sum_i I_{i,z} \right) B_z(t) \quad . \tag{IV.80}$$

The fluctuating magnetic field at audio frequency can be produced by a noise generator. The power level and the band width of the noise can be controlled by an amplifier and an audio frequency filter.

Since the non-adiabatic part of the relaxation is very small, the transverse relaxation rate is completely determined by the

adiabatic process, and[6]

$$\Gamma_{\alpha\beta} = \frac{1}{2\hbar^2} J_A^{(0)}(0) (m_\alpha - m_\beta)^2 \quad . \tag{IV.81}$$

The linewidth of multiple quantum transition has a simple quadratic dependence of the decay rates on the number of quanta.

By changing the width of the filter that corresponds to τ_c^{-1}, and the amplifier gain for the noise generator, we can systematically vary the spectral density of fluctuation $J_A^{(0)}(0)$. From the linewidth measurements of the multiple quantum transition, the quadratic dependence can be testified.

4.7 References

1. A. Abragam, The Principles of Nuclear Magnetism, Chapter 3 (Oxford Univ. Press, London, 1961).
2. A. G. Redfield, IBM J. Res. Div. 1, 19 (1957).
3. A. G. Redfield, Adv. Magn. Reson. 1, 1 (1965).
4. Reference 1, Chapter 8.
5. Reference 1, Chapter 10.
6. J. Tang and A. Pines, J. Chem. Phys. 72, 3290 (1980).
7. R. L. Vold and R. R. Vold, Prog. in NMR Spectroscopy, vol. 12. ed. by J. W. Emsley, et al. (Pergamon Press, New York, 1979).
8. A. Wokaun and R. R. Ernst, Mol. Phys. 36, 317 (1978).
9. A. Wolaun and R. R. Ernst, Chem. Phys. Lett. 52, 407 (1977).
10. R. Poupko, R. L. Vold, and R. R. Vold, J. Magn. Reson. 34, 67 (1979).
11. M. E. Stoll, A. J. Vega, and R. W. Vaughan, J. Chem. Phys. 67, 2029 (1977).
12. L. G. Werbelow and D. M. Grant, Adv. in Mag. Res. 9, 180 (1977).
13. S. Emid, R. J. Baarda, J. Smidt, and R. A. Wind, Physica 93B, 327 (1978).
14. G. Drobny, A. Pines, S. Sinton, D. Weitekamp, and D. Wemmer, Faraday Div. of the Chem. Soc. Symposium 13, 49 (1979).
15. S. Vega, T. W. Shattuck, and A. Pines, Phys. Rev. Lett. 37, 43 (1976).
16. A. Pines, D. Wemmer, J. Tang, and S. Sinton, Bull. of Amer. Phys. Soc. 23, 21 (1978).
17. S. Clough and T. Hobson, J. Phys. C7, 3387 (1974).

18. M. Tinkham, Group Theory and Quantum Mechanics, Chapter 5 (McGraw-Hill, New York, 1964).

19. R. A. Hoffman, Adv. in Mag. Res. 4, 87 (1970).

20. E. L. Hahn, Phys. Rev. 80, 580 (1959).

21. J. Tang and A. Pines, J. Chem. Phys. 73, 2512 (1980).

V

MULTIPLE QUANTUM NMR STUDY OF CORRELATION OF TWO METHYL GROUPS

5.1 Introduction

Molecules having two rotating groups may show coupled motions. An interesting question for us to consider is the characterization of conformation and correlated motion of molecular groups which are sterically hindered. For example, two adjacent methyl groups may exhibit some degree of correlated motion as do two wheels in gear. The coupling of rotational motion is very difficult to measure by microwave spectroscopy. Although the traditional single quantum NMR can yield some information about the molecular conformation and correlated motions, the spectra obtained may sometimes be complicated and difficult to analyze.[1]

In this chapter, we shall demonstrate the application of multiple quantum NMR technique to the study of the potentially correlated motion of two adjacent methyl groups in the same molecular framework.[2]

We shall show that four-quantum spectrum is sensitive to the two-body correlations and distinguishes simply between the cases of uncorrelated and correlated motion.[2] The two-body correlation also reveals in other lower order spectra, though their complexity in the spectrum makes the assignment difficult. The number of four-quantum transitions (five expected for uncorrelated and seven for correlated motion) provides a ready test of the limits for two methyl groups.

We shall also discuss the intermediate case, namely, when the inverse of the correlation time of gearing motion is comparable to the dipole coupling strength.

We should expect that the two distant methyl groups will rotate or reorient independently. Yet, if we bring these two groups closer, their mutual interaction will force them to move in a copperative way. This kind of correlated motion is very interesting. We shall see how the correlated motion affects both molecular symmetry and multiple quantum NMR spectra.

Let us now consider a system of two methyl groups as is shown in Figure V.1a. For the uncorrelated case, these two methyl groups move independently; their relative orientations are random. Consequently, the dipole couplings between protons of a different group are equal in average. nevertheless, this is not true if these two methyl groups move in a correlated way as do two wheels in gear. Although each methyl group rotates very fast about its three-fold axis, their relative orientation is in good order--as we have shown in Figure V.1b. The methyl group on the left rotates clock-wise, however, the right one rotates counterclockwise. A complete correlation signifies that the gearing motion is not interrupted.

Let us define several dipole coupling constants according to the top configuration of the Figure V.Ib as

$$\begin{aligned} a &= D_{24} = D_{34} \\ b &= D_{14} = D_{25} = D_{36} \\ c &= D_{35} = D_{26} \\ d &= D_{16} = D_{15} \quad . \end{aligned} \tag{V.I}$$

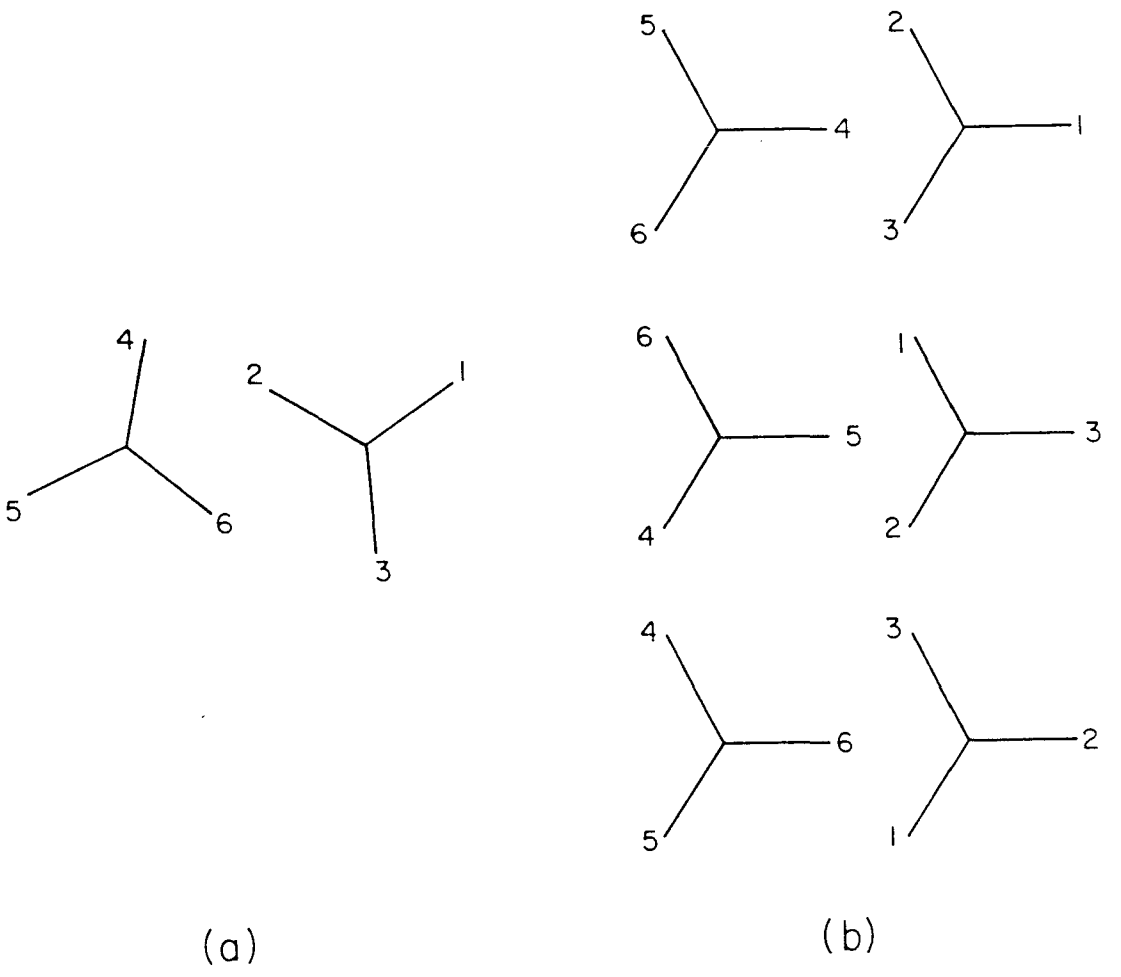

XBL 7912-5207

Figure V.1a The geometry of two adjacent methyl groups. In the case of uncorrelated motion the two methyl groups move independently. On the average, the couplings between protons belonging to different methyl groups are equal. Figure V.1b With gearing motion, the averaged coupling between protons 1 and 4 is not equal to the coupling between 1 and 5. Thus, there are two intermethyl couplings and one intramethyl coupling.

The time-averaged dipole coupling strengths are averaged over the three possible orientations as in Figure V.1b, and they are

$$w = \langle D_{24} \rangle = \langle D_{34} \rangle = \langle D_{25} \rangle = \langle D_{36} \rangle = \langle D_{16} \rangle = \langle D_{15} \rangle$$

$$= \frac{1}{3} (a + b + d) \quad . \tag{V.3}$$

As a result, there are two different intermethyl dipole coupling constants for the correlated motion.

If the motion is not correlated, we need to average the dipole couplings over an additional six different orientations. We shall find that all of the intermethyl dipole couplings are equal and have a value of

$$x = \frac{1}{3} (v + 2w) = \frac{1}{3} (2a + 3b + 2c + 2d) \quad . \tag{V.4}$$

For both cases, the intramethyl dipole couplings are all equal since each methyl group is identical; also, the distance between protons of same group is equal.

The difference in the number of intermethyl dipole couplings has a striking effect on the symmetry and the NMR spectrum, and will be discussed extensively later.

We shall use a simple rule and diagram representations to find out the number of possible four, five, and six-quantum transitions for the system of two-methyl groups. The rule is stated as:[3]

The number of n-quantum transitions is given by the number of combinations of non-equivalent configurations. For a system

of N coupled spin-1/2 particles, the rule holds only for N, N-1, and N-2 quantum transitions. The rule is based on the group theory and holds exactly for the transitions within the manifold of totally symmetric representation. It turns out that the N, N-1, and N-2 quantum transitions are of totally symmetric representation.

As illustrated in Figure V.2, there is only one six-quantum transition, since it connects the state with all spins up and the state with all the spins down. A similar argument can be applied to the five-quantum transitions. There is only one configuration with one spin down. The location of the down spin at any one of the six different sites is equal. Therefore, there are two five-quantum transitions. For each case of correlated and uncorrelated motion, the number of six and five-quantum transitions is the same.

As shown in Figures V.3 and V.4, there are seven four-quantum transitions for correlated motion and five four-quantum transitions for uncorrelated motion. The difference results from the way we assign the two down or up spins. For the case of uncorrelated motion, there is only one intermethyl coupling. The assignment with one of the two down (or up) spins to each separate methyl group is equal. Nevertheless, it is not the case for a correlated motion that has two intermethyl couplings. As we discussed before, the averaged couplings $\langle D_{14} \rangle$ and $\langle D_{15} \rangle$ are not equal. As a consequence, the configuration with spins 1 and 4 down is not equal to the configuration with spins 1 and 5 down. Therefore, there are two additional transitions for the correlated motion.

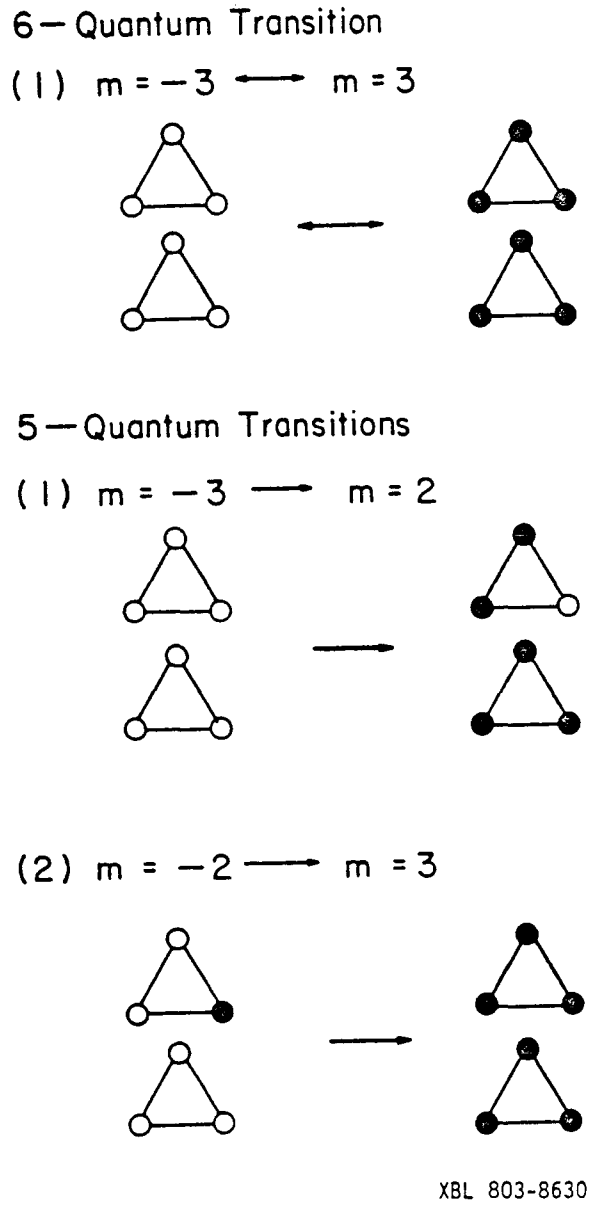

Figure V.2 Diagrams representing multiple quantum transitions. Full (empty) circles represent up (down) spins. There is only one 6-quantum transition and two 5-quantum transitions for both correlated and uncorrelated motion.

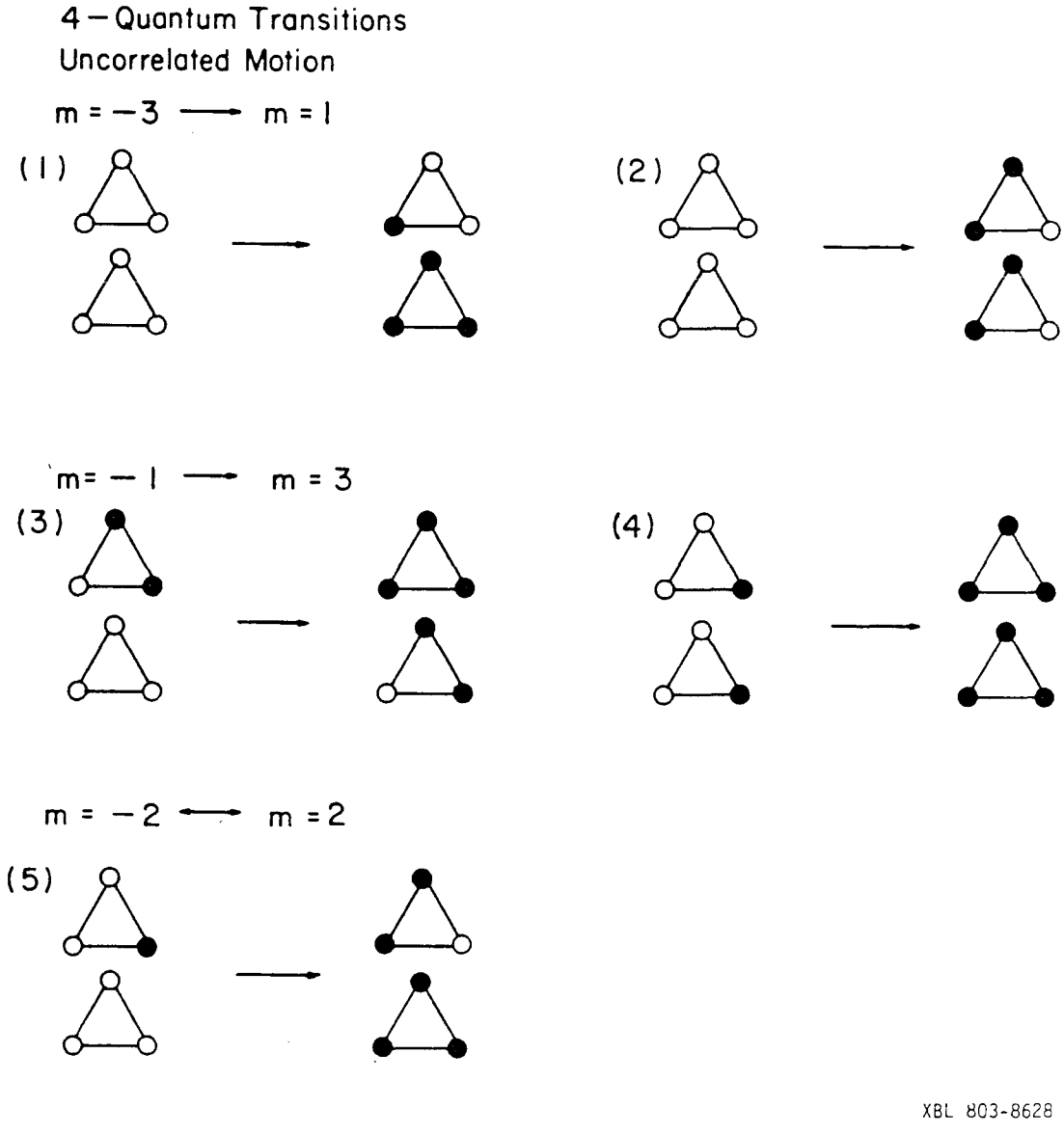

Figure V.3 Allowed 4-quantum transitions for two methyl groups with uncorrelated motion. There are five 4-quantum transitions.

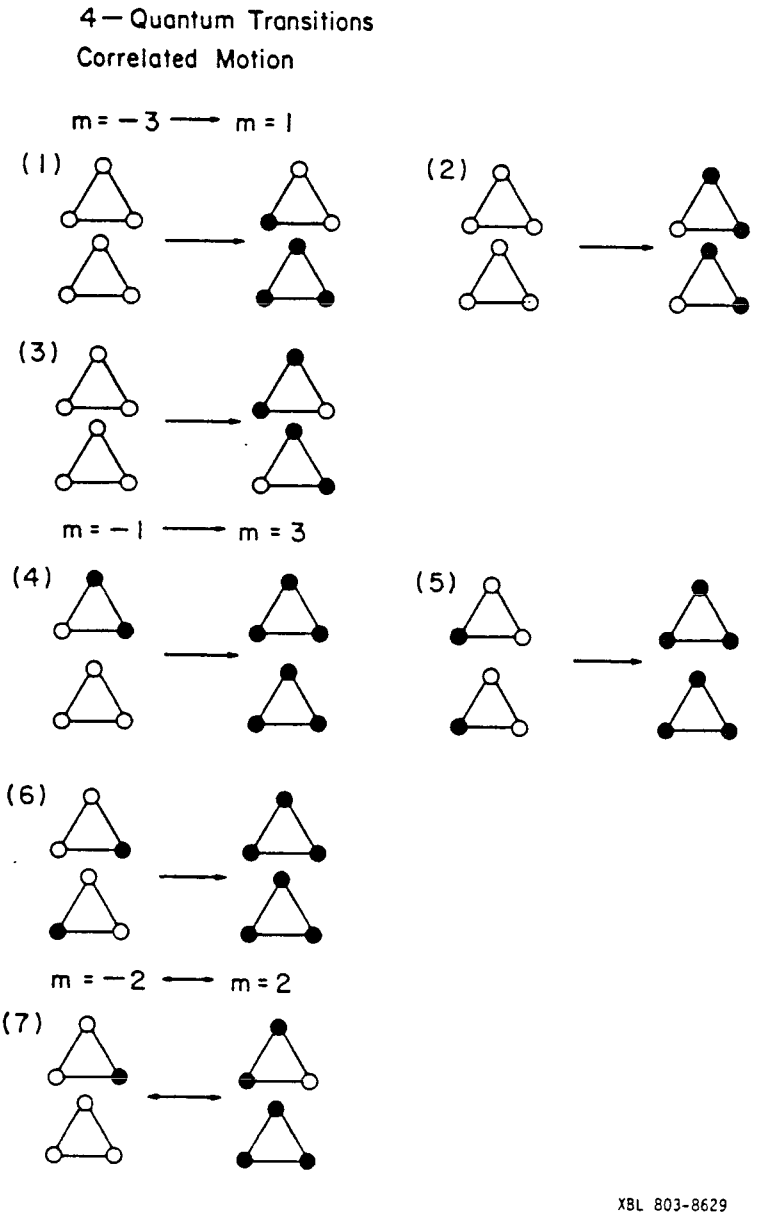

Figure V.4 Allowed 4-quantum transitions for the case of correlated motion. Seven 4-quantum transitions are expected. Since there are two intermethyl couplings, the configuration in (2) is different from the configuration in (3).

The four-quantum spectrum provides a direct and ready test of the limits for the motion of two methyl groups.

5.2 Two methyl groups in correlated motion

The symmetry group for two methyl groups in correlated motion is isomorphic to the symmetry group of cyclopropane molecule.[4] In the molecule of cyclopropane as we have shown in Figure V.5, the dipolar couplings D_{14}, D_{25}, and D_{35} are all equal and different than the value of D_{24}, D_{34}, D_{25}, D_{36}, D_{16} or D_{15}. Since there is a one-to-one correspondence between the dipolar couplings for cyclopropane molecule and the two correlated methyl groups, we do not need to find the symmetry group for the latter case from the first principle. Instead, we can use the symmetry group D_{3h} of cyclopropane for it.

Using the characteristic table for D_{3h} group,[5] we can decompose the eigenstates of m-quantum manifold into several irreducible representations. The result is shown as follows,

$$m = 3 \qquad A_1'$$

$$m = 2 \qquad A_1' + A_2'' + E' + E''$$

$$m = 1 \qquad 3A_1' + A_1'' + A_2'' + 3E' + 2E''$$

$$m = 0 \qquad 3A_1' + A_1'' + A_2' + 3A_2'' + 3E'' \quad .$$

The states with negative quantum number m have the same decomposition as their mirror states with positive m. With the above decomposition, we can construct the energy-level diagram as shown in Figure V.6.

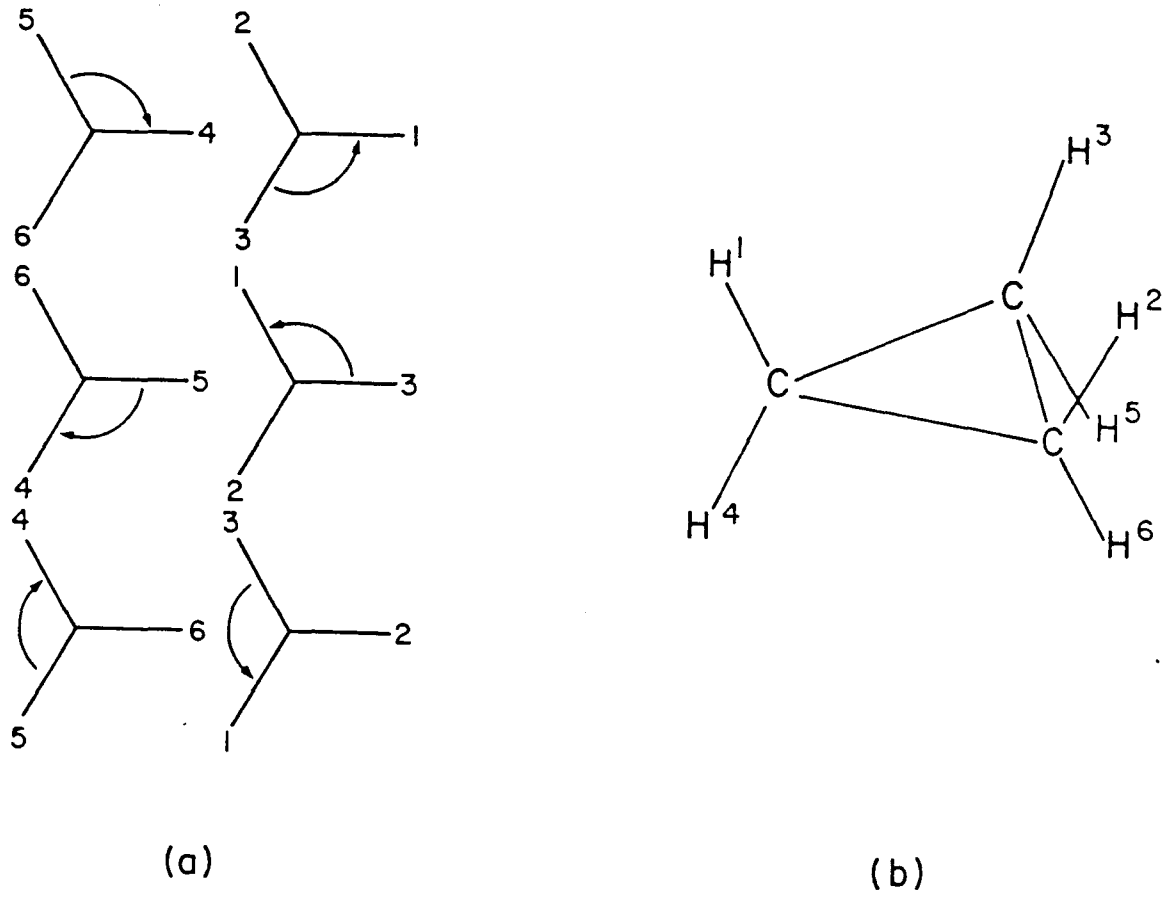

Figure V.5 (a) Methyl groups in correlated motion. (b) The symmetry group for the system in (a) is isomorphic to the symmetry group of cyclopropane. The average coupling constants $\langle D_{14} \rangle$ and $\langle D_{15} \rangle$ are different.

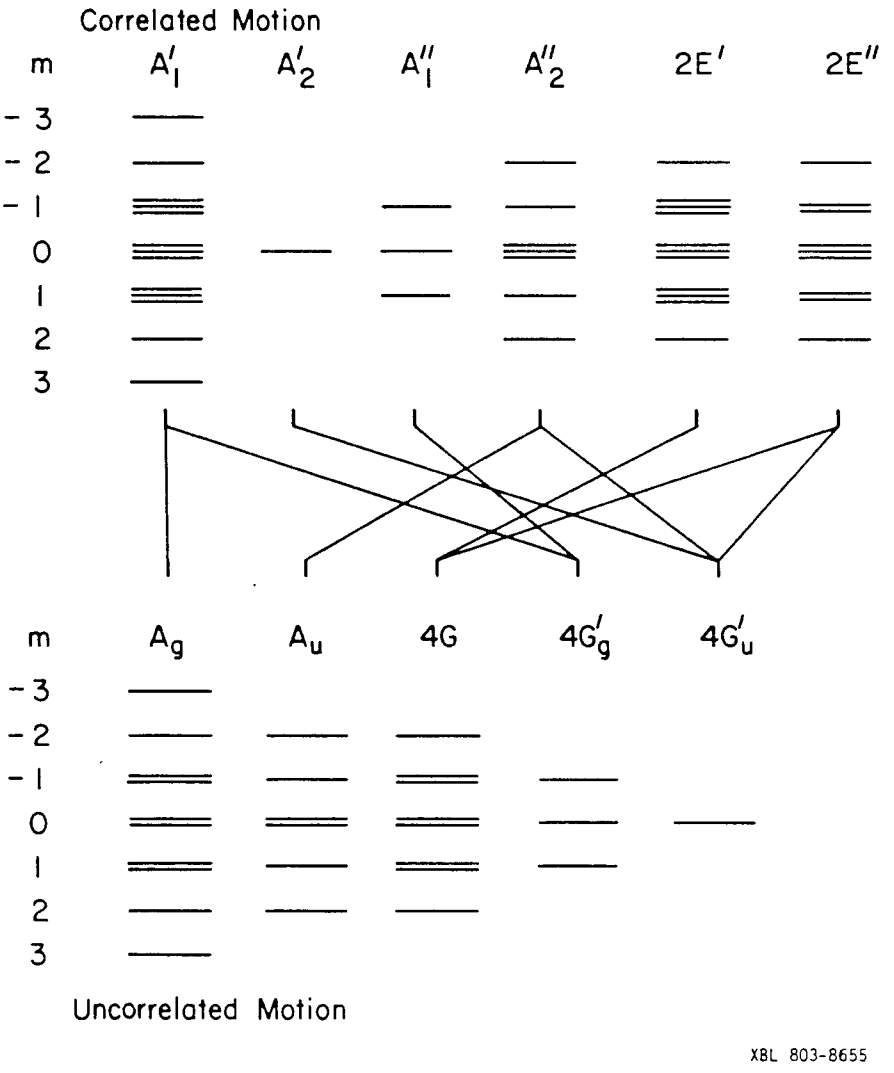

Figure V.6 Energy level diagrams for two methyl groups in correlated motion or uncorrelated motion. The number of multiple quantum transitions can be found from the diagrams. There are one 6-quantum, two 5-quantum transitions for both cases, but five 4-quantum transitions for uncorrelated motion, and seven for correlated motion.

There are one six-quantum transition $A_1'(m=-3) \rightarrow A_1'(m=3)$, and two five-quantum transitions $A_1'(m=-3) \rightarrow A_1'(m=2)$, $A_1'(m=-2) \rightarrow A_1'(m=3)$. These transitions are of A_1' type. Any pair of mirror states has a similar dipolar energy shift. The transition between the two occurs at the center of the corresponding m-quantum domain, and does not contain information about dipolar coupling. The four-quantum transitions of $A_1'(-2) \rightarrow A_1'(2)$, $A_2''(-2) \rightarrow A_2''(2)$, $2E'(-2) \rightarrow 2E'(2)$, and $2E''(-2) \rightarrow 2E''(2)$ are mirror-state transitions. They are located at the center of 4-quantum domain. Yet, there are three pairs of transitions $3A_1'(-1) \rightarrow A_1'(2)$, $A_1'(-2) \rightarrow 3A_1'(1)$, which have a non-zero frequency shift. Consequently, there are seven four-quantum transitions. The three pairs of A_1'-type transition appears on each side, and the central peak consists of several degenerate transitions of a different type.

The dipole-dipole interaction Hamiltonian H of two methyl groups in correlated motion is given by

$$H = H_u + H_v + H_w$$

$$= u \sum_{i<j} U_{ij} + v \sum_{i<j} V_{ij} + w \sum_{i<j} W_{ij} \quad . \qquad (V.5)$$

H_u is the Hamiltonian for the intramethyl dipolar interaction, H_v and H_w are the intermethyl dipolar Hamiltonian. The blinear operators U_{ij}, V_{ij}, and W_{ij} are given by the same form as

$$U_{ij},\ V_{ij},\ W_{ij} = I_{iz}I_{jz} - \frac{1}{4}\left(I_{i+}I_{j-} + I_{i-}I_{j+}\right) \quad . \qquad (V.6)$$

The indices i and j refer to different sets of protons as follows,

$$U_{ij}: \quad (i,j) = (1,2),\ (1,3),\ (2,3),\ (4,5),\ (4,6),\ (5,6)$$

$$V_{ij}: \quad (i,j) = (1,4),\ (2,6),\ (3,5)$$

$$W_{ij}: \quad (i,j) = (2,4),\ (3,4),\ (1,5),\ (2,5),\ (1,6),\ (3,6) \quad .$$

We can show that

$$H|A_1'(3)\rangle = H|\alpha\alpha\alpha\alpha\alpha\alpha\rangle = (\frac{3}{2}u + \frac{3}{4}v + \frac{3}{2}w)\ |A_1'(3)\rangle \qquad (V.7)$$

and

$$H|A_1'(2)\rangle = H\ \frac{1}{\sqrt{6}}\ (|1\rangle + |2\rangle + |3\rangle + |4\rangle + |5\rangle + |6\rangle$$

$$= 0 \quad , \qquad (V.8)$$

where state $|i\rangle$ means the state with all spins up except i-th spin.

The eigenenergies for the triplet of $A_1'(1)$ can be found by matrix diagonalization of

$$H = \begin{pmatrix} -\frac{v}{4} - \frac{w}{2} & -\frac{w}{\sqrt{2}} & -\frac{v}{2} - \frac{w}{2} \\ -\frac{w}{\sqrt{2}} & -\frac{u}{2} + \frac{3}{4}v - \frac{w}{2} & -\frac{u}{\sqrt{2}} \\ -\frac{v}{2} - \frac{w}{2} & -\frac{u}{\sqrt{2}} & -u - \frac{v}{4} + \frac{w}{2} \end{pmatrix}, \qquad (V.9)$$

and will be discussed later in the section on partially correlated motion.

5.3 Two methyl groups in uncorrelated motion

The symmetry group for each methyl group is D_3. The molecule with two non-equivalent methyl groups (AA'A"BB'B") forms a symmetry group by the direct product of two D_3 groups. It is represented by

$$(A_1 + 2E) \times (A_1 + 2E)$$

$$= A_1 \times A_1 + 2A_1 \times E + 2E \times A_1 + 4E \times E \quad . \qquad (V.10)$$

If two methyl groups are identical, we should include the permutation symmetry that they share and introduce the symmetric or anti-symmetric form for the wavefunction. The representations A_g, A_u signify the symmetric and antisymmetric wavefunctions of $A_1 \times A_1$ type. Similarly, we should classify the four-fold degenerate representation $4(E \times E)$ by $4G_g'$ and $4G_u'$. The two doubly degenerate representations $2A_1 \times E$ and $2E \times A_1$ are put together to form a new representation 4G. We can decompose the total 2^6 spin states into irreducible representations A_g, A_u, 4G, $4G_g'$ and $4G_u'$ as shown in Figure V.6.

By decomposing the representations of D_{3h} for the correlated motion into the new representations above, we can obtain the information about the correlation between these two symmetry groups. The correlation diagram is also shown in Figure V.6. For example, representation A_1' is the direct sum of A_g and G_g'. Since G_g' does not have states with m = 2 or 3, states $A_1'(2)$ and $A_1'(3)$ are simply the states $A_g(2)$ and $A_g(3)$. In the cases of partially correlated and uncorrelated motion, the correlated motion is frequently

interrupted. The triplets of $A_1'(1)$ are no longer pure states and are mixed with different representations A_g and G_g'. The corresponding four-quantum transitions become broadened once phase interruption sets in. The five and six-quantum transitions, however, remain unaffected because their associated states are pure states. We shall discuss the effects of phase interruption on multiple quantum spectrum later in more detail.

As we found in the previous figure for uncorrelated motion, there are one six-quantum transition $A_g(-3) \rightarrow A_g(3)$, and two five quantum transitions $A_g(-2) \rightarrow A_g(3)$, $A_g(-3) \rightarrow A_g(2)$. The transitions $A_g(-2) \rightarrow A_g(2)$, $A_u(-2) \rightarrow A_u(-2)$, and $4G(-2) \rightarrow 4G(2)$ are all degenerate because they are transitions between mirror states. There are two pairs of transitions $2A_g(-2) \rightarrow A_g(1)$, $A_g(-1) \rightarrow 2A_g(2)$, and they have non-zero frequency shift. As a consequence, there are five four-quantum transitions derived from the simple rule for counting the number of N-2 quantum transitions.

The dipole-dipole interaction Hamiltonian H of two uncorrelated methyl groups is given by

$$H = H_u + H_v \quad . \tag{V.11}$$

It is a special case of Eq. (V.5), when we make the coupling constants v and w equal. The Hamiltonian H_v describes the dipolar coupling between protons of different methyl groups. We can show that

$$H|A_g(3)\rangle = (\frac{3}{2}u + \frac{9}{4}v) \quad A_g(3) \quad , \tag{V.12}$$

$$H|A_g(2)> = 0 \quad . \tag{V.13}$$

The eigenenergy for the doublet of $A_g(1)$ can be found by diagonalizing a 2 x 2 matrix, and is given by

$$\lambda_{\pm} = -\frac{3}{4}u - \frac{1}{4}v \pm \frac{1}{2}\left(\frac{9}{4}u^2 + 7u^2 - 3uv\right)^{1/2} \quad . \tag{V.14}$$

As a consequence, the dipolar frequency shifts in the five and four-quantum spectra are given by

$$\Delta m = 5 \; : \; \pm \left(\frac{3}{2}u + \frac{9}{4}v\right) \quad , \tag{V.15}$$

$$\Delta m = 4 \; : \; \pm \left(\frac{9}{4}u + \frac{5}{2}v \pm \frac{1}{2}\left(\frac{9}{4}u^2 + 7v^2 - 3uv\right)^{1/2}\right). \tag{V.16}$$

From experimental four-quantum spectra, five-quantum spectra, and the above relation, we can specifically determine the coupling strength u and v.

5.4 Experiments

We have shown earlier that the high n-quantum spectra distinguish simply between the cases of uncorrelated motion (independent rotation) and correlated motion (geared rotation). For N spins we can show that the N-2 quantum spectrum is sensitive to the two-body correlations and has many triplets equal to the number of different dipole couplings, (that is, the number of different pairs of spins).[3] For the system of two methyl groups, we should make a distinction in the four-quantum spectrum between these two cases.

The extent of the correlated motion that two adjacent rotating methyl groups have is determined by the potential barrier of the

coupling, and by the temperature of observation. The lifetime τ_c characterizes the duration of the correlation and may be classified into three main categories: (1) completely uncorrelated motion ($\tau_c^{-1} >> 10$ kHz), (2) completely correlated motion ($\tau_c^{-1} << 0.1$ kHz), and (3) the intermediate case. The time scale defined here refers to the magnitude of the dipolar splittings.

For example, a sample of 2,3-dimethylmaleic anhydride (30% in mole), dissolved in a liquid crystal solvent of p-octylphenyl 2-chloro-4-(p-heptybenzoxyloxy) benzoate, was studied by using multiple quantum NMR techniques in a magnetic field of 42.5 KG at 50.0°C.

An ensemble average process was performed on the multiple quantum spectra. By using the TPPI method we were able to take the average of each magnitude spectra. The various preparation periods, ranged from 1.0 msec to 7.0 msec. The experimental multiple quantum spectra of four, five, and six-quantum regions are shown in Figure V.7.

Assuming that the intramethyl dipolar coupling constant u is equal to 2.00 kHz and that intermethyl coupling constant v is equal to -0.59 kHz the spectra are best fitted with the model of completely uncorrelated motion. The calculated stick spectrum using above parameters is shown in Figure V.7; it is in agreement with the experimental spectra.

The molecule of 1,8-dimethylnaphthalene, with two methyl groups in closer position, was studied. The experimental spectra of multiple quantum transitions are shown in Figures V.8 and V.9. The calculated stick spectrum assuming uncorrelated motion is also

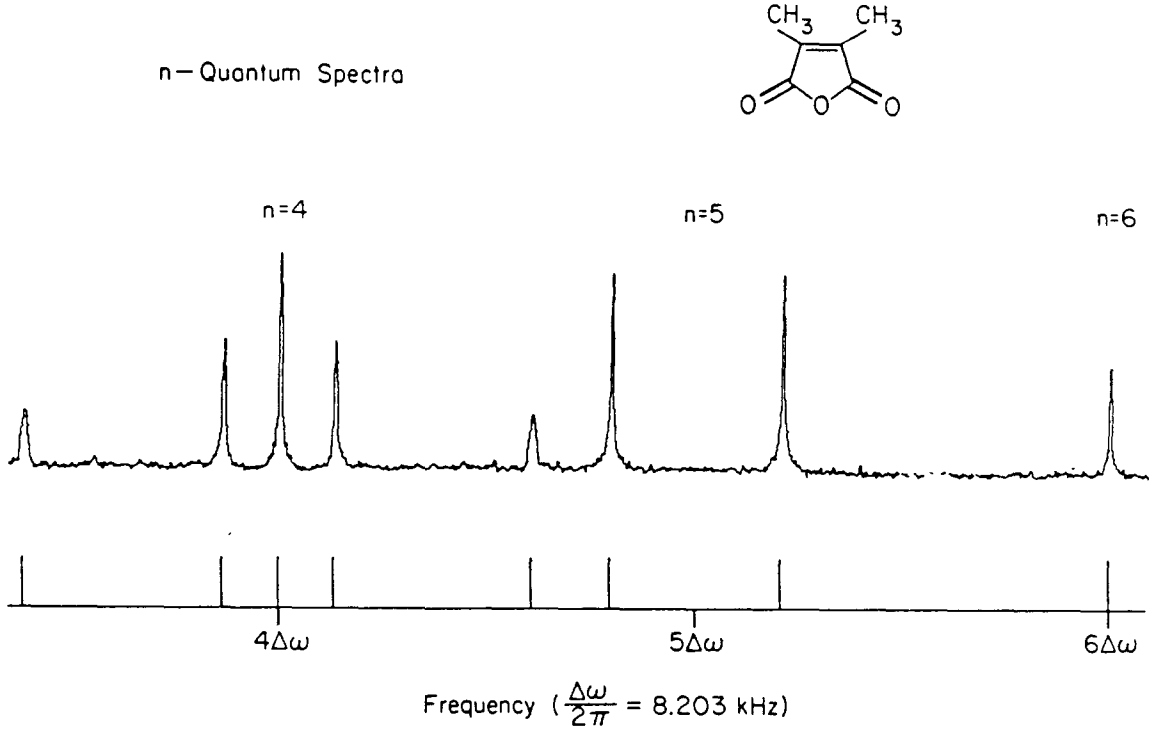

Figure V.7 (a) Spectrum of 4, 5, and 6-quantum transitions in dimethyl maleic anhydride. Five of the 4-quantum transition were observed. (b) Calculates stick spectrum assuming uncorrelated motion with intramethyl coupling constant equal to 2.00 kHz and intermethyl coupling constant equal to -0.59 kHz.

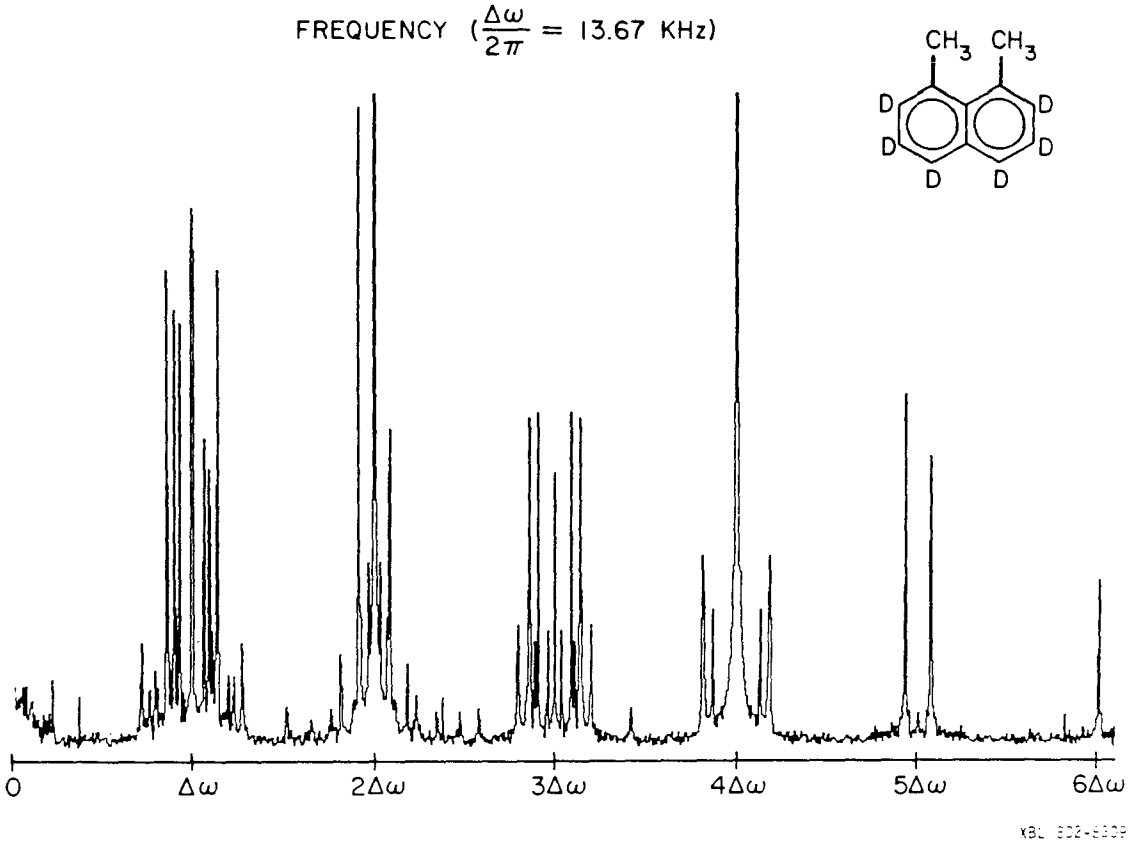

Figure V.8 Multiple quantum spectra of 1,8-dimethylnaphthalene with ring protons deuterated.

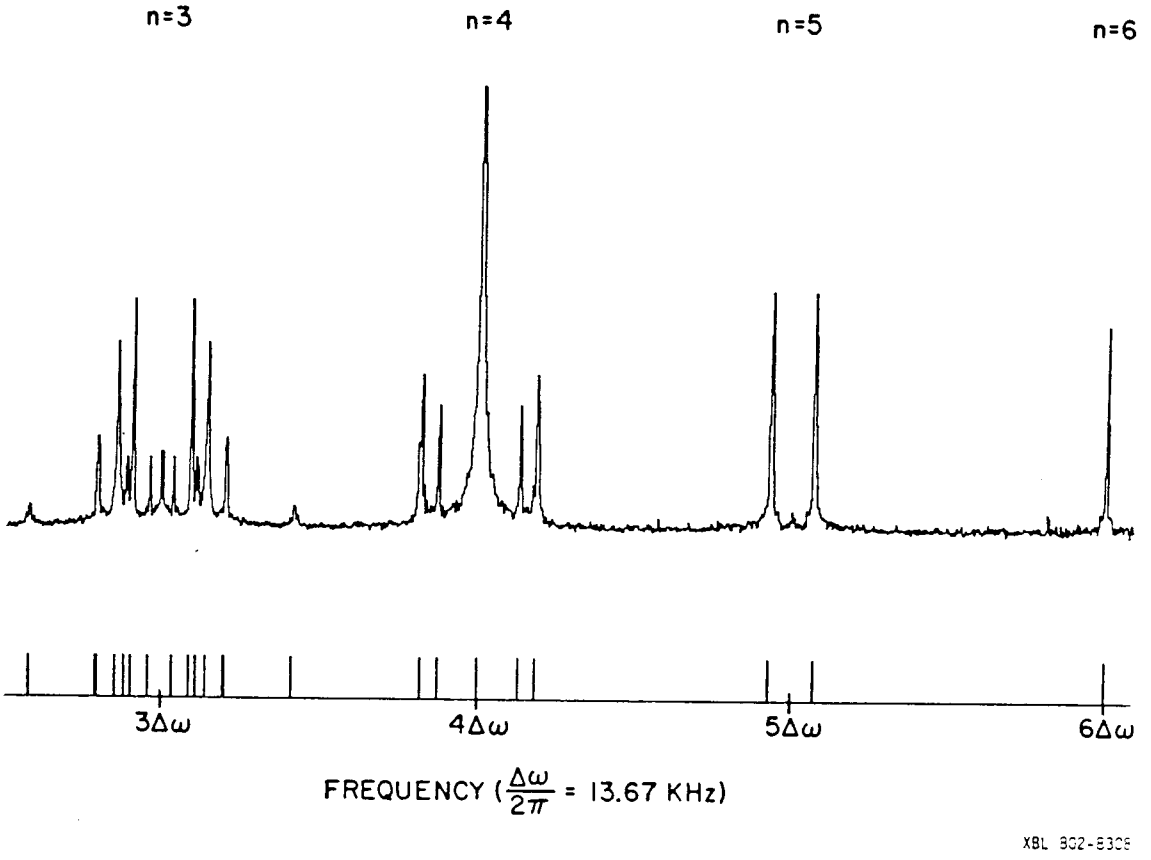

Figure V.9 The top figure shows the experimental spectra of 3, 4, 5, and 6-quantum transitions of 1,8-dimethylnapthalene. The lower stick spectra are obtained by assuming uncorrelated motion.

in agreement with the experimental spectra.

5.5 Partially correlated motion and chemical exchange process

5.5.1 Chemical exchange for J-coupled AB system

Besides nuclear magnetic relaxation, the molecular motion also affects its NMR lineshapes. NMR has been a successful tool in studying chemical exchange processes. In this section we shall illustrate the first application of multiple quantum NMR study of exchange process among two methyl groups as caused by steric hindrance. Before any further discussion, however, we shall demonstrate how to apply density formalism to the study of a simple chemically exchanging system.

The motion equation of the density matrix ρ for a chemically exchanging system is given by[6]

$$\frac{d}{dt}\rho = i[\rho,H] + \frac{1}{\tau}(R\rho R^{+}-\rho) \qquad (V.17)$$

where we neglect the T_2 relaxation caused by other mechanisms.

The first term on the right-hand side is familiar. The second term describes the effect of the chemical exchange on the evolution of the density matrix. The unitary operator R is the exchange operator that connects the various states or configurations caused by chemical exchange with a correlation time τ. The inverse of the correlation time is also known as the exchange rate. For the system of no chemical exchange, the operator R is a unity operator; consequently, the second term on the right-hand side of eq. (V.17) is, as we expected, identical to zero.

By using the projector operator $U_{\alpha\beta} = |\alpha><\beta|$, we can expand

the density matrix ρ into its components as

$$\rho(t) = \sum \rho_{\alpha\beta} U_{\alpha\beta} \quad . \tag{V.18}$$

The equation of motion for any particular matrix element of $\rho(t)$ is given by

$$\begin{aligned} \frac{d}{dt}\rho_{\alpha\beta} &= -i\,\omega_{\alpha\beta}\rho_{\alpha\beta} - \frac{1}{\tau}\left(\rho_{\alpha\beta} - \sum_{\alpha',\beta'} \rho_{\alpha'\beta'}\, R_{\alpha\alpha'}\, R^{+}_{\beta'\beta}\right) \\ &= -i\,\omega_{\alpha\beta}\rho_{\alpha\beta} - \frac{1}{\tau}\left(1 - R_{\alpha\alpha}R^{+}_{\beta\beta}\right) \\ &\quad + \frac{1}{\tau} \sum_{\substack{\alpha'\beta' \\ (\alpha'\neq\alpha,\,\beta'\neq\beta)}} \rho_{\alpha'\beta'}\, R_{\alpha\alpha'}\, R^{+}_{\beta'\beta} \quad . \end{aligned} \tag{V.19}$$

For the case of non-degenerate transitions, namely, $|\omega_{\alpha'\beta'} - \omega_{\alpha\beta}|\tau >> 1$, the last term of the above equation is very small and may be neglected because it consists of components that oscillate very fast in time.

As a result, the evolution of element $\rho_{\alpha\beta}$ is not coupled to other components and is given by

$$\begin{aligned} \frac{d}{dt}\rho_{\alpha\beta} &= -i\omega_{\alpha\beta}\rho_{\alpha\beta} - \frac{1}{\tau}\rho_{\alpha\beta}\left(1 - R_{\alpha\alpha}R^{+}_{\beta\beta}\right) \\ &= -(i\omega_{\alpha\beta} + \Gamma_{\alpha\beta})\rho_{\alpha\beta} \quad , \end{aligned} \tag{V.20}$$

or

$$\rho_{\alpha\beta}(t) = \rho_{\alpha\beta}(0)\, \exp(-i\omega_{\alpha\beta}t - \Gamma_{\alpha\beta}t) \quad , \tag{V.21}$$

where

$$\Gamma_{\alpha\beta} = (1-R_{\alpha\alpha}R^{+}_{\beta\beta})/\tau \quad .$$

If there is only one other quasi-degenerate transition between states $|\alpha'>$ and $|\beta'>$, i.e., $|\omega_{\alpha'\beta'}-\omega_{\alpha\beta}|\tau \lesssim 1$, the equations of motion for $\rho_{\alpha\beta}$ and $\rho_{\alpha'\beta'}$ are coupled and are given by

$$\begin{cases} \dfrac{d}{dt}\rho_{\alpha\beta} = -(i\omega_{\alpha\beta} + \dfrac{1-R_{\alpha\alpha}R^{+}_{\beta\beta}}{\tau})\rho_{\alpha\beta} + \dfrac{1}{\tau} R_{\alpha\alpha'}R^{+}_{\beta'\beta'}\rho_{\alpha'\beta'} \quad , \\ \dfrac{d}{dt}\rho_{\alpha'\beta'} = -(i\omega_{\alpha'\beta'} + \dfrac{1-R_{\alpha'\alpha'}R^{+}_{\beta'\beta'}}{\tau})\rho_{\alpha'\beta'} + \dfrac{1}{\tau} R_{\alpha'\alpha}R^{+}_{\beta\beta'}\rho_{\alpha\beta} \quad . \end{cases} \tag{V.22}$$

We can obtain the eigenfrequencies by solving the secular equation. The result is given by

$$\begin{aligned} \lambda_{\pm} = &- \frac{i}{2}(\omega_{\alpha\beta}+\omega_{\alpha'\beta'}) - \frac{1}{2\tau}(2 - R_{\alpha\alpha}R^{+}_{\beta\beta}-R_{\alpha'\alpha'}R^{+}_{\beta'\beta'}) \\ &\pm \frac{1}{2}\{[i(\omega_{\alpha\beta}-\omega_{\alpha'\beta'}) - \frac{1}{\tau}(R_{\alpha\alpha}R^{+}_{\beta\beta}-R_{\alpha'\alpha'}R^{+}_{\beta'\beta'})]^2 \\ &+ \frac{4}{\tau^2} R_{\alpha\alpha'}R_{\alpha'\alpha}R^{+}_{\beta'\beta}R^{+}_{\beta\beta'}\}^{1/2} \quad . \end{aligned} \tag{V.23}$$

We shall now discuss two extreme cases which have simpler results:

(i) Slow exchange limit (very large τ).

In this case, we may neglect all of the higher order terms except terms that contain $1/\tau$. We can show

$$\lambda_{\pm} \simeq \begin{cases} -i\omega_{\alpha\beta} - \dfrac{1}{\tau}(1-R_{\alpha\alpha}R_{\beta\beta}) \\ -i\omega_{\alpha'\beta'} - \dfrac{1}{\tau}(1-R_{\alpha'\alpha'}R_{\beta'\beta'}) \end{cases} \quad . \tag{V.24}$$

This is just the case of non-degenerate transitons.

(ii) Fast exchange limit (very short τ).

We can show that there are two eigenfrequencies and they are given by

$$\lambda_{\pm} \simeq -\frac{i}{2}(\omega_{\alpha\beta}+\omega_{\alpha'\beta'}) \pm \frac{1}{\tau}(R_{\alpha\alpha'}R_{\alpha'\alpha}R^{+}_{\beta'\beta}R^{+}_{\beta\beta'})^{1/2} - \frac{1}{2\tau}(2-R_{\alpha\alpha}R^{+}_{\beta\beta}-R_{\alpha'\alpha'}R^{+}_{\beta'\beta'}) \quad . \tag{V.25}$$

One of the above solutions with positive sign in $1/\tau$ corresponds to exponentially increasing function in time. It is a non-physical solution and should be omitted. The other solution is physical and it indicates that two separate peaks in the slow exchange limit will coalesce into one peak in the fast exchange limit. The new resonant frequency is the average of the two.

For example, we shall discuss the exchange system of two J-coupled unlike spin-1/2 particles. The energy diagrams for both slow and fast exchange limits are shown in Figure V.10. The eigenstates and eigenfrequencies for slow exchange limit are listed as follows:

$$|1\rangle = |\alpha\alpha\rangle \qquad E_1 = \nu_0[1-\tfrac{1}{2}(\sigma_A+\sigma_B)] + \tfrac{1}{4}J \quad ,$$

$$|2\rangle = \cos\theta|\alpha\beta\rangle + \sin\theta|\beta\alpha\rangle \qquad E_2 = -\frac{J}{4} + \frac{1}{2}\sqrt{(\nu_0\delta)^2+J^2} \quad ,$$

$$|3\rangle = -\sin|\alpha\beta\rangle + \cos\theta|\beta\alpha\rangle \qquad E_3 = -\frac{J}{4} - \frac{1}{2}\sqrt{(\nu_0\delta)^2+J^2} \quad ,$$

$$|4\rangle = |\beta\beta\rangle \qquad E_4 = -\nu_0[1-\tfrac{1}{2}(\sigma_A+\sigma_B)] + \tfrac{1}{4}J \quad , \tag{V.26}$$

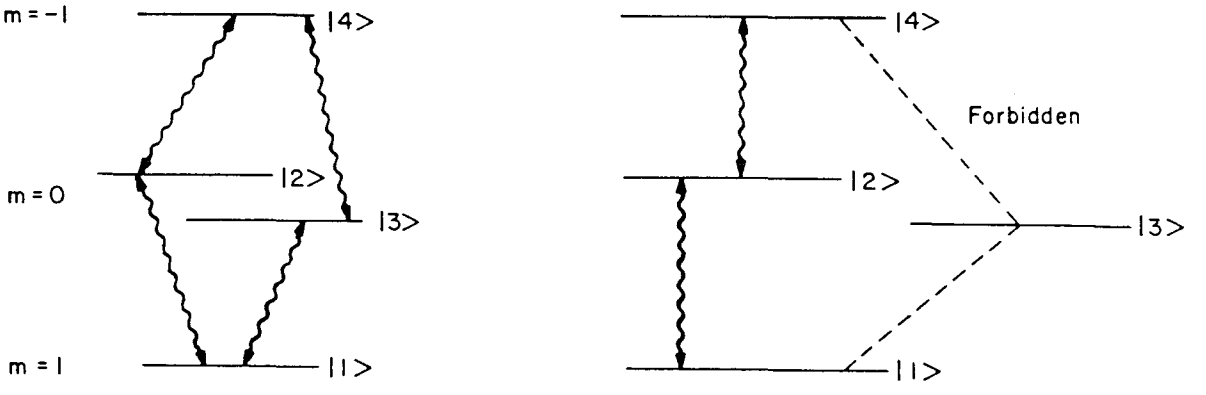

Figure V.10 Energy level diagrams for a J-coupled AB system undergoing chemical exchange, (a) for slow exchange and (b) for fast exchange. There are four single quantum transitions for the slow exchange case. Only one transition is expected for a fast exchange, because the transitions $|2\rangle \rightarrow |4\rangle$, $|1\rangle \rightarrow |2\rangle$ are degenerate, and $|3\rangle \rightarrow |4\rangle$, $|1\rangle \rightarrow |3\rangle$ are forbidden.

where $\delta = \sigma_B - \sigma_A$ and $\tan 2\theta = J/\delta\nu_0$.

Similarly, for the case of a fast exchange limit, we can show

$$|1\rangle = |\alpha\alpha\rangle \qquad E_1 = \nu_0(1-\sigma) + \frac{1}{4}J \ ,$$

$$|2\rangle = \frac{1}{\sqrt{2}}(|\alpha\beta\rangle + |\beta\alpha\rangle) \qquad E_2 = \frac{J}{4} \ ,$$

$$|4\rangle = |\beta\beta\rangle \qquad E_4 = -\nu_0(1-\sigma) + \frac{1}{4}J \ ,$$

$$|3\rangle = \frac{1}{2}(-|\alpha\beta\rangle + |\beta\alpha\rangle) \qquad E_3 = -\frac{3}{4}J \ , \qquad (V.27)$$

where $\sigma = \sigma_A = \sigma_B$. We notice that it is the special case with $\theta = \pi/4$.

The spectrum of the slow exchange case contains four peaks, but only contains one peak for the fast exchange case as shown in Figure V.11.. We shall use density formalism to solve the problem for the general exchange rate.

The operator R describes the exchange operation on particles between two sites. Since R does not change the magnetic quantum number, it can only connect states of the same magnetic quantum number.

We can show that the states $|1\rangle$ and $|4\rangle$ are invariant under operation R and that

$$\begin{aligned} R|2\rangle &= R(\cos\theta|\alpha\beta\rangle + \sin\theta|\beta\alpha\rangle) \\ &= \cos\theta|\beta\alpha\rangle + \sin\theta|\alpha\beta\rangle \\ &= \cos\theta(\sin\theta|2\rangle + \cos\theta|3\rangle) + \sin\theta(\cos\theta|2\rangle - \sin\theta|3\rangle) \\ &= \sin 2\theta|2\rangle + \cos 2\theta|3\rangle \ , \end{aligned} \qquad (V.28)$$

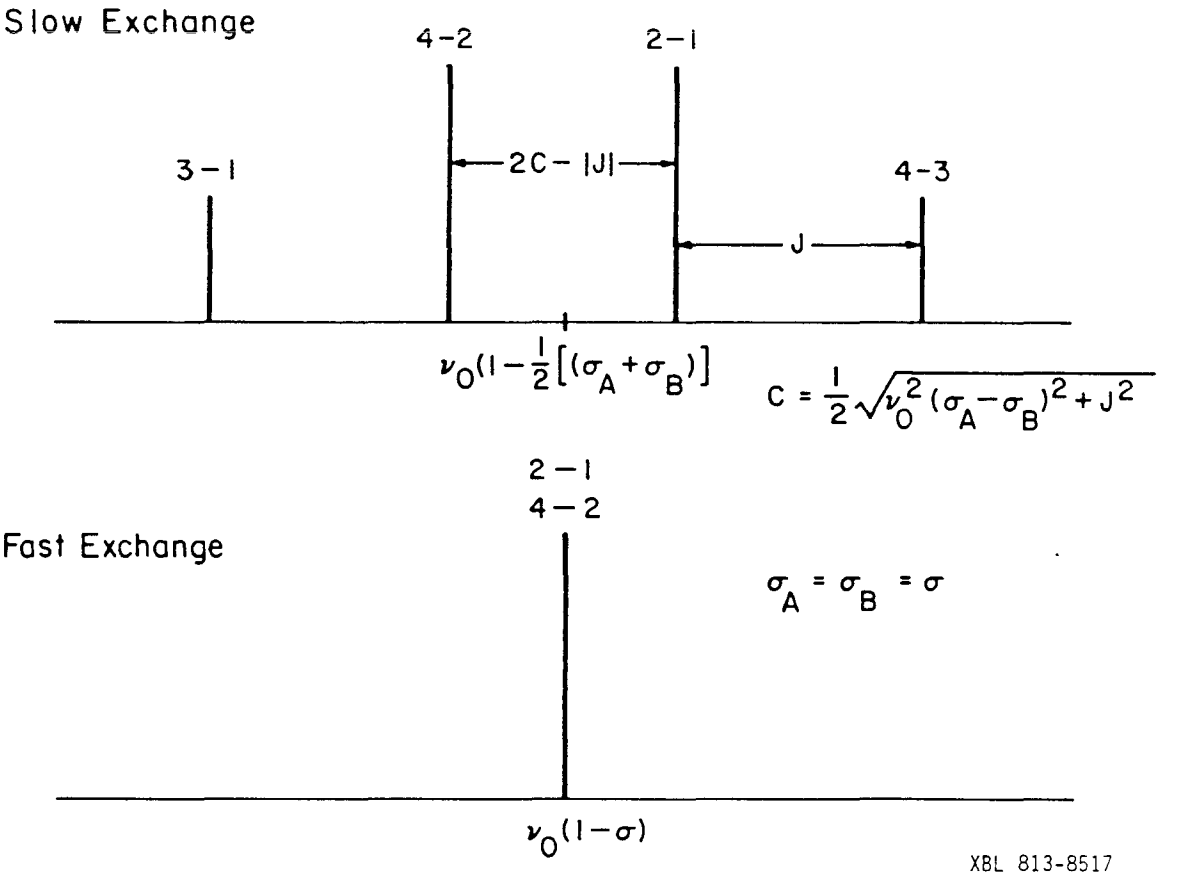

Figure V.11 Theoretical stick spectra for a J-coupled AB system undergoing chemical exchange. There are four peaks in the slow exchange limit but only one peak in the fast exchange limit.

$$R|3\rangle = -\sin\theta|\beta\alpha\rangle + \cos\theta|\alpha\beta\rangle$$

$$= \cos2\theta|2\rangle - \sin2\theta|3\rangle \quad . \tag{V.29}$$

Using $|2\rangle$ and $|3\rangle$ as a basis set, the operator R can be represented by a 2 x 2 matrix as follows

$$R = \begin{pmatrix} \sin2\theta & \cos2\theta \\ \cos2\theta & -\sin2\theta \end{pmatrix} = R^{+} \quad . \tag{V.30}$$

We can show that the equation of motion for density matrix elements ρ_{12}, ρ_{13} and ρ_{24}, and ρ_{34} are coupled and are given by

$$\begin{cases} \frac{d}{dt}\rho_{12} = -i\omega_{12}\rho_{12} - \frac{1}{\tau}\rho_{12}(1-\sin2\theta) + \frac{1}{\tau}\rho_{13}\cos2\theta \\ \frac{d}{dt}\rho_{13} = -i\omega_{13}\rho_{13} - \frac{1}{\tau}\rho_{13}(1+\sin2\theta) + \frac{1}{\tau}\rho_{12}\cos2\theta \end{cases} , \tag{V.31}$$

$$\begin{cases} \frac{d}{dt}\rho_{24} = -i\omega_{24}\rho_{24} - \frac{1}{\tau}\rho_{24}(1+\sin2\theta) + \frac{1}{\tau}\rho_{34}\cos2\theta \\ \frac{d}{dt}\rho_{34} = -i\omega_{34}\rho_{34} - \frac{1}{\tau}\rho_{34}(1-\sin2\theta) + \frac{1}{\tau}\rho_{24}\cos2\theta \end{cases} . \tag{V.32}$$

By solving the above equation for either stationary or transient conditions, we can obtain the spectrum for the general case of exchange rate. The computed spectra with various values of τ are shown in Figure V.12.

5.5.2 Two methyl groups in partially correlated motion

We shall discuss an interesting system of two methyl groups having steric hindrance. We have discussed the characteristic features between two extreme cases of completely uncorrelated

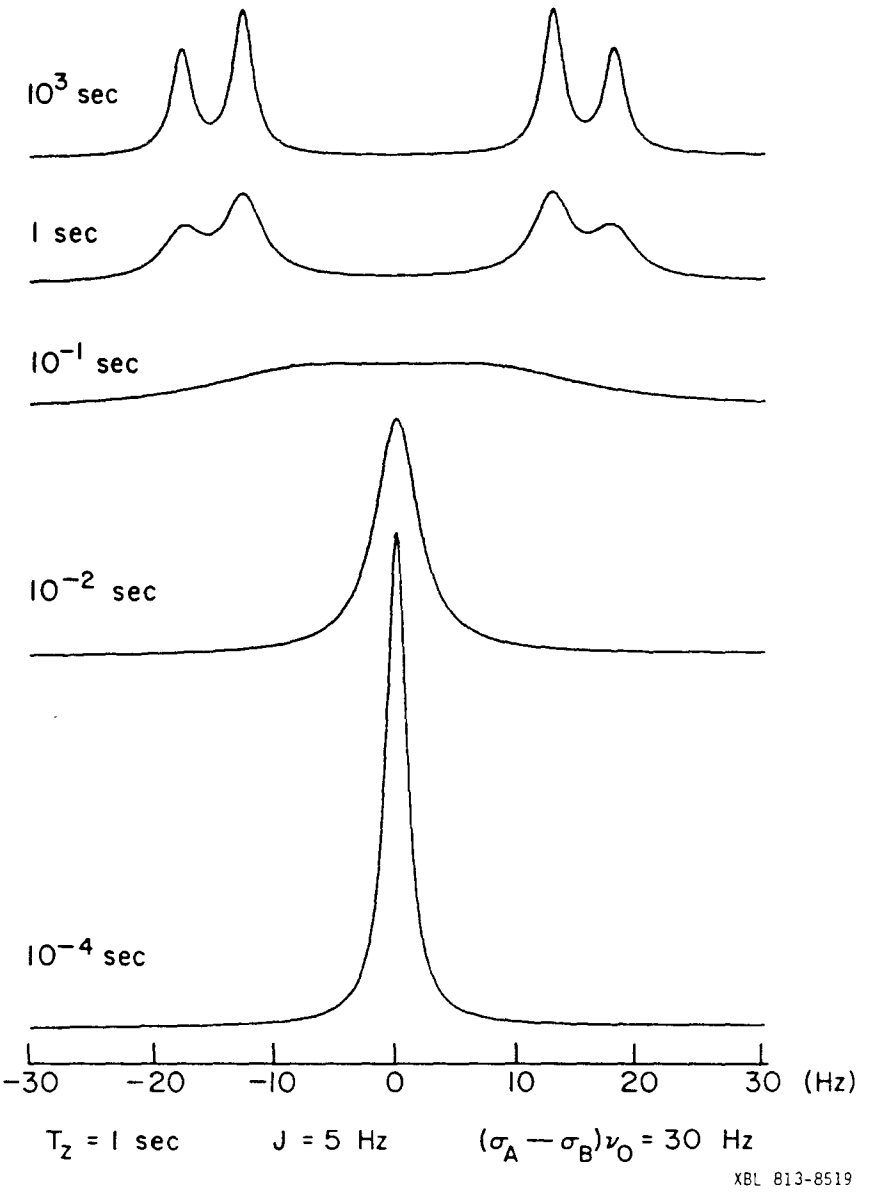

Figure V.12 Theoretical spectra of a J-coupled AB system. The molecule undergoes chemical exchange with a correlation time τ_c from 10^3 sec to 10^{-4} sec.

and completely correlated motion. Particularly, we have shown that there are five and seven peaks of 4-quantum transitions for the first and latter cases. In this section, we shall discuss the intermediate case when the exchange rate namely, the inverse of the correlation time, is comparable to the dipolar coupling strength. The six and five quantum transitions remain unchanged because the exchange operator does not affect their corresponding states. That is, states $|Ag\ (m = \pm 3)> = |A_1'\ (m = \pm 3)>$ and $|Ag\ (m = \pm 2)> = |A_1'\ (m = \pm 2)|$ are also eigenstates of the exchange operator. Since those 5- and 6-quantum spectra are invariant they are not relevant to our discussion of the exchange process. Particularly, we shall discuss how the correlated motion affects the 4-quantum spectra. The associated states of 4-quantum transitions are shown in Figure V.13. The central peak, which actually consists of several degenerate transitions, has a complicated dependence on the exchange rate and thus, will not be discussed. We shall only deal with the satellite peaks.

The exchange operators R and R' describe the interruption of the geared motion of the two methyl groups as shown in Figure V.14. The duration of the geared motion before interruption is the correlation time τ. To observe the effect of the geared motion on the NMR spectrum, the correlation time should be longer than the inverse of the dipolar coupling. Frequent interruption of the correlated motion (between the two methyl groups) makes each groupt rotate as if independent.

We shall assume that the correlation times for exchange processes R and R' are identical because of the symmetry consideration. As

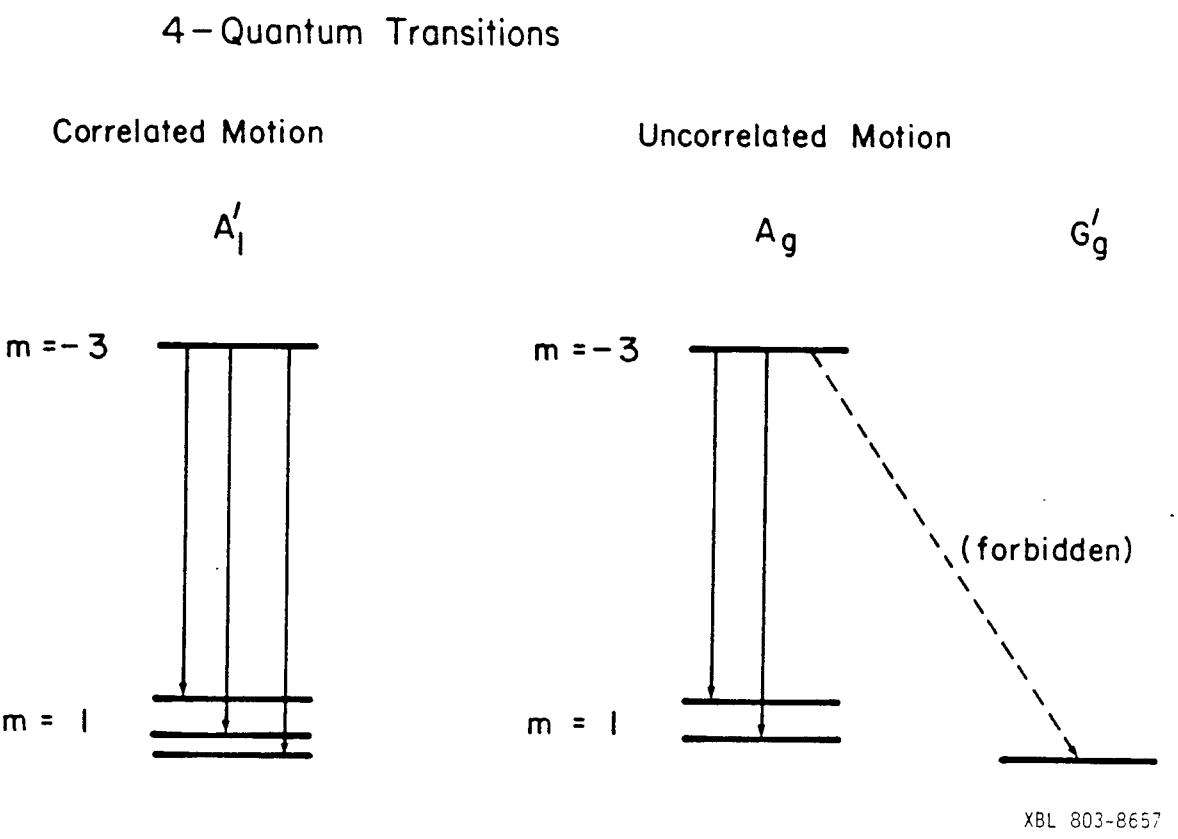

Figure V.13 The relevant energy level diagram for 4-quantum transitions is shown above. One pair of 4-quantum transitions $A_g(3) \rightarrow G_g'(-1)$ and $A_g(-3) \rightarrow G_g'(1)$ is forbidden for the case of uncorrelated motion. Consequently, the 4-quantum transitions for correlated motion have one extra pair of transitions.

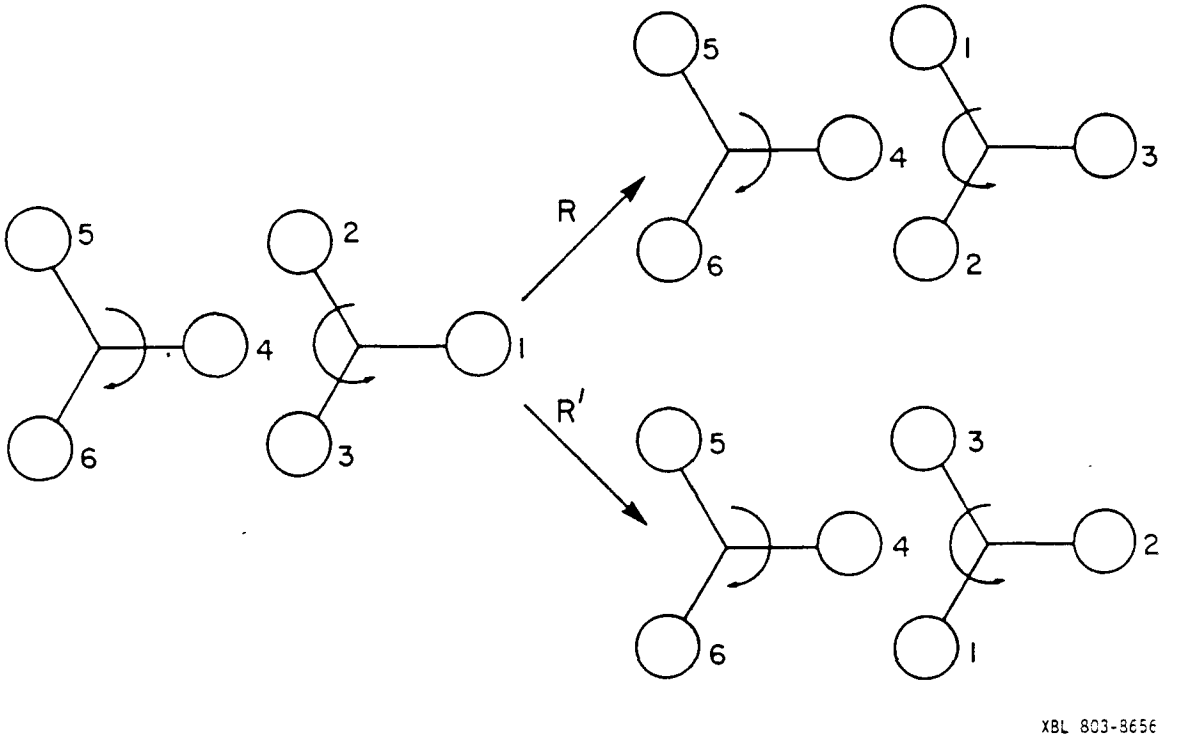

Figure V.14 The exchange operators R and R' represent the process of slipping that interrupts the correlated motion.

shown in Figure V.14, the exchange operators R and R' rearrange the ordering of the methyl protons cyclically and can be expressed mathematically by permutation symbols as follows

$$R = \begin{pmatrix} 1 & 2 & 3 & 4 & 5 & 6 \\ 3 & 1 & 2 & 4 & 5 & 6 \end{pmatrix}, \qquad R = \begin{pmatrix} 1 & 2 & 3 & 4 & 5 & 6 \\ 2 & 3 & 1 & 4 & 5 & 6 \end{pmatrix}. \tag{V.33}$$

The original position for each proton is shifted to the position indicated in the lower line. We may notice that $R^{-1} = R$ and $R' = R^2$.

The state $|A_1'(m = -3)\rangle$ $(=|Ag(m = -3)\rangle)$ is invariant under operations R and R'. The remaining three eigenstates (those with m=1 and A_1' symmetry of special interest) are superpositions of the following three basis functions,

$$|a\rangle = \frac{1}{\sqrt{6}} (|12\rangle + |13\rangle + |23\rangle + |45\rangle + |46\rangle + |56\rangle)$$

$$|b\rangle = \frac{1}{\sqrt{3}} (|14\rangle + |26\rangle + |35\rangle)$$

$$|c\rangle = \frac{1}{\sqrt{6}} (|15\rangle + |16\rangle + |24\rangle + |25\rangle + |34\rangle + |36\rangle) \tag{V.34}$$

where state $|ij\rangle$ means that the spins of i-th and j-th protons are down. The above states are not eigenstates of the Hamiltonian in eq. (V.5). If we separate the dipolar Hamiltonian into three parts H_u, H_v, and H_w according to their different couplings u, v and w, we can show that the matrix representations of the above Hamiltonians with $|a\rangle$, $|b\rangle$, and $|c\rangle$ as basis set are given by

$$H_u = u \begin{pmatrix} 0 & 0 & 0 \\ 0 & -\frac{1}{2} & -\frac{1}{\sqrt{2}} \\ 0 & -\frac{1}{\sqrt{2}} & -1 \end{pmatrix} , \qquad (V.35)$$

$$H_v = v \begin{pmatrix} -\frac{1}{4} & 0 & -\frac{1}{2} \\ 0 & \frac{3}{4} & 0 \\ -\frac{1}{2} & 0 & -\frac{1}{4} \end{pmatrix} , \qquad (V.36)$$

$$H_w = w \begin{pmatrix} -\frac{1}{2} & -\frac{1}{\sqrt{2}} & -\frac{1}{2} \\ -\frac{1}{\sqrt{2}} & -\frac{1}{2} & 0 \\ -\frac{1}{2} & 0 & \frac{1}{2} \end{pmatrix} , \qquad (V.37)$$

and

$$H = \begin{pmatrix} -\frac{v}{4}-\frac{w}{2} & -\frac{w}{\sqrt{2}} & -\frac{v}{2}-\frac{w}{2} \\ -\frac{w}{\sqrt{2}} & -\frac{u}{2}+\frac{3}{4}v-\frac{w}{2} & -\frac{u}{\sqrt{2}} \\ -\frac{v}{2}-\frac{w}{2} & -\frac{u}{\sqrt{2}} & -u-\frac{v}{4}+\frac{w}{2} \end{pmatrix} . \qquad (V.38)$$

Calculating the matrix representations for R and R' is straightforward, however, a few remarks should be made. First of all, $|a\rangle$ is an invariant state. Secondly, Operators R and R' mix states $|b\rangle$, $|c\rangle$ and another state $|A_1''(m = 1)\rangle$ of a different

symmetry. Using $|a>$, $|b>$, $|c>$ and $|A_1''(m = 1)>$ as a basis set we can show

$$R = \begin{pmatrix} 1 & 0 & 0 & 0 \\ 0 & 0 & \frac{1}{\sqrt{2}} & -\frac{1}{\sqrt{2}} \\ 0 & \frac{1}{\sqrt{2}} & \frac{1}{2} & \frac{1}{2} \\ 0 & \frac{1}{\sqrt{2}} & -\frac{1}{2} & -\frac{1}{2} \end{pmatrix} , \qquad (V.39)$$

$$R' = \begin{pmatrix} 1 & 0 & 0 & 0 \\ 0 & 0 & \frac{1}{\sqrt{2}} & \frac{1}{\sqrt{2}} \\ 0 & \frac{1}{\sqrt{2}} & \frac{1}{2} & -\frac{1}{2} \\ 0 & -\frac{1}{\sqrt{2}} & \frac{1}{2} & -\frac{1}{2} \end{pmatrix} , \qquad (V.40)$$

and

$$R + R' = \begin{pmatrix} 2 & 0 & 0 & 0 \\ 0 & 0 & \sqrt{2} & 0 \\ 0 & \sqrt{2} & 1 & 0 \\ 0 & 0 & 0 & -1 \end{pmatrix} . \qquad (V.41)$$

As we shall see later only R + R' will enter the equation of motion as a whole; the exotic state $|A_1''(m = 1)>$ does not mix with the remained states since R + R' has no off-diagonal elements in the 4-th column and row. Consequently, we can completely

eliminate it.

The equation of motion for exchange processes R and R' is given by

$$\frac{d}{dt}\rho = i[\rho,H] + \frac{1}{\tau}(R\rho R^{+}-\rho) + \frac{1}{\tau}(R'\rho R'^{+}-\rho) \quad . \qquad (V.42)$$

Let $|A_1'(m = 3)|\rho|i\rangle = \rho_i$; by using the facts $R|A_1'(m = -3)\rangle = |A_1'(m = -3)\rangle$ and $H|A_1'(m = -3)\rangle = (\frac{3}{2}u + \frac{3}{4}v + \frac{3}{2}w)|A_1'(m = -3)\rangle \equiv E_o|A_1'(m = -3)\rangle$, we can show that

$$\frac{d}{dt}\rho_i = \sum_k [iH_{ki} + \frac{1}{\tau}(R_{ki}+R'_{ki}+R'_{ik})]\rho_k - (iE_o + \frac{2}{\tau})\rho_i \quad . \qquad (V.43)$$

By rearranging the superposition between states $|2\rangle$ and $|3\rangle$ as

$$\begin{cases} |2'\rangle = \sqrt{\frac{2}{3}}|2\rangle - \sqrt{\frac{1}{3}}|3\rangle \quad , \\ |3'\rangle \quad \sqrt{\frac{1}{3}}|2\rangle + \sqrt{\frac{2}{3}}|3\rangle \end{cases} \qquad (V.44)$$

the operator R + R' becomes diagonal in this basis set and is given by

$$R + R' = \begin{pmatrix} 2 & 0 & 0 \\ 0 & -1 & 0 \\ 0 & 0 & 2 \end{pmatrix} \quad . \qquad (V.45)$$

The equation (V.43) can be written in a simpler form as follows

$$\frac{d}{dt}\rho_i + \{i E_o - \frac{1}{\tau}[(R+R')_i - 2]\}\rho_i = i \sum H_{ki}\rho_k \quad . \qquad (V.46)$$

The corresponding secular equation can be found by using $d\rho_i/dt = i\lambda_i\rho_i$ and is written explicitly as follows

$$\begin{vmatrix} \frac{3}{2}u + v + 2w - \lambda & \frac{\sqrt{3}}{6}(v-w) & \frac{1}{\sqrt{6}}(v+2w) \\ \frac{\sqrt{3}}{6}(v-w) & \frac{3}{2}u + \frac{v}{3} + \frac{5}{3}w + \frac{3i}{\tau} - \lambda & \frac{\sqrt{2}}{3}(v-w) \\ \frac{1}{\sqrt{6}}(v+2w) & \frac{\sqrt{2}}{3}(v-w) & 3u + \frac{2}{3}v + \frac{4}{3}w - \lambda \end{vmatrix} = 0 \quad . \qquad (V.47)$$

One remark needs to be made about matrix element H_{ki} in the new basis set. It is related to the old H_{ki} in eq. (V.38) by a similarity transformation A and

$$H_{(new)} = A\, H_{(old)}\, A^{+} \quad , \qquad (V.48)$$

where

$$A_{(old)} = \begin{pmatrix} 1 & 0 & 0 \\ 0 & \sqrt{\frac{2}{3}} & -\sqrt{\frac{1}{3}} \\ 0 & \sqrt{\frac{1}{3}} & \sqrt{\frac{2}{3}} \end{pmatrix} \quad . \qquad (V.49)$$

The solution of the above secular equation gives three 4-quantum transition frequencies. The three satellites on the other side are the images of these three with respect to the central frequency of a 4-quantum transition domain.

We shall now discuss two extreme cases of the above solution. In the limit of short correlation time, $|(v-w)_\tau| << 1$, the two methyl group move quite independently. The transitions frequencies are given by

$$\lambda_{1,2} = \frac{9}{4} u + \frac{5}{2} x \pm \frac{1}{2} (\frac{9}{4} u^2 + 7 x^2 - 3 ux)^{1/2} \quad , \qquad (V.50)$$

and

$$\lambda_3 = \frac{3}{2} u + x + w + \frac{3i}{\tau}$$

where

$$x = (u + 2w)/3 \quad . \qquad (V.51)$$

Since τ is very small, the transition with λ_3 is very broad in lineshape and is very weak in intensity and thus, cannot be observed. Actually, only two pairs of satellites can be observed. The transition frequencies λ_1 and λ_2 are also in agreement with our previous result. The coupling x is the averaged value of the intramethyl couplings v and w according to their weight.

In the limit of a completely correlated motion, $1/\tau$ is negligibly small and can be dropped out of the secular equation. The three roots of the secular equation correspond to the transition frequencies. There are seven 4-quantum transitions, including the central peak, in all.

5.6 References

1. E. E. Gurnell and P. Diehl, Mol. Phys. 24, 489 (1972).

2. J. Tang and A. Pines, J. Chem. Phys. 73, 2512 (1980).

3. W. S. Warren and A. Pines, J. Am. Chem. Soc. 103, 1613 (1981).

4. P. Diehl and C. L. Khetrapal, NMR Basic Principles and Progress, Vol. 1, ed. by P. Diehl et al. (Springer-Verlag, New York, 1969).

5. M. Tinkham, Group Theory and Quantum Mechanics, Appendix B (McGraw-Hill, New York, 1971).

6. P. D. Buckley, K. W. Jolly, and D. N. Pinder, Prog. Nucl. Mag. Res. Spectr. 10, 1 (1975).

VI

SECOND MOMENT OF MULTIPLE QUANTUM SPECTRUM AND STATISTICAL MODEL

6.1 Introduction

In our experiments we observed that the overall intensity for each order of multiple quantum transitions is dependent on the preparation and detection of the coherence. Generally, it depends on the time interval of: the preparation and detection periods, the phase of the pulses, the frequency offset, and some other factors. The behavior of the intensity for each order Δm seems to have some correlation with Δm. The spectral width of the multiple quantum spectra for each order seems also to have a correlation with Δm. In order to understand these general behaviors, and other effects caused by the method of preparation and the detection of the multiple quantum coherence should be diminished. We should average the spectra over various conditions for the external factors. Averaging the spectra over different values of the preparation and the detection periods is a frequently used method. To understand the correlation among the intensity, spectral width, and the order of multiple quantum coherence Δm, we shall present in this chapter a statistical model. This model assumes an equal transition intensity for each pair of states and does not consider molecular symmetry. The theoretical predictions of the MQ intensity and second moment versus Δm are in good agreement with the experimental results.

6.2 Intensity of the multiple quantum spectra

In general, the single quantum spectra are usually obtained by Fourier transformation of the FID, followed by a single excitation pulse. The FID is actually the correlation function of the transverse magnetization in time. In terms of the spin angular momentum operator I, we may express the FID S(t) by

$$\begin{aligned} S(t) &\propto \mathrm{Tr}(I_x \rho(t)) \\ &= \mathrm{Tr}(I_x e^{-iHt} I_x e^{iHt}) \\ &= \mathrm{Tr}(I_x(0)\ I_x(t)) \quad . \end{aligned} \tag{VI.1}$$

By either continuous wave method or pulse method, the intensity of the single quantum transition between states $|\alpha\rangle$ and $|\beta\rangle$ is given by the value of $|\langle\alpha|I_x|\beta\rangle|^2$ or $|\langle\alpha|I_y|\beta\rangle|^2$. For the case of continuous wave method, we can easily prove the above statement by using the Fermi golden rule. For the latter case, we may prove it by Fourier transformation of the FID S(t) into a frequency domain.

As we discussed in Chapter III, the multiple quantum FID can be expressed in terms of the correlation function of multiple quantum spin operators $U(\tau)$ and $V(-\tau')$. Unlike I_x or I_y, which contain single raising and lowering operators I_+ and I_-, the multiple quantum operators U and V may contain all possible orders of the raising and lowering operators. In addition, the intensity of the multiple quantum transition between states $|\alpha\rangle$ and $|\beta\rangle$ depends on the parameters τ and τ', because of the intensity is given by $U_{\alpha\beta}(\tau)\ V_{\beta\alpha}(-\tau')$. Accordingly, the intensity of the multiple quantum

spectra depends on the method of the preparation, and the detection of the multiple quantum coherence. Because of the implicit dependence of the pulse sequence, some transitions may accidentally be low in intensity. To avoid this situation, we can take the average of the spectra of various τ and τ'. In most cases the spectra were obtained by setting τ be equal to τ'.

The overall intensity for each order of the τ-averaging multiple quantum spectra (of partially oriented benzene) is shown in Figure VI.1.[1]

The dependence of the intensity on Δm follows a gaussian curve. It indicates that the intensity of multiple quantum spectra behaves statistically.

6.3 Statistical model for intensity of the MQ spectra

Let us consider a system of isolated molecules of N spin-1/2 particles, for example, benzene molecules in liquid crystal. Because of the translational diffusion, the dipolar interaction among different molecules is decoupled. The number of states with n spins down is given by the binomial coefficient C(N,n) and

$$C(N,n) = \frac{N!}{(N-n)!n!} \quad . \qquad \text{(VI.2)}$$

In terms of magnetic quantum number m, we can express the number of states by

$$C(N,n) = C_N(m) = \frac{N!}{\{\frac{1}{2}(N-2m)\}!\{\frac{1}{2}(N+2m)\}!} \quad . \qquad \text{(VI.3)}$$

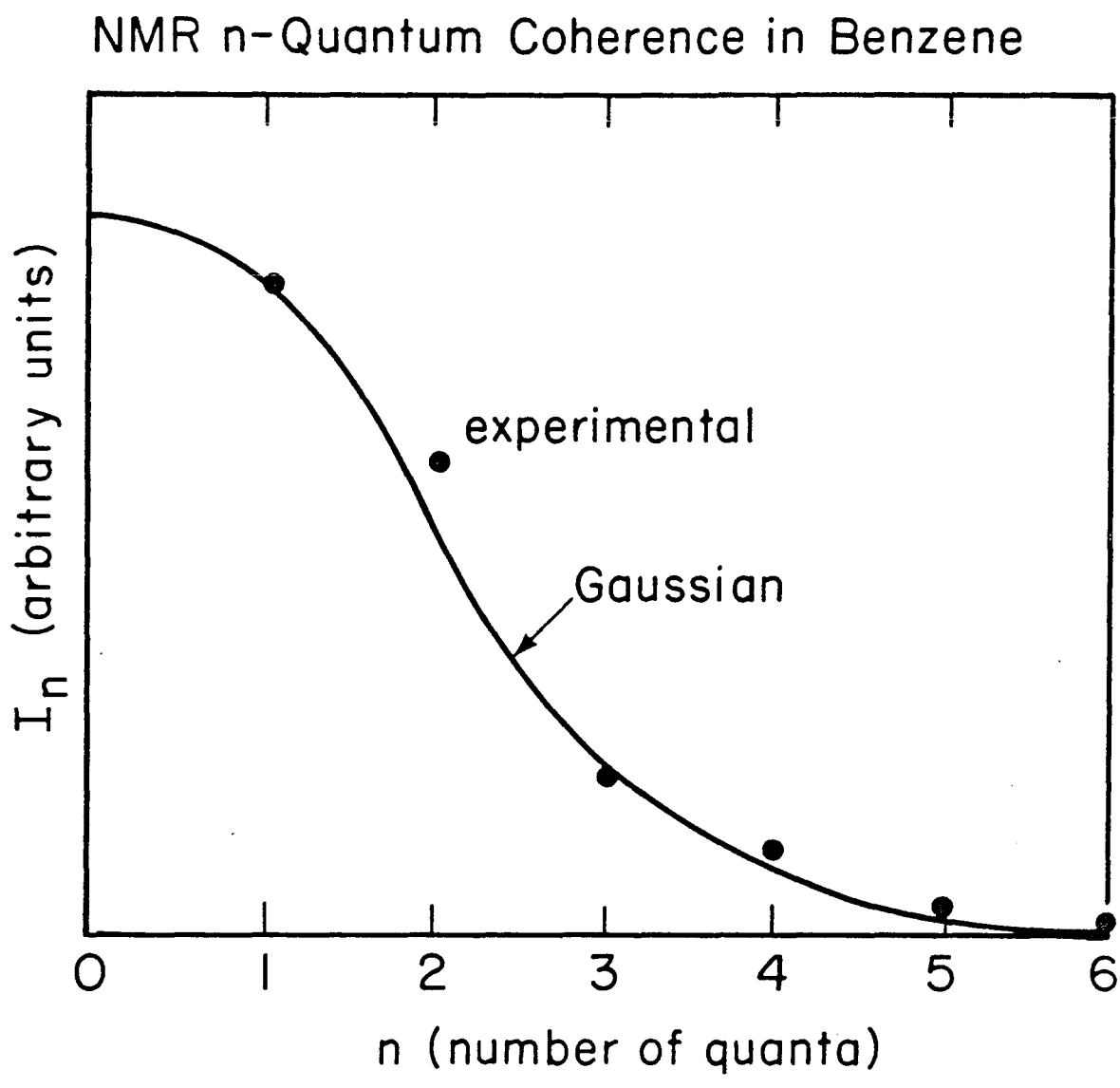

Figure VI.1 The integrated intensity of multiple quantum spectra versus the number of quanta. The experimental data follow a gaussian curve.

Using Stirling's approximation for factorial,

$$\ln n! \simeq (x+\tfrac{1}{2}) \ln x - x + \tfrac{1}{2} \ln 2\pi \quad , \tag{VI.4}$$

we will obtain an approximated form for $C_N(m)$ if $m \ll N$,

$$C_N(m) \simeq \frac{2^{N+1}}{\sqrt{2\pi N}} \exp(-2\, m^2/N) \quad . \tag{VI.5}$$

The approximation is pretty good even for $N = 6$ as shown in Table VI.1. The gaussian forms of $C_N(m)$ for several N are shown in Figures VI.2 and VI.3.

In this statistical model, we shall assume that the transition between each pair of states has an equal intensity. In addition, we do not include a symmetry consideration. Specifically, no selection rule caused by molecular symmetry is assumed.

The intensity of the transition between the manifold with a magnetic quantum number m and $m - \Delta m$ is then given by the product of the number of the associated states, namely, $C_N(m)\ C_N(m-\Delta m)$. The overall intensity of a particular order of multiple quantum transition is then given by

$$\begin{aligned} I(\Delta m) &\propto \sum_m C_N(m)\ C_N(m-\Delta m) \\ &\simeq \int dm\ e^{-\frac{\Delta m^2}{N}}\ e^{-\frac{4(m-\frac{1}{2}\Delta m)^2}{N}} \\ &\propto \exp(-\Delta m^2/N) \quad . \end{aligned}$$

As we expected, the intensity decreases as Δm increases; it is characterized by a gaussian as is shown in Figures VI.4 and VI.5.

TABLE VI.1

N=6

Magnetic quantum number	Number of states	$C_N(m)$
3	1	1.04
2	6	5.42
1	15	15.01
0	20	20.85
-1	15	15.01
-2	6	5.42
-3	1	1.04

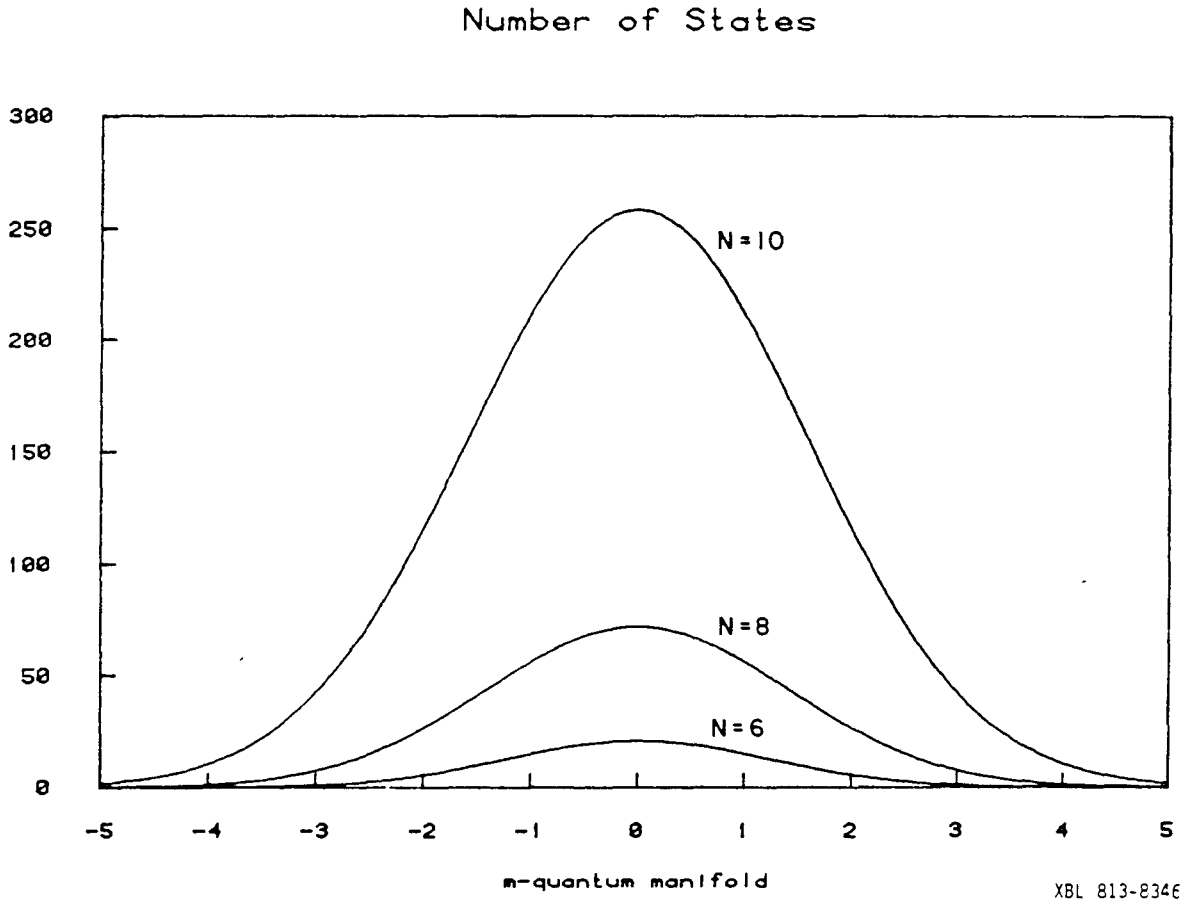

Figure VI.2 The number of states of N spin-1/2 particles in each m-quantum manifold using Stirling's approximation. The curves have a gaussian form.

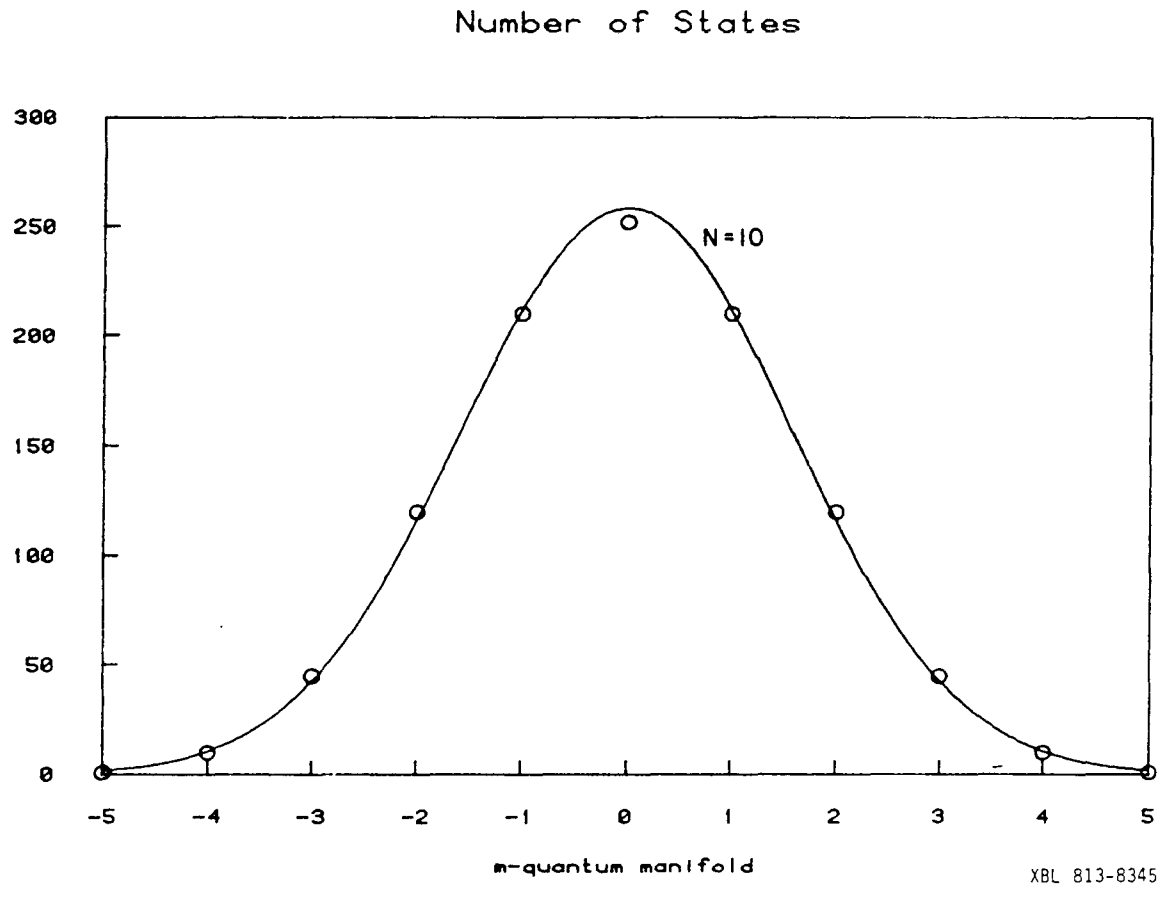

Figure VI.3 Number of states of ten spin-1/2 particles in each m-manifold. The exact value of the binomial coefficient is indicated by a circle. The gaussian curve is obtained by using Stirling's approximation.

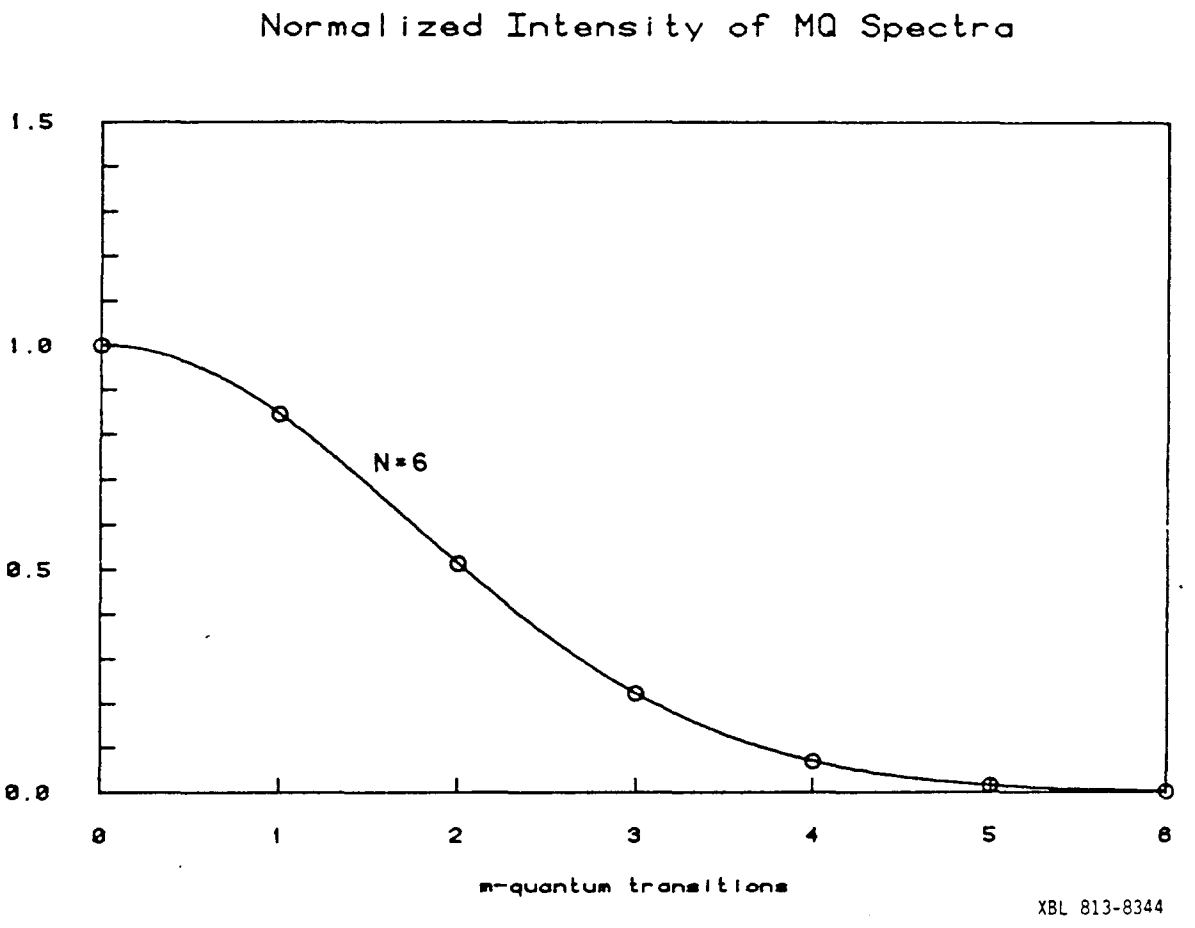

Figure VI.4 Normalized overall intensity of the multiple quantum spectra for each order m based on the statistical model (N=6). The curve has a gaussian form.

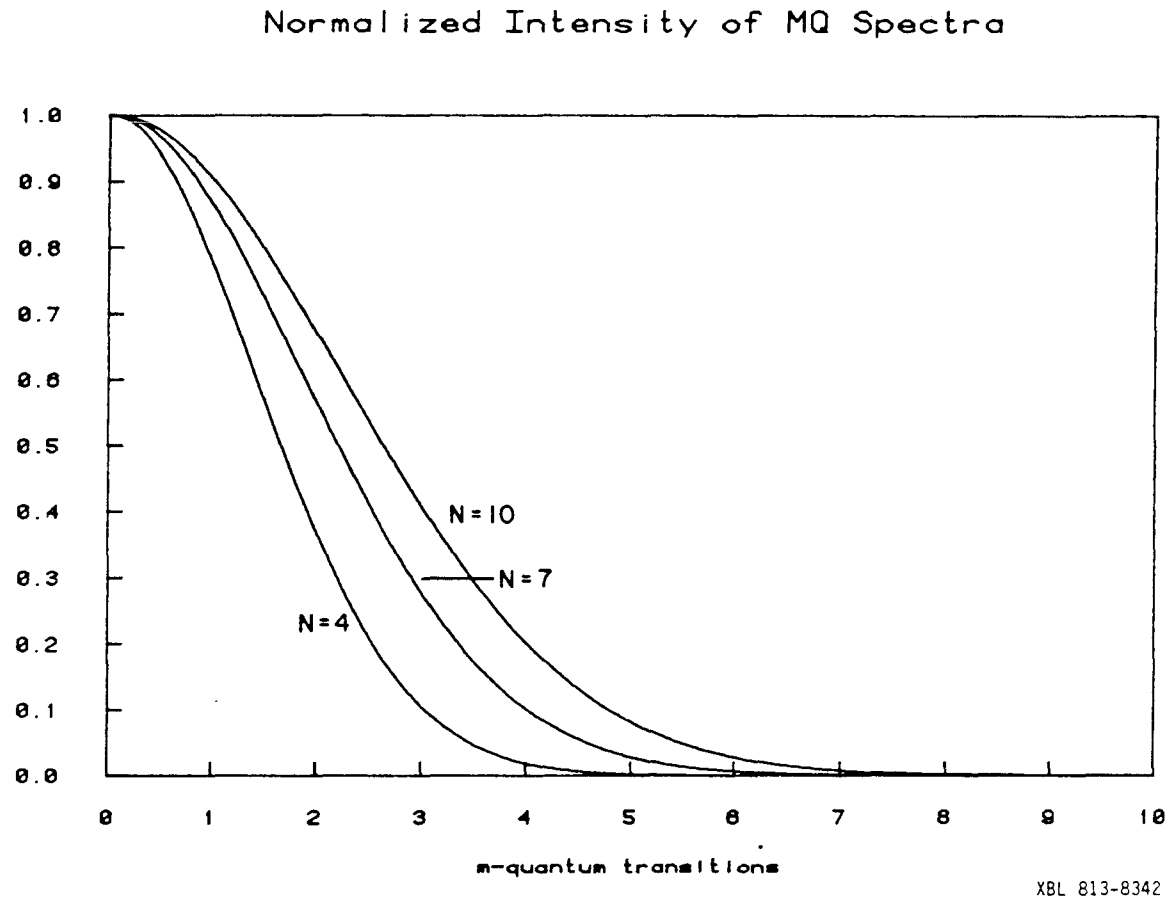

Figure VI.5 Normalized overall intensity of multiple quantum spectra for each order m based on the statistical model (N = 4, 7 and 10).

Our prediction of the statistical model is in good agreement with the experimental results.[1]

6.4 Second moment of MQ spectra

6.4.1 Introduction

The NMR spectrum in solids is generally very broad and almost structureless. A study of lineshape and spectral width, however, provides some information about the system. For example, second moment measurements can provide some information about molecular structure and motions in the solid state.[2] One of the nice things about moments study is that their values can be calculated from the first principles, without having to find the eigenstates of the Hamiltonian. The second moment of an ordinary single quantum spectrum can be calculated by using the Van Vleck formula and can be related to the molecular structure.

We generalized the expression of the second moment for usual single quantum spectrum to the case for the multiple quantum spectrum.

Let us consider a system of dipole-coupled spin-1/2 particles. The Hamiltonian consists of two parts, the Zeeman Hamiltonian H_z and the truncated dipole-dipole interaction $H_D^{(0)}$,

$$H = H_z + H_D^{(0)} = -\Delta\omega\ I_z + H_D^{(0)} \quad , \tag{VI.6}$$

where $\Delta\omega$ is the frequency-offset and

$$[H_z\ ,\ H_D^{(0)}] = 0 \quad . \tag{VI.7}$$

The FID S(t) of multiple quantum transitions is given by

$$J(t) = Tr(e^{-iHt}\, U(\tau)\, e^{iHt}\, V(-\tau')) \quad . \tag{VI.8}$$

We can decompose the multiple quantum operators U and V into components of a different order of m, such as,

$$U(\tau) = \sum_m U_m(\tau) \quad , \tag{VI.9}$$

and

$$V(-\tau') = \sum_m V_m(-\tau') \quad . \tag{VI.10}$$

By the definition of the tensor operator, the operators U_m and V_m satisfy the following commutation relations;

$$\begin{cases} [I_z, U_m] = m\, U_m \quad , \\ [I_z, V_m] = m\, V_m \quad . \end{cases} \tag{VI.11}$$

As a consequence, we can prove easily that

$$e^{i\Delta\omega t\, I_z}\, U_m\, e^{-i\Delta\omega t\, I_z} = e^{im\Delta\omega t}\, U_m \quad . \tag{VI.12}$$

We may express S(t) in terms of U_m by

$$S(t) = \sum_m e^{im\Delta\omega t}\, Tr(e^{-iH_D^{(0)}t}\, U_m\, e^{iH_D^{(0)}t}\, V_{-m}) \quad . \tag{VI.13}$$

Since $H_D^{(0)}$ conserves the magnetic quantum number, the non-vanishing component in $V(-\tau')$ is the one with a magnetic quantum number -m,

$V_{-m}(-\tau')$. We can further reduce the FID $S(t)$ to a simple form:

$$S(t) = \sum_m e^{im\Delta\omega t}\, \mathrm{Tr}(e^{-iH_D^{(0)}t}\, U_m\, e^{iH_D^{(0)}t}\, V_{-m})$$

$$= \sum_m e^{im\Delta\omega t}\, S_m(t)$$

where

$$S_m(t) = \mathrm{Tr}(e^{-iH_D^{(0)}t}\, U_m\, e^{iH_D^{(0)}t}\, V_{-m}) \quad . \tag{VI.14}$$

The spectral function of the m-quantum transitons $G_m(\omega)$ is the Fourier transformation of $S_m(t)$:

$$G_m(\omega) = \frac{1}{\sqrt{2\pi}} \int e^{-i\omega t}\, S_m(t)\, dt \quad . \tag{VI.15}$$

We define the normalized spectral function $g(\omega)$ by

$$g(\omega) = \sqrt{2\pi}\, G_m(\omega) / \int G(\omega)\, d\omega$$

$$= \sqrt{2\pi}\, G_m(\omega)/S_m(0) \quad ; \tag{VI.16}$$

this can be expressed explicitly by

$$g_m(\omega) = \frac{\int e^{-i\omega t}\, dt\, \mathrm{Tr}(e^{-iH_D^{(0)}t}\, U_m\, e^{iH_D^{(0)}t}\, V_{-m})}{\mathrm{Tr}(U_m V_{-m})}$$

$$= \frac{1}{\mathrm{Tr}(U_m V_{-m})} \int e^{-i\omega t}\, dt \sum_n (-i)^n\, t^n\, \mathrm{Tr}^{(n)}([H_D^{(0)}, U_m] V_{-m}) \quad , \tag{VI.17}$$

where

$$\mathrm{Tr}^{(n)}([H_D^{(0)},U_m]V_{-m})$$

$$= \mathrm{Tr}(\underbrace{[H_D^{(0)},[H_D^{(0)},\ldots}_{n \text{ times}} [H_D^{(0)},U_m]\ldots]]V_{-m}) \quad .$$

Using an inverse Fourier transformation, we will obtain

$$\int g_m(\omega)\ e^{i\omega t}\ \frac{d\omega}{2\pi} = \frac{1}{\mathrm{Tr}(U_m V_{-m})}\ \mathrm{Tr}(e^{-iH_D^{(0)}t}\ U_m\ e^{iH_D^{(0)}t}\ V_{-m}) \quad . \tag{VI.18}$$

By expanding the expressions on both sides into Taylor's series of t and by comparing the terms of same power of t, we can obtain this useful result for the n-th moment:

$$\int g_m(\omega)\ \omega^n\ \frac{d\omega}{2\pi} = \frac{(-1)^n}{\mathrm{Tr}(U_m V_{-m})}\ \mathrm{Tr}^{(n)}\ ([H_D^{(0)},U_m(\tau)]V_{-m}(-\tau'))$$

$$\equiv M_n(m) \tag{VI.19}$$

where $M_n(m)$ is the n-th moment of the m-quantum spectrum.

Since U_m and V_{-m} depend on τ and τ', however, the value of the n-th moment is not a constant. Its average value, however, can be obtained by measuring the n-th moment of the τ-averaging multiple quantum spectra.

Particularly, we are interested in the behavior of the second moment of the m-quantum spectrum. Based on the statistical model, we are able to explain qualitatively the general behavior of the second moment of the m-quantum spectrum, in terms of simple parameters such as the dipole couplings.

The second moment of m-quantum spectrum is given by

$$M_z(m) = \frac{1}{Tr(U_m V_{-m})} \quad Tr([H_D^{(0)},[H_D^{(0)},U_m]]V_{-m})$$

$$= \frac{1}{Tr(U_m V_{-m})} \quad Tr([H_D^{(0)},U_m][H_D^{(0)},V_{-m}])$$

$$= \frac{1}{Tr(U_m V_{-m})} \quad \sum_{\alpha,\beta} E_{\alpha\beta}^2 \langle\alpha|U_m|\beta\rangle\langle\beta|V_{-m}|\alpha\rangle \quad . \qquad \text{(VI.20)}$$

As a special case in the ordinary single quantum NMR method, operators U and V are the spin angular momentum operators I_x and I_y, and are constant in time. The corresponding second moment was first calculated by Van Vleck and is expressed by[3]

$$M_z = \frac{1}{Tr(I_x^2)} Tr([H_D^{(0)},I_x]^2)$$

$$= \frac{1}{4}\gamma^4\hbar^2 \sum_k d_{jk}^2 \quad , \qquad \text{(VI.21)}$$

where

$$d_{jk} = \frac{3}{2}(1-3\cos^2\theta_{jk})/\gamma_{jk}^3 \quad .$$

In the case of the multiple quantum NMR method, the single quantum operator is not simply I_x or I_y. We should not expect the value of M_2 to be same as in the previous case. Because of the complexity of the multiple quantum operators U and V, we cannot calculate the second moment in a simple way. In the spirit of the statistical model, however, we can assume that the transition matrix elements, $\langle\alpha|U_m|\beta\rangle$ and $\langle\beta|V_{-m}|\alpha\rangle$, are equal for each transition. Accordingly, the selection rule due to molecular symmetry is not considered.

We shall make another approximation on the transition frequency $E_{\alpha\beta}$. We assume that the distribution of the energy levels for a particular manifold of a magnetic quantum n can be described by the distribution function $g(\omega)$. This function is also known as the density of state.

Let us consider two particular manifolds with distribution functions, $g_1(\omega)$ and $g_2(\omega)$ as we have shown in Figure VI.6.

The spectrum of the transitions between two manifolds is given by the convolution of their distribution functions, and is expressed by

$$f(\Omega) = \int g_1(\omega)\ g_2(\Omega-\omega)d\omega \quad . \tag{VI.22}$$

Consequently, we can make an approximation on eq. (VI.19) for second momentum by

$$M_z = \int g_1(\omega)\ g_2(\omega-\Omega)\ \Omega^2\ d\omega\ d\Omega = \int f(\Omega)\ \Omega^2\ d\Omega \quad . \tag{VI.23}$$

We shall now prove a theorem for the second moment of the spectral functions that will be useful.

Theorem: The second moment of a spectral function is the additive sum of the second moments of the distribution functions.

Proof: Assuming that the distribution functions $g_1(\omega)$ and $g_2(\omega)$ are normalized, their second moments are given by

$$\sigma_1^2 = \int (\omega-\bar{\omega}_1)^2\ g_1(\omega)\ d\omega = \int (\omega^2-\bar{\omega}_1^2)\ g_1(\omega)d\omega \quad , \tag{VI.24}$$

and

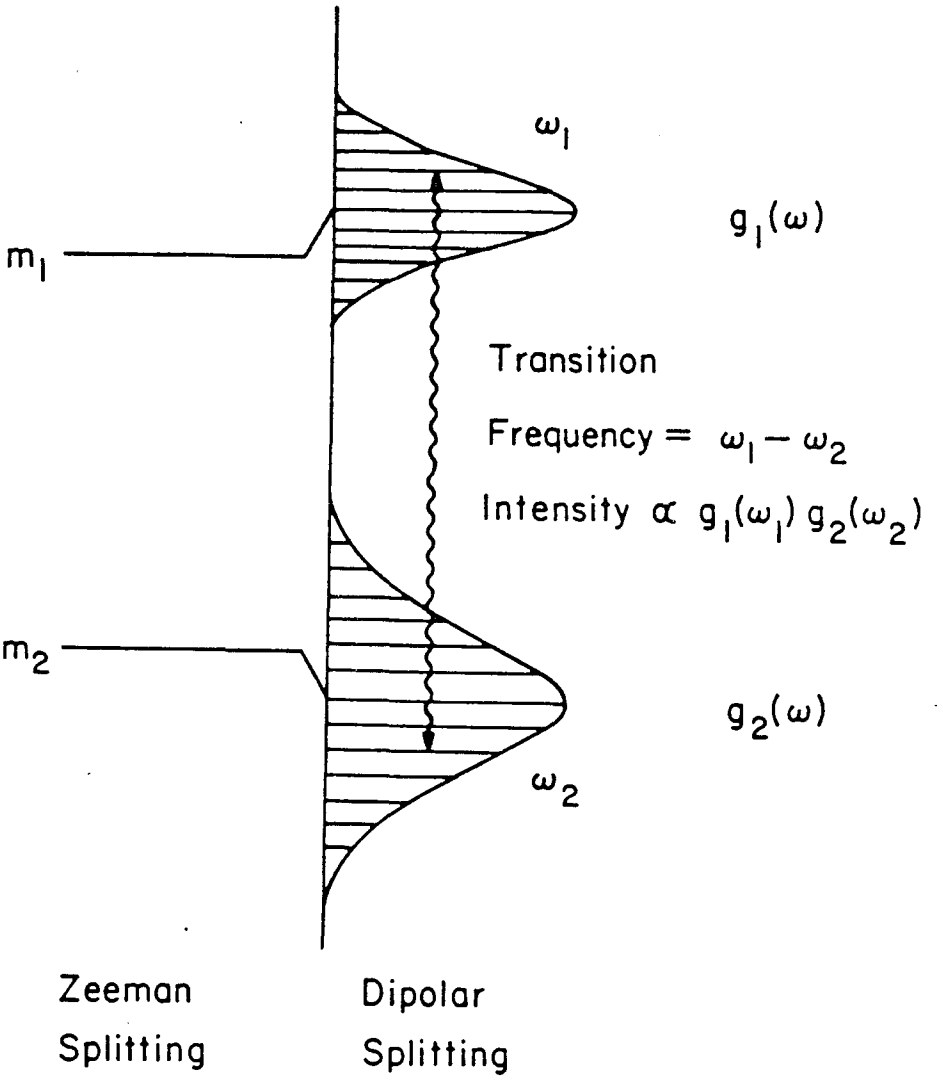

XBL 813-8353

Figure VI.6 Schematic diagram for the transition between two m-manifolds. The function $g(\omega)$ describes the distribution of states. The spectrum of the transitions between the two manifolds is given by the convolution of their distribution functions.

$$\sigma_2^2 = \int (\omega-\bar{\omega}_2)^2 \, g_2(\omega) \, d\omega = \int (\omega^2-\bar{\omega}_2^2) \, g_2(\omega) d\omega \quad , \qquad \text{(VI.25)}$$

where $\bar{\omega}$ is the average value of ω, and is defined by

$$\bar{\omega} = \int \omega g(\omega) d\omega \quad . \qquad \text{(VI.26)}$$

Since

$$\begin{aligned} \int \Omega \, f(\Omega) d\Omega &= \int g_1(\omega) d\omega \int \Omega \, d\Omega \, g_2(\Omega-\omega) \\ &= \int g_1(\omega) d\omega \int (x+\omega) \, dx \, g_2(x) \\ &= \int g_1(\omega) d\omega \, (\omega+\bar{\omega}_2) \\ &= \bar{\omega}_1 + \bar{\omega}_2 \quad , \end{aligned} \qquad \text{(VI.27)}$$

we can prove that

$$\bar{\Omega} = \bar{\omega}_1 + \bar{\omega}_2 \quad . \qquad \text{(VI.28)}$$

The second moment of the spectrum is given by

$$\begin{aligned} \sigma^2 &= \int (\Omega^2-\bar{\Omega}^2) \, f(\Omega) d\Omega \\ &= \int g_1(\omega) d\omega \int (\Omega^2-(\bar{\omega}_1+\bar{\omega}_2)^2] g_2(\Omega-\omega) d\Omega \\ &= \int g_1(\omega) d\omega \int [(x+\omega)^2-(\bar{\omega}_1+\bar{\omega}_2)] g_2(x) dx \\ &= \int g_1(\omega) d\omega \, [\sigma_2^2 + 2 \, \bar{\omega}_2(\omega-\bar{\omega}_1) + \omega^2-\bar{\omega}_1^2] \\ &= \sigma_1^2 + \sigma_2^2 \quad . \end{aligned} \qquad \text{Q.E.D.} \qquad \text{(VI.29)}$$

As a special case, if the density of states is a gaussian, the

spectral distribution is again a gaussian, but with a larger width.

Using the above theorem, we can relate the second moment of the spectrum to the distribution of the associated states by evaluating the second moment of the density of states. The spreading of the energy levels in the same manifold is caused by dipole-dipole coupling. The second moment of the density states is given by

$$\sigma^2 = \langle H_D^{(0)2} \rangle - \langle H_D^{(0)} \rangle^2 \quad , \tag{VI.30}$$

where $H_D^{(0)}$ is the Hamiltonian of a dipole-dipole interaction and $\langle\ \rangle$ is the averaged value. More explicitly, $\langle H_D^{(0)} \rangle$ is the trace of the Hamiltonian $H_D^{(0)}$ and is divided by the total number of states in a particular manifold. Since the trace by any operator does not depend on a particular choice of a basis set, we can calculate its value without knowing the eigenfunctions.

6.4.2 Calculation of $\langle H_D^{(0)} \rangle$

The truncated Hamiltonian $H_D^{(0)}$ of the dipole-dipole interaction consists of two parts:

$$H_D^{(0)} = \sum_{i \neq j} D_{ij} [2\ I_{iz} I_{jz} - \frac{1}{2} (I_{i+} I_{j-} + I_{i-} I_{j+})] \quad . \tag{VI.31}$$

To more easily evaluate the trace of $H_D^{(0)}$, we may use some special properties of the trace. As stated before, the trace of an operator does not depend on the way of choosing the basis set. We may choose the direct product of states for each spin, for

example, $|\alpha\alpha\alpha...\alpha\rangle$, $|\beta\alpha\alpha...\alpha\rangle$, and so on. Since the second part of the dipolar Hamiltonian contains fli-flop operators $I_{i+}I_{j-}$ and $I_{i-}I_{j+}$, their matrix representation using this particular set of basis is off-diagonal and traceless. As a consequence, we can completely omit this part of Hamiltonian when evaluating the trace of the dipolar Hamiltonian. In short hand, we can write the dipolar Hamiltonian as

$$H_D^{(0)} = \sum_{i\neq j} 2\, D_{ij}\, I_{iz} I_{jz} \quad . \tag{VI.32}$$

We will derive an analytic form for the trace of $H_D^{(0)}$ for each manifold of magnetic quantum number m. For illustration purposes, we shall first discuss several simple cases:

(1) Case of all spins up:

$$\mathrm{Tr}(H_D^{(0)}) = \langle\alpha\alpha...\alpha| \sum_{i\neq j} 2\, D_{ij}\, I_{iz}\, I_{jz}\, |\alpha\alpha...\alpha\rangle$$

$$= \frac{1}{2} \sum_{i\neq j} D_{ij} \equiv \frac{1}{2} \sum_{i,j}{}' D_{ij} \quad . \tag{VI.33}$$

(2) Case of one spin down:

Let $|k\rangle$ describes the state with the k-th spin down, namely,

$$|k\rangle = |\alpha\alpha..\underset{\substack{\uparrow \\ \text{k-th spin}}}{\alpha\beta}\alpha..\alpha\rangle$$

$$\langle k|H_D^{(0)}|k\rangle = \sum_{i,j\neq k}{}' \frac{1}{2} D_{ij} - \frac{1}{2}\sum_i{}' D_{ik} - \frac{1}{2}\sum_j{}' D_{jk} \quad , \tag{VI.34}$$

$$\mathrm{Tr}(H_D^{(0)}) = \sum_{i,j,k}{}' \frac{1}{2} D_{ij} - \frac{1}{2} \sum_{i,k}{}' D_{ik} - \frac{1}{2} \sum_{j,k}{}' D_{kj}$$

$$= \sum_{i,j,k}{}' \frac{1}{2} D_{ij} - \sum_{i,k}{}' D_{ik}$$

$$= (N-2) \sum_{i,j}{}' \frac{1}{2} D_{ij} - \sum_{i,j}{}' D_{ij}$$

$$= \frac{1}{2} (N-4) \sum_{i,j}{}' D_{ij} \quad . \qquad \text{(VI.35)}$$

The subscript "," above the summation notation indicates that the sum is taken for all indice i,j (or k), except $i \neq j$ ($\neq k$).

(3) Case of two spins down:

Let $|kl\rangle$ describes the state with k-th and l-th spin down, namely,

$$|kl\rangle = |\alpha\alpha\ldots\underset{\uparrow}{\beta}\ldots\underset{\uparrow}{\beta}\ldots\alpha\rangle$$

k-th l-th spin

$$\mathrm{Tr}(H_D^{(0)}) = \sum_{\{k,\ell\}} \frac{1}{2} \sum_{i,j}{}' D_{ij} - \sum_{\{k,\ell\}} \sum_{i} (D_{ik}+D_{i\ell})$$

$$= \frac{N(N-1)}{2} \sum_{i,j}{}' \frac{1}{2} D_{ij} - \left[\frac{N(N-1)}{2} - \frac{(N-2)(N-3)}{2} - 1\right] \sum_{i,j}{}' D_{ij}$$

$$= \frac{1}{4} (N^2 - 9N + 16) \sum_{i,j}{}' D_{ij} \quad . \qquad \text{(VI.36)}$$

(4) Case of three spins down:

Similar to the previous case,

$$\mathrm{Tr}(H_D^{(0)}) = \sum_{\{k,\ell,m\}} \frac{1}{2} \sum_{i,j}{}' D_{ij} - \sum_{\{k,\ell,m\}} \sum_{i} (D_{ik}+D_{i\ell}+D_{im})$$

$$= C(N,3)\,\frac{1}{2} \sum_{i,j}{}' D_{ij} - [C(N,3)-C(N-2,3)-(N-2)] \sum_{i,j}{}' D_{ij}$$

$$= \frac{1}{12}\,(N-2)[(N-6)^2-N] \sum_{i,j}{}' D_{ij} \quad , \qquad \text{(VI.37)}$$

where C(N,3), etc., are the binomial coefficients.

Generally, for the manifold with n spins down, the trace of $H_D^{(0)}$ can be shown as:

$$\mathrm{Tr}(H_D^{(0)}) = \frac{1}{2}\,C(N,n) \sum_{i,j}{}' D_{ij}$$

$$- \sum_{i,j}{}' D_{ij}\,[C(N,n)-C(N-2,n)-C(N-2,n-2)]$$

$$= \frac{C(N,n)}{2N(N-1)}\,[(N-2n)^2-N] \sum_{i,j}{}' D_{ij} \quad . \qquad \text{(VI.38)}$$

Since the magnetic quantum number m is related to the number of spins down n by $m = \frac{1}{2}N-n$, we can express the trace in terms of m:

$$\mathrm{Tr}_m(H_D^{(0)}) = \frac{C_N(m)}{2N(N-1)}\,[4\,m^2 - N] \sum_{i,j}{}' D_{ij} \quad . \qquad \text{(VI.39)}$$

The average value of the dipolar splitting $\langle H_D^{(0)} \rangle$ is given by the value of the trace, divided by the number of states that equals C(N,n). Finally, we obtain an analytic expression for the averaged dipolar splitting as follows:

$$\langle H_D^{(0)} \rangle = \frac{1}{2N(N-1)} [(N-2n)^2 - N] \sum_{i,j}' D_{ij}$$

$$= \frac{1}{2N(N-1)} [4\,m^2 - N] \sum_{i,j}' D_{ij} \qquad \text{(VI.40)}$$

$$= \frac{1}{4} [4\,m^2 - N] \langle D \rangle$$

where $\langle D \rangle$ is the average dipolar couplings and $\langle D \rangle = \sum_{i,j}' D_{ij}/C(N,2)$.

The value of the magnetic quantum number m is an integer or a half-integer if N is an even or an odd number. The value varies from -N/2 to N/2.

If the distribution function of the states has a gaussian form, the distribution center is shifted away from the Zeeman level by the amount of $\langle H_D^{(0)} \rangle$.

Since $H_D^{(0)}$ is a traceless operator, the sum of $Tr_m(H_D^{(0)})$ is zero, namely,

$$\sum_{m=-N/2}^{N/2} Tr_m(H_D^{(0)}) = 0 \quad . \qquad \text{(VI.41)}$$

Accordingly, we can easily show that

$$Tr_m(H_D^{(0)}) = Tr_{-m}(H_D^{(0)}) \quad . \qquad \text{(VI.42)}$$

We shall give some illustrations for the equation of the trace of H_D that we have just proved. Let us consider a dipole-coupled system of N spins with N = 2, 3,...6.

$$\mathcal{H}_D = H_D^{(0)}$$

(1) $N = 2$

$m = 1 \quad Tr(\mathcal{H}_D) = \frac{1}{2} \Sigma' D_{ij}$

$m = 0 \quad Tr(\mathcal{H}_D) = - \Sigma' D_{ij}$

(2) $N = 3$

$m = \frac{3}{2} \quad Tr(\mathcal{H}_D) = \frac{1}{2} \Sigma' D_{ij}$

$m = \frac{1}{2} \quad Tr(\mathcal{H}_D) = - \frac{1}{2} \Sigma' D_{ij}$

(3) $N = 4$

$m = 2 \quad Tr(\mathcal{H}_D) = \frac{1}{2} \Sigma' D_{ij}$

$m = 1 \quad Tr(\mathcal{H}_D) = 0$

$m = 0 \quad Tr(\mathcal{H}_D) = -\Sigma' D_{ij}$

(4) $N = 5$

$m = \frac{5}{2} \quad Tr(\mathcal{H}_D) = \frac{1}{2} \Sigma' D_{ij}$

$m = \frac{3}{2} \quad Tr(\mathcal{H}_D) = \frac{1}{2} \Sigma' D_{ij}$

$m = \frac{1}{2} \quad Tr(\mathcal{H}_D) = -\Sigma' D_{ij}$

(5) $N = 6$

$m = 3 \quad Tr(\mathcal{H}_D) = \frac{1}{2} \Sigma' D_{ij}$

$m = 2 \quad Tr(\mathcal{H}_D) = \Sigma' D_{ij}$

$m = 1 \quad Tr(\mathcal{H}_D) = - \frac{1}{2} \Sigma' D_{ij}$

$m = 0 \quad Tr(\mathcal{H}_D) = -2 \Sigma' D_{ij}$

As a special case, we can compare the results for the methyl group or benzene molecule systems with the above equations. We

show that they are identical.

6.4.3 Calculation of $\langle \mathcal{H}_D^2 \rangle$ and discussion

To estimate the second moment of the density of states, we need to calculate the trace of $\mathcal{H}_D^2$, where

$$\mathcal{H}_D^2 = \Sigma' D_{ij}[2 I_{iz}I_{jz} - \frac{1}{2}(I_{i+}I_{j-}+I_{i-}I_{j+})]$$

$$\times \Sigma' D_{k\ell}[2 I_{kz}I_{\ell z} - \frac{1}{2}(I_{k+}I_{\ell-}+I_{k-}I_{\ell+})] \quad . \qquad \text{(VI.43)}$$

We can omit the off-diagonal elements that do not contribute to the trace. Those elements are $I_{iz}J_{jz}I_{k+}I_{-}$, $I_{iz}J_{jz}I_{k-}I_{+}$, and so on. Consequently, we can show

$$\mathcal{H}_D^2 = (\Sigma' 2 D_{ij} I_{iz}I_{jz})(\Sigma' 2 D_{k\ell}I_{kz} I_{\ell z})$$

$$+ \frac{1}{4}\Sigma' D_{ij}D_{k\ell}(I_{i+}I_{j-}I_{k+}I_{\ell-} + I_{i+}I_{j-}I_{k-}I_{\ell+}$$

$$+ I_{i-}I_{j+}I_{k+}I_{\ell-} + I_{i-}I_{j+}I_{k-}I_{\ell+}) \quad . \qquad \text{(VI.44)}$$

We can make further simplifications by noticing that the trace of $I_{i+}I_{j-}I_{k+}I_{\ell-}$ is non-zero only if $i = \ell$ and $j = k$. Finally, we have

$$\mathcal{H}_D^2 = (\Sigma' 2 D_{ij}I_{iz}I_{jz})(\Sigma' 2 D_{k\ell}I_{kz}I_{\ell z})$$

$$+ \frac{1}{2}\Sigma' D_{ij}^2 (I_{i+}I_{i-}I_{j-}I_{j+} + I_{i-}I_{i+}I_{j+}I_{j-}) \quad . \qquad \text{(VI.45)}$$

The calculation of the trace of the second part is rather easy. We can show that the matrix element for the second part is non-zero for those states where spins i and j are anti-parallel.

Consequently, we will obtain

$$\mathrm{Tr}\left[\frac{1}{2}\,\Sigma'\, D_{ij}^2\ (I_{i+}I_{i-}I_{j-}I_{j+} + I_{i-}I_{i+}I_{j+}I_{j-})\right]$$

$$= \frac{1}{2}\ \Sigma'\, D_{ij}^2\ [C(N-n)-C(N-2,n)-C(N-2,n-2)]$$

$$= \frac{1}{N(N-1)}\ \Sigma'\, D_{ij}^2\ C(N,n)(N,n)n$$

$$= \frac{1}{2}\, C(N,n)(N-n)n\, \langle D^2\rangle \quad . \tag{VI.46}$$

The trace calculation of the first part is rather complicated. We shall first discuss a special case and assume that all the coupling constants are equal, that is, $D_{ij} = D$.

In this case, we find

$$\mathrm{Tr}(\Sigma'\ 2\ D_{ij}I_{iz}I_{jz})(\Sigma'\ 2\ D_{k\ell}I_{kz}I_{\ell z})$$

$$= 4\ D^2\ \mathrm{Tr}(\Sigma'\ I_{iz}I_{jz})(\Sigma'\ I_{kz}I_{\ell z})$$

$$= \frac{1}{16}\, D^2\ [(N-2n)^2-N]^2\ C(N,n) \quad . \tag{VI.47}$$

The average values of $\mathcal{H}_D^{\,2}$ and $\mathcal{H}_D$ are given by

$$\langle \mathcal{H}_D^{\,2}\rangle = \frac{\mathrm{Tr}(\mathcal{H}_D^{\,2})}{C(N,n)} = \frac{D^2}{2}\,(N-n)n + \frac{D^2}{16}\,[(N-2n)^2-N]^2 \quad , \tag{VI.48}$$

$$\langle \mathcal{H}_D\rangle = \frac{D}{4}\,[(N-2n)^2 - N] \quad . \tag{VI.49}$$

The second moment of the density of states is defined by

$$\langle \mathcal{H}_D^{\,2}\rangle - \langle \mathcal{H}_D\rangle^2 = \frac{D^2}{2}\,(N-n)n \quad . \tag{VI.50}$$

Since n is related to m by

$$m = \frac{N}{2} - n \quad ,$$

we find

$$\sigma_m^2 \equiv \langle \mathcal{H}_D^2 \rangle - \langle \mathcal{H}_D \rangle^2 = \frac{D^2}{2}\left(\frac{N^2}{4} - m^2\right) \tag{VI.51}$$

$$\omega_m \equiv \langle \mathcal{H}_D \rangle_m = \frac{D}{4}[4m^2 - N] \quad , \tag{VI.52}$$

where ω_m is the averaged frequency shift in the manifold with the magnetic quantum number m.

The second moment of the density of states ω_m^2 is a monotonically decreasing function of m. Nevertheless, the averaged frequency shift increases monotonically with m.

Assuming a gaussian form for the distribution of the states, the density of states is given by

$$\begin{aligned} g_m(\omega) &= C_N(m) \frac{1}{\sqrt{2\pi}\sigma_m} \exp[-(\omega-\omega_m)^2/2\sigma_m^2] \\ &\simeq \frac{2^N}{\sqrt{N\pi}\sigma_m} e^{-2m^2/N} e^{-(\omega-\omega_m)^2/2\sigma_m^2} \quad , \end{aligned} \tag{VI.53}$$

where $C_N(m)$ is the total number of states in the manifold of m.

The spectral function of the m-quantum transition is given by

$$\begin{aligned} F_m(\Omega) &= \sum_{\substack{n_1,n_2 \\ |n_1-n_2|=m}} \int_{-\infty}^{\infty} g_{n_1}(\omega)\, g_{n_2}(\omega-\Omega)\, d\omega \\ &= \sum_{\substack{n_1,n_2 \\ |n_1-n_2|=m}} \frac{2^{2N+1}}{N\pi} e^{\frac{2}{N}(n_1^2+n_2^2)} \frac{1}{\sqrt{2\pi}\sigma_{n_1,n_2}^2} \exp[-(\Omega-\omega_{n_1,n_2})^2/2\sigma_{n_1,n_2}^2] , \end{aligned} \tag{VI.54}$$

where

$$\sigma^2_{n_1,n_2} = \sigma^2_{n_1} + \sigma^2_{n_2} = \frac{D^2}{2}\left(\frac{N^2}{2} - n_1^2 - n_2^2\right) \quad , \tag{VI.55}$$

and

$$\omega_{n_1,n_2} = D(n_1^2 - n_2^2) \quad . \tag{VI.56}$$

The second moment of any particular m-quantum transitions associated with the manifolds of magnetic quantum number n_1 and n_2, is given by

$$\begin{aligned}\Omega^2_{n_1,n_2} &= \int_{-\infty}^{\infty} \Omega^2 \, d\Omega \, \frac{1}{\sqrt{2\pi}\,\sigma^2_{n_1,n_2}} \exp[-(\Omega-\omega_{n_1,n_2})^2/2\,\sigma^2_{n_1,n_2}] \\ &= \sigma^2_{n_1,n_2} + \omega^2_{n_1,n_2} \\ &= \frac{D^2}{2}\left[\frac{N^2}{2} - n_1^2 - n_2^2\right] + D^2(n_1-n_2)^2(n_1+n_2)^2 \quad , \end{aligned} \tag{VI.57}$$

where $m = n_1 - n_2$.

All transactions between any pair of manifolds of n_1 and n_2 with $m = n_1 - n_2$ contribute to the m-quantum spectrum. The second moments of the m-quantum spectrum is given by

$$\begin{aligned}\langle\Omega^2\rangle_m &= \int F_m(\Omega)\ \Omega^2\ d\Omega \Big/ \int F_m(\Omega) d\Omega \\ &= \frac{\sum_{|n_1,n_2|=m} (\sigma^2_{n_1,n_2} + \omega^2_{n_1,n_2})\ C_N(n_1)\ C_N(n_2)}{\sum_{|n_1-n_2|=m} C_N(n_1)\ C_N(n_2)} \\ &= A_m + B_m \quad , \end{aligned} \tag{VI.58}$$

where

$$A_m = \frac{D^2}{2}\left\{\frac{N^2}{2} - \frac{\Sigma\ (n_1^2+n_2^2)\ \exp(-\frac{2}{N}\ (n_1^2+n_2^2)]}{\Sigma\ \exp[-\frac{2}{N}\ (n_1^2+n_2^2)]}\right\} \qquad \text{(VI.59)}$$

and

$$B_m = D^2 m^2\ \frac{\Sigma\ (n_1+n_2)^2\ \exp[-\frac{2}{N}\ (n_1^2+n_2^2)]}{\Sigma\ \exp[-\frac{2}{N}\ (n_1^2+n_2^2)]}\ . \qquad \text{(VI.60)}$$

Two sources contribute to the second moment of the spectrum. Firstly, the A_m term comes from the second moment of the density of states. Secondly, the B_m term results from the averaged frequency shift of each manifold.

Generally speaking, the A_m is a monotonically decreasing function with m, whereas B_m is a monotonically increasing function for small m and a decreasing function for large m. To illustrate the systems of 6, 10, and 20 spins having equal couplings, the normalized values of $\langle\Omega^2\rangle_m$, A_m and B_m are plotted in Figures VI.7-VI.9. The dependence of $\langle\Omega^2\rangle_m$ for various N is shown in Figure VI.10.

The summations in eqs. (VI.58), (VI.59), and (VI.60) are taken for n_1 and n_2 with $n_1-n_2 = m$ and $\frac{N}{2} \leq n_1, n_2 \leq N/2$.

By suitable rearrangement of the indices, we can obtain a symmetric form for the summation. Let $n_2 = n, n_1 = n+m$ and $x = n + \frac{m}{2}$; we can rewrite eq. (VI.59) and (VI.60) as

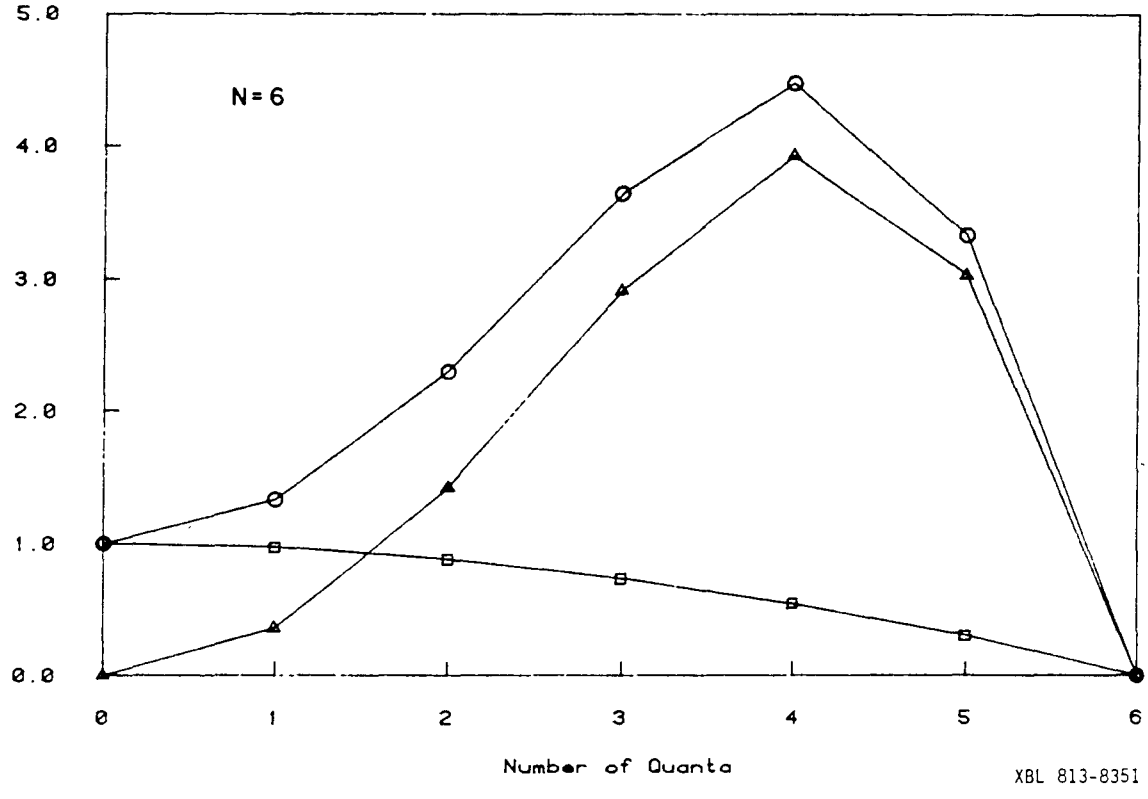

Figure IV.7 This illustration demonstrates the normalized dependence of the second moment of the number of quanta assuming equal coupling constants (circle: $\langle\Omega^2\rangle_m$; square: A_m; triangle: B_m).

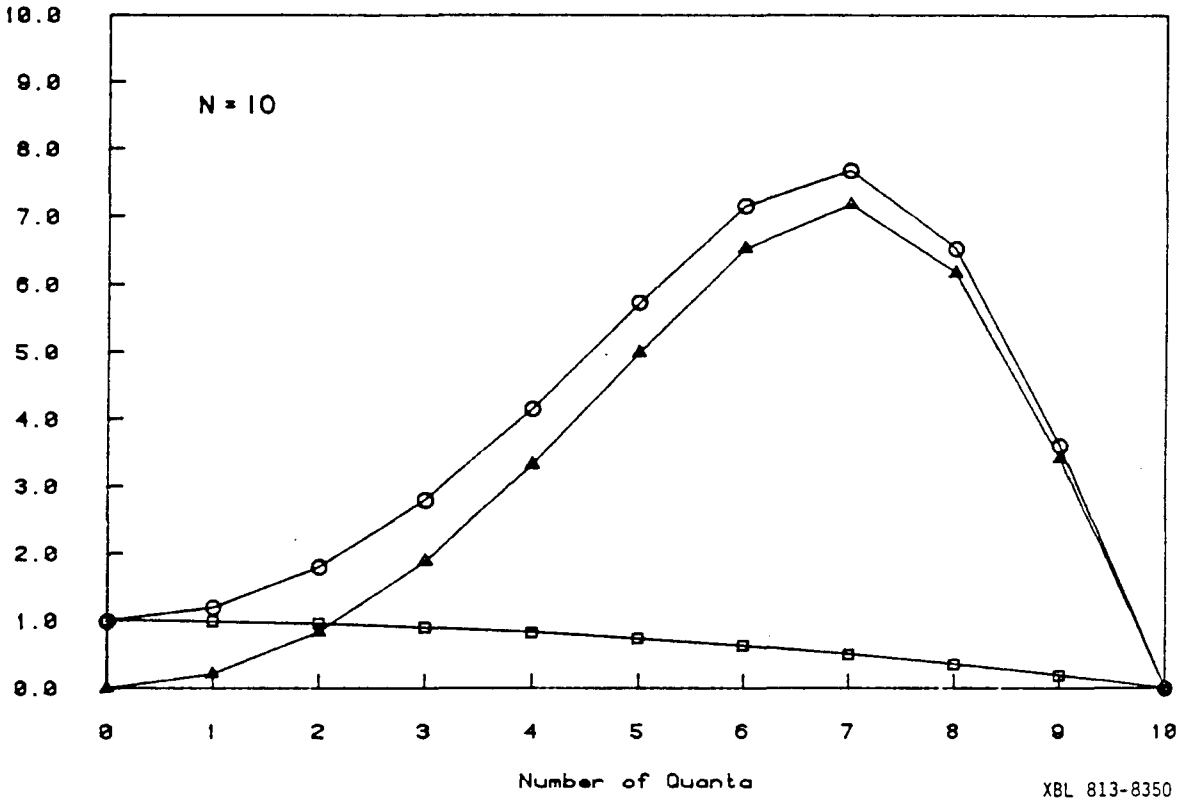

Figure VI.8 This figure is similar to Figure VI.7, except that N = 10 (circle: $\langle\Omega^2\rangle_m$; square: A_m; triangle: B_m).

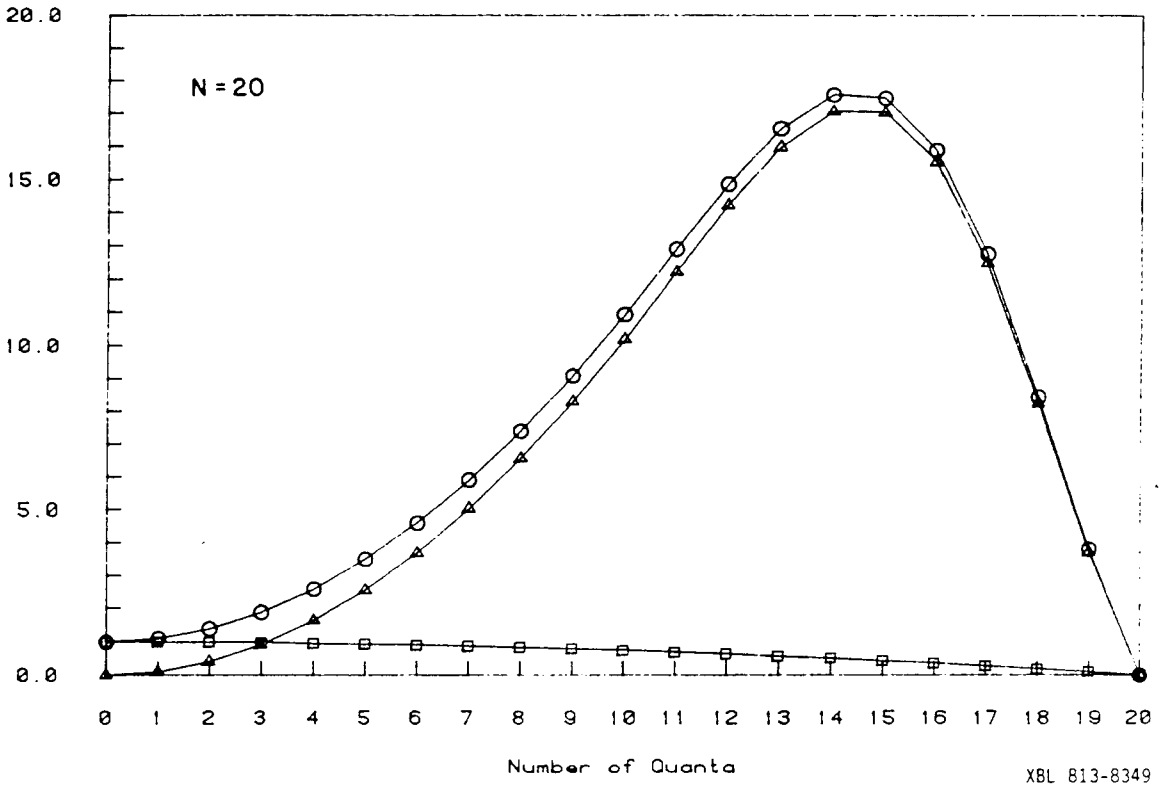

Figure VI.9 This graph is similar to Figure VI.7, except that N = 20 (circle: $\langle\Omega^2\rangle_m$; square: A_m; triangle: B_m).

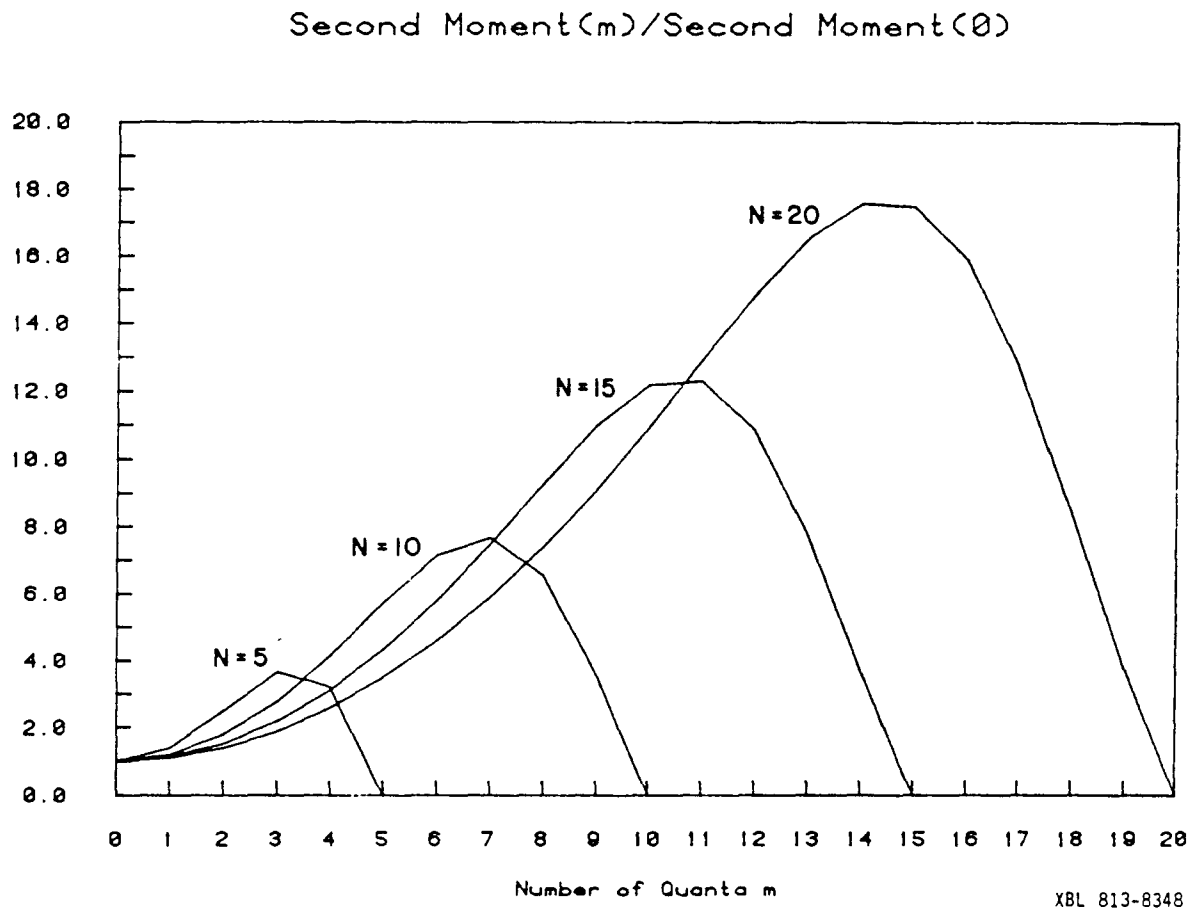

Figure VI.10 Normalized dependence of $\langle\Omega^2\rangle_m$ on m for N = 5, 10, 15, and 20.

$$A_m = \frac{D^2}{4}\left[N^2-m^2-4\,\frac{E^{-\frac{m^2}{N}}}{Z_m}\sum_{x=-\frac{N-m}{2}}^{\frac{N-m}{2}} e^{-\frac{4}{N}x^2}\,x^2\right] , \qquad \text{(VI.61)}$$

$$B_m = 4\,D^2\,m^2\,\frac{E^{-\frac{m^2}{N}}}{Z_m}\sum_{x=-\frac{N-m}{2}}^{\frac{N-m}{2}} e^{-\frac{4}{N}x^2}\,x^2 , \qquad \text{(VI.62)}$$

where Z_m is the partition function and is given by

$$Z_m = \sum_{x=-\frac{N-m}{2}}^{\frac{N-m}{2}} e^{-\frac{4}{N}x^2} . \qquad \text{(VI.63)}$$

The sumation in the above expressions can be approximated by using integration to avoid the complicated calculation. Using the definition of error function as

$$\mathrm{erf}(x) = \frac{1}{\sqrt{\pi}} \int_{-x}^{x} d^{-t^2}\, dt \quad , \tag{VI.64}$$

we can show that

$$Z_m = \int_{-\frac{N-m+1}{2}}^{\frac{N-m+1}{2}} e^{-\frac{4}{N}x^2}\, dx = \frac{1}{2}\sqrt{N\pi}\ \mathrm{erf}\left(\frac{N-m+1}{\sqrt{N}}\right) \quad , \tag{VI.65}$$

and

$$\sum_{x=-\frac{N-m}{2}}^{\frac{N-m}{2}} x^2 e^{-\frac{4}{N}x^2} \simeq \int_{-\frac{N-m+1}{2}}^{\frac{N-m+1}{2}} e^{-\frac{4}{N}x^2} x^2\, dx$$

$$= \frac{N}{8}\left[\frac{\sqrt{N\pi}}{2}\ \mathrm{erf}\left(\frac{N-m+1}{\sqrt{N}}\right) - (N-m+1)\, e^{-\frac{(N-m+1)^2}{N}}\right] \quad . \tag{VI.66}$$

The approximated value for A_m and B_m can be obtained:

$$A_m = \frac{D^2}{4}\left\{N^2-m^2-N\left[\frac{1}{2} - \frac{\frac{n-m+1}{\sqrt{N}}\ \exp\left(-\frac{(N-m+1)^2}{N}\right)}{\sqrt{\pi}\ \mathrm{erf}\left(\frac{N-m+1}{\sqrt{N}}\right)}\right]\right\} , \tag{VI.67}$$

$$B_m = D^2 m^2 N\left[\frac{1}{2} - \frac{\frac{N-m+1}{\sqrt{N}}\ \exp\left(-\frac{(n-m+1)^2}{N}\right)}{\sqrt{\pi}\ \mathrm{erf}\left(\frac{N-m+1}{\sqrt{N}}\right)}\right] \quad . \tag{VI.68}$$

The value of the error function can be found in most books of mathematical tables.[4] In the special case of small m and larger N, the value of the error function in the above expression is approximately equal to unity.

Using an integration approximation, the calculated value of $\langle\Omega^2\rangle_m$ ($= A_m + B_m$) is very close to its exact value, except for large m. The comparison is illustrated for the cases N = 6 and 10 and is shown in figures (VI.11) and (VI.12).

We shall proceed with the discussion on the general case without assuming that the coupling constants are all equal.

The complex calculation for the general case comes from finding the square trace of the diagonal dipolar Hamiltonians,

$$\mathrm{Tr}\Big[\Big(\sum_{i,j}{}' 2\, D_{ij}\, I_{iz}\, I_{jz}\Big)\Big(\sum_{k,\ell}{}' 2\, D_{k\ell}\, I_{kz}\, I_{\ell z}\Big)\Big]$$

$$= \sum_{\{A,B\}} \Big(\frac{1}{2} \sum_{\substack{i,j \\ i,j\in AUB}}{}' D_{ij} - \sum_{i,k} D_{ik}\Big)^2 \quad . \qquad \text{(VI.69)}$$

The first summation is carried out over all possible sets, with subset A containing N-n spins up and subset B containing n spins down. The notation AUB represents the union set of subsets A and B.

The trace calculation is straightforward, yet tedious. The computer program needed to perform the trace calculation for each manifold and for the second moment of the multiple quantum spectra, based on the statistical model, is shown in the appendix A.
The second moment of the density of states in the manifold having magnetic quantum number n is defined by

$$\sigma_n^2 = \langle \mathcal{H}_D^{\,2} \rangle - \langle \mathcal{H}_D \rangle^2 \quad . \qquad \text{(VI.70)}$$

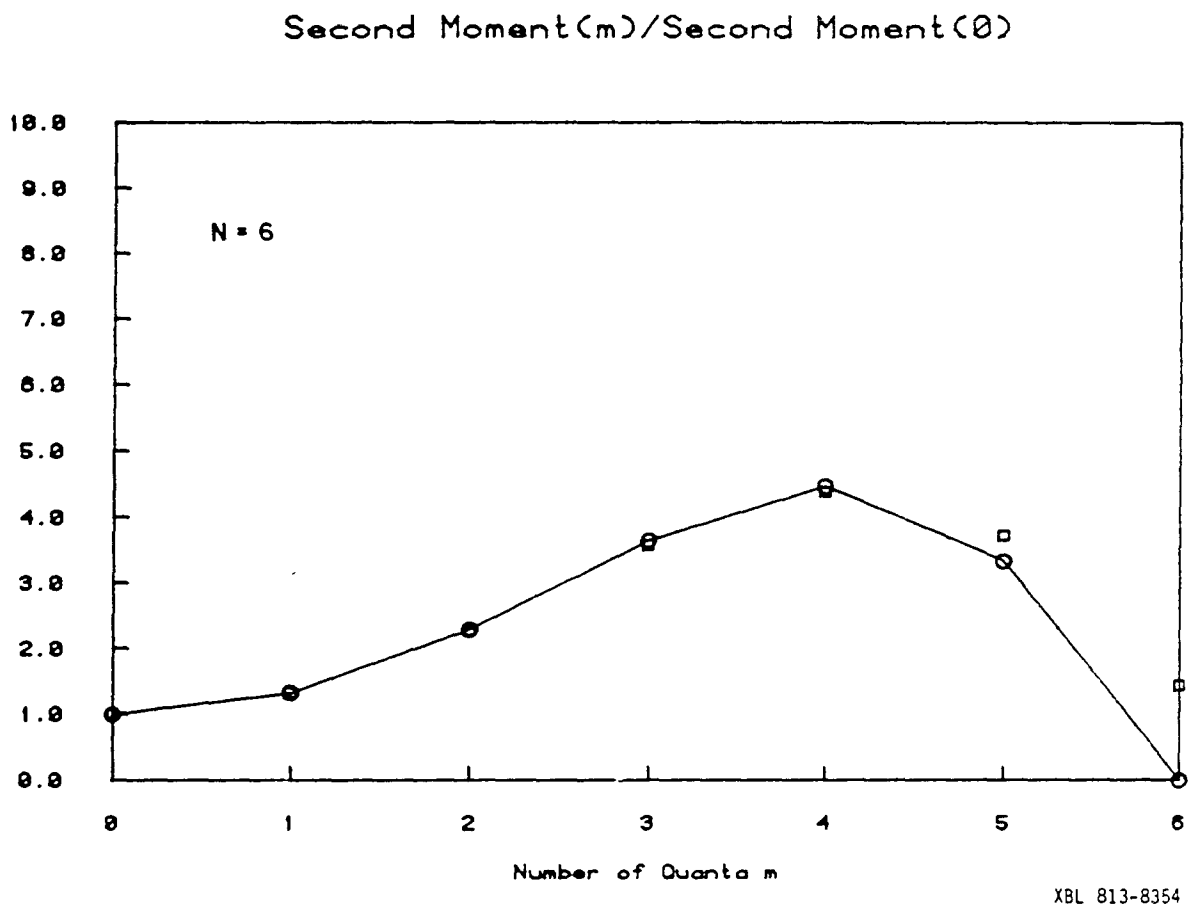

Figure VI.11 Here we observe the normalized dependence of the second moment on the number of quanta if we assume they have equal coupling constants. The value obtained by the integration approximation (square) is very close to the value based on the statistical model (circle), except for large m (N = 6).

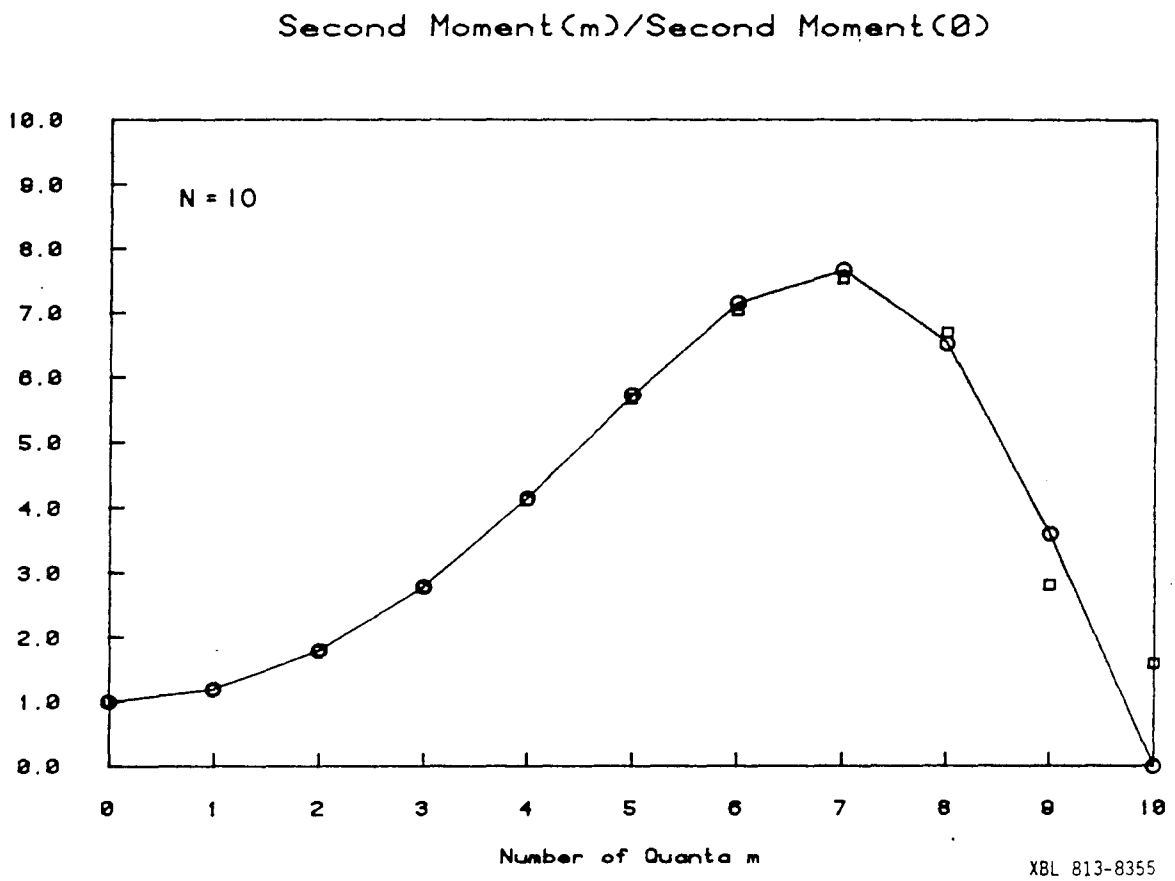

Figure VI.12 This graph is similar to Figure VI.11, except that N = 10.

It has a complicated dependence on the distribution of the dipole couplings and can be caluclated by using the computer program shown in the appendix.

Yet, the averaged frequency shift ω_n in the manifold with a magnetic quantum number m has a simple relation, and is given by

$$\omega_n = \langle \mathcal{H}_D \rangle_n = \frac{\langle D \rangle}{4} (4\, n^2 - N) \quad , \tag{VI.71}$$

where <D> is the averaged dipole coupling constant.

The second moments of the m-quantum spectrum is given by

$$\langle \Omega^2 \rangle_m = \frac{\sum_{|n_1 - n_2| = m} (\sigma^2_{n_1,n_2} + \omega^2_{n_1,n_2})\, C_N(n_1)\, C_N(n_2)}{\sum_{|n_1 - n_2| = m} C_N(n_1)\, C_N(n_2)} \quad , \tag{VI.72}$$

where $\sigma^2_{n_1,n_2} = \sigma^2_{n_1} + \sigma^2_{n_2}$ and $\omega_{n_1,n_2} = \omega_{n_1} - \omega_{n_2}$. The contribution of $\langle \Omega^2 \rangle_m$ from the averaged dipolar shift $\omega^2_{n_1,n_2}$ is large for the case with $\langle D^2 \rangle - \langle D \rangle^2$, and has a simple form

$$B_m = \frac{\Sigma\, \omega^2_{n_1,n_2}\, C_N(n_1)\, C_N(n_2)}{\Sigma\, C_N(n_1)\, C_N(n_2)}$$

$$= \langle D \rangle^2\, m^2\, \frac{\Sigma\, (n_1 + n_2)^2\, C_N(n_1)\, C_N(n_2)}{\Sigma\, C_N(n_1)\, C_N(n_2)} \quad . \tag{VI.73}$$

The complicated calculation of A_m, which comes from $\sigma^2_{n_1,n_2}$, is carried out by a computer program in the appendix.

For example, the second moments of six spin systems, that have various sets of dipole couplings, are illustrated in Figure

VI.13. The top curve refers to the system with all the dipole couplings equal. This particular system has a very large B_m component. The bottom curve refers to the system with coupling constants of equal magnitude, but that alternate in sign. Its B_m component is zero. The second moments decrease monotonically with m. The central curve is for the benzene molecule. Its coupling constants are not all equal, but have same sign.

Another example is illustrated in Figure VI.14. The curve A is a monotonically decreasing function of m, since the dipole couplings between the two methyl protons alternate in sign and have a small <D>.

The curve of second moments has a strong dependence on the ratio of γ (= $<D>^2 / <D^2>$)--as we illustrated in the comparison between the benzene molecule and dimethylmaleic anhydride molecule. This is also shown in Figure VI.14. In the case A, all couplings are equal to one and $\gamma = 1$. As more couplings have negative sign as in the cases B, C, and D, the value of γ decreases. For all the above cases, $<D^2>$ is the same and equals one, however, <D> becomes smaller in the sequence from A to D.

Even the distribution of dipole couplings has the same value of γ, although some small variation of the second moments' dependence of m still exists. A few examples are shown in Figures VI.15 and VI.16. In each figure, the value of γ is equal. It appears that the second moments are large if several spins with an opposite sign in coupling are in common. For example, the system A in Figure VI.15 has two negative coupling constants D(1,2) and D(1,3). They have a common spin index 1.

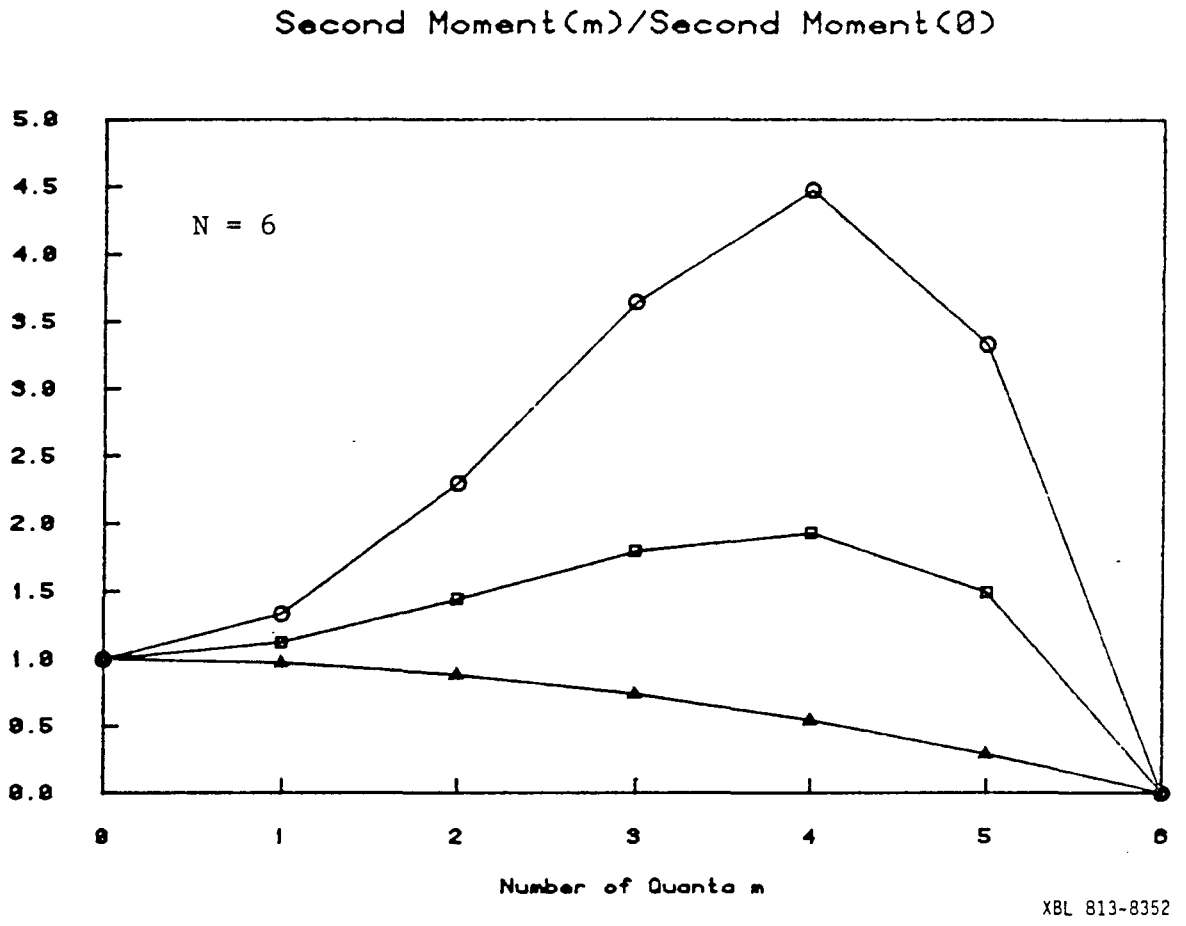

Figure VI.13 Here we see the normalized dependence of the second moment on the number of quanta (circle: equal coupling constants; square: benzene, triangle: couplings equal in magnitude, but alternating in sign).

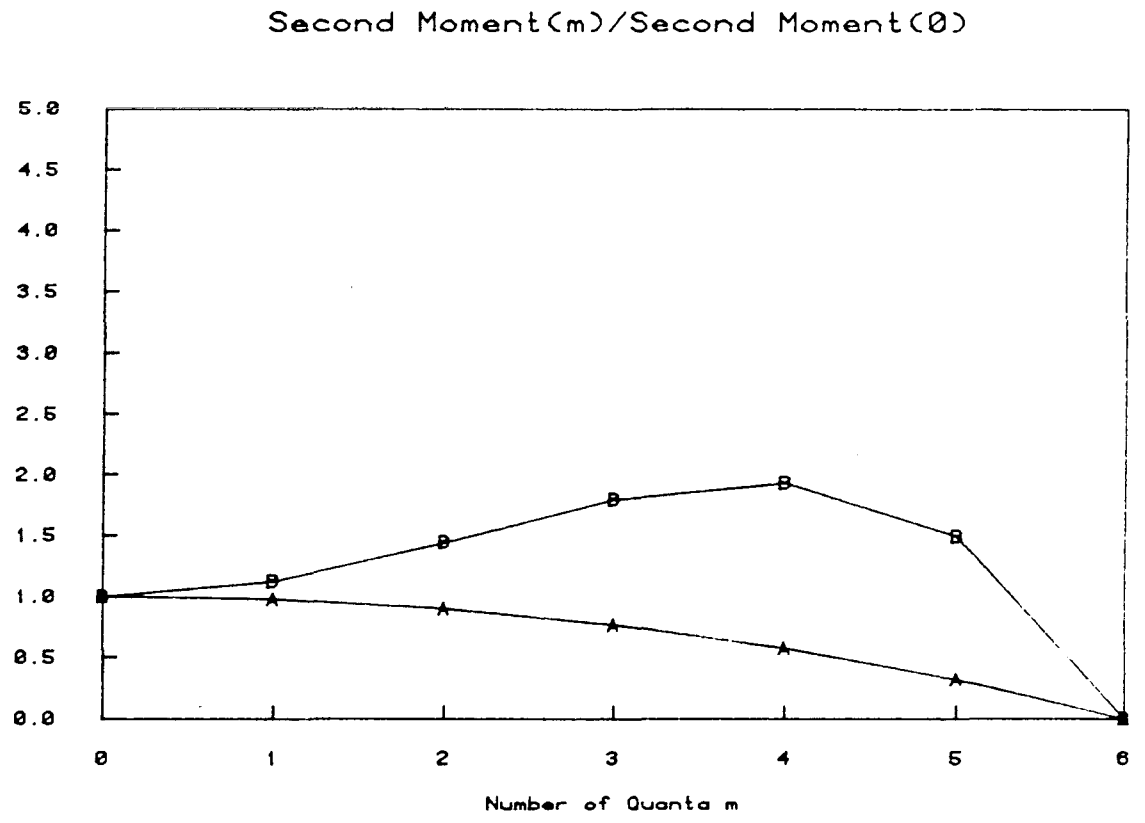

Figure VI.14 Normalized dependence of the second moment on the number of quanta for N = 6 (A: dimethyl maleic anhydrice which has couplings alternating in sign; B: benzene which has couplings of the same sign).

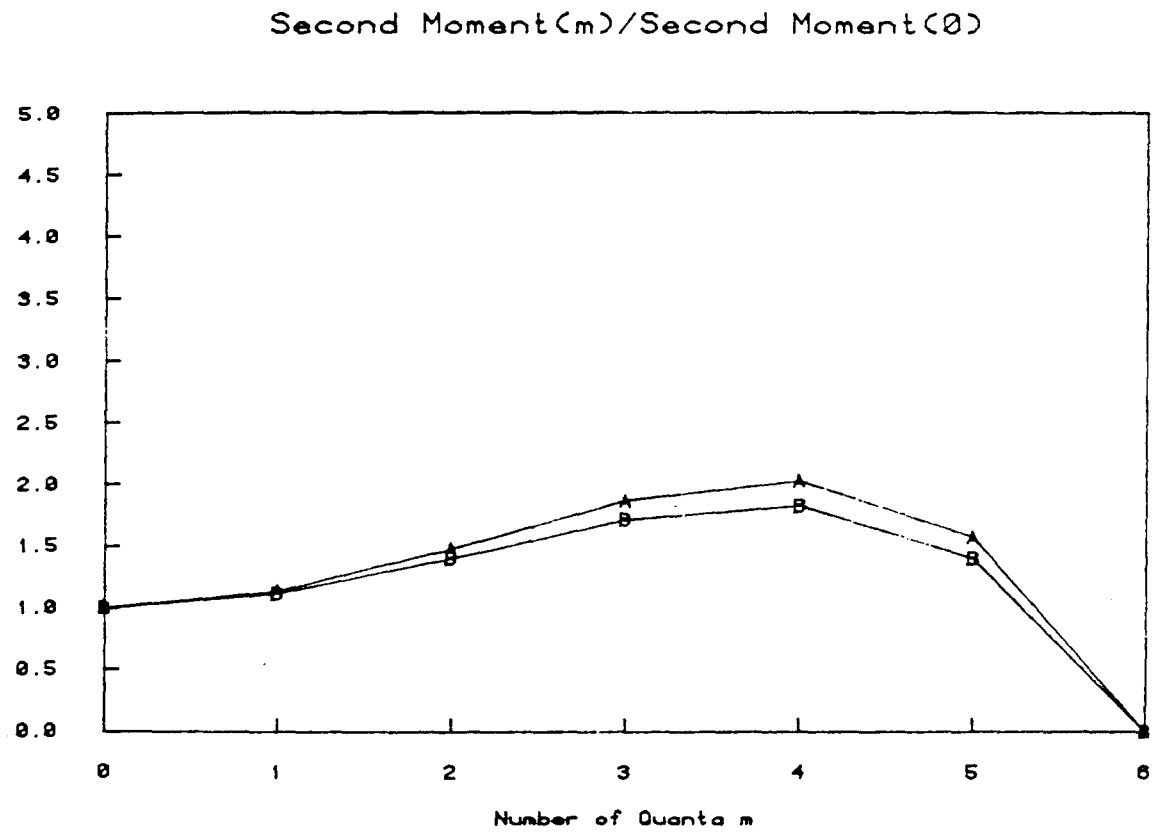

Figure VI.15 Normalized dependence of the second moment on the number of quanta for N = 6 (A: all D(i,j) = 1 except two couplings D(1,2) and D(1,3); B: D(i,j) = 1 except D(1,2) and D(3,4)). In case A the couplings having a negative sign share a common particle 1.

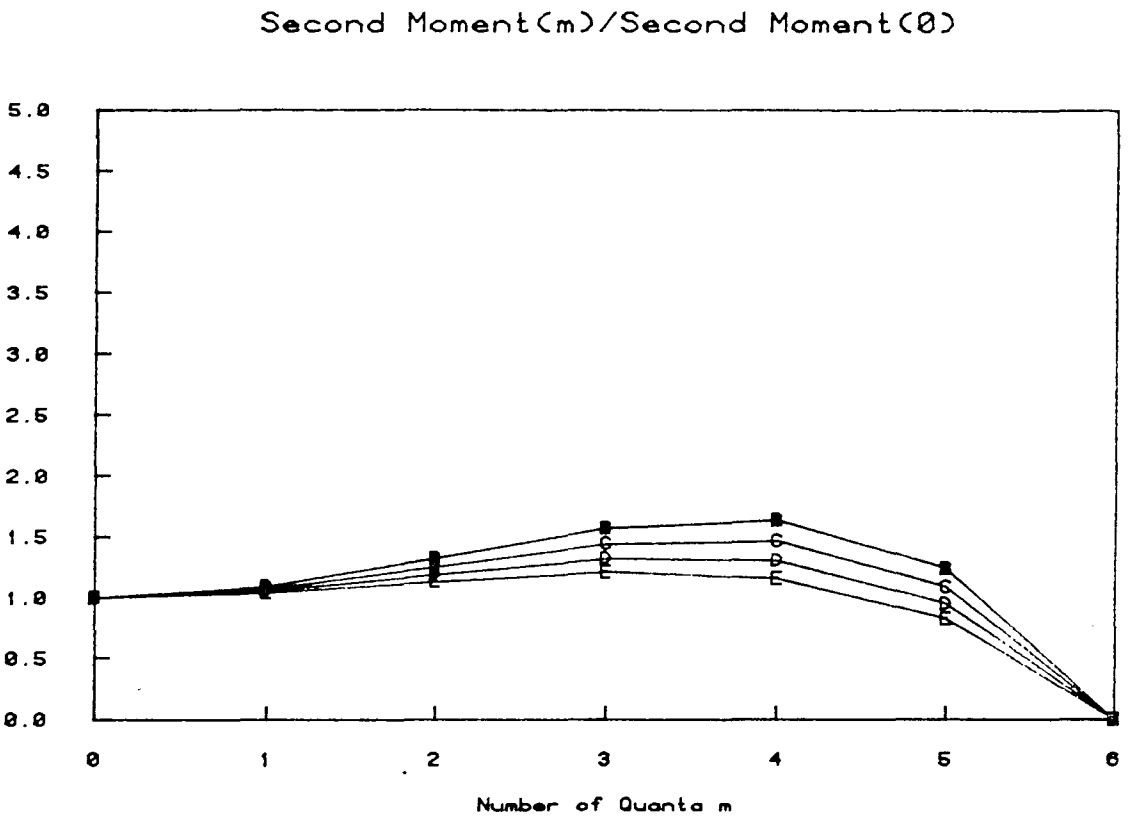

Figure VI.16 Normalized dependence of the second moment on the number of quanta for N = 6 with all D(i,j) = 1, except for three coupling constants shown in cases A through E.

Although there is a small variation in the function of second moments, their overall behavior is largely determined by the value of γ (Figure VI.17). The qualitative dependence of the second moments of the multiple quantum spectra on the value of $\langle D^2 \rangle$, $\langle D \rangle^2$, and γ predicts different behavior of the second moments for molecules of benzene and dimethylmaleic anhydride. The experimental spectra in Figures II.9 and V.8 show a good agreement with the statistical model for the second moments.

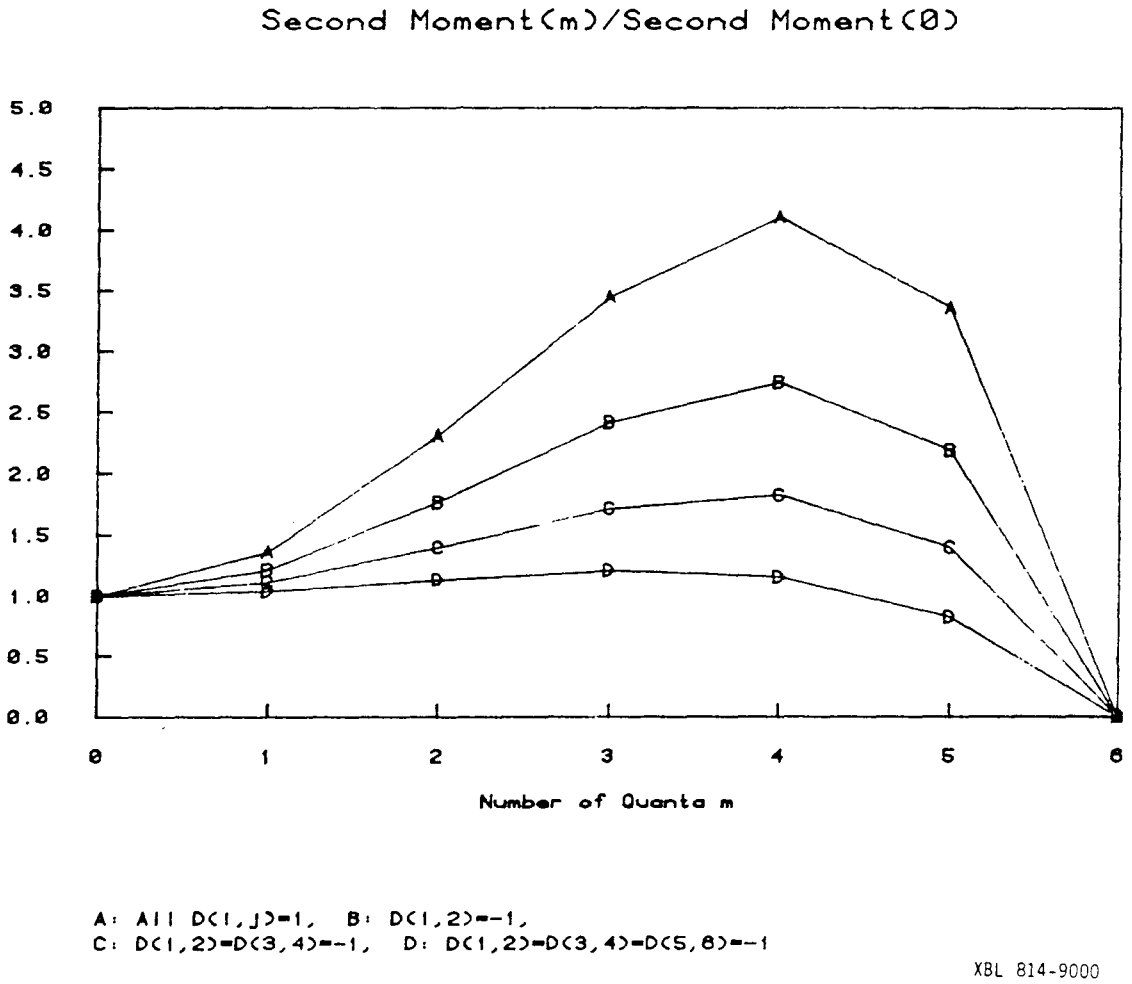

Figure VI.17 Normalized dependence of the second moment on the number of quanta for N = 6 (A: all coupling constants equal to unity; B: D(i,j) = 1 except that D(1,2) = -1; C: D(i,j) = 1 except that D(1,2) = D(3,4) = -1, and so on).

6.5 References

1. S. Mukamel, J. Murdoch, and A. Pines, Lawrence Berkeley Laboratory MMRD Annual Report p. 262 (1977).

2. A. Carrington and A. D. McLachlan, Introduction to Magnetic Resonance, Chapter 3 (Harper & Row, New York, 1967).

3. A. Abragam, The Principles of Nuclear Magnetism, Chapter 4, (Oxford Univ. Press, London, 1961).

4. H. B. Dwight, Tables of Integrals and Other Mathematical Data (MacMillan, New York).

VII

SPIN-LATTICE RELAXATION OF METHYL GROUPS IN SOLIDS

7.1 Spin-lattice relaxation

As discussed earlier in chapter IV, the time-dependent Hamiltonian $H_1(t)$ describes the fluctuation of the interaction between spins and lattice. This fluctuation is responsible for the relaxation of the spin system toward thermal equilibrium. The spin-lattice relaxation time characterizes the recovery of the non-equilibrium diagonal elements of the density matrix. The diagonal part of the density matrix describes the population of states.

In general, the spin-lattice interaction can be written as a inner product of two tensors of rank j:[1]

$$H_1(t) = \sum_{\mu,m} (-1)^m V^{(m)}_{(j)\mu} [f^{(m)}_{(j)\mu}(t)]^+ \quad , \quad (|m| \leq j) \quad , \text{(VII.1)}$$

with

$$[I_z, V^{(m)}_{(j)\mu}] = m V^{(m)}_{(j)\mu} \quad ,$$

$$[I_\pm, V^{(m)}_{(j)\mu}] = \sqrt{j(j+1)-m(m\pm1)}\ V^{(m\pm1)}_{(j)\mu} \quad ,$$

and

$$[V^{(m)}_{(j)\mu}]^+ = (-1)^m V^{(-m)}_{(j)\mu} \quad .$$

There are several common forms for the tensor operator $V^{(m)}_{(j)\mu}$.[2]

(1) V_μ is linear with respect to the spin operators, for example, the interaction of spins with the random fluctuation fields.

(2) V_μ is bilinear with respect to the spin operators of single nuclei, such as the quadrupole interaction of nuclei with spin $I \geq 1$ with the fluctuating electric field gradient.

(3) V_μ is bilinear with respect to the spin operators of two different nuclei, such as the fluctuating spin-spin interaction. In case (1) $j = 1$, and $j = 2$ in cases (2) and (3). The subscript j will be dropped out in a later discussion.

The correlation functions $G_\mu^{(m)}(\tau)$ are assumed to have an exponential decay form characterized by a single correlation time τ_c,

$$(-1)^m \overline{f_\mu^{(-m)}(t)\, f_\nu^{(n)}(t-\tau)} = \delta_{mn}\, \delta_{\mu\nu}\, G_\mu^{(m)}(0)\, \exp(-\tau/\tau_c). \quad \text{(VII.2)}$$

Using the above explicit expressions for the time-dependent Hamiltonian $H_1(t)$ and correlation function, the master equation of motion in equation (IV.11) is expressed:

$$\frac{d\rho}{dt} = -i[H_o,\rho] - \int_0^\infty d\tau\, \overline{[e^{-iH_o\tau}\, H_1(t+\tau)\, e^{iH_o\tau}, [H_1(t),\rho-\rho_o]]}$$

and becomes

$$\frac{d\rho}{dt} = -i[H_o,\rho] - \frac{1}{2} \sum_{\mu,m} J_\mu(m\,\omega_o)\, [V_\mu^{(m)},[V_\mu^{+(m)},\rho-\rho_o]] \quad , \quad \text{(VII.3)}$$

where the spectral density $J_\mu(m\,\omega_o)$ is defined by the Fourier

transform of $G_\mu^{(m)}(\tau)$ as

$$J_\mu(m\,\omega_o) = G_\mu^{(m)}(0)\,\frac{2\,\tau_c}{1 + m^2\,\omega_o{}^2\,\tau_c{}^2} \quad . \tag{VII.4}$$

7.2 Spin thermodynamics in solids

It is generally assumed that after any disturbance the density matrix of a dipole-coupled spin system in solids takes the form:[3]

$$\rho \simeq 1 + \alpha_z\,H_z + \alpha_D\,H_D^{(0)} \tag{VII.5}$$

due to a complete spin diffusion. The time-dependent Lagrange multipliers α_z and α_D are the inverse temperatures of the subsystems of the Zeeman reservoir and dipolar reservoir. As a result, the Zeeman as well as the dipolar relaxation, is characterized by a single exponential decay; they are not coupled.

The above traditional model, however, is not adequate for describing dipolar solids that contain reorienting or tunneling symmetrical groups, such as CH_3, CF_3, and NH_4. They have a general feature of non-exponential relaxation.[4-6]

Without losing generality, we can assume that the spin system has no subsystems. As far as the spin-lattice relaxation is concerned, only the diagonal part of the density matrix is relevant. The Zeeman subsystem is characterized by the operator I_z; each subsystem is associated with an operator.

It is convenient to define a set of n orthonormal, traceless diagonal matrices O_k's,[7]

$$\mathrm{Tr}\ O_k = 0 \quad , \tag{VII.6}$$

and

$$\mathrm{Tr}(O_k O_j) = \delta_{ij} \quad . \tag{VII.7}$$

Using high temperature approximation, we can assume that

$$\rho \simeq 1 + \sum_k \alpha_k O_k \quad , \tag{VII.8}$$

where $\alpha_k = \mathrm{Tr}(O_k\ \rho)$.

Using the following relations,

$$\mathrm{Tr}(O_k[H_0,\rho] = \mathrm{Tr}([O_k,H_0]\rho) = 0 \quad ,$$

and

$$\mathrm{Tr}(O_k[V_\mu^{(m)},[V_\mu^{+(m)},O_j]]) = \mathrm{Tr}([O_k,V_\mu^{(m)}][V_\mu^{+(m)},O_j]) \quad ,$$

we can express the master equation for the density matrix in terms of these orthonormal operators,

$$\frac{d}{dt}\alpha_k = -\sum_j S_{kj}(\alpha_k - \alpha_{k,o}) \quad , \tag{VII.9}$$

where

$$S_{kj} = \frac{1}{2}\sum_{\mu,m} J_\mu(m\ \omega_o)\ \mathrm{Tr}([O_k,V_\mu^{(m)}][V_\mu^{+(m)},O_j])$$

$$= \frac{1}{2}\sum_{\mu,m} J_\mu\ (m\ \omega_o)\ \mathrm{Tr}([O_k,V_\mu^{(m)}][O_j,V_\mu^{(m)}]^+) \quad . \tag{VII.10}$$

The off-diagonal elements of the relaxation rate matrix S describes the cross-relaxation between the two associated subsystems.

The transition rate matrix W is related to the matrix S by

$$S_{kj} = \frac{1}{2} \sum_{\alpha,\beta} (0_{k,\alpha} - 0_{k,\beta})(0_{j,\alpha} - 0_{j,\beta}) W_{\alpha\beta} \quad , \tag{VII.11}$$

where $W_{\alpha\beta}$ is the transition rate between states $|\alpha\rangle$ and $|\beta\rangle$, and

$$W_{\alpha\beta} = \sum_{\mu,m} J_{\mu}(m\,\omega_o) \; |\langle\alpha|V_{\mu}^{(m)}|\beta\rangle|^2$$

$$= \frac{1}{\hbar^2} \int_{-\infty}^{\infty} d\tau \; \overline{\langle\alpha|H_1(t)|\beta\rangle\langle\beta|H_1(t-\tau)|\alpha\rangle} \; \exp(i\omega_{\alpha\beta}\tau) \quad . \tag{VII.12}$$

Both matrices S and W are symmetric, namely,

$$S_{kj} = S_{jk} \quad , \quad W_{\alpha\beta} = W_{\beta\alpha} \quad . \tag{VII.13}$$

The lifetime t_α of state $|\alpha\rangle$ is related to the elements of W by the equations (IV.25) expressed as

$$1/t_\alpha = \sum_{\beta\neq\alpha} W_{\alpha\beta} \quad . \tag{VII.14}$$

Defining a new matrix $\hat{W}$ by

$$\hat{W}_{\alpha\beta} = W_{\alpha\beta} - \delta_{\alpha\beta} \sum_{\gamma} W_{\alpha\gamma} \quad , \tag{VII.15}$$

we can show that

$$\sum_{\alpha} \hat{W}_{\alpha\beta} = 0 \quad , \tag{VII.16}$$

$$\hat{W}_{\alpha\beta} = \hat{W}_{\beta\alpha} \quad , \tag{VII.17}$$

$$S_{kj} = - \sum_{\alpha,\beta} O_{k,\alpha} O_{j,\beta} \hat{W}_{\alpha\beta} \quad . \tag{VII.18}$$

The Pauli equation for the population change is related to $\hat{W}_{\alpha\beta}$ by

$$\frac{d}{dt} \rho_{\alpha} = - \sum_{\beta} \hat{W}_{\alpha\beta} (\rho_{\alpha}-\rho_{\alpha,0}-\rho_{\beta}+\rho_{\beta,0}) \quad , \tag{VII.19}$$

where ρ_{α} is the population at state $|\alpha>$. The above equation is completely equivalent to the equation (VII.9). Yet, by choosing an appropriate set of the operators O_i's, we may obtain a better physical picture about the relaxation mechanism.[7]

7.3 Relaxation of protonated methyl groups in solids

The cross-correlation in the fluctuation of the dipole-dipole interaction in solids has strong impact on the behavior of relaxation. Generally this leads to an non-exponential spin-lattice relaxation.[4]

The methyl groups in solids undergo hindered rotation about their three-fold symmetry axes. The first random reorientation modulates the dipole-dipole interaction among methyl protons.

The spin state of methyl protons consists of eight levels as shown in Figure VII.1.[8] The E^a and E^b states are shifted upward in energy with respect to A states that result from rotor-lattice interactions. The energy splitting is $\hbar\omega_t$. At high temperature, where semiclassical description is valid, the tunneling frequency ω_t is approximately equal to zero.

Because of the conservation of total population, the distribution of population among eight levels can be described by seven independent occupation operators 0_k. It is convenient to choose them according to physical properties. Two of them, 0_1 and 0_5, correspond to the Zeeman and dipolar system. Another two, 0_4 and 0_6, correspond to the rotational polarization, being defined as the excess in population of E^a over E^b states, 0_6 to the tunneling system, being defined as the excess in population of A over E spin species.[8] The eigenvalues of these operators are given in Table (VII.1).

Using the above set of occupation operators, the relaxation rate matrix can be evaluated if we assume a three-fold random reorientation of the methyl groups. Their values are listed elsewhere.[8]

Up to now, the effects caused by the interaction among methyl groups has not been taken into account, this leads to a spin diffusion process at a rate much faster than the spin-lattice relaxation.

The traditional spin temperature model, assuming a complete spin diffusion which mixes up the A, E^a, and E^b spin states, shows that the Zeeman and dipolar systems are the only quasi-constants

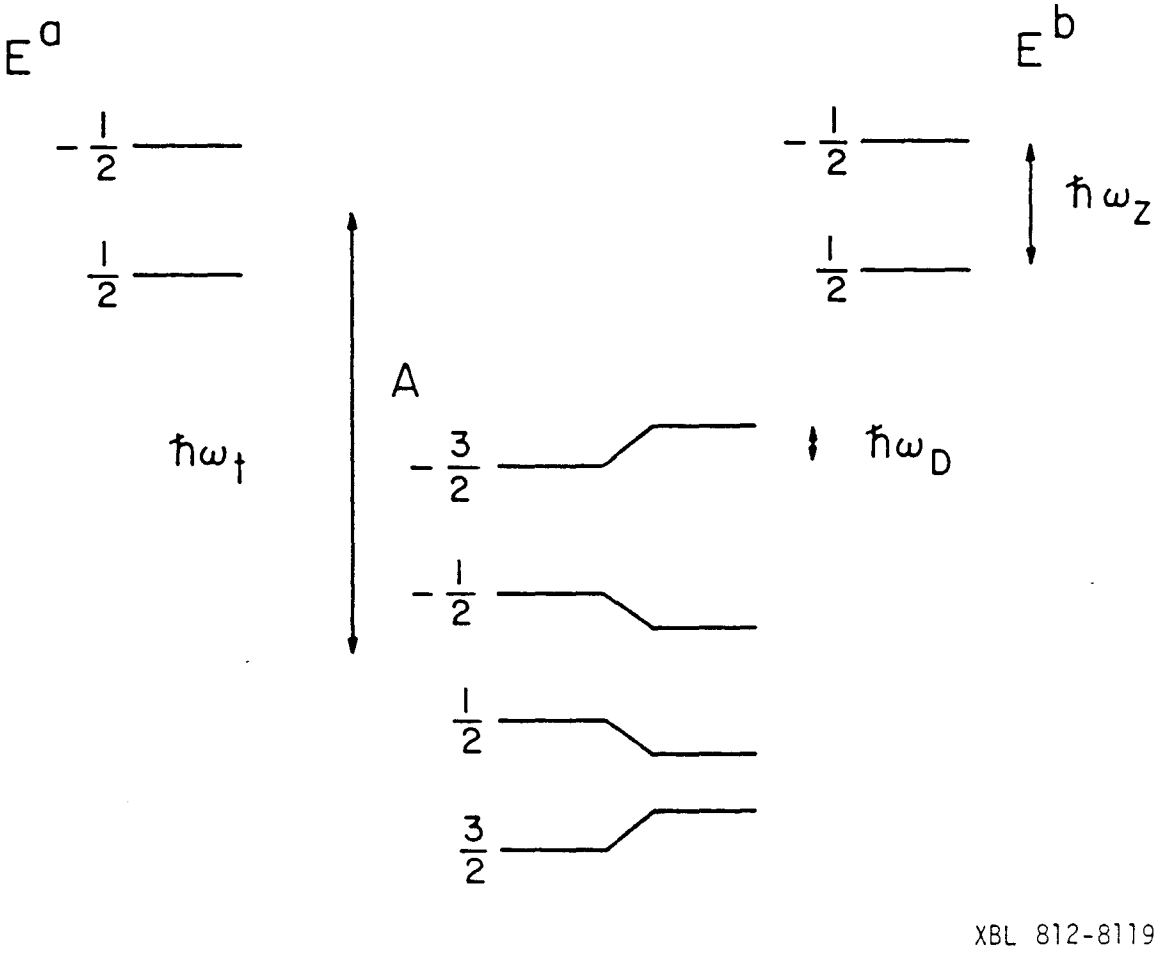

Fig. VII.1 This figure illustrates the energy levels of the three protons of a methyl group considering the Zeeman, intramethyl dipolar, and tunneling interactions. The appearance of a tunneling energy in the spin Hamiltonian is a consequence of the Pauli exclusion principle that couples spin and rotor symmetries.

Table VII.1

Eigenvalues[a] of the Occupation Operators[b,c]

	$A_{3/2}$	$A_{1/2}$	$A_{-1/2}$	$A_{-3/2}$	$E^a_{1/2}$	$E^a_{-1/2}$	$E^b_{1/2}$	$E^b_{-1/2}$
$\sqrt{6}\ 0_1$	3/2	1/2	-1/2	-3/2	1/2	-1/2	1/2	-1/2
$\sqrt{2}\ 0_2$	1/2	-1/2	1/2	-1/2	-1/2	1/2	-1/2	1/2
$\sqrt{3}\ 0_3$	0	1	- 1	0	-1/2	1/2	-1/2	1/2
0_4	0	0	0	0	1/2	1/2	-1/2	-1/2
0_5	1/2	-1/2	-1/2	1/2	0	0	0	0
$\sqrt{2}\ 0_6$	1/2	1/2	1/2	1/2	-1/2	-1/2	-1/2	-1/2
0_7	0	0	0	0	1/2	-1/2	-1/2	1/2

[a]The eigenvalues are for the spin eigenstates of the Zeeman and secular dipolar Hamiltonians. At quasi-equilibrium, all of the number operators are diagonal.

[b]The identity operator which, may be taken as the eighth occupation operator, is not needed since the total population of the spin states is constant.

[c]This table is taken from reference 8.

of the motion.[2] The density matrix at quasi-equilibrium is of the form

$$\rho = 1 + \alpha_1 0_1 + \alpha_5 0_5 \quad .$$

The spin-lattice relaxation of α_1 and α_5 are independent at a high temperature when $\omega_t = 0$. They relax exponentially at rates S_{11} and S_{55}. At low temperature when $\omega_t \neq 0$, the cross-relaxation rate S_{15} is not zero, and the Zeeman and dipolar systems are coupled.[7] The spin-lattice relaxation is characterized by two exponentials.

The prediction of the above model does not agree with the experimental facts of the non-exponential spin-lattice relaxation. Because of the rapid reorientation, the flip-flop terms of the inter-methyl dipolar interaction conserve the symmetry of spin states. The protons of the same methyl group experience the same averaged local dipolar field than protons in neighbor methyl groups. This is the basic assumption of symmetry-restricted spin diffusion (SRSD).[8,9] In this case, four degrees of freedom are expected.[8] Instead of equation(VII.5), the quasiequilibrium density matrix takes the form:

$$\rho = 1 + \alpha_1 0_1 + \alpha_4 0_4 + \alpha_5 0_5 + \alpha_6 0_6 \quad .$$

When $(\omega_t + n\,\omega_o)^2\,\tau_c^2 << 1$, i.e., $\omega_t = 0$ or $\omega_t >> \omega_o$, the Zeeman system is only coupled to the rotational polarization, and the dipolar system is coupled to the tunneling system, as shown in Figure (VII.2). These predictions have been verified experimentally by discoveries of the Haupt effect[10-12] and

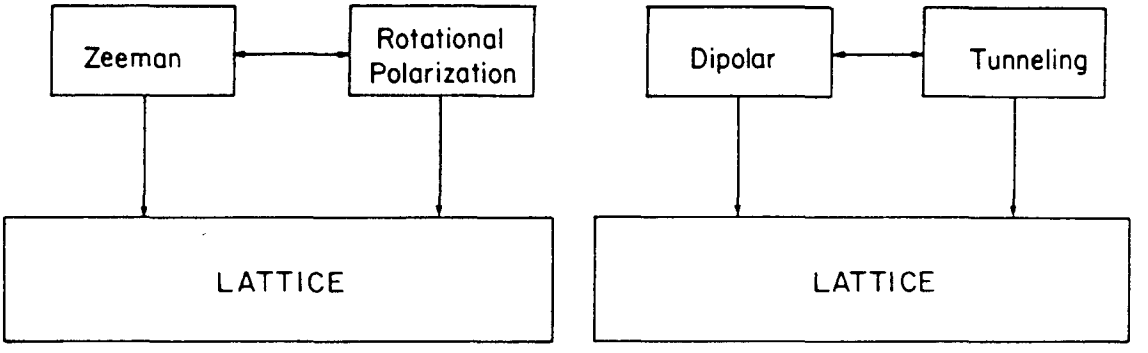

XBL 803-8663

Figure VII.2 At high temperature, when $\omega_t = 0$, the Zeeman system is only coupled to the rotational polarization, and the dipolar system is coupled to the tunneling system. This leads to non-exponential spin-lattice relaxation and the Haupt effect.

and non-exponential spin-lattice relaxation. For an arbitrary value of $\omega_t - \omega_o$, the relaxation of α_1, α_4, α_5, and α_6 are mutually coupled as is shown in Figure (VII.3).

7.4 Relaxation of deuterated methyl groups in solids.[23]

7.4.1 Introduction

The relaxation mechanism of reorienting or tunneling methyl groups in solids has been under intensive investigation.[4-20] The non-exponential nature of spin lattice relaxation[4-6,8,17] and the Haupt effect[10-12] of thermally induced dipolar polarization can be explained as being a result of the dynamical couplings among Zeeman, dipolar, tunneling, and the rotational polarization systems. At high temperatures, the non-zero couplings exist only between the Zeeman and rotational polarization systems and between the dipolar and tunneling systems.

In this section, we shall study the system of deuterated methyl (CD_3) groups in solids. Some interesting new features arise because of the deuterium quadrupole coupling. In a manner analogous to the CH_3 case,[7] let us assume that the relevant quasi-constants of the motion are the Zeeman, quadrupole, tunneling, and rotational polarization systems. The dipolar reservoir is negligibly small in the CD_3 case. In particular, we assume, that the fluctuation of quadrupole coupling of the deuterons, by random reorientation or tunneling of the methyl group, is the dominant relaxation mechanism. We shall derive the relaxation equations for the above subsystems and see which subsystems are mutually coupled by relaxation. The full calculation is given in Section 7.4.2. Here we shall mention

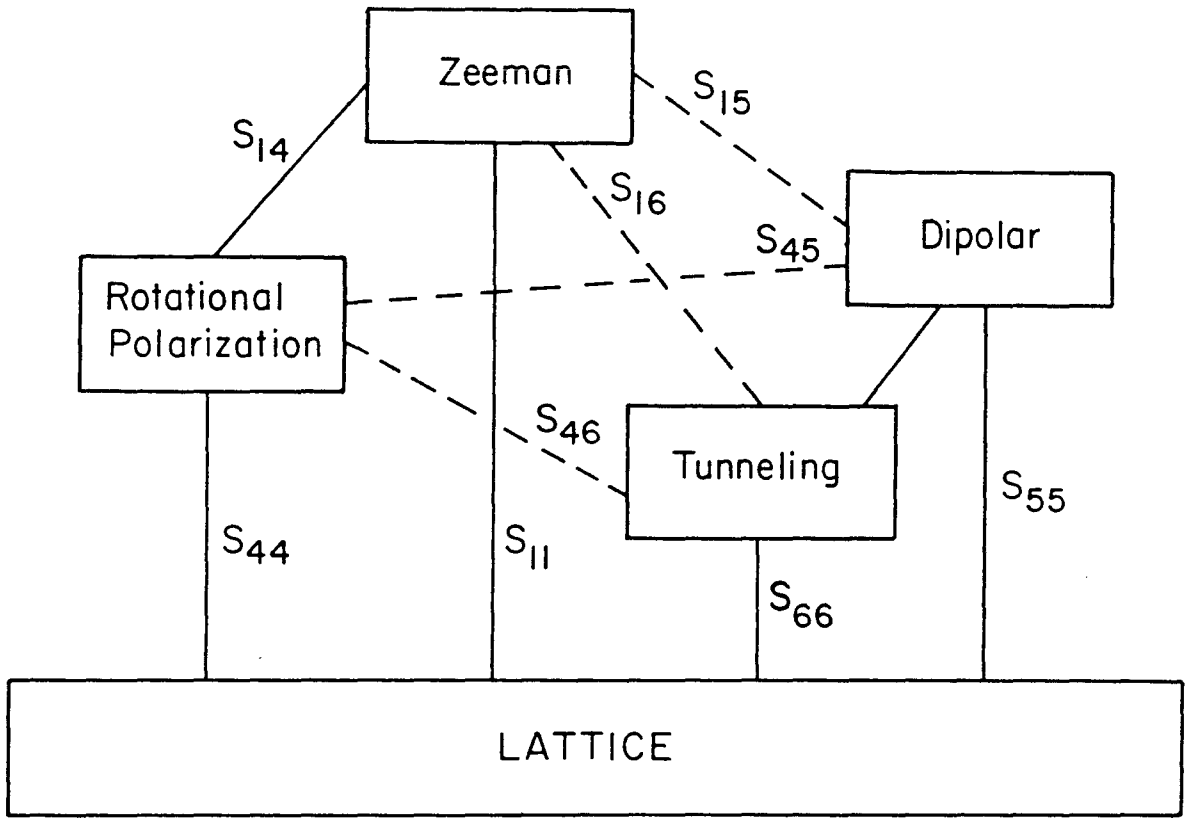

XBL 816-10420

Fig. VII.3 In general, the lattice, Zeeman, rotational polarization, dipolar, and tunneling systems are all coupled together. The cross-relaxation rates S_{15}, S_{16}, S_{45}, and S_{46} vanish when $\omega_t = 0$ or $\omega_t >> \omega_o$.

the main findings. For random reorientation at high temperatures (i.e., $\geq$ 77°K) Zeeman, quadrupole, tunneling, and the rotation polarization systems are predicted to be uncoupled. This is a contrast to the CH_3 case. As a result, the Zeeman spin lattice relaxation is expected to be exponential. For tunneling CD_3 groups at low temperatures ($<<$ 77°K) the Zeeman and tunneling systems are coupled, and consequently, the Zeeman spin lattice relaxation is predicted to become non-exponential. The experiments that we have done to test the calculations consist of measuring the Zeeman spin lattice relaxation of dilute toluene, with the methyl group having been deuterated, at liquid nitrogen and liquid helium temperatures. The experimental results are discussed in Section 7.4.3. We mention here that the relaxation is exponential at liquid nitrogen temperature and becomes non-exponential at liquid helium temperature, thus verifying the unique expectations for CD_3 relaxation.

7.4.2 Theory

Consider a CD_3 group with geometrical parameters shown in Figure VII.4. Unlike the system of methyl protons, the dominant relaxation mechanism of deuterated methyl groups is caused by the fluctuation of quadrupole coupling through random rotation of the reorienting or tunneling methyl groups. The much less efficient relaxation process due to fluctuating dipolar interactions may be neglected. The Hamiltonian of the rotating methyl deuterons in a high field consists of a Zeeman term (H_Z), tunneling term (H_t), the time-averaged truncated quadrupole interaction ($\bar{H}_Q$), and its fluctuating nonsecular part ($H_1(t)$) responsible for relaxation:

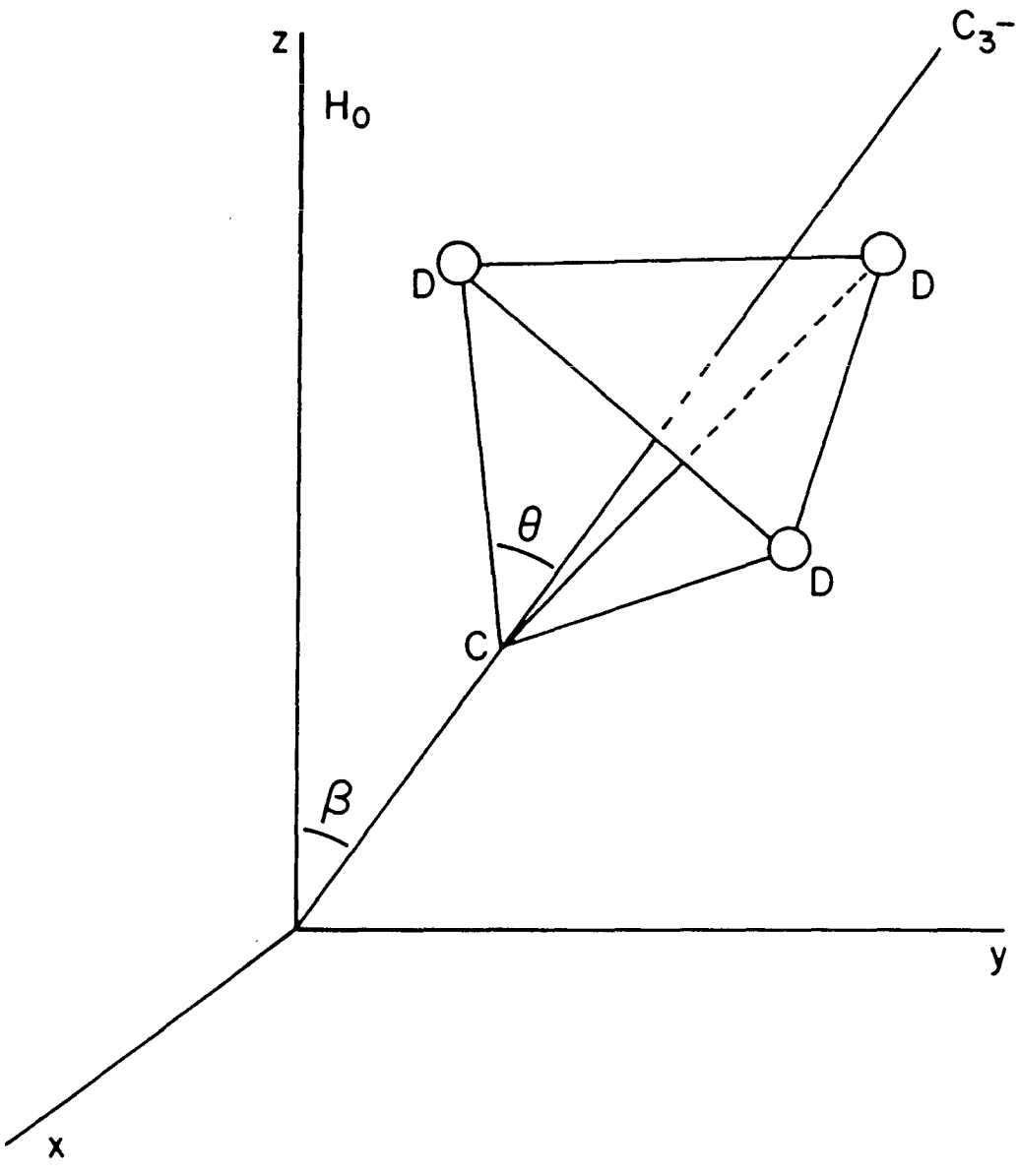

XBL 7912-13588

Figure VII.4 This figure shows the geometry of a methyl group. θ is the angle between the C_3 axis and C-D bond, and β is the angle between the C_3 axis and the magnetic field.

$$H = H_z + H_t + \bar{H}_Q + H_1(t) \quad .$$

The energy level diagram with the classification of irreducible representations of the C_3 group is shown in Figure VII.5. The truncated quadrupole interaction $\bar{H}_Q$, averaged over the random rotation, is reduced by a factor of $P_2(\cos\theta)$

$$\bar{H}_Q = \frac{\omega_Q}{3} P_2(\cos\theta)\ P_2(\cos\theta) T_A^{(0)} \quad ,$$

where $T_\mu^{(m)}$ is the component of the symmetry-adapted tensor operator of the second rank[1] and $\mu = A, E^a, E^b$ are the irreducible representations of the C_3 group,[21]

$$T_\mu^{(m)} = T_1^{(m)} + \lambda T_2^{(m)} + \lambda^* T_3^{(m)} \quad , \quad \text{with } \mu = A,\ E^a \text{ or } E^b$$

for $\lambda = 1$, ε or ε^*, $\varepsilon = \exp(i2\pi/3)$ and $T_i^{(0)} = 3\, I_{iz}^2 - I(I+1)$, $i = 1, 2, 3$. Here the tensor components $T^{(\pm1)}$ and $T^{(\pm2)}$ are generated from $T_\mu^{(0)}$ by commutation relation[1]

$$[(I_\pm, T_\mu^{(m)})] = \sqrt{I(I+1)-m(m\pm1)}\ \ T_\mu^{(m\pm1)}$$

As shown in Figure VII.4 β is the angle between the C_3 axis and the magnetic field; θ is the angle between the C_3 axis and the principle axis of the electric field gradient tensor.

The fluctuating term $H_1(t)$ can be expressed as being a product of the symmetry-adapted tensor operators and spatial functions,

$$H_1(t) = \sum_{\mu=E^a,E^b} \sum_{m=-2}^{2} \frac{\omega_Q}{2} T_\mu^{(m)} (F_\mu^{(m)}(t))^+ \quad ,$$

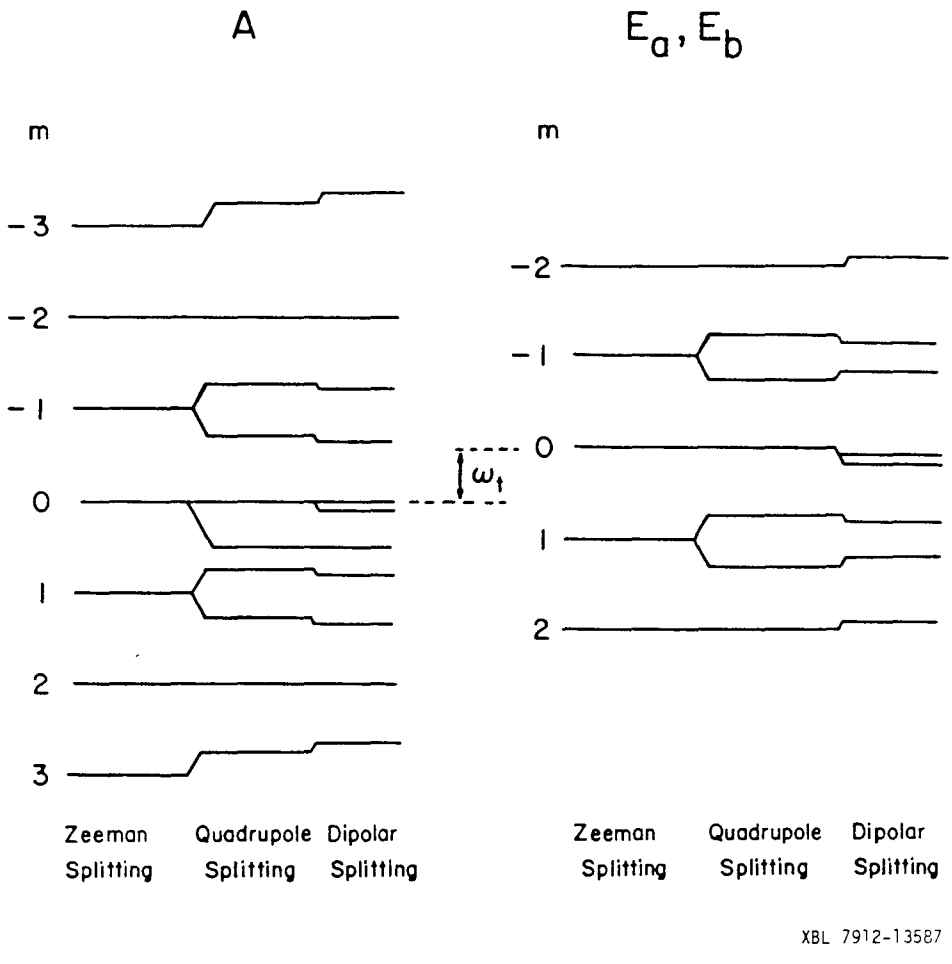

Fig. VII.5 This figure illustrates the energy level scheme with a classification according to A, E^a, and E^b states. ω_t is the tunneling splitting between the A and E states.

where

$$F_{E^a}^{(0)} = -\frac{3}{8} e^{2i\phi} \sin^2\theta \sin^2\beta - \frac{3}{8} i e^{i\phi} \sin 2\theta \sin 2\beta \quad ,$$

$$F_{E^a}^{(\pm 1)} = -\frac{\sqrt{6}}{8} i e^{2i\phi} \sin^2\theta \sin\beta (\pm 1 + \cos\beta) + \frac{\sqrt{6}}{8} e^{i\phi} \sin 2\theta (\cos 2\beta \mp \cos\beta) \quad ,$$

$$F_{E^a}^{(\pm 2)} = \frac{\sqrt{6}}{16} e^{2i\phi} \sin^2\theta (1 \pm \cos\beta)^2 - \frac{\sqrt{6}}{8} i e^{i\phi} \sin 2\theta \sin\beta (\mp 1 + \cos\beta) \quad ,$$

and

$$F_{E^b}^{(m)} = (-1)^m (F_{E^a}^{(-m)})^* \quad .$$

The angle ϕ fluctuates randomly by a fast rotation of the methyl group about the C_3 axis.

The correlation functions $G_\mu^{(m)}(t)$ are assumed to decay exponentially and to be characterized by a single correlation time τ_c,

$$(\frac{\omega_Q}{3})^2 \overline{F_\mu^{(m)}(t) \, F_\mu^{(m')*}(t+\tau)} = \delta_{mm'} \, G_\mu^{(m)}(0) \exp(-t/\tau_c) \quad .$$

They are evaluated as tabulated in Table VII.2.

For spin-lattice relaxation only the evolution of the diagonal part ρ_D of the density matrix is relevant.[22] Based on the Symmetry Restricted Spin Diffusion (SRSD) model,[8] we can assume that there are four degrees of freedom that characterize the quasi-equilibrium during the relaxation process. In the high spin temperature assumption, we can decompose ρ_D into a set of four traceless and mutually orthonormal operators, and the unit operator with their corresponding Lagrange multipliers α_k,

Table VII.2

The Symmetry-Adapted Correlation Functions $G_{\mu}^{(m)}(0)$

$$G_{E^a}^{(0)}(0) = G_{E^b}^{(0)}(0) = \frac{\omega_Q^2}{64} \sin^4\theta \sin^4\beta \, (1+16 \cos^2\theta \cos^2\beta)$$

$$G_{E^a}^{(1)}(0) = G_{E^b}^{(-1)}(0) = \frac{\omega_Q^2}{96} [\sin^4\theta \sin^2\beta \, (1+\cos\beta)^2 + \sin^2 2\theta \, (\cos 2\beta - \cos\beta)^2]$$

$$G_{E^a}^{(-1)}(0) = G_{E^b}^{(1)}(0) = \frac{\omega_Q^2}{96} [\sin^4\theta \sin^2\beta \, (1-\cos\beta)^2 + \sin^2 2\theta \, (\cos 2\beta + \cos\beta)^2]$$

$$G_{E^a}^{(2)}(0) = G_{E^b}^{(-2)}(0) = \frac{\omega_Q^2}{96} [\frac{1}{4} \sin^4\theta \, (1+\cos\beta)^4 + \sin^2 2\theta \sin^2\beta \, (-1+\cos\beta)^2]$$

$$G_{E^a}^{(-2)}(0) = G_{E^b}^{(2)}(0) = \frac{\omega_Q^2}{96} [\frac{1}{4} \sin^4\theta \, (1-\cos\beta)^4 + \sin^2 2\theta \sin^2\beta \, (1+\cos\beta)^2]$$

$$\rho_D \sim 1 + \alpha_1 0_1 + \alpha_2 0_2 + \alpha_3 0_3 + \alpha_4 0_4 \quad .$$

0_1, 0_2, 0_3 and 0_4 defined below, correspond to the Zeeman, tunneling, quadrupole, and rotational polarization systems respectively, namely,

$$0_1 = I_Z / \sqrt{\mathrm{Tr}(Iz)^2} = \frac{I_Z}{\sqrt{54}} \quad ,$$

$$0_2 = \sqrt{\frac{176}{27}} \left(\frac{1}{11}|A\rangle\langle A| - \frac{1}{16}|E\rangle\langle E|\right) \quad ,$$

$$0_3 = \frac{1}{3\sqrt{2}} T_A^{(0)} \quad ,$$

$$0_4 = \frac{1}{4} \left(|E^a\rangle\langle E^a| - |E^b\rangle\langle E^b|\right) \quad ,$$

where $|A\rangle\langle A|$, $|E^a\rangle\langle E^a|$ and others are projection operators.

The equation governing the relaxation of the system toward an equilibrium with the lattice can be expressed as[7,8]

$$\dot{\alpha} = -S \cdot (\alpha - \alpha^{eq}) \quad ,$$

where α is a column-vector with components α_k. The symmetric relaxation matrix S have the components[7,8]

$$S_{k\ell} = \frac{1}{2} \sum_{\mu=E^a,E^b} \sum_{m=-2}^{2} G_\mu^{(m)}(0) \int_{-\infty}^{\infty} d\tau \, e^{-|\tau|/t_c} \, \mathrm{Tr}([0_k, e^{-iH\tau} T_\mu^{(m)} \, e^{iH\tau}$$

$$= \sum_\mu \sum_m G_\mu^{(m)}(0) \frac{2\tau_c}{1+(m\omega_o + \omega t)^2 \, \tau_c^2} \mathrm{Tr}(P[0_k, T_\mu^{(m)}][T_\mu^{+(m)}, 0_\ell]) \quad ,$$

where ω_t is the observable tunneling frequency[7] and the projection operator $p = |A><A|$.

The non-zero relaxation rates $S_{k\ell}$ were evaluated, yielding:

$$S_{11} = \sum_{m=-1,2} \sum_{\mu=E^a,E^b} \left[\frac{G_\mu^{(m)}(o)}{1+(m\omega_o+\omega_t)^2\tau_c^2} + \frac{G_{\bar{\mu}}^{(m)}(0)}{1+(-m\omega_o+\omega_t)^2\tau_c^2} \right] 3m^2\tau_c \quad ,$$

$$S_{12} = \sum_{m=1,2} \sum_{\mu=E^a,E^b} \left[\frac{G_\mu^{(m)}(0)}{1+(m\omega_o+\omega_t)^2\tau_c^2} - \frac{G_{\bar{\mu}}^{(m)}(0)}{1+(-m\omega_o+\omega_t)^2\tau_c^2} \right] 162\sqrt{\frac{27}{176}}\, m\tau_c$$

$$S_{22} = \sum_{m=0,\pm1,\pm2} \sum_{\mu=E^a,E^b} \frac{G_\mu^{(m)}(0)}{1+(m\omega_o+\omega_t)^2\tau_c^2} \cdot \left(\frac{81}{2}\right)^2 \tau_c \quad ,$$

$$S_{33} = \sum_{\mu=E^a,E^b} \left[\frac{G_\mu^{(1)}(0)}{1+(\omega_o+\omega_t)^2\tau_c^2} + \frac{G_{\bar{\mu}}^{(1)}(0)}{1+(-\omega_o+\omega_t)^2\tau_c^2} \right] 81\,\tau_c \quad ,$$

$$S_{44} = \sum_{m=0,\pm1,\pm2} \sum_{\mu=E^a,E^b} \left[\frac{G_\mu^{(m)}(0)}{1+(m\omega_o+\omega_t)^2\tau_c^2} \right] 162\,\tau_c \quad .$$

The quadrupole system and the rotational polarization system are characterized by a single relaxation rate S_{33} and S_{44}. The Zeeman system and the tunneling system, however, are coupled through S_{12}, which is non-zero for $\omega_t \neq 0$. The spin lattice relaxation is non-exponential, in fact, a sum of two exponentials. At high temperatures, when $\omega_t = 0$, the Zeeman system and the tunneling system become decoupled, since $S_{12} = 0$.

7.4.3 Experimental results and discussion

The spin-lattice relaxation of toluene, when the methyl groups is deuterated and diluted in a normal protonated toluene matrix ($\sim$ 10% by mole), was measured at liquid nitrogen and liquid helium temperatures in a field of 42.5 kG. The corresponding resonance frequency of the deuteron NMR is 28.4 MHz. A three-pulse sequence 180_X-τ-90_X-τ'-90_Y is used to measure the spin-lattice relaxation. The first π pulse is used to reverse the magnetization. The second and third $\pi/2$ pulses are used to generate a quadrupole echo for improving the S/N ratio and for achieving easier detection.

The spin-lattice relaxation time was measured on the recovery of the sharp singularity in the powder spectrum. The recovery of intensity at liquid nitrogen and liquid helium temperatures are plotted on a semi-logarithmic scale as we have shown in Figure VII.6. We found the relaxation to be exponential with a T_1 of 1.1 ± 0.1 sec at liquid nitrogen temperature. At liquid helium temperature, the spin-lattice relaxation is characterized by two exponents with relaxation rates λ_1 and λ_2; λ_1^{-1} = 0.9 ± 0.1 sec and λ_2^{-1} = 26 ± 3 sec. λ_1 and λ_2 are related to $S_{k\ell}$ by

$$\lambda_1 + \lambda_2 = S_{11} + S_{22}$$

$$\lambda_1\lambda_2 = S_{11}S_{22} - S_{12}^2 \quad .$$

S_{11}, the initial slope of curve in Figure VII.6b, is measured with S_{11}^{-1} = 12 ± 1 sec. S_{12} and S_{22} are calcualted to be S_{12} = -0.23 ± 0.02 sec^{-1} and S_{22} = 0.9 ± 0.1 sec^{-1}. The non-exponentiality

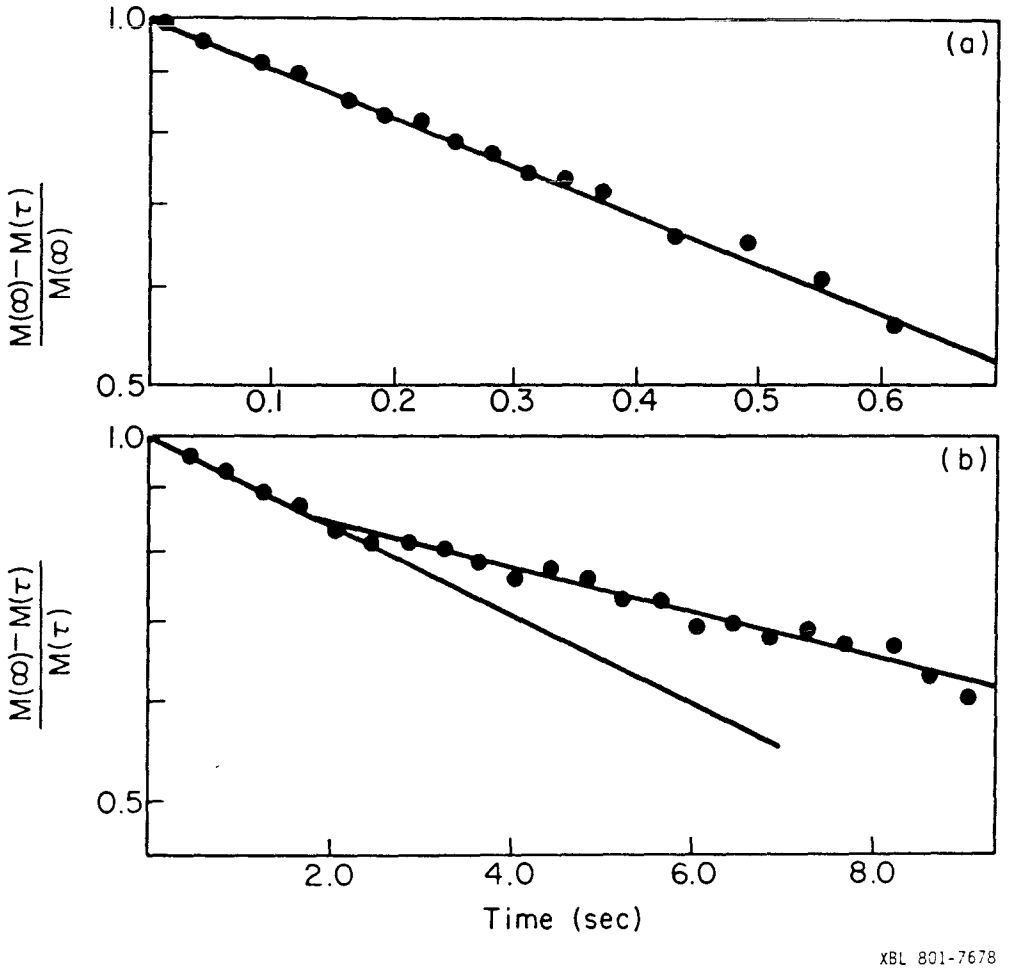

Figure VII.6 The recovery of the intensity of the spectrum is plotted on a semi-logarithmic scale. (a) The spin-lattice relaxation at liquid nitrogen temperature is exponential with $T_1 = 1.1 \pm 0.1$ sec. (b) The spin-lattice relaxation at liquid helium temperature is the sum of two exponentials.

of spin-lattice provides us with evidence of the coupling between the Zeeman and tunneling systems. The inter-system coupling S_{12} is non-zero at low temperature when the tunneling is in communication with the Zeeman system, i.e., $\omega_t \sim \omega_o$ or $\sim 2\omega_o$--such that both systems may exchange energy through phonons (Figure VII.7).

Finally, we briefly compared the relaxation processes between the methyl protons and the methyl deuteron systems. In the first case, the protons are coupled to the lattice by a dipolar interaction. This is a two-body interaction between protons. The existence of cross-correlations among the intramolecular dipolar interactions results in coupled, namely, non-exponential spin-lattice relaxations. In the CD_3 case, however, the deuterons are coupled to the lattice by quadrupole interactions that are single particle interactions. We expect that each deuteron should be relaxed by its own interaction with the lattice and that the relaxation should be exponential. Then it is not surprising to find that the relaxation of three identical deuterons is exponential, as in the case of high temperatures. At low temperature, however, we apparently cannot consider each deuteron independently from the others. We are forced by the Bose-Einstein statistics to consider the three deuterons as a collective system and to classify the eigenstates in an appropriate manner. We then find coupled relaxation becuase of the statistics and because when $\omega_t \neq 0$, the A states are lower in energy than the E states.

The above illustrates that the relaxation coupling is not caused by cross-correlation effects,[5] but rather, by what we call

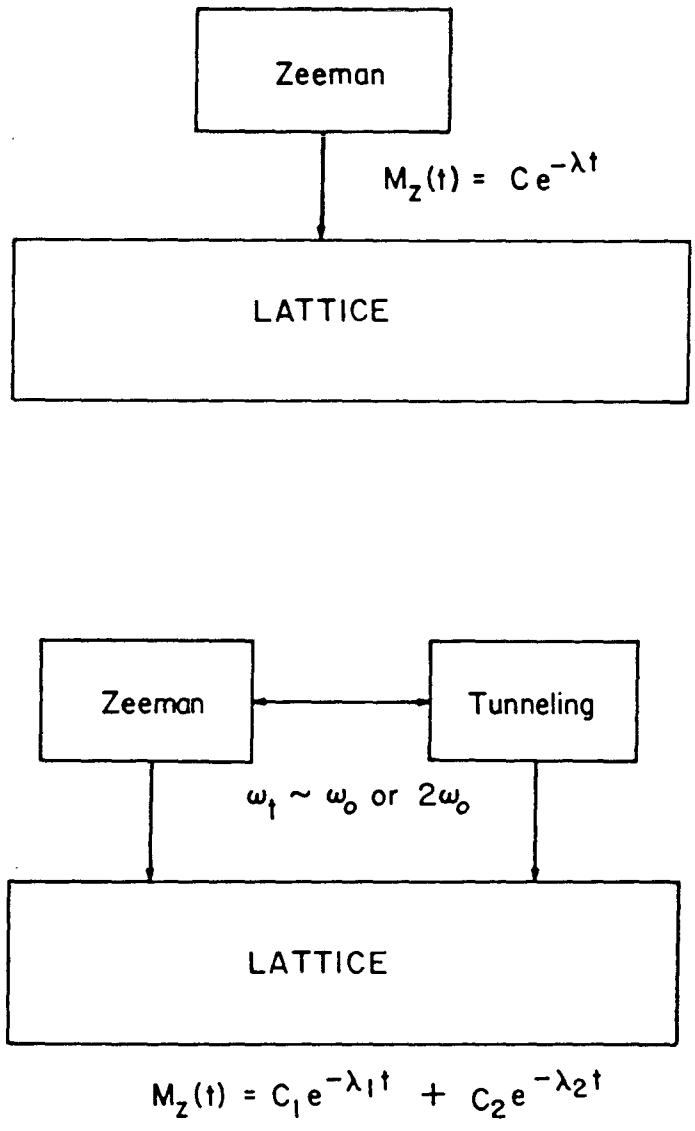

Figure VII.7 The top figure shows that the spin-lattice relaxation at high temperature is characterized by a single exponential decay. The bottom figure shows that at low temperature, when $\omega_t \sim \omega_o$ or $2\ \omega_o$, the tunneling system is in communication with the Zeeman system. The spin-lattice relaxation is a bi-exponential decay.

a statistical interference. Some of the couplings in the CH_3 case[7,8] that vanish when ω_t becomes zero, are of the same nature.

7.5 References

1. M. Tinkham, Group Theory and Quantum Mechanics, Chapter 5 (McGraw-Hill, New York, 1964).
2. M. Goldman, Spin Temperature and Nuclear Magnetic Resonance in Solids, Chapter 3 (Clarendon Press, Oxford, 1970).
3. Ibid., Chapter 1.
4. P. S. Hubbard, Phys. Rev. 109, 1153 (1958).
5. R. L. Hill and P. S. Hubbard, Phys. Rev. 134, A392 (1964).
6. M. F. Baud and P. S. Hubbard, Phys. Rev. 170, 384 (1968).
7. S. Emid and R. A. Wind, Chem. Phys. Lett. 33, 269 (1975).
8. S. Emid, R. J. Baarda, J. Smidt, and R. A. Wind, Physica (Utrecht) B93, 327 (1978).
9. S. Emid and R. A. Wind, Chem. Phys. Lett. 27, 312 (1974).
10. J. Haupt, Naturforsch. 26A, 1578 (1971).
11. J. Haupt, Phys. Lett. 38A, 389 (1972).
12. J. Haupt, Naturforsch. 28A, 98 (1973).
13. P. S. Allen, J. Chem. Phys. 48, 3031 (1968).
14. F. Apaydin and S. Clough, J. Phys. C1, 932 (1968).
15. S. Clough, J. Phys. C4, 2180 (1971).
16. S. Clough, Phys. Lett. 42A, 371 (1973).
17. M. Mehring and H. Raber, J. Chem. Phys. 59, 1116 (1973).
18. S. Emid, R. A. Wind, and S. Clough, Phys. Rev. Lett, 33, 769 (1974).
19. R. A. Wind, S. Emid, J. F. J. M. Pourquiré, and J. Smidt, J. Phys. C9, 139 (1976).

20. P. Beckmann, S. Clough, J. W. Hennel, and J. R. Hill, J. Phys. C10, 729 (1977).

21. H. Eyring, J. Waller, and G. E. Kimble, Quantum Chemistry (Wiley, New York, 1949).

22. S. Emid, Physica (Utrecht) 82B, 347 (1976).

23. J. Tang, A. Pines, and S. Emid, J. Chem. Phys. 73, 172 (1980).

VIII

ANISOTROPIC SPIN-LATTICE RELAXATION OF DEUTERATED HEXAMETHYLBENZENE

8.1 Introduction

Some molecules in solids may exhibit reorientating motion other than thermal vibration. The motional group does not rotate freely, but rather, jumps (or reorients) among all possible equivalent positions. In most cases, only part of the molecule is able to reorient, for example, the methyl group. Yet, there are a few cases where the whole molecule may undergo reorienting motion; some examples are benzene, hexamethylbenzene and adamantane.

Because the motional group or molecule does not tumble isotropically, but rather, reorients about some special direction, the spin-lattice relaxation is generally not isotropic. In general, the special direction of reorientation is along the symmetry axis of the motional group. For example, the methyl group jumps about its three-fold axis; the benzene reorients about its six-fold axis. Although the spin-lattice relaxation of individual motional group is anisotropic, the spin-diffusion among each different molecule may diminish or completely wash out the anisotropy.

Some single crystals may greatly facilitate the anisotropy study of spin-lattice relaxation if all the motional groups reorient about the same direction. The single crystal of silver-trifluoroacetate (CF_3COOAg) has been studied by ^{19}F NMR.[1] The CF_3 groups in the crystal all point to the same direction. The orientation of the methyl group is determined by the measurement of the anisotropic chemical shift of ^{19}F.

The three-fold reorientation of the CF_3 groups creates a fluctuating local field through the dipole-dipole interaction. The cross-correlated fluctuation of the local field caused by the reorientation produces an additional pathway for the relaxation. As a consequence, the spin-lattice relaxation of the methyl groups (CH_3 or CF_3), is generally anisotropic and non-exponential.[1-3]

Nevertheless, in the case of the deuterated methyl group (CD_3), the relaxation is characterized by a single exponential. Unlike the dipolar interaction, the quadrupole interaction for the spin 1 nucleus is associated with a single particle. Even in the presence of correlated reorientation, the cross-correlated fluctuation between two nucleus is zero and does not contribute to the spin-lattice relaxation.

The deuterated hexamethylbenzene (HMB-d_{18}) molecule in the solid state undergoes a reorienting motion about its hexad axis (C_6 motion) over a wide range of temperature--as shown by second moment, T_1, and $T_{1\rho}$ studies of the protonated material[4-6]. As a result of this anisotropic C_6 reorientation, the nuclear spin-lattice relaxation exhibits a strong dependence on the orientation of the molecular hexad axis with respect to the applied magnetic field (Figure VIII.1). The T_1 anisotropy of a single crystal of deuterated hexamethylbenzene was measured on both sides of the T_1 minimum.[7] We shall present a model that uses only the single-particle relaxation to explain the temperature dependence of this anisotropy. In addition, from the measured temperature dependence of T_1 over the range -85 to 70°C, the activation energy and correlation time for the C_6 motion is

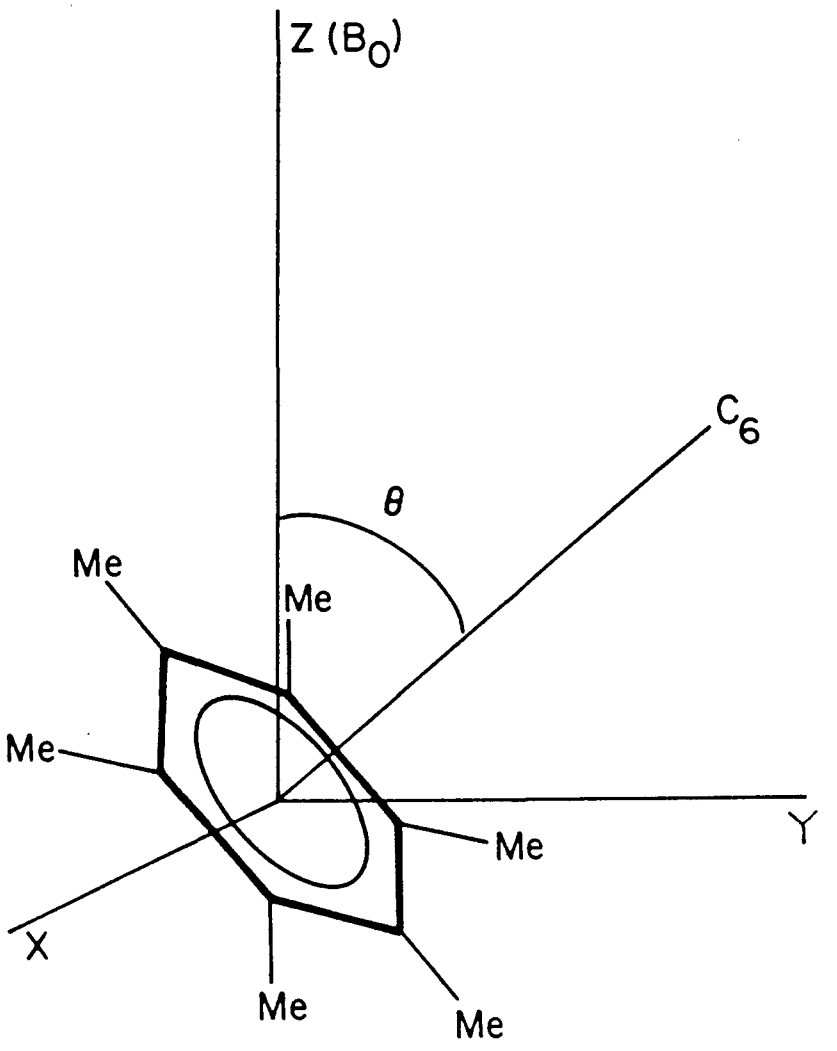

XBL 803-8658

Fig. VIII.1 This figure shows a hexamethylbenzene-d_{18} molecule oriented in a magnetic field with field direction along the z-axis.

determined[7] and compared with the values previously reported for the protonated compound.

8.2 Theory

There are two motions associated with the hexamethylbenzene molecule. In addition to the aforementioned C_6 motion of the entire molecule, each of the six methyl groups undergoes rapid reorientation about its C_3 axis. The C_3 and C_6 reorientations cause fluctuations in the deuterium quadrupole interaction; these quadrupole fluctuations are responsible for the deuterium spin-lattice relaxation. The spin-lattice relaxation is most efficient (T_1 minimum) when the rate of fluctuation is near the Larmor frequency or near the second harmonic of the Larmor frequency. In the temperature range of our measurements, the rate of the methyl group C_3 motion is much larger than the rate of the molecular C_6 motion, and is far away from the Larmor frequency. Consequently, it is a very good approximation to neglect the contribution by the fast C_3 motion to the spin-lattice relaxation. Since the deuterium dipole-dipole coupling is much smaller than the quadrupole interaction, we can legitimately neglect the contribution (estimated to be less than 1%) of the fluctuating dipolar interaction that it makes to the relaxation.

Unlike the dipolar interaction, the quadrupole interaction is associated with a single nucleus. With this in mind, and by ignoring fluctuations due to the fast C_3 motion, the system of 18 deuterons can be simplified down to the treatment of a single deuteron having reduced quadrupole strength and having a principal axis along the methyl group C_3 axis. Because of the fast

reorientation of the methyl groups, the principal axis of quantization for the quadrupole interaction is along the C_3 axis. Since the rate of the three-fold reorientation is much faster than the Larmor frequency in the temperature range of our experiments, the C_3 motion does not contribute significantly to the spin-lattice relaxation. As a consequence, the non-secular time-dependent part of the Hamiltonian can be neglected. The quadrupole Hamiltonian of a methyl deuteron, with C_3 axis parallel to the field direction, can be expressed by

$$H_Q'' = \frac{1}{3}\omega_Q T^{(0)} \quad , \tag{VIII.1}$$

where $T^{(0)} = 3 I_z^2 - I(I+1)$, and ω_Q is the reduced quadrupole frequency by C_3 motion.

To include the six-fold reorientation of the whole molecule, we can apply two consecutive transformations, $\exp(i \frac{\pi}{2} I_x)$ and $\exp(i \phi I_z)$, to the previous Hamiltonian. The new Hamiltonian, with a C_6 axis along the z-direction, is given by

$$H_Q' = e^{i\phi I_z} e^{i \frac{\pi}{2} I_x} H_Q'' e^{-i \frac{\pi}{2} I_x} e^{-i\phi I_z} \quad . \tag{VIII.2}$$

The quadrupole Hamiltonian for a general orientation of the molecule (Figure VIII.1) can be obtained by an additional transformation $\exp(-i \phi I_x)$,

$$H_Q = e^{-i\theta I_x} H_Q' e^{i\theta I_x}$$

$$= -\frac{1}{2}\left[\frac{1}{2}(3\cos^2\theta-1)T^{(0)} + i\frac{\sqrt{6}}{4}(T^{(1)}+T^{(-1)})\sin 2\theta\right.$$

$$\left. - \frac{\sqrt{6}}{8}(T^{(2)}+T^{(-2)})(1-\cos 2\theta)\right]$$

$$- \frac{\sqrt{6}}{4}\left[-\frac{\sqrt{6}}{4}\sin^2\theta\, T^{(0)} - iT^{(1)}\sin\theta\,(1-\cos\theta)\right.$$

$$+ i\,T^{(-1)}\sin\theta\,(1+\cos\theta) + \frac{1}{2}T^{(2)}(1-\cos\theta)^2$$

$$\left. + \frac{1}{2}T^{(-2)}(1+\cos\theta)^2\right]\exp(2i\phi)$$

$$- \frac{\sqrt{6}}{4}\left[-\frac{\sqrt{6}}{4}\sin^2\theta\, T^{(0)} - iT^{(-1)}\sin\theta\,(1-\cos\theta)\right.$$

$$+ i\,T^{(1)}\sin\theta\,(1+\cos\theta) + \frac{1}{2}T^{(-2)}(1-\cos\theta)^2$$

$$\left. + \frac{1}{2}T^{(2)}(1+\cos\theta)^2\right]\exp(-2i\phi) \quad , \qquad \text{(VIII.3)}$$

where the θ is the angle between the molecular C_6 axis and the magnetic field (Figure VIII.1).

The time-independent terms in $T^{(1)}$, $T^{(-1)}$, $T^{(2)}$, and $T^{(-2)}$ that do not contain a fluctuating angle $\phi(t)$ can be neglected because they do not contribute to the relaxation, but rather, only have a negligible second-order effect on the quadrupole shift.

The static quadrupole Hamiltonian is then given by

$$\bar{H}_Q = -\frac{1}{2}\omega_Q P_2(\cos\theta)\, T^{(0)} \quad . \tag{VIII.4}$$

The fluctuating quadrupole Hamiltonian can be expressed explicitly as being a sum of the products of tensor operators $T^{(m)}$ and the time-dependent spatial function $F^{(-m)}(t)$:

$$H_1(t) = \frac{1}{3}\omega_Q \sum_{m=-2}^{2} (-1)^m T^{(m)} F^{(-m)}(t) \quad , \tag{VIII.5}$$

where

$$F^{(0)} = \frac{3}{4}\sin^2\theta \cos 2\phi \quad ,$$

$$F^{(1)} = -i\frac{\sqrt{6}}{8}\cos 2\phi \sin 2\theta - \frac{\sqrt{6}}{4}\sin 2\phi \sin\theta \quad ,$$

$$F^{(2)} = -\frac{\sqrt{6}}{8}\cos 2\phi (1+\cos^2\theta) + i\frac{\sqrt{6}}{4}\sin 2\phi \cos\theta \quad ,$$

and $F^{(-m)} = (-1)^m (F^{(m)})^*$. $F^{(0)}$ is included for completeness, although it does not contribute to the T_1 relaxation.

The time-dependence of $F^{(m)}$ is contained in the randomly fluctuating angle ϕ. This angle ϕ describes reorientation of the molecule about its C_6 axis with a correlation time τ_c. Since all of the time-dependence enter into $H_1(t)$ as 2ϕ, only one correlation time is necessary to describe the relaxation. With one correlation time it is impossible to distinguish sixfold reorientation from rotational diffusion.[8]

Nevertheless, x-ray analysis shows that the hexamethylbenzene molecules do have a specific sixfold equilibrium orientation.[9] Thus, τ_c can be viewed as an inverse jumping rate.

In general, the relaxation of a multi-spin system must be described by a relaxation matrix $S^{(0)}$. Since our treatment involves

only a single particle relaxation, the spin-lattice relaxation rate, (that is, $1/T_1$) is given by the single matrix element S_{11}, previously evaluated to be:

$$S_{11} = 6\, J^{(1)} + 24\, J^{(2)} \quad , \qquad \text{(VIII.6)}$$

where $J^{(1)}$ and $J^{(2)}$ are the special densities:

$$J^{(1)} = \left(\frac{\omega_Q}{3}\right)^2 \frac{3}{16} (1-\cos^4\theta) \frac{\tau_c}{1+\omega^2\tau_c^2}$$

$$J^{(2)} = \left(\frac{\omega_Q}{3}\right)^2 \frac{3}{64} (1 + 6\cos^2\theta + \cos^4\theta) \frac{\tau_c}{1+4\omega^2\tau_c^2} \quad .$$

The dependence of T_1 (S_{11}^{-1}) upon the angle θ is evident from the spectral densities. T_1 has a minimum for the C_6 axis parallel to the magnetic field, and increases monotonically as θ increases up to 90° (Figure VIII.2). The anisotropy of T_1 depends on the temperature because τ_c is temperature-dependent (Figure VIII.3). The spectral density $J^{(1)}$ vanishes when the C_6 axis is parallel to the applied magnetic field, meaning that only $J^{(2)}$, or the double quantum transition contributes to the relaxation at this orientation.

8.3 Experiment and discussion

All experiments were performed using a single crystal of HMB-d_{18}. This greatly facilitates the study of the anisotropic spin-lattice relaxation because all molecular C_6 axes are parallel in the single crystal.[9] T_1 was measured using a saturation-recovery pulse sequence, that is, $(90°\text{-}\tau')_n - \tau - 90°$, $T_2 << \tau' << T_1$ in a field of 25.8 KG that had a corresponding deuterium resonance

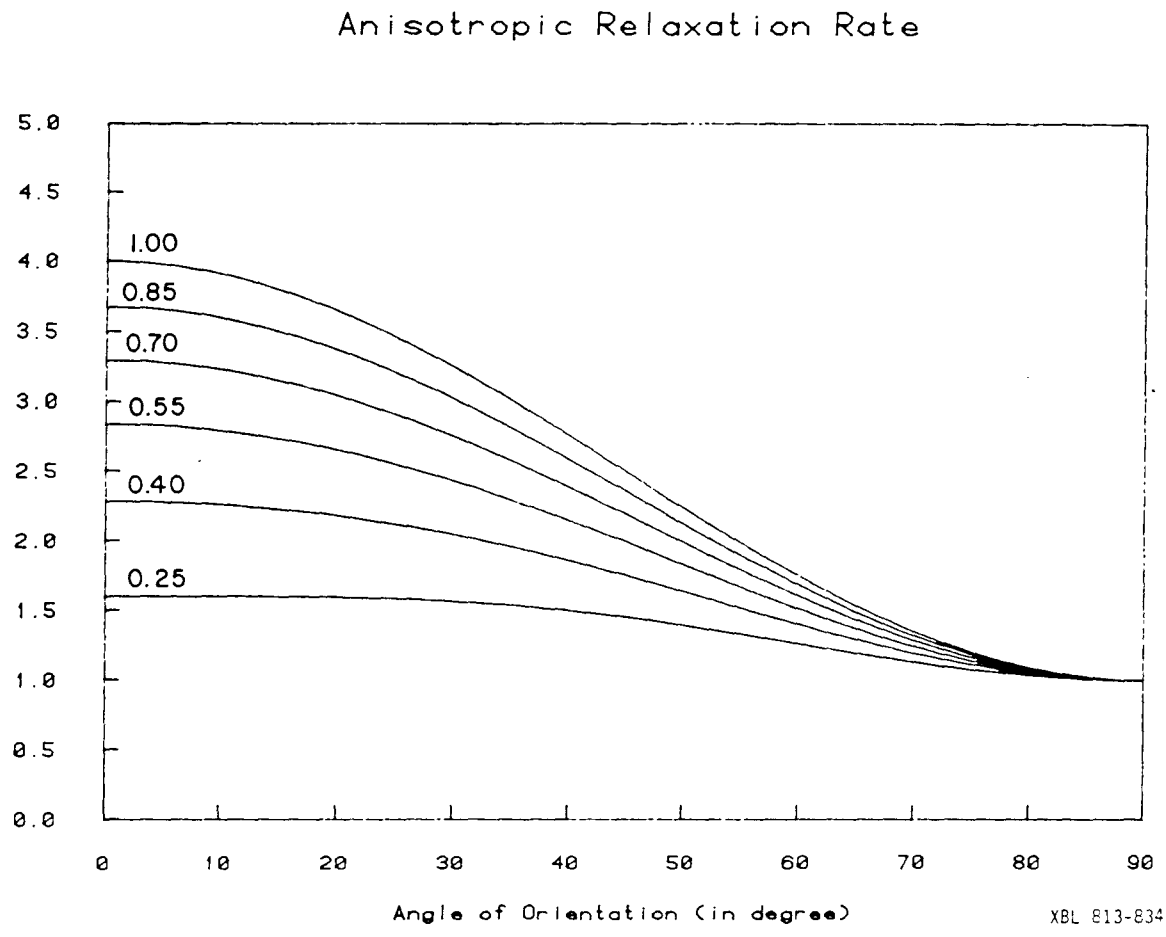

Fig. VIII.2 Here we see the dependence of the relaxation rate S_{11}^{-1} on the orientation of the C_6 axis and the parameter ε defined as $\varepsilon = (1+\omega^2\tau_c^2)/(1+4\omega^2\tau_c^2)$.

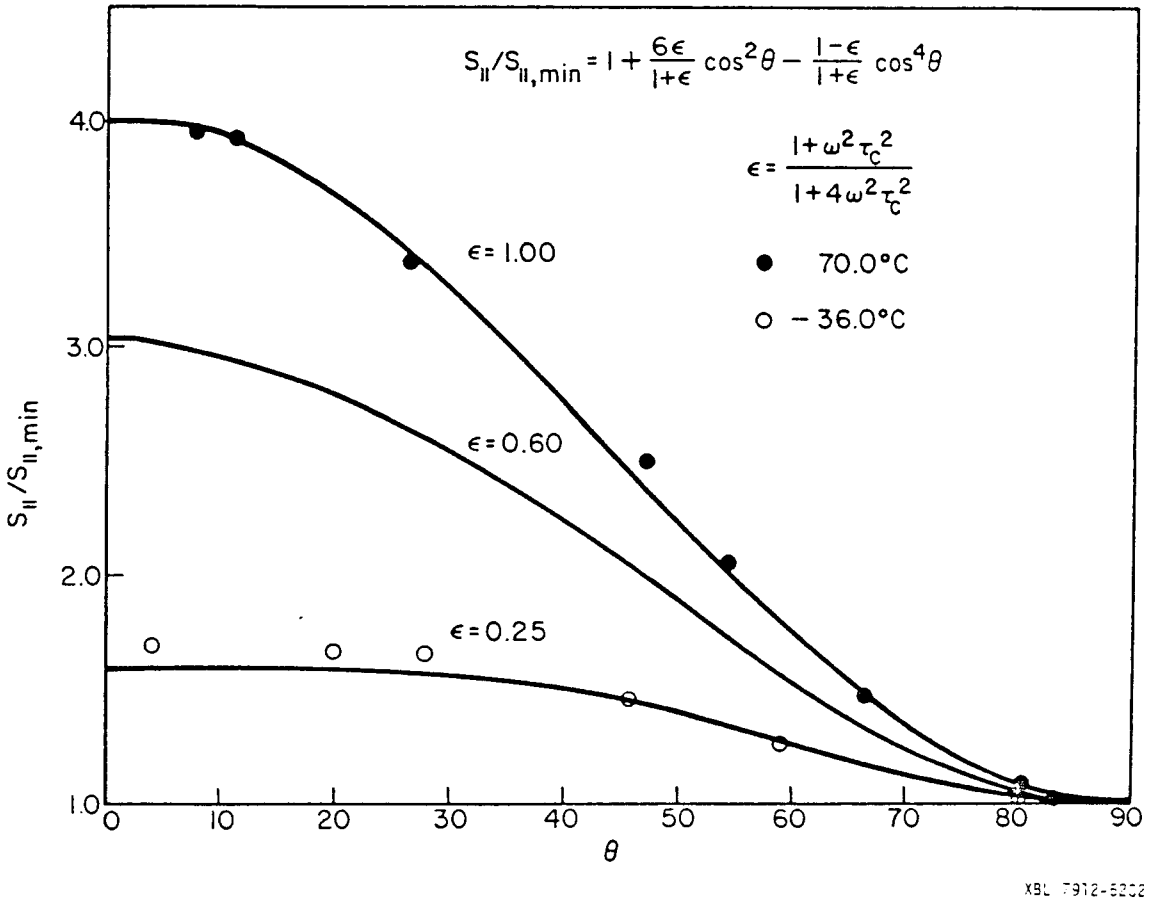

Fig. VIII.3 The angular dependence of the spin-lattice relaxation rate at two temperatures (-36°C and 70°C) is shown along with the theoretical fit (solid line) for three different values of the parameter ε defined in the figure. $\varepsilon = 0.25$ corresponds to the low temperature limit (i.e. $\omega^2\tau_c^2 >> 1$) and $\varepsilon = 1.00$ corresponds to the high temperature limit (i.e. $\omega^2\tau_c^2 << 1$).

frequency of 16.8 MHz.

The angular dependence of the spin-lattice relaxation rate S_{11} was measured at two temperatures -36°C and 70°C. The results are shown in Figure VIII.3. With the single crystal oriented so that all of the molecular C_6 axes are parallel to the field, (that is, $\theta = 0$), the temperature dependence of S_{11} was measured over the range -85°C to 70°C. The observed temperature dependence is shown in Figure VIII.4.

For the single orientation of the C_6 axes parallel to the field, only the second term ($J^{(2)}$ term) in equation (VIII.6), is expected to contribute to the relaxation:

$$S_{11} = A \frac{\tau_c}{1+4\omega^2\tau_c^2} \quad . \qquad \text{(VIII.7)}$$

Assuming an Arrhenius form for the correlation time:

$$\tau_c = \tau_{c_o} \exp(E_a/RT); \qquad \text{(VIII.8)}$$

the data are best fitted to the above expression for S_{11} with the following values:

$$A = (6.1 \pm 0.1) \times 10^{10} \text{ sec}^{-1}$$

$$\tau_{c_o} = (1.8 \pm 0.3) \times 10^{-15} \text{ sec}$$

$$E_a = 7.8 \pm 0.1 \text{ kcal/mole} \quad ,$$

where E_a is the energy of activation needed for the molecule to reorient about its C_6 axis. The theoretical fit of the data is shown in Figure VIII.4. The deviation of the theoretical fit from

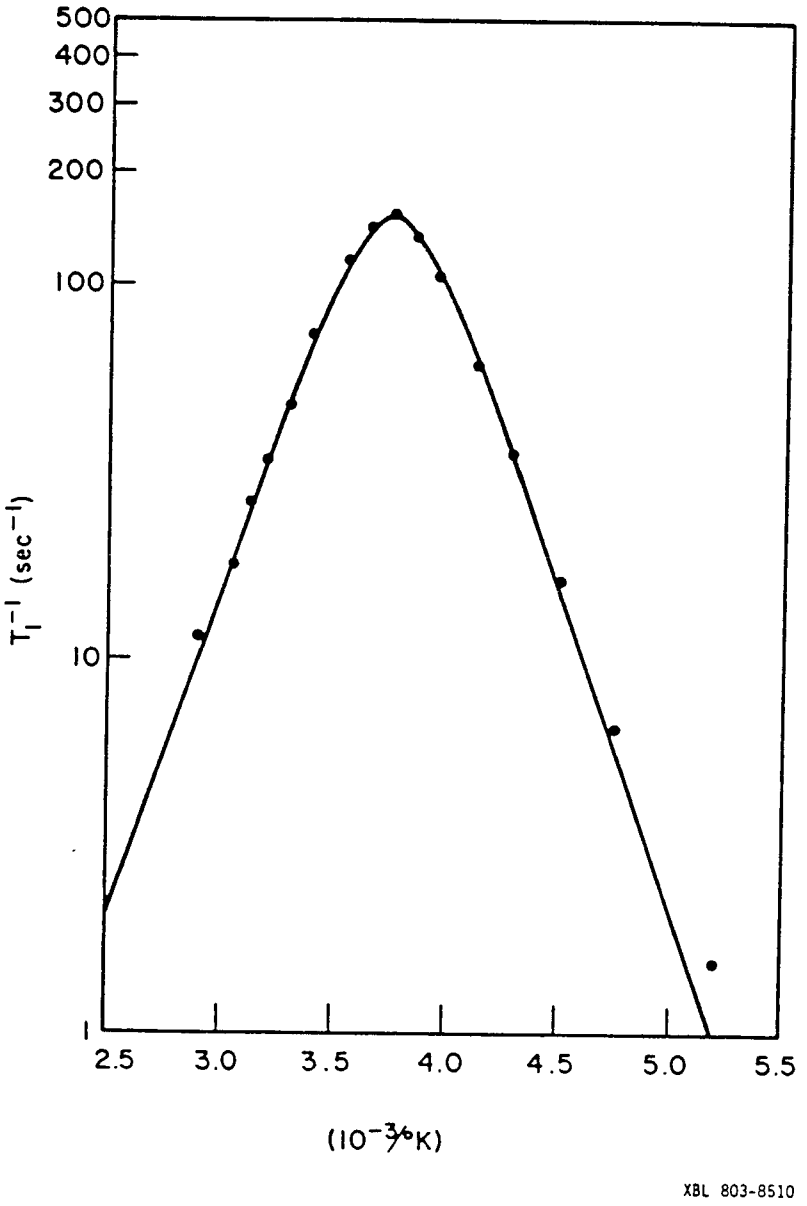

Figure VIII.4 The temperature dependence of the spin-lattice relaxation rate for the HMB-d_{18} single crystal oriented with all molecular C_6 axes parallel to the magnetic field. The solid curve is the best fit of equation VIII.7 to the data.

the data at a low temperature can result from our neglect of the methyl group rotation (C_3 motion). This rotation becomes increasingly important at a low temperature.

Our measured activation energy for HMB-d_{18} is substantially higher than the reported value (6.7 ± 0.1 kcal/mole) for the fully protonated HMB. If we view the molecule as a torsional oscillator that sits in a sixfold well, the activation energy for reorientation can be expected to decrease upon deuteration. Deuteration increases the moment of molecule inertia, thus, the torsional energy levels are shifted down and the spacing between zero point energy and barrier top is increased.

From the value of A given above, the effective quadrupole strength is found to be: $\nu_{Q,eff} = 39.1 \pm 0.3$ kHz. This agrees quite well with our measurement of the powder pattern at -170°C, where the C_6 motion is essentially frozen, $\nu_{Q,-170°C} = 38.2 \pm 0.4$ kHz. This agreement indicates that it is valid to consider only the methyl-group-averaged quadrupole strength as a contributing factor to the relaxation.

There is a problem, however, in comparing the effective quadrupole strength with the powder pattern value for HMB-d_{18} at room temperature. At room temperature, where the C_6 motion is rapid, the powder pattern value is expected to be exactly one-half of the effective quadrupole strength. In fact, the measured value is: $\nu_{Q,25°C} = 16.6 \pm 0.2$ kHz. This is about 15% smaller than expected. One explanation for this reduced value is that besides the in-plane reorientation of the molecule, some additional motion exists. One explanation for this is that the

molecule is not constrained to lie in a plane, but rather, its C_6 axis rocks about in a cone. Such an out-of-plane motion seems unlikely, however, since measurements of the C^{13} chemical shielding anisotropy in HMB do not indicate any significant change in σ_{33} over the temperature range -186°C to 23°C.[11] σ_{33} is the element of the chemical shielding tensor that corresponds to a principal axis that is perpendicular to the molecular plane. Additionally, $T_{1\rho}$ measurements that are sensitive to slow motion, have not indicated the existence of any motion besides the C_6 motion.

Also, we can explain that the principal axis of the quadrupole interaction of a CD_3 group is not perpendicular to the molecular C_6 axis. This is possible if the three deuterons of the CD_3 group experience different local electric field gradients, so that when they are averaged over the C_3 motion, the effective quadrupole axis lies outside the molecular plane. For a free C_3 rotor, the average could never be out of plane, but in HMB, where there are many methyl-methyl steric interactions, the methyl groups can be staggered in such a way that some groups give above-plane averages, whereas others give below-plane averages.

8.4 References

1. M. Mehring and H. Raber, J. Chem. Phys. 59, 1116 (1973).
2. R. L. Hill and P. S. Hubbard, Phys. Rev. 134, A392 (1964).
3. M. F. Baud and P. S. Hubbard, Phys. Rev. 170, 384 (1968).
4. E. R. Andrew, J. Chem. Phys. 18, 607 (1950).
5. P. S. Allen and A. Cowking, J. Chem. Phys. 47, 4286 (1967).
6. H. W. Bernard, J. E. Tanner, and J. G. Aston, J. Chem. Phys. 50, 5016 (1969).
7. J. Tang, L. Sterna, and A. Pines, J. Magn. Reson. 41, 389 (1980).
8. D. E. Woessner, J. Chem. Phys. 36, 1 (1962).
9. L. O. Brockway and J. M. Robertson, J. Chem. Soc., 1324 (1939).
10. S. Emid, R. J. Baarda, J. Smidt, and R. A. Wind, Physica B93, 327 (1978).
11. A. Pines, M. G. Gibby, and J. W. Waugh, Chem. Phys. Lett. 15, 373 (1972).

IX

THE SPECTROMETERS

All the experiments on multiple quantum NMR and the experiments of deuterated methyl groups at low temperatures were done on the β-spectrometer. Only the experiments on the deuterated hexamethylbenzene were carried out on the α-spectrometer.

9.1 The β spectrometer

9.1.1 Magnet

The β spectrometer has a superconducting magnet with a 3.5 inch bore from Bruker. It is operated at 42.5 KGauss and has a proton resonance frequency at 185.0 MHz and a deuterium resonance frequency at 28.4 MHz. The magnet has both superconducting and room temperature shims. The field can be shimmed to less than 1 ppm over a 1 cm^3 region. The field is very stable and no other field or frequency locking is necessary.

9.1.2 Pulse generation

The proton RF is generated by mixing the 30 MHz IF from a General Radio 1061 frequancy synthesizer with 155 MHz from the same synthesizer. Only the upper sideband is kept. The 30 MHz IF is generated by tripling the synthesizer's 10 MHz reference signal. The low frequency for deuteron is generated directly by a Hewlett-Packard 3320A. The RF is passed through the commercial quadrature hybrids and switches to produce four phases (x, $\bar{x}$, y and $\bar{y}$). The x and $\bar{x}$ channels are fed into a Daico 100D0898 phase shifter. This produces a phase shift in any multiple of $2\pi/256$.

The output goes to the high power transmitter (a class C cavity-tuned transmitter or AR model 100/model 200) and provides a pulse of up to 200 watts.

The timing of the pulses and the data acquisition is controlled by a 16-step pulse programmer that is interfaced with a NOVA 820 computer.

9.1.3 Receivers

The signal from the probe is first amplified by a commercial wideband low noise (noise figure $\sim$ 2.5 dB) preamplifier (Avantek UTO-511, UTO-512) with about 35 dB of gain. The output is mixed and filtered to $\sim$ MHz, amplified with a variable gain IF strip up to 70 dB (RHG EVT 3010), and then mixed with 30 MHz down to audio frequencies with two phases (0° and 90°).

9.1.4 Digitizers

The audio signals in two channels are digitized by a pair of analog-digital converters (Datel SHM2 S/H in series with 10 bit Datel ADCE10B A/D). The digitized signal is transferred to a NOVA 820 computer at a maximum rate of 3 μsec per point.

9.1.5 Probe

The double resonance probe used has a single coil, double-tuned configuration, with a Q of $\sim$ 150 for protons. The solenoid coil contains eight turns of 18 gauge uninsulated copper wire (8 mm x 15 mm).

The probe head is covered by a glass dewar to provide thermal isolation. Temperature control is achieved by regulating the flow of heated air (or cooled N_2 gas for low temperatures) into the dewar

trough vacuum jacketed tube. The gas is heated by a resistive heater at the end of the tube. The temperature is constantly sensored by a copper/constantan thermocouple and compared to a reference setting. A differential voltage between the two is used to drive the current source (up to 3 amps) for the constantan heating coil. The temperature may be regulated to within ±0.2°C over the range -175°C to 150°C.

9.2 The α spectrometer

The spectrometer has a Westinghouse superconducting magnet of 25.8 KGauss with 2.5 inch bore. The corresponding resonance frequency for deuterium is 16.8 MHz. The deuterium RF is generated directly from a General Radio 1164-A frequency synthesizer that provides IF at 30 MHz.

The audio signal is digitized by an 8 bit Biomation transient recorder model 802 at an maximum rate of 0.5 μsec per point. All other aspects of the α spectrometer are very similar to the β spectrometer.

X

APPENDIX (COMPUTER PROGRAMS)

```
      program anisct1
c     This program calculates the anisotropic spin-lattice relaxation rate for
c     hexamethylbenzene-d18
c     theta: angle between the C6-axis of the molecule and the magnetic field
c     epsilo: parameter defined by the ratio between spectral densities
c        J(w) and J(2w)
c     s: spin-lattice relaxation rate
      dimension s(60,10)
      open(unit=01,name='anisot1.val',type='new')
      do 100 k=1,51
      theta=(k-1.)*3.14159265/100.
      x1=cos(theta)**2
      x2=cos(theta)**4
      do 60 i=1,6
      epsilo=(i-1.)*0.15+0.25
      a=6.*epsilo/(1.+epsilo)
      b=(1.-epsilo)/(1.+epsilo)
      s(k,i)=1.+a*x1-b*x2
60    continue
      angle=theta*180./3.14159265
      write(1,70)angle,(s(k,i),i=1,6)
70    format(1x,f8.3,6(2x,f9.4))
100   continue
      close(unit=01)
      stop
      end
```

```
      program ch3exc
      complex c(3), f(3)
      write(6,2)
2     format(10x,'enter the value of T2 (in sec): ',$)
      read(5,4)t2
4     format(f10.0)
      write(6,25)
25    format(10x,'enter the value of max. omega (in Hz): ',$)
      read(5,27)xmax
27    format(f10.0)
      open(unit=01,name='ch3exc.data',type='old',readonly)
      do 30 i=1,3
      read(1,29)c(i)
29    format(f13.6,5x,f13.6)
30    continue
      close(unit=01)
      open(unit=01,name='ch3exc.val',type='new')
      do 100 kk=1,800
      omega=(kk-401.)/400.*xmax
      do 40 i=1,3
      f(i)=cmplx(0.,-1.)/(cmplx(omega,-1./t2)-c(i))
40    continue
      sum=cabs(f(1)+f(2)+f(3))
      write(1,60)omega,sum
60    format(3x,f10.3,5x,f13.6)
100   continue
      close(unit=01)
      stop
      end
```

```
      program ch3fid
      complex a(8,8)
      dimension tau(3),iph(3),angle(3),phase(3),sx(100),sy(100)
      open(unit=01,name='ch3fid.data',type='old',readonly)
      pi=3.14159265
      read(1,1)dx
1     format(f10.0)
      write(6,2)
2     format(10x,'The value of dipole coupling (Khz):  ',$)
      write(6,3)dx
3     format(1x,f10.4)
      omegad=dx*1000.0
      read(1,8)npulse
8     format(i2)
      write(6,10)
10    format(/,10x,'The number of the pulses:  ',$)
      write(6,11)npulse
11    format(1x,i2)
      do 110 n=1,npulse
      read(1,105)iph(n)
105   format(i2)
      read(1,106)angle(n)
106   format(f10.0)
      read(1,107)phase(n)
107   format(f10.0)
      if(n.eq.npulse)go to 110
      read(1,108)tau(n)
108   format(f10.0)
110   continue
      do 30 n=1,npulse
      write(6,12)
12    format(/,10x,'The phase & angle of the pulses:  ')
      write(6,14)n
14    format(15x,'Pulse no.',i2,5x,'phase 0 or 1(x or y): ',$)
      write(6,15)iph(n)
15    format(1x,i2)
      write(6,17)
17    format(15x,'angle of flip (in degree): ',$)
      write(6,18)angle(n)
18    format(1x,f10.4)
      write(6,19)
19    format(15x,'phaseshift of the pulse (in degree): ',$)
      write(6,20)phase(n)
20    format(1x,f10.4)
      if (n.ec.npulse) go to 30
      write(6,22)
22    format(/,10x,'The evolution time tau (microseccnd): ')
      write(6,24)n
24    format(15x,'tau(',i2,')= ',$)
      write(6,26)tau(n)
26    format(1x,f10.4)
30    continue
      read(1,31)ti
31    format(1x,f10.0)
      write(6,32)
32    format(/,10x,'The time increment (microsecond): ',$)
      write(6,33)ti
33    format(1x,f10.4)
      read(1,34)nfid
34    format(i4)
```

```
      write(6,35)
35    format(/,10x,'The total no. of FID: ',$)
      write(6,36)nfic
36    format(1x,i4)
      read(1,37)narg
37    format(i3)
      write(6,38)
38    format(/,10x,'The no. of angles between 0 & 90: ',$)
      write(6,39)nang
39    format(1x,i3)
      close(unit=01)
      rang=nang.
c     The followings are the initial density matrix elements of Iz
      nang1=narg+1
      do 40 nf=1,nfic
      sx(nf)=0.
      sy(nf)=0.
40    continue
      do 60 ia=1,nang1
      do 42 n1=1,8
      do 42 n2=1,8
      a(n1,n2)=cmplx(0.,0.)
42    continue
      a(1,1)=cmplx(1.5,0.)
      a(2,2)=cmplx(0.5,0.)
      a(3,3)=cmplx(-0.5,0.)
      a(4,4)=cmplx(-1.5,0.)
      a(5,5)=cmplx(0.5,0.)
      a(6,6)=cmplx(-0.5,0.)
      a(7,7)=cmplx(0.5,0.)
      a(8,8)=cmplx(-0.5,0.)
43    rangle=0.5*pi*(ia-1.)/rang
      p2cos=1.5*cos(rangle)**2-0.5
      d=omegac*p2ccs
      do 50 k=1,npulse
      ipnase=ip(k)
      theta=angle(k)*pi/180.
      tp=tau(k)*1.0e-6
      phi=phase(p)
      call unirot(a,ipnase,theta,phi)
      if(k.eq.npulse) go to 50
      call timevol(a,tp,d)
50    continue
c     The following calculates the trace Ix & Iy of FID
      t=ti*1.0e-6
      do 55 nf=1,nfic
      call timevol(a,t,d)
      call tracexy(a,tr1,tr2)
      sx(nf)=tr1+sx(nf)
      sy(nf)=tr2+sy(nf)
55    continue
60    continue
      do 80 nf=1,nfic
      write(6,70)sx(nf),sy(nf)
70    format(/,15x,'trace(A*Ix)= ',f10.4,10x,'trace(A*Iy)= ',f10.4)
80    continue
90    call lgplot(sx,nfic,25)
      call lgplot(sy,nfic,25)
      stop
      end
```

```
      program ch3in
      dimension tau(3),iph(3),angle(3),phase(3)
      open(unit=01,name='ch3fid.data',type='new')
      write(6,2)
2     format(10x,'enter the value of dipole coupling (Khz):  ',$)
      read(5,4)dx
4     format(f10.0)
      write(1,5)dx
5     format(1x,f10.0)
      write(6,7)
7     format(//,10x,'enter the number of the pulses:  ',$)
      read(5,8)npulse
8     format(i2)
      write(1,9)npulse
9     format(1x,i2)
      write(6,11)
11    format(//,10x,'enter the phase, angle, phaseshift of the pulses:  ')
      do 30 n=1,npulse
      write(6,12)n
12    format(/,15x,'Pulse no.',i2,5x,'phase 0 or 1(x or y): ',$)
      read(5,13)iph(n)
13    format(i2)
      write(1,14)iph(n)
14    format(1x,i2)
      write(6,15)
15    format(15x,'angle of flip (in degree): ',$)
      read(5,16)angle(n)
16    format(f10.0)
      write(1,17)angle(n)
17    format(1x,f10.0)
      write(6,18)
18    format(15x,'phaseshift of the pulse: ',$)
      read(5,19)phase(n)
19    format(f10.0)
      write(1,20)phase(n)
20    format(1x,f10.0)
      if (n.ec.npulse) go to 30
      write(6,22)
22    format(//,10x,'enter the evolution time tau (microsecond): ')
      write(6,24)n
24    format(/,15x,'tau(',i2,')= ',$)
      read(5,26)tau(n)
26    format(f10.0)
      write(1,27)tau(n)
27    format(1x,f10.0)
30    continue
      write(6,31)
31    format(//,10x,'enter the time increment (microsecond): ',$)
      read(5,32)ti
32    format(f10.0)
      write(1,33)ti
33    format(1x,f10.0)
      write(6,34)
34    format(//,10x,'enter the total no. of FID: ',$)
      read(5,35)nfid
35    format(i4)
      write(1,36)nfid
36    format(1x,i4)
      write(6,38)
38    format(//,10x,'enter the no. of angles between 0 & 90: ',$)
```

```
      read(5,39)narg
39    format(i3)
      write(1,40)narg
40    format(1x,i3)
      close(unit=01)
      stop
      end
```

```
      subroutine unirot(a,iphase,theta,phi)
c     This program calculates the transformation of the initial density
c     matrix a by pulse with phase x or y (iphase= 0 or 1), angle theta
c     and phaseshift phi. The output is written over a.
      complex a(8,8),v(8),ab(8,8)
      complex prod,sum
      dimension u(8,8)
      call phaseshft(a,phi)
      z=theta/2.
      u(1,1)=cos(z)**3
      u(1,2)=-cos(z)**2*sin(z)*3.**0.5
      u(1,3)=cos(z)*sin(z)**2*3.**0.5
      u(1,4)=-sin(z)**3
      u(2,1)=-u(1,2)
      u(2,2)=2.*cos(z)*(1.5*cos(z)**2-1.)
      u(2,3)=2.*sin(z)*(1.5*sin(z)**2-1.)
      u(2,4)=u(1,3)
      u(3,1)=u(1,3)
      u(3,2)=-u(2,3)
      u(3,3)=u(2,2)
      u(3,4)=u(1,2)
      u(4,1)=-u(1,4)
      u(4,2)=u(1,3)
      u(4,3)=-u(1,2)
      u(4,4)=u(1,1)
      u(5,5)=cos(z)
      u(5,6)=-sin(z)
      u(6,5)=-u(5,6)
      u(6,6)=u(5,5)
      u(7,7)=u(5,5)
      u(7,8)=u(5,6)
      u(8,7)=u(6,5)
      u(8,8)=u(6,6)
      do 80 i=1,8
      do 75 j=1,8
      sum=cmplx(0.,0.)
      do 50 m=1,8
      do 45 n=1,8
      prod=u(m,i)*a(m,n)*u(n,j)
      sum=sum+prod
45    continue
50    continue
      ab(i,j)=sum
75    continue
80    continue
      do 110 i=1,8
      do 100 j=1,8
      a(i,j)=ab(i,j)
100   continue
110   continue
      if(iphase.eq.1) go to 300
      g=0.5**0.5
      v(1)=cmplx(-g,-g)
      v(2)=cmplx(g,-g)
      v(3)=cmplx(g,g)
      v(4)=cmplx(-g,g)
      v(5)=v(2)
      v(6)=v(3)
      v(7)=v(2)
      v(8)=v(3)
```

```
      do 205 i=1,8
      do 200 j=1,8
      a(i,j)=conjg(v(i))*ab(i,j)*v(j)
200   continue
205   continue
300   call phaseshft(a,-phi)
      return
      end


      subroutine phaseshft(a,phi)
      complex a(8,8),a1(8,8),w(8)
      z1=cos(1.5*phi)
      z2=sin(1.5*phi)
      z3=cos(0.5*phi)
      z4=sin(0.5*phi)
      w(1)=cmplx(z1,z2)
      w(2)=cmplx(z3,z4)
      w(3)=conjg(w(2))
      w(4)=conjg(w(1))
      w(5)=w(2)
      w(6)=w(3)
      w(7)=w(2)
      w(8)=w(3)
      do 100 i=1,8
      do 100 j=1,8
      a1(i,j)=conjg(w(i))*a(i,j)*w(j)
100   continue
      do 150 i=1,8
      do 150 j=1,8
      a(i,j)=a1(i,j)
150   continue
      return
      end


      subroutine timevol(a,t,d)
      complex a(8,8),w(8),a1(8,8)
      z1=cos(c*t)
      z2=sin(c*t)
      w(1)=cmplx(z1,-z2)
      w(2)=cmplx(z1,z2)
      w(3)=w(2)
      w(4)=w(1)
      w(5)=cmplx(1.,0.)
      w(6)=cmplx(1.,0.)
      w(7)=cmplx(1.,0.)
      w(8)=cmplx(1.,0.)
      do 100 i=1,8
      do 100 j=1,8
      a1(i,j)=conjg(w(i))*a(i,j)*w(j)
100   continue
      do 150 i=1,8
      do 150 j=1,8
      a(i,j)=a1(i,j)
150   continue
      return
      end
```

```
      subroutine tracexy(a,tr1,tr2)
      complex a(8,8),yi(8,8)
      dimension xi(8,8)
      xi(1,2)=3.**0.5/2.
      xi(2,1)=xi(1,2)
      xi(2,3)=1.
      xi(3,2)=1.
      xi(3,4)=xi(1,2)
      xi(4,3)=xi(1,2)
      xi(5,6)=0.5
      xi(6,5)=0.5
      xi(7,8)=0.5
      xi(8,7)=0.5
      yi(1,2)=cmplx(0.,-3.**0.5/2.)
      yi(2,1)=conjg(yi(1,2))
      yi(2,3)=cmplx(0.,-1.)
      yi(3,2)=cmplx(0.,1.)
      yi(3,4)=yi(1,2)
      yi(4,3)=yi(2,1)
      yi(5,6)=cmplx(0.,-0.5)
      yi(6,5)=cmplx(0.,0.5)
      yi(7,8)=yi(5,6)
      yi(8,7)=yi(6,5)
      sum1=0.
      sum2=0.
      do 100 m=1,8
      do 100 n=1,8
      sum1=sum1+a(m,n)*xi(n,m)
      sum2=sum2+a(m,n)*yi(n,m)
100   continue
      tr1=sum1
      tr2=sum2
      return
      end
```

```
      subroutine diagni(h,un,nm)
c     subroutine for  complex matrix diagonization
c     h: matrix element arrays
c     nm: dimension of the matrix
c     un: unitary transform matrix which diagonizes the given matrix h
      complex h(nm,nm),un(nm,nm),ull,ulm,uml,umm,th,tu
      nmm=nm-1
      an=nm
      range=1.0e-4
      do 20 i=1,nm
      do 10 j=1,nm
10    un(i,j)=0.
20    un(i,i)=1.
      anorm=0.
      do 30 i=1,nmm
      ii=i+1
      do 30 j=1,nm
30    anorm=anorm+real(h(i,j)*conjg(h(i,j)))
      if(anorm.le.range) return
      anorm=sqrt(2.*anorm)
      anormx=anorm*range/an
      ind=0
      thr=anorm
40    thr=thr/an
50    do 80 l=1,nmm
      ll=l+1
      do 80 m=ll,nm
      if (cabs(h(l,m)).lt.thr) go to 80
      ind=1
      diff=real(h(m,m)-h(l,l))
      if(diff.eq.0.) diff=1.0e-15
      ar=0.5*atan(-2.*real(h(l,m))/diff)
      ai=0.5*atan(-2.*aimag(h(l,m))/diff)
      sini=sin(ai)
      cosi=cos(ai)
      sinr=sin(ar)
      cosr=cos(ar)
      ull=cmplx(cosr*cosi,sinr*sini)
      ulm=cmplx(sinr*cosi,cosr*sini)
      uml=cmplx(-sinr*cosi,cosr*sini)
      umm=cmplx(cosr*cosi,-sinr*sini)
      do 60 j=1,nm
      th=ull*h(l,j)+ulm*h(m,j)
      h(m,j)=uml*h(l,j)+umm*h(m,j)
      h(l,j)=th
60    continue
      do 70 i=1,nm
      th=conjg(ull)*h(i,l)+conjg(ulm)*h(i,m)
      h(i,m)=conjg(uml)*h(i,l)+conjg(umm)*h(i,m)
      h(i,l)=th
      tu=conjg(ull)*un(i,l)+conjg(ulm)*un(i,m)
      un(i,m)=conjg(uml)*un(i,l)+conjg(umm)*un(i,m)
      un(i,l)=tu
70    continue
80    continue
      if(ind.eq.0) go to 100
      ind=0
      go to 50
100   if(thr.gt.anormx) go to 40
      return
```

```
end
```

```
      program dimeth
c     This program calculates the inter-proton distances, scaling factor
c     S matrix elements for u, v, and w couplings for the single crystal
c     of 1,8-dimethylnaphthalene
      dimension x(2,3,3),vect(3,3,3,3),dist(3,3,3),a(3,3),univ(3,3,3,3)
      dimension s(3,5),su(5),sv(5),sw(5)
      x(1,1,1)=3.622
      x(1,1,2)=-1.851
      x(1,1,3)=6.308
      x(1,2,1)=2.225
      x(1,2,2)=-2.566
      x(1,2,3)=6.215
      x(1,3,1)=2.444
      x(1,3,2)=-1.704
      x(1,3,3)=7.451
      x(2,1,1)=4.255
      x(2,1,2)=-2.083
      x(2,1,3)=4.473
      x(2,2,1)=2.818
      x(2,2,2)=-2.875
      x(2,2,3)=4.295
      x(2,3,1)=3.638
      x(2,3,2)=-2.447
      x(2,3,3)=3.058
      write(6,5)
5     format('1',5x,'list of the coordinates of methyl proton',$)
      write(6,6)
6     format(2x,'x(i,j,k), i=1,2, j=a,b,c, k=x,y,z',//)
      do 50 i=1,2
      do 40 j=1,3
      do 30 k=1,3
      write(6,10)i,j,k,x(i,j,k)
10    format(5x,'x(',i1,',',i1,',',i1,')= ',f7.3,$)
30    continue
      write(6,31)
31    format(1x,/)
40    continue
50    continue
      do 90 j1=1,3
      do 85 j2=1,3
      do 80 k=1,3
      if(j1.eq.j2) go to 60
      vect(1,j1,j2,k)=x(1,j1,k)-x(1,j2,k)
      vect(2,j1,j2,k)=x(2,j1,k)-x(2,j2,k)
60    vect(3,j1,j2,k)=x(1,j1,k)-x(2,j2,k)
80    continue
85    continue
90    continue
      do 110 i=1,3
      do 105 j1=1,3
      do 100 j2=1,3
      sum=0.
      do 95 k=1,3
      sum=sum+vect(i,j1,j2,k)**2
95    continue
      dist(i,j1,j2)=sum**0.5
100   continue
105   continue
110   continue
      write(6,111)
```

```
111     format(1x,///)
        write(6,112)
112     format('1',5x,'list of the vectors & distance between')
        write(6,113)
113     format(8x,'proton vect(i,j1,j2,k), i=1-1,2-2,1-2',$)
        write(6,114)
114     format(2x,'j1,j2=a,b,c, k=x,y,z',//)
        do 150 i=1,3
        do 145 j1=1,3
        do 140 j2=1,3
        do 130 k=1,3
        if(i.eq.3) go to 115
        if(j1.ge.j2) go to 140
115     write(6,116)i,j1,j2,k,vect(i,j1,j2,k)
116     format(5x,'v(',3(i1,','),i1,')= ',f7.3,$)
130     continue
        write(6,135)i,j1,j2,dist(i,j1,j2)
135     format(10x,'distance(',i1,',',i1,',',i1,')= ',f7.3,/)
140     continue
145     continue
150     continue
        write(6,151)
151     format('1',//,5x,'list of the directional cosine of',$)
        write(6,152)
152     format(2x,'vector in the molecular frame given',$)
        write(6,153)
153     format(2x,'by unit vector a(i,k)',//)
        a(1,1)=0.427
        a(1,2)=-0.861
        a(1,3)=0.277
        a(2,1)=-0.299
        a(2,2)=0.157
        a(2,3)=0.941
        a(3,1)=0.854
        a(3,2)=0.485
        a(3,3)=0.190
        do 200 i=1,3
        do 195 j1=1,3
        do 190 j2=1,3
        do 185 k=1,3
        if(i.eq.3) go to 160
        if(j1.ge.j2) go to 190
160     tr=0.
        do 180 m=1,3
        tr=tr+vect(i,j1,j2,m)*a(k,m)/dist(i,j1,j2)
180     continue
        univ(i,j1,j2,k)=tr
        write(6,170)i,j1,j2,k,univ(i,j1,j2,k)
170     format(8x,'univ(',3(i1,','),i1,')= ',f7.3,$)
185     continue
        write(6,186)
186     format(1x,/)
190     continue
195     continue
200     continue
        write(6,201)
201     format('1',5x,'list of 5 S-matrix elements s(m,n)',$)
        write(6,202)
202     format(2x,'m=1-1,2-2,1-2, n=1,5',//)
        do 255 i=1,3
```

```
      sum1=0.
      sum2=0.
      sum3=0.
      sum4=0.
      sum5=0.
      do 250 j1=1,3
      do 240 j2=1,3
      if(i.eq.3) go to 205
      if(j1.ge.j2) go to 240
205   ddd=dist(i,j1,j2)**3
      sa=3.*univ(i,j1,j2,1)**2-1.
      sum1=sum1+sa/ddd
      sa=univ(i,j1,j2,2)**2-univ(i,j1,j2,3)**2
      sum2=sum2+sa/ddd
      sa=univ(i,j1,j2,1)*univ(i,j1,j2,2)*2.
      sum3=sum3+sa/ddd
      sa=univ(i,j1,j2,1)*univ(i,j1,j2,3)*2.
      sum4=sum4+sa/ddd
      sa=univ(i,j1,j2,2)*univ(i,j1,j2,3)*2.
      sum5=sum5+sa/ddd
240   continue
250   continue
      if(i.eq.3) rm=9.
      if(i.lt.3) rm=3.
      s(i,1)=sum1/rm
      s(i,2)=sum2/rm
      s(i,3)=sum3/rm
      s(i,4)=sum4/rm
      s(i,5)=sum5/rm
255   continue
      write(6,256)
256   format(1x,/)
      do 300 m=1,3
      do 270 n=1,5
      write(6,260)m,r,s(m,n)
260   format(5x,'s(',i1,',',i1,')= ',f8.4,$)
270   continue
      write(6,275)
275   format(1x,/)
300   continue
      write(6,301)
301   format('1',//,5x,'list of the S-matrix elements',3)
      write(6,302)
302   format(2x,'of u,v,w couplings',//)
      sum1=0.
      sum2=0.
      sum3=0.
      sum4=0.
      sum5=0.
      do 350 j=1,3
      ddd=dist(3,j,j)**3
      sb=3.*univ(3,j,j,1)**2-1.
      sum1=sum1+sb/ddd
      sb=univ(3,j,j,2)**2-univ(3,j,j,3)**2
      sum2=sum2+sb/ddd
      sb=univ(3,j,j,1)*univ(3,j,j,2)*2.
      sum3=sum3+sb/ddd
      sb=univ(3,j,j,1)*univ(3,j,j,3)*2.
      sum4=sum4+sb/ddd
      sb=univ(3,j,j,2)*univ(3,j,j,3)*2.
```

```
      sum5=sum5+sb/dcd
350   continue
      sv(1)=sum1/3.
      sv(2)=sum2/3.
      sv(3)=sum3/3.
      sv(4)=sum4/3.
      sv(5)=sum5/3.
      do 390 n=1,5
      su(n)=(s(1,n)+s(2,n))/2.
      sw(n)=(s(3,n)*9.-sv(n)*3.)/6.
      write(6,360)r,su(n),n,sv(n)
360   format(1x,/,5x,'su(',i1,')= ',f8.4,10x,'sv(',i1,')= ',f8.4,5)
      write(6,361)r,sw(n)
361   format(10x,'sw(',i1,')= ',f8.4)
390   continue
      stop
      end
```

```
      dimension d(7,7)
      open(unit=01,name='varmain.data',type='new')
      write(6,2)
2     format(1x,'enter the number of spins=',$)
      read(5,4)nspin
4     format(i2)
      write(1,6)nspin
6     format(1x,i2)
      do 50 i=1,nspin
      do 50 j=1,nspin
      if(j.le.i) go to 50
      write(6,10)i,j
10    format(10x,'enter the value of d(',i2,',',i2,')=',$)
      read(5,12)d(i,j)
12    format(f10.0)
      write(1,15)d(i,j)
15    format(1x,f10.3)
50    continue
      close(unit=01)
      stop
      end
```

```
      program gauss
      write(6,10)
10    format(10x,'enter the number of spins: ',$)
      read(5,15)n
15    format(i2)
      rn=n
      write(6,20)
20    format(10x,'enter the max of display: ',$)
      read(5,25)xmax
25    format(f10.0)

c     Calculation of MW intensity - for each order
      open(unit=01,name='gauss1.val',type='new')
      n1=n+1
      do 50 k=1,n1
      x=k-1.
      y=x*x/rn
      fx=exp(-y)
      write(1,30)x,fx
30    format(10x,f10.4,10x,f13.6)
50    continue
      close(unit=01)

c     Calculation of MO intensity - gaussian curve
      open(unit=01,name='gauss.val',type='new')
      do 100 k=1,401
      x=(k-1.)/400.*xmax
      y=x*x/rn
      fx=exp(-y)
      write(1,60)x,fx
60    format(5x,f13.6,10x,f13.6)
100   continue
      close(unit=01)

c     Calculation of the approximate number of states for each manifold
c     by Stirling's formula
      open(unit=01,name='gauss2.val',type='new')
      do 200 k=1,2*n+1,2
      rm=(k-1.-n)/2.
      cx=2.**(rn+1.)/sqrt(2.*3.1416*rn)*exp(-2.*rm*rm/rn)
      write(1,120)rm,cx
120   format(5x,f13.6,10x,f13.6)
200   continue
      close(unit=01)

      open(unit=01,name='gauss3.val',type='new')
      do 300 k=1,400
      r=(k-201.)/200.*xmax/2.
      cx=2.**(rn+1.)/sqrt(2.*3.1416*rn)*exp(-2.*r*r/rn)
      write(1,220)r,cx
220   format(5x,f13.6,10x,f13.6)
300   continue
      close(unit=01)
      stop
      end
```

```
      program heigen
c     This program calculates the eigenvalues of the 3x3 matrix for the
c     4-quantum transitions of two methyl groups in partially correlated
c     motion.  Output stored in file ch3exc.data
c
c     tau=1/g, the correlation time for the gearing motion
c
c     dipole couplings u, v, w in Hz

      complex h(3,3),un(3,3),g
      u=1196.
      v=-2684.
      w=-494.
      write(6,3)
3     format(10x,'enter the correlation time tau: ',$)
      read(5,5)tau
5     format(f13.0)
      g=cmplx(0.,1./tau)
      h(1,1)=1.5*u+v+2.*w
      h(1,2)=1.732*(v-w)/6.
      h(1,3)=(v+2.*w)/sqrt(6.)
      h(2,2)=3.*u/2.+v/3.+5.*w/3.+3.*g
      h(2,3)=1.414*(v-w)/3.
      h(3,3)=3.*u+2.*v/3.+4.*w/3.
      h(2,1)=h(1,2)
      h(3,1)=h(1,3)
      h(3,2)=h(2,3)
      write(6,40)g
40    format(///,5x,'g= ',f4.1,'+ i  ',f10.3,/)
      call diagni(h,un,3)
      open(unit=01,name='ch3exc.data',type='new')
      do 60 i=1,3
      write(6,50)i,h(i,i)
50    format(10x,'eigenvalue (',i2,')= ',f10.3,5x,'+ i  ',f10.3)
      write(1,55)h(i,i)
55    format(1x,f13.6,5x,f13.6)
60    continue
      close(unit=01)
      stop
      end


      subroutine diagni(h,un,nm)
      complex h(nm,nm),un(nm,nm),ull,ulm,uml,umm,th,tu
      nmm=nm-1
      an=nm
      range=1.0e-2
      do 20 i=1,nm
      do 10 j=1,nm
10    un(i,j)=0.
20    un(i,i)=1.
      anorm=0.
      do 30 i=1,nmm
      ii=i+1
      do 30 j=ii,nm
30    anorm=anorm+real(h(i,j)*conjg(h(i,j)))
      if(anorm.le.range) return
      anorm=sqrt(2.*anorm)
      anormx=anorm*range/an
      ind=0
```

```
      thr=anorm
40    thr=thr/on
50    do 80 l=1,nm
      ll=l+1
      do 80 m=ll,nm
      if (cabs(h(l,m)).lt.thr) go to 80
      ind=1
      diff=real(h(m,m)-h(l,l))
      if(diff.eq.0.) diff=1.0e-15
      ar=0.5*atan(-2.*real(h(l,m))/diff)
      ai=0.5*atan(-2.*aimag(h(l,m))/diff)
      sini=sin(ai)
      cosi=cos(ai)
      sinr=sin(ar)
      cosr=cos(ar)
      ull=cmplx(cosr*cosi,sinr*sini)
      ulm=cmplx(sinr*cosi,cosr*sini)
      uml=cmplx(-sinr*cosi,cosr*sini)
      umm=cmplx(cosr*cosi,-sinr*sini)
      do 60 j=1,nm
      th=ull*h(l,j)+ulm*h(m,j)
      h(m,j)=uml*h(l,j)+umm*h(m,j)
      h(l,j)=th
60    continue
      do 70 i=1,nm
      th=conjg(ull)*h(i,l)+conjg(ulm)*h(i,m)
      h(i,m)=conjg(uml)*h(i,l)+conjg(umm)*h(i,m)
      h(i,l)=th
      tu=conjg(ull)*un(i,l)+conjg(ulm)*un(i,m)
      un(i,m)=conjg(uml)*un(i,l)+conjg(umm)*un(i,m)
      un(i,l)=tu
70    continue
80    continue
      if(ind.ec.0) go to 100
      ind=0
      go to 50
100   if(thr.gt.anorm*x) go to 40
      return
      end
```

```
      subroutine irvmax(a)
      complex a(3,3),b(3,3)
      complex cet
      det=a(1,1)*a(2,2)*a(3,3)+a(1,2)*a(2,3)*a(3,1)
      det=det+a(1,3)*a(2,1)*a(3,2)-a(1,3)*a(2,2)*a(3,1)
      det=det-a(1,1)*a(2,3)*a(3,2)-a(1,2)*a(2,1)*a(3,3)
      b(1,1)=a(2,2)*a(3,3)-a(2,3)*a(3,2)
      b(1,2)=-a(2,1)*a(3,3)+a(2,3)*a(3,1)
      b(1,3)=a(2,1)*a(3,2)-a(2,2)*a(3,1)
      b(2,1)=-a(1,2)*a(3,3)+a(3,2)*a(1,3)
      b(2,2)=a(1,1)*a(3,3)-a(1,3)*a(3,1)
      b(2,3)=-a(1,1)*a(3,2)+a(3,1)*a(1,2)
      b(3,1)=a(1,2)*a(2,3)-a(1,3)*a(2,2)
      b(3,2)=-a(1,1)*a(2,3)+a(1,3)*a(2,1)
      b(3,3)=a(1,1)*a(2,2)-a(1,2)*a(2,1)
      do 10 i=1,3
      do 10 j=1,3
      a(i,j)=b(i,j)/cet
10    continue
      return
      end
```

```
      subroutine invmax(a)
      complex a(2,2),b(2,2)
      complex cet
      det=a(1,1)*a(2,2)-a(1,2)*a(2,1)
      b(1,1)=a(2,2)
      b(1,2)=-a(2,1)
      b(2,1)=-a(1,2)
      b(2,2)=a(1,1)
      do 10 i=1,2
      do 10 j=1,2
      a(i,j)=b(i,j)/cet
10    continue
      return
      end
```

```
      subroutine lescft(n,ncata,x)
      dimension a(20,20),b(20,20),x(7,20,3)
      dimension secmom(8),summ(3,4),err(8)
c     This subprogram calculates the least square fit for a
c     simultaneous linear equations
      write(6,10)
10    format(//,10x,'The least square fit for second moment',5)
      write(6,12)
12    format(2x,'x(1)=dave**2, x(2)=dsqave',/)
      nn=2
      mm=1
      do 200 k=1,n
      do 46 i=1,nn
      do 45 j=1,nn+1
      sum=0.
      do 20 km=1,ncata
      sum=sum+x(k,km,i)*x(k,km,j)/x(k,km,3)**2
20    continue
      summ(i,j)=sum
      nn1=nn+1
      if (j.ec.nn1) go to 40
      a(i,j)=summ(i,j)
      go to 45
40    b(i,1)=summ(i,3)
45    continue
46    continue
      call matinv(a,nn,b,mm,det)
      k1=k-1
      sb=0.
      do 70 km=1,ncata
      sa=0.
      do 60 i=1,nn
      sa=sa+b(i,1)*x(k,km,i)/x(k,km,3)
60    continue
      sb=sb+(sa-1.)**2
70    continue
      nca=ncata-1
      err(k)=(sb/nca)**0.5
      do 80 i=1,nn
      write(6,75)k1,i,b(i,1)
75    format(6x,'b(',i2,',',i2,')= ',f10.4,5)
80    continue
      write(6,85)k1,err(k)
85    format(10x,'error(',i2,')= ',e10.3,/)
200   continue
      open(unit=01,name='var.val',type='new')
      do 500 km=1,rdata
      sc=0.
      do 350 i=1,nn
      sc=sc+b(i,1)*x(1,km,i)
350   continue
      do 450 k=1,n+1
      sa=0.
      do 420 i=1,nn
      sa=sa+b(i,1)*x(k,km,i)/sc
420   continue
      k1=k-1
      if(k1.ec.n) sa=0.
      if(k1.eo.n) y2=0.
      y2=x(k,km,3)/x(1,km,3)
```

```
      write(1,430)k1,y2,sa
430   format(1x,i2,5x,f13.6,5x,f13.6)
450   continue
500   continue
      close(unit=01)
      return
      end
```

```
      subroutine lgplot(data,ndata,iyscal)
      dimension data(100),ipos(100,50)
      data istar,itblank,ihyphe/'*',' ','-'/
      write(6,5)(ihyphe, k=1,100)
5     format(10x,100A1)
      dmax=data(1)
      dmin=data(1)
      do 10 k=2,ndata
      if(data(k).gt.dmax) dmax=data(k)
      if(data(k).lt.dmin) dmin=data(k)
10    continue
      if((dmin/dmax).ge.0.99) go to 120
      do 20 i=1,ndata
      data(i)=(data(i)-dmin)*iyscal/(dmax-dmin)
20    continue
      do 25 i=1,ndata
      do 25 j=1,iyscal
      ipos(i,j)=itblank
25    continue
      do 40 i=1,ndata
      itest=iyscal+1
30    itest=itest-1
      if((itest-data(i)).ge.0.5) go to 30
      ipos(i,itest)=istar
40    continue
      do 80 i=1,iyscal
      j=iyscal+1-i
80    write(6,90)(ipos(k,j),k=1,ndata)
90    format(10x,100A1)
      write(6,100)(ihyphe,k=1,100)
100   format(10x,100A1)
120   return
      end
```

```
      subroutine matinv(a,nn,b,mm,det)
      dimension a(20,20),b(20,20),ipvot(20),index(20,2),pivot(20)
      common ipvot,index,pivot
      equivalence (irow,jrow),(icol,jcol)
57    det=1.
      do 17 j=1,nn
17    ipvot(j)=0
      do 135 i=1,nn
      t=0.
      do 9 j=1,nn
      if(ipvot(j).eq.1) go to 9
13    do 23 k=1,nn
      if(ipvot(k)-1) 43,23,81
43    if(abs(t).ge.abs(a(j,k))) go to 23
83    irow=j
      icol=k
      t=a(j,k)
23    continue
9     continue
      ipvot(icol)=ipvot(icol)+1
      if(irow.eq.icol) go to 109
73    det=-det
      do 12 l=1,nn
      t=a(irow,l)
      a(irow,l)=a(icol,l)
12    a(icol,l)=t
      if(mm.le.0) go to 109
33    do 2 l=1,mm
      t=b(irow,l)
      b(irow,l)=b(icol,l)
2     b(icol,l)=t
109   index(i,1)=irow
      index(i,2)=icol
      pivot(i)=a(icol,icol)
      det=det*pivot(i)
      a(icol,icol)=1.
      do 205 l=1,nn
205   a(icol,l)=a(icol,l)/pivot(i)
      if(mm.le.0) go to 347
66    do 52 l=1,mm
52    b(icol,l)=b(icol,l)/pivot(i)
347   do 135 ll=1,nn
      if(ll.eq.icol) go to 135
21    t=a(ll,icol)
      a(ll,icol)=0.
      do 89 l=1,nn
89    a(ll,l)=a(ll,l)-a(icol,l)*t
      if(mm.le.0) go to 135
18    do 68 l=1,mm
68    b(ll,l)=b(ll,l)-b(icol,l)*t
135   continue
222   do 3 i=1,nn
      l=nn-i+1
      if(index(l,1).eq.index(l,2)) go to 3
19    jrow=index(l,1)
      jcol=index(l,2)
      do 549 k=1,nn
      t=a(k,jrow)
      a(k,jrow)=a(k,jcol)
      a(k,jcol)=t
```

```
549     continue
3       continue
81      return
        end
```

```
      program moment
c     the program to calculate the second moment of multiple quantum spectra
c     of n coupled spin-1/2 particles assuming equal coupling constants based
      on statistical model
      dimension z(50), b(50),a(50),omega(50),sqrome(50),ratome(50)
      dimension ratscr(50)
      write(6,2)
2     format(10x,'enter the number of spins: ',$)
      read(5,4)n
4     format(i3)
11    do 100 k=1,n+1
      m=k-1
      x=-(n-m)/2.
      zs=0.
      bs=0.
20    zs=zs+exp(-4.*x**2/n)
      bs=bs+exp(-4.*x**2/n)*x**2.
      x=x+1.
      if (x-(n-m)/2.) 20,20,30
30    rm=m
      rn=n
      z(k)=zs*exp(-rm**2./rn)
      b(k)=4.*bs*rm**2/zs
      a(k)=(n**2-rm**2-4.*bs/zs)/4.
      omega(k)=a(k)+b(k)
      sqrome(k)=omega(k)**0.5
      ratome(k)=omega(k)/omega(1)
      ratscr(k)=sqrome(k)/sqrome(1)
100   continue
      write (6,110)
110   format(//,2x,'number of spins n',3x,'m-quantum m',6x,'a(m)',$)
      write (6,115)
115   format(11x,'b(m)',10x,'omega(m)',4x,'sqrome(m)',$)
      write (6,116)
116   format(5x,'omega(m)/omega(0)',4x,'sqrome(m)/sqrome(0)')
      do 130 k=1,n+1
      m=k-1
      write(6,120)n,m,a(k),b(k),omega(k),sqrome(k),ratome(k),ratscr(k)
120   format(10x,i3,11x,i3,4x,4(4x,e10.4),2(5x,e10.4))
130   continue
      open(unit=01,name='moment.val',type='new')
      do 160 k=1,n+1
      k1=k-1
      ratioa=a(k)/omega(1)
      ratiob=b(k)/omega(1)
      write(1,155)k1,ratome(k),ratioa,ratiob
155   format(1x,i3,3(5x,f10.5))
160   continue
      close(unit=01)
210   stop
      end
```

```
      subroutine plot(data,ndata,scale)
      dimension data(100)
      data star,blank/'*',' '/
      write(6,5)
5     format(1H1)
      dmax=data(1)
      dmin=data(1)
      do 10 k=2,ndata
      if(data(k).gt.dmax) dmax=data(k)
      if(data(k).lt.dmin) dmin=data(k)
10    continue
      if(dmin/dmax.le.0.99) go to 25
      do 20 k=1,ndata
20    data(k)=(data(k)-dmin)*100./(dmax-dmin)
      go to 30
25    length=50
30    do 40 k=1,ndata
      length=data(k)*scale
40    write(6,50)k,(blank,m=1,length-1),star
50    format(3x,i3,4x,100A1)
      return
      end
```

```
      program plot1
      dimension data(100),ipos(100,50)
      data istar,iblank/'*',' '/
      ndata=10
      do 5 k=1,ndata
5     data(k)=k
      dmax=data(1)
      dmin=data(1)
      do 10 k=2,ndata
      if(data(k).gt.dmax) dmax=data(k)
      if(data(k).lt.dmin) dmin=data(k)
10    continue
      do 20 i=1,ndata
      data(i)=(data(i)-dmin)*50./(dmax-dmin)
20    continue
      do 25 i=1,ndata
      do 25 j=1,50
      ipos(i,j)=iblank
25    continue
      do 40 i=1,ndata
      itest=51
30    itest=itest-1
      if((itest-data(i)).ge.0.5) go to 30
      ipos(i,itest)=istar
40    continue
      do 80 i=1,50
      j=51-i
80    write(6,90)(ipos(k,j),k=1,ndata)
90    format(10x,100A1)
      stop
      end
```

```
      open(unit=01,name='rel.val',type='new')
      do 100 i=1,101
      x=(i-1.)/100.
      f1=(20.+18.*x)/(18.+7.*x)
      f2=(21.+15.*x)/(18.+7.*x)
      f3=(18.+18.*x)/(9.+7.*x)
      f4=(13.+12.*x)/(9.+7.*x)
      f5=(90.+72.*x)/(63.+28.*x)
      f6=(76.+57.*x)/(63.+28.*x)
      write(1,20)x,f1,f2,f3,f4,f5,f6
20    format(1x,f8.4,6(5x,f10.5))
100   continue
      close(unit=01)
      stop
      end
```

```
      program siteex
c     This program calculates the lineshape of ordinary single quantum
c     spectrum for the exchanging system of J-coupled AB spins
c     rj: J coupling constant
c     t2: transverse relaxation time
c     tau: inverse of the exchange rate
c     delta: difference in the resonance frequency between A and B spins
c     xmax: max. value of the frequency display
      complex a(2,2),alpha1,alpha2
      write(6,2)
2     format(10x,'enter the value of T2 (in sec): ',$)
      read(5,4)t2
4     format(f10.0)
      write(6,10)
10    format(10x,'enter the value of tau (in sec): ',$)
      read(5,12)tau
12    format(f10.0)
      write(6,15)
15    format(10x,'enter the value of chemical shift freq. :',$)
      read(5,16)delta
16    format(f10.0)
      write(6,20)
20    format(10x,'enter the value of J coupling (in Hz): ',$)
      read(5,22)rj
22    format(f10.0)
      write(6,25)
25    format(10x,'enter the value of max. omega (in Hz): ',$)
      read(5,27)xmax
27    format(f10.0)
      open(unit=01,name='siteex.val',type='new')
      c=sqrt(delta**2+rj**2)/2.
      s1=0.5*rj/c
      c1=0.5*delta/c
      do 100 kk=1,800
      omega=(kk-401.)/400.*xmax
      sum=0.
      do 60 m=1,2
      if(m.eq.1) go to 30
      if(m.eq.2) go to 40
30    xa=rj/2.-c-omega
      xb=rj/2.+c-omega
      go to 50
40    xa=rj/2.-c+omega
      xb=rj/2.+c+omega
50    alpha1=cmplx(1./t2+(1.-s1)/tau,xa)
      alpha2=cmplx(1./t2+(1.+s1)/tau,xb)
      a(1,1)=alpha1
      a(2,2)=alpha2
      a(1,2)=cmplx(-c1/tau,0.)
      a(2,1)=a(1,2)
      call invmax(a)
      sum=sum+(a(1,1)+a(2,1))*(1.+s1)+(a(1,2)+a(2,2))*(1.-s1)
60    continue
      write(1,70)omega,sum
70    format(3x,2(5x,f13.7))
100   continue
      close(unit=01)
      stop
      end
```

```
      program speccn
      write(6,1)
1     format(5x,'enter 0 or 1 for correlated motion cr',$)
      write(6,9)
9     format(1x,' uncorrelated motion: ',$)
      read(5,2)logic
2     format(i2)
      if(logic.eq.1) go to 3
      alarge=3.504*12.013e3
      asmall=0.953*12.013e3
      rnorm1=2./3.
      rnorm2=1./3.
      go to 4
3     alarge=1.790*12.013e3
      asmall=1.790*12.013e3
      rnorm1=0.5
      rnorm2=0.5
      write(6,60)
60    format(10x,'enter the max frequency: ',$)
      read(5,65)amax
65    format(f10.4)
4     write(6,5)alarge,asmall
5     format(1x,/,5x,'alarge= ',f8.2,5x,'asmall= ',f8.2,$)
      write(6,6)rnorm1,rnorm2
6     format(5x,'rnorm1= ',f6.2,5x,'rnorm2= ',f6.2,///)
      open(unit=01,name='speccn.val',type='new')
      do 50 i=1,500
      y=(i-251.)/250.*amax/alarge
      x=y*alarge
      z=x/asmall
      gn=funct(z,asmall)*rnorm1+funct(y,alarge)*rnorm2
      write(1,81)x,gn
81    format(5x,f13.6,10x,f13.6)
50    continue
      close(unit=01)
      stop
      end


c  funct follows.
      function funct(y,a)
      yplus=0.5+abs(y)
      yminus=0.5-abs(y)
      if(abs(y)-1.000) 5,5,3
3     funct=0.000
      go to 50
5     if(abs(y)-0.500) 10,30,20
10    funct=(1./sqrt(yminus)+1./sqrt(yplus))/a
      go to 50
20    funct=1./(a*sqrt(yplus))
      go to 50
30    funct=1./(a*sqrt(0.0005))
50    return
      end
```

```
      program trplct
c     This program plots the data in file 'trplot.data'
      dimension data(120),ipos(120,50)
      data istar,iblank,ihyphe/'*',' ','-'/
      data iyscal/50/
      open(unit=01,name='trplot.data',type='old',readonly)
      read(1,1)ndata,ymax,ymin
1     format(i3,2e13.6)
      do 2 k=1,ndata
2     read(1,3)data(k)
3     format(e13.6)
      close(unit=01)
      write(6,8)(ihyphe, k=1,120)
8     format(10x,120A1)
      do 20 i=1,ndata
      data(i)=(data(i)-ymin)*iyscal/(ymax-ymin)
20    continue
      do 25 i=1,ndata
      do 25 j=1,iyscal
      ipos(i,j)=iblank
25    continue
      do 40 i=1,ndata
      itest=iyscal+1
30    itest=itest-1
      if((itest-data(i)).ge.0.5) go to 30
      ipos(i,itest)=istar
40    continue
      do 80 i=1,iyscal
      j=iyscal+1-i
80    write(6,90)(ipos(k,j),k=1,ndata)
90    format(10x,120A1)
      write(6,100)(ihyphe,k=1,120)
100   format(10x,120A1)
120   stop
      end
```

```
      program var
      dimension d(7,7),hdave(8),hofsav(8),hdsav(8),sigma(8),bn(8)
      dimension hdisav(8),secmom(8),x(7,20,4)
c     This program calculates the second moment of the multiple quantum
c     spectra for each order m. The number of spins: 3 to 7.
      open(unit=01,name='var.data',type='old',readonly)
      read(1,2)ndata
2     format(i2)
      do 100 km=1,ndata
      read(1,5)n
5     format(i2)
      do 16 i=1,n
      do 15 j=1,n
      if(i.ge.j) go to 15
      read(1,13)c(i,j)
13    format(f10.3)
15    continue
16    continue
      go to 35
      write(6,20)n
20    format(1x,///,25x,'number of spins: ',i2,//)
      do 30 i=1,n
      do 25 j=1,n
      if(i.ge.j) go to 25
      write(6,22) i,j,d(i,j)
22    format(23x,'c(',i2,',',i2,'): ',2x,f10.3)
25    continue
30    continue
35    call subr1(n,d,dsum,dave,dsqave,hdave,hofsav,gamma,)
      call subr2(n,d,dsum,hcave,hofsav,hdsav,hdisav,sigma,bn)
      go to 65
      write(6,40)
40    format(///,6x,'m',14x,'hdave(m)',12x,'hdsav(m)',12x,'sigma(m)')
      do 60 k=1,n+1
      rm=0.5*n-k+1
      write(6,50)rm,hdave(k),hdsav(k),sigma(k)
50    format(/,3x,f4.1,3(10x,f10.3))
60    continue
65    call subr3(n,bn,hdsav,hdisav,hdave,sigma,gamma,secmom)
      do 70 k=1,n
      x(k,km,1)=cave**2
      x(k,km,2)=cscave
      x(k,km,3)=secmom(k)
70    continue
100   continue
      close(unit=01)
      call lescft(n,ndata,x)
      stop
      end
```

```
      program varcpl
      dimension d(7,7)
c     This program generates random dipole couplings for N coupled
c     spins within dmax and dmin
      open(unit=01,name='varmain.data',type='new')
      write(6,2)
2     format(10x,'enter the total number of spins:',$)
      read(5,4)nspin
4     format(i2)
      write(1,5)nspin
5     format(1x,i2)
c     write(6,10)
c10   format(10x,'enter the max. of dipole coupling:',$)
c     read(5,12)dmax
c12   format(f10.0)
c     write(6,15)
c15   format(10x,'enter the min. of dipole coupling:',$)
c     read(5,17)dmin
c17   format(f10.0)
      write(6,19)
19    format(10x,'enter rancom number k=',$)
      read(5,20)k
20    format(1x,i6)
      write(6,21)
21    format(10x,'enter rancom number m=',$)
      read(5,22)m
22    format(1x,i6)
      do 50 i=1,nspin
      do 50 j=1,nspin
      if(j.le.i) cc to 50
24    x=ran(k,m)
      if(x-0.5)25,24,26
25    d(i,j)=1.
      go to 50
26    d(i,j)=-1.
      go to 50
50    continue
      do 100 i=1,nspin
      do 100 j=1,nspin
      if(j.le.i) cc to 100
      write(1,60)d(i,j)
60    format(1x,f10.3)
100   continue
      close(unit=01)
      stop
      end
```

```
      dimension d(5,5),dpasum(5,5),hdave(5),hdfsav(5),cn(5),hdisav(5)
      dimension hdsav(5),sigma(5)
      write(6,1)
1     format(//,10x,'enter the number of spins: ',$)
      read(5,5)n
5     format(i2)
      write(6,10)
10    format(//,10x,'enter the dipole couplings d(i,j): ')
      do 15 i=1,n
      do 15 j=1,n
      if(i.ge.j) go to 15
      write(6,12)i,j
12    format(/,10x,'c(',i2,',',i2,')= ',$)
      read(5,13)d(i,j)
13    format(f8.2)
15    continue
      write(6,16)n
16    format(//,10x,'number of spins: ',i2,//,'list of dipole couplings')
      do 18 i=1,n
      do 18 j=1,n
      if (i.ge.j) go to 18
      write(6,17)i,j,d(i,j)
17    format(/,10x,'c(',i2,',',i2,'): ',1x,e10.4)
18    continue
      do 20 i=1,n
      d(i,i)=0.
20    continue
      do 30 i=1,n
      do 30 j=1,n
      if(i.le.j) go to 30
      d(i,j)=d(j,i)
30    continue
      dsum=0.
      dsqsum=0.
      do 40 i=1,n
      do 40 j=i,n
      if(i.ge.j) go to 40
      dsum=dsum+d(i,j)
      dsqsum=dsqsum+d(i,j)**2
      dpasum(i,j)=0.
40    continue
      cn2=n*(n-1)/2.
      dave=dsum/cn2
      dsqave=dsqsum/cn2
      do 50 k=1,n+1
      sn=k-1
      hdave(k)=0.25*dave*((n-2*sn)**2-sn)
      hdfsav(k)=0.5*dsqave*(n-sn)*sn
50    continue
      cn(1)=n
      do 60 k=2,n
      cn(k)=cn(k-1)*(n-k+1)/k
60    continue
      hdisav(1)=0.25*dsum**2
      do 70 i=1,n
      do 70 j=1,n
      do 70 k=1,n
      if (i.ge.j) go to 70
      dpasum(i,j)=dpasum(i,j)+d(i,k)+d(j,k)-d(i,j)-d(j,i)
70    continue
```

```
c
            trsohd=0.
            do 80 i=1,n
c           do 80 j=1,n
            if(i.ne.j) go to 80
            trsqhd=trsohc+(0.5*dsum-ddasum(i,j))**2
c    80     continue
            hdisav(3)=trsqhd/cn(2)
            trsqhd=0.
c           do 90 i=1,n
            trsqhd=trsohc+(0.5*dsum-0.5*ddasum(i,j))**2
    90      continue
c           hdisav(2)=trsqhd/cn(1)
            if(n-3)110,100,110
    100     hdisav(4)=hdisav(1)
c   110     if(n-4)130,120,130
    120     hdisav(4)=hdisav(2)
            hdisav(5)=hdisav(1)
c   130     if(n-5)150,140,150
    140     hdisav(4)=hdisav(3)
            hdisav(5)=hdisav(2)
c           hdisav(6)=hdisav(1)
    150     do 160 k=1,n+1
            hdsav(k)=hdisav(k)+hdfsav(k)
c           sigma(k)=(hdsav(k)-hdave(k)**2)**0.5
    160     continue
            write(6,600)cave,dsqave
c   600     format(//,10x,'dave= ', e10.4,10x,'dsqave= ',e10.4)
            write(6,610)
    610     format(//,3x,'m',12x,'hdave(m)',12x,'hdsav(m)',12x,'sigma(m)')
c           do 650 k=1,n+1
            rm=0.5*n-k+1
            write(6,640)rm,hdave(k),hdsav(k),sigma(k)
c   640     format(/,3x,e10.4,3(10x,e10.4))
    650     continue
            stop
c           end
```

```
      program varin
c     This program enters the number of spins n and the dipole couplings
c     d(i,j) for the calculateion of program var.
      dimension d(7,7)
      open(unit=01,name='varmain.data',type='new')
      write(6,1)
1     format(1x,/,10x,'enter the number of spins(3 to 7): ',$)
      read (5,5)n
5     format(i2)
      write(1,6)n
6     format(1x,i2)
      write(6,10)
10    format(1x,/,10x,'enter the dipole couplings d(i,j): ')
      do 16 i=1,n
      do 15 j=1,n
      if (i.ge.j) go to 15
      write(6,12)i,j
12    format(1x,/,10x,'d(',i2,',',i2,')= ',$)
      read(5,13)d(i,j)
13    format(f10.0)
      write(1,14)d(i,j)
14    format(1x,f10.3)
15    continue
16    continue
      close(unit=01)
      stop
      end
```

```
      program varmain
      dimension d(7,7),hdave(8),hofsav(8),hdsav(8),sigma(8),bn(8)
      dimension hdisav(8),secmom(8),x(7,20,4)
c     This program calculates the second moment of the multiple quantum
c     spectra for each order m. The number of spins: 3 to 7.
      open(unit=01,name='varmain.data',type='old',readonly)
      read(1,5)n
5     format(i2)
      do 16 i=1,n
      do 15 j=1,n
      if(i.ne.j) go to 15
      read(1,13)d(i,j)
13    format(f10.3)
15    continue
16    continue
      close(unit=01)
      go to 35
      write(6,20)n
20    format(1x,///,25x,'number of spins: ',i2,//)
      do 30 i=1,n
      do 25 j=1,n
      if(i.ne.j) go to 25
      write(6,22) i,j,d(i,j)
22    format(23x,'d(',i2,',',i2,'): ',2x,f10.3)
25    continue
30    continue
35    call subr1(n,d,dsum,dave,dsqave,ndave,hofsav,gamma,)
      call subr2(n,d,dsum,hdave,hofsav,hdsav,hdisav,sigma,bn)
      write(6,40)
40    format(///,6x,'m',14x,'hdave(m)',12x,'hdsav(m)',12x,'sigma(m)')
      do 60 k=1,n+1
      rm=0.5*n-k+1
      write(6,50)rm,hdave(k),hdsav(k),sigma(k)
50    format(/,3x,f4.1,3(10x,f10.3))
60    continue
65    call subr3(n,bn,hdsav,hdisav,hdave,sigma,gamma,secmom)
      stop
      end
```

```
      subroutine subr1(n,d,csum,dave,dsqave,hdave,hofsav,gamma)
      dimension d(7,7),hdave(8),hofsav(8)
c     The subroutine calculate the averaged values of the trace of the dipole
c     hamiltonian and the square of the dipole hamiltonian for each manifold
      do 20 i=1,n
      do 10 j=1,n
      if(j.ge.i) go to 10
      d(i,j)=c(j,i)
10    continue
      d(i,i)=0.
20    continue
      dsum=0.
      dsqsum=0.
      do 50 i=1,n
      do 40 j=1,n
      dsum=dsum+c(i,j)/2.
      dsqsum=csqsum+c(i,j)**2/2.
40    continue
50    continue
      rn=n
      cn2=rn*(rn-1.)/2.
      dave=dsum/cn2
      dsqave=csqsum/cn2
      gamma=(dsqave-cave**2)/dsqave
      write(6,60) cave,dsqave,gamma
60    format(////,3x,'dave= ',f10.3,7x,'dsqave= ',f10.3,7x,'gamma= ',f10.3)
      do 70 k=1,n+1
      sn=k-1.
      hdave(k)=0.25*cave*((rn-2.*sn)**2-rn)
      hofsav(k)=0.5*csqave*(rn-sn)*sn
70    continue
      return
      end


      subroutine subr2(n,d,csum,hdave,hofsav,hqsav,hcisav,sigma,bn)
      dimension c(7,7),hdave(8),hofsav(8),hdisav(8),bn(8),dpasum(7,7,7)
      dimension hqsav(8),sigma(8)
c     This subprogram calculates the variance of the dipole hamiltonian
c     for each manifold. sigma= <H**2>-<H>**2.
      do 100 i=1,n
      do 100 j=1,n
      do 100 k=1,n
100   dpasum(i,j,k)=0.
      do 150 i=1,n
      do 140 j=1,n
      if(i.gt.j) go to 140
      do 130 k=1,n
      if(j.gt.k) go to 130
      dijk=0.
      do 120 l=1,n
      dijk=dijk+c(i,l)+d(j,l)+d(k,l)
120   continue
      dpasum(i,j,k)=dpasum(i,j,k)-d(i,j)*2.-d(j,k)*2-d(i,k)*2+dijk
130   continue
140   continue
150   continue
      trsqhd=0.
      do 220 i=1,n
      do 210 j=1,n
```

```
            if(i.ge.j) go to 210
            do 200 k=1,n
            if(j.ge.k) go to 200
            trsqhd=trsqhd+(0.5*dsum-dpasum(i,j,k))**2
  200       continue
  210       continue
  220       continue
            rn=n
            bn(1)=1.
            do 250 k=2,n+1
            bn(k)=bn(k-1)*(rn-k+2.)/(k-1.)
  250       continue
            hdisav(4)=trsqhd/bn(4)
  c         Calculation of the averaged value of the square of the diagonal
  c         part of dipolar hamiltonian with 3 spins down. The value is given above
  c         by hdisav(4).
            trsqhd=0.
            do 310 i=1,n
            do 300 j=1,n
            if(i.ge.j) go to 300
            dpa=(dpasum(i,i,j)+dpasum(i,j,j)+2*d(i,j))/3.
            trsqhd=trsqhd+(0.5*dsum-dpa)**2
  300       continue
  310       continue
            hdisav(3)=trsqhd/bn(3)
  c         The value of hdisav(3) is the averaged value of the square of the
  c         diagonal part of dipolar hamiltonian with 2 spins down.
            trsqhd=0.
            do 400 i=1,n
            dpas=dpasum(i,i,i)/3.
            trsqhd=trsqhd+(0.5*dsum-dpas)**2
  400       continue
            hdisav(2)=trsqhd/bn(2)
            hdisav(1)=0.25*dsum**2
  c         The above values of hdisav(2) and hdisav(1) for 1 and 0 spin down,
  c         respectively.
            i=n-2
            go to(500,410,430,450,470),i
  410       hdisav(5)=hdisav(1)
            go to 500
  430       hdisav(6)=hdisav(1)
            hdisav(5)=hdisav(2)
            go to 500
  450       hdisav(7)=hdisav(1)
            hdisav(6)=hdisav(2)
            hdisav(5)=hdisav(3)
            go to 500
  470       hdisav(8)=hdisav(1)
            hdisav(7)=hdisav(2)
            hdisav(6)=hdisav(3)
            hdisav(5)=hdisav(4)
  500       do 510 k=1,n+1
            hdsav(k)=hdisav(k)+hdfsav(k)
            sigma(k)=(hdsav(k)-hdave(k)**2)**0.5
  510       continue
            return
            end


            subroutine subr3(n,bn,hdsav,hdisav,hdave,sigma,gamma,secmom)
```

```
      dimension bn(8),hdave(8),hdsav(8),hdisav(8),secmom(8),hofsav(8)
      dimension ratio(8),sigma(8),sigmom(8),pigmom(8),rb(8),ra(8)
c     Calculation of the second moment of m-quantum spectra with given second
c     moments for each pair of manifolds of magnetic quantum number m1 and m2
c     so that m1-m2=m.
      do 40 j=1,n+1
      i=j-1
      upsum=0.
      dowsum=0.
      usum=0.
      psum=0.
      kf=n-i+1
      do 20 k=1,kf
      ki=k+i
      hki=hdsav(k)+hdsav(ki)-2.*hdave(k)*hdave(ki)
      bki=bn(k)*bn(ki)
      ski=sigma(k)**2+sigma(ki)**2
      pki=hdisav(k)+hdisav(ki)-hdave(k)**2-hdave(ki)**2
c     pki=hki-hofsav(k)-hofsav(ki)
      upsum=upsum+bki*hki
      dowsum=dowsum+bki
      usum=usum+bki*ski
      psum=psum+bki*pki
20    continue
      secmom(j)=upsum/dowsum
      sigmom(j)=usum/dowsum
      pigmom(j)=psum/dowsum
40    continue
      write(6,50)
50    format(//,3x,'m-quantum',7x,'secmom(m)',$)
      write(6,51)
51    format(5x,'secmom(m)/secmom(0)',5x,'sigmom(m)/secmom(0)',$)
      write(6,52)
52    format(6x,'pigmom(m)/secmom(0)')
      open(unit=01,name='var.val',type='new')
      do 70 j=1,n+1
      m=j-1
      ratio(j)=secmom(j)/secmom(1)
      ra(j)=sigmom(j)/secmom(1)
      rb(j)=pigmom(j)/secmom(1)
      write(6,60)m,secmom(j),ratio(j),ra(j),rb(j)
60    format(/,5x,i2,9x,f10.3,8x,f10.3,13x,f10.3,15x,f10.3)
      write(1,65)m,ratio(j)
65    format(5x,i2,5x,f13.7)
70    continue
      close(unit=01)
80    return
      end
```